Biophysical Aspects of Transdermal Drug Delivery and Chemical Enhancement

by

Mark E. Johnson

B.S., Chemical Engineering
University of California at Davis, 1990

M.S., Chemical Engineering Practice
Massachusetts Institute of Technology, 1992

Submitted to the Department of Chemical Engineering
in Partial Fulfillment of the Requirements for the Degree of

DOCTOR OF PHILOSOPHY IN CHEMICAL ENGINEERING

at the

MASSACHUSETTS INSTITUTE OF TECHNOLOGY

June 1996

Signature of Author: _____
Department of Chemical Engineering
May 22, 1996

Certified by: _____
Professor Daniel Blankschtein
Thesis Supervisor

Certified by: _____
Professor Robert Langer
Thesis Supervisor

Accepted by: _____
Professor Robert Cohen
Chairman, Committee for Graduate Students

Biophysical Aspects of Transdermal Drug Delivery and Chemical Enhancement

by

Mark E. Johnson

Submitted to the Department of Chemical Engineering
on May 22, 1996 in Partial Fulfillment of the
Requirements for the Degree of
Doctor of Philosophy in Chemical Engineering

ABSTRACT

Transdermal drug delivery offers several advantages over other drug delivery methods, such as oral delivery and intravenous administration, including the ability to deliver drugs at a nearly constant rate for extended durations, and ease of use. However, the outermost layer of the skin, the stratum corneum (SC), exhibits tremendous barrier properties and effectively retards the transport of exogenous compounds into the body. As a result, there has been significant interest in expanding the repertoire of drugs that can be delivered transdermally, and in using enhancers (chemical and others) to achieve this goal. This thesis examined, both experimentally and theoretically, diffusive transport across human SC, and the effect of enhancers (including chemical and sonophoretic) on transdermal drug permeation.

An image-based fluorescence recovery after photobleaching (video-FRAP) technique was used to measure the lateral diffusion coefficients of a series of lipophilic fluorescent probes in human stratum corneum extracted lipids (SCE) and in two model lipid bilayer systems, dimyristoylphosphatidylcholine (DMPC) and DMPC/cholesterol (40 mol%). The probes varied in molecular weight from 223 to 854 Da, and were chosen in order to characterize the lateral diffusion of small compounds in these bilayer systems. The measurements in SCE lipids, which represent a novel examination of diffusion in this unique lipid system, exhibited a strong molecular weight dependence, with values ranging from 0.31×10^{-8} to 2.3×10^{-8} cm^2/sec. Similar trends were exhibited by the DMPC and DMPC/cholesterol bilayer systems. These strong molecular weight dependencies were shown to extend to even smaller compounds than those examined in this study, by using literature data.

Partition coefficients of a series of compounds were measured with SCE lipids and water, as well as with octanol/water and three different liposome systems. The partition coefficient measurements made with SCE lipids correlated reasonably well with those made in all four model systems. In particular, a power-law relationship was found to relate the SCE partition coefficient values with the octanol/water values, for which thousands of measurements are available in the literature.

Solute permeation across human SC was then examined in terms of the fundamental bilayer transport properties. A mathematical model was developed to describe the macroscopic SC permeation via the interkeratinocyte lipid domain in terms of: i) the structure and dimensions of the SC, and ii) the micro-scale lipid bilayer transport properties, which include the bilayer/water partition coefficient, the lateral diffusion coefficient, the interfacial transbilayer mass transfer coefficient, and the intramembrane transbilayer mass transfer coefficient. The relative importance of the diffusive resistances associated with the bilayer transport properties was evaluated using the model and experimental data. Lateral diffusion coefficients in SC lipid bilayers were calculated from 120 human skin permeability measurements, and compared with the measurements made in SCE lipids. Good qualitative and quantitative agreement was observed. This indicates that the diffusive resistance associated with lateral diffusion is sufficient to explain the overall resistance of solute permeation through the SC. A similar analysis shows that the diffusive resistance associated with interfacial transbilayer transport is not capable of explaining the experimental permeation values, thus supporting this finding. The lateral diffusion analysis also revealed a bimodal size dependence of transport within the SC, with a strong size dependence for small solutes (<300 Da) and a weak size dependence for larger solutes.

Lastly, the effects of chemical enhancers, and of the combination of chemical enhancers and therapeutic ultrasound, on transdermal drug transport were investigated. A series of chemical enhancer formulations were evaluated using model drugs. In particular, the extent of enhancement produced by the bilayer disordering agent, linoleic acid, increased with increasing molecular weight of the drug examined. Likewise, ultrasound and linoleic acid produced an enhancement which exhibited a similar size dependence. Bilayer disordering agents appear to transform the SC lipid bilayers into a fluid lipid bilayer phase or to create a separate bulk oil phase. The *difference* in diffusivity of a given solute in SC bilayers and in either fluid bilayers or bulk oil is *larger for larger solutes*, thereby producing greater enhancements for larger solutes. A reexamination of permeation data from the literature, in which different bilayer disordering agents were utilized, further supports these findings.

Thesis Advisor:	Daniel Blankschtein
Title:	Associate Professor of Chemical Engineering
Thesis Advisor:	Robert Langer
Title:	Germeshausen Professor of Chemical and Biomedical Engineering

Acknowledgments

The years I have spent here at MIT have been remarkable, and I wish to thank all who have made them so memorable. I would like to thank my thesis advisors, Professors Daniel Blankschtein and Robert Langer, who had the foresight to see an intriguing research opportunity: Professor Blankschtein, for his intrinsic scientific curiosity, dedication to the project, careful attention to detail, and tremendous personal efforts, which constituted a guiding influence on the course of the project. Bob, for creating a positive environment in which it seems anything can be accomplished, allowing me the freedom to explore my ideas, his ability to motivate, providing extraordinary opportunities, chocolate, and group beach and ski trips.

I have also had the good fortune to work with many talented and outstanding individuals, whom I wish to thank.

The members of my thesis committee, Ken Smith, and Mary Roberts, for their interest in my project, insightful comments and questions, and their support, which was greatly appreciated.

Samir Mitragotri for our research collaborations, our many talks about research, football, and life, coffee, and his generosity.

David Berk and Rakesh Jain, for teaching me the experimental and theoretical aspects of the video-FRAP system.

Scott Canazaro for his humorous stories, and his valiant attempts at separating the inseparable molecular weight probes.

The Langer-group chemists, Kathryn Uhrich, Jeff 'radiophobe' Hrkach, Prasad Shastri, Kevin Shakeshef, Eric Krumpler, and Scott Canazaro, who answered my many questions, and taught me a little chemistry in the process.

Lisa Freed for sharing baby stories. Laura Niklason, my favorite mud-fud-anesthesiologist, for helping me with my high cholesterol 'problem', and in tracking down esoteric drug information.

Mark Prausnitz, for the free and open exchange of ideas, and our adventures in harvesting.

Noah Lotan, for Israeli chocolates, advice about research, life, and little ones, making me laugh, and fun with the ICE course.

Lab mates, both past and present, Craig Boyce, Lon Cook, Tani Chen, Hongming Chen, Yosi Kost, Guillermo Ameer, Gizette, Justin Hanes, Karen Fu, Joe Seidel,

Christine Schmidt, Kristi Anseth, Ginger Tse, Anat Shiloach, Nancy Zoeller, Chi-li Lue, Leo Lue, and Pak Yuet, for their advice and assistance on a myriad of experimental and theoretical issues.

The excellent undergraduates I have worked with, including Ashish Patel, Jason Wertheim, Camille Anderson, Nikki Caruthers, Ji Chang, Jean Ou, Jeanette Kao, Matt Edstrom, Matt Grice, and Aaron Day, for their hard work, and positive outlooks, and bright futures.

Pam Brown, Janet Fischer, and Elaine Aufiero, for always providing interesting conversations about anything and everything, and their expert assistance with the logistics of research and graduate school.

Special thanks to Kodak for a four-year graduate fellowship, and to Kelco, for funding.

Thanks to my Boston friends for the many good times: Debbie, Bill, Christine, Tom, Diane, John, Eric, Deb, Scott, Jolene, and Amy, Mike Fife, David Stracher, and the other Rugby boys.

My family, Mom, Dad, Karen, Matt, Kim, and Bo, for their optimism and support, long talks, great ski trips, two weddings and a baby, and spending holidays together.

My wife, Erin, for her love and support, listening, being there for the highs and lows, long drives, getting to know Boston together, three wonderful years of marriage, and for our beautiful daughter, Kathryn, who is an incredible blessing.

Contents

List of Figures

List of Tables

Chapter 1

Background

1.1 Advantages of Transdermal Drug Delivery

Transdermal drug delivery has many advantages over other drug delivery methods, such as the more traditional oral delivery and the more cumbersome intravenous administration. Foremost, transdermal drug delivery systems are capable of delivering drugs at a nearly constant flux for relatively long periods of time, up to and including seven days. With a constant flux, the "peaks and valleys" of the drug concentration in the blood, often associated with oral delivery, are, hence, avoided. These peaks in drug concentration can produce unwanted, and sometimes harmful, side effects, while the valleys can represent drug concentrations which are too low to be therapeutically effective. Nicotine patches, for example, are more successful than nicotine gum, and grossed nearly $1 billion in sales in their first year on the market (1992). One of the principal problems with nicotine gum, the primary alternative to the nicotine patches, is that the nicotine peaks can often induce addiction to the gum itself. Other advantages of using transdermal delivery systems include: (i) a reduced need for, and reliance upon, patient compliance, (ii) avoidance of the highly variable gastro-intestinal tract, and (iii) avoidance of rapid drug clearance associated with the first pass hepatic metabolism.

Despite the advantages of, and large interest in, transdermal drug delivery, there are currently only seven drugs on the market that are delivered

transdermally: chlonodine, estradiol, fentanyl, nicotine, nitroglycerine, scopolamine, and testosterone. The primary reason that there are so few transdermal delivery systems available is that the skin is an effective barrier for keeping exogenous compounds out of the body. Moreover, a closer examination of these seven drugs reveals that they have several properties in common. They are all small and lipophilic, as shown in Table 1.1 which lists the molecular weights (MW), octanol/water partition coefficients ($K_{o/w}$), and human skin permeabilities (P) of these drugs. Moreover, all these drugs are fairly potent, which reduces the transdermal fluxes that are required to achieve therapeutic efficacy. As a result, there has been substantial interest in expanding the repertoire of drugs that can be delivered transdermally, as well as in using enhancers (chemical and others) to achieve this goal.

1.2 Anatomy of the Skin

The skin is the largest organ of the human body, comprising approximately two square-meters, and is the most accessible to exogenous materials. It is composed of three primary multilaminate structures, as shown in Figure 1.1, the hypodermis, the dermis, and the epidermis. Figure 1.1 shows that hair follicles cross dermis and epidermis layers and protrude outside the skin. The blood vessels which comprise the papillary layer are also shown to lie just beneath the epidermis. Since transdermal drug delivery is generally utilized for systemic delivery, as opposed to local delivery, the papillary layer constitutes the primary route of systemic uptake.

The epidermis, which is 50-100 μm thick, is the outer structure of the skin. It is comprised of several different layers, as shown in Figure 1.2, including the stratum basale, stratum spinosum, stratum granulosum, stratum lucidum, and

Table 1.1 List of drugs for which transdermal delivery systems are currently available.

Drug	MW (Da)	$K_{o/w}$	P (cm/hr)
Clonidine	266.6	27 [a]	4.42×10^{-4} [f]
Estradiol	272.4	7200 [e]	4.16×10^{-3} [e]
Fentanyl	336.5	23442 [d]	5.60×10^{-3} [g]
Nicotine	162.2	15 [c]	2.03×10^{-2} [h]
Nitroglycerin	227.09	100 [b]	1.10×10^{-2} [i]
Scopolamine	303.4	17 [c]	5.16×10^{-5} [i]
Testosterone	288.4	2042 [c]	5.36×10^{-3} [e]

[a] Chloroform/water partition coefficient, pH corrected (Hansch and Leo, 1979). [b] 'oils'/water partition coefficient (Hansch and Leo, 1979). [c] (Hansch and Leo, 1979). [d] (Roy and Flynn, 1989). [e] (Johnson et al., (in preparation)). [f] Estimated by the Potts-Guy correlation (Potts and Guy, 1992). [g] (Roy and Flynn, 1990). [h] (Hadgraft and Ridout, 1987). [i] (Michaels et al., 1975).

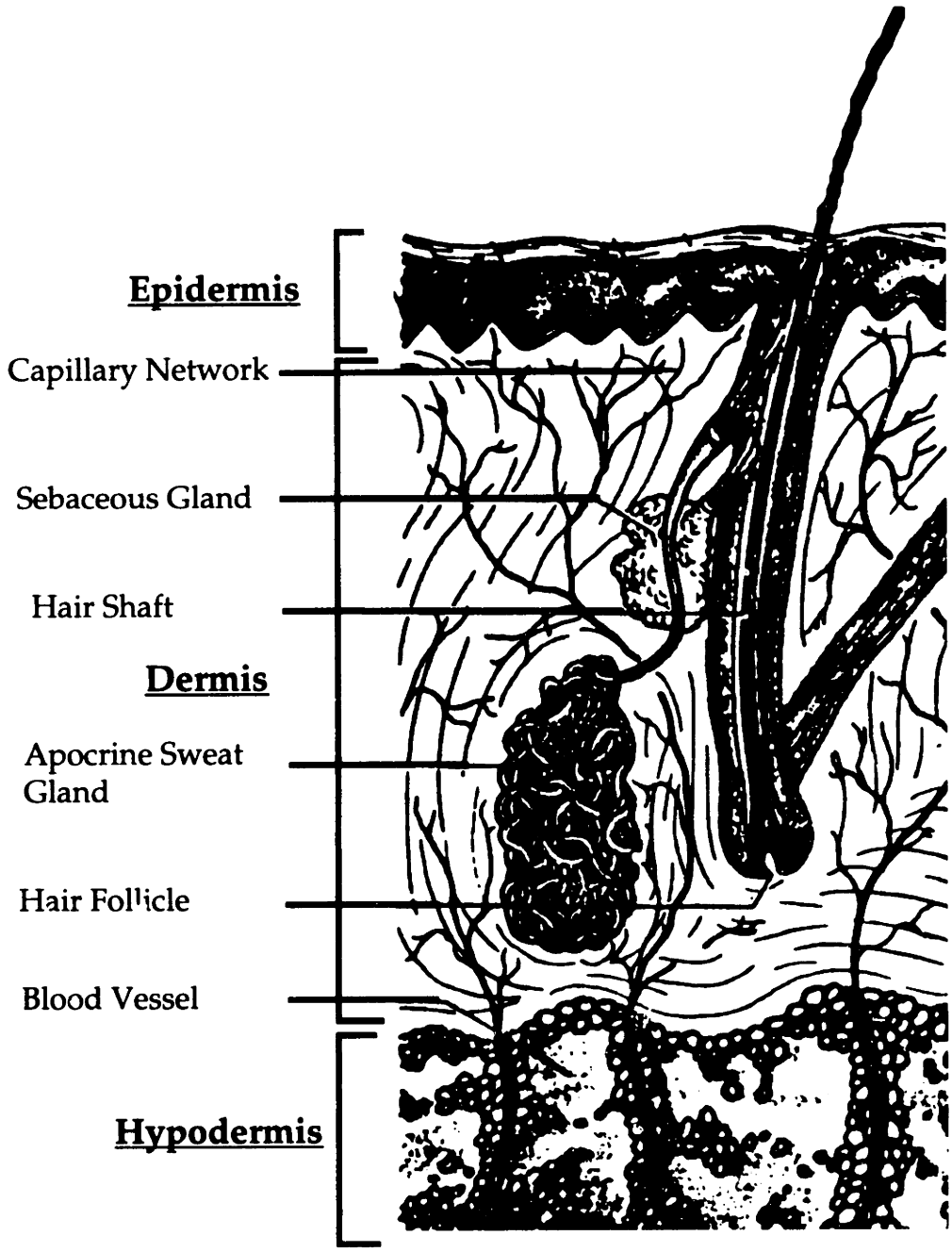

Figure 1.1 Schematic diagram of human skin. The three primary multilaminate structures of the skin, the epidermis, dermis, and hypodermis are shown, as are the various appendages and structures, including hair follicles, glands, and blood vessels. Reproduced from (Chien, 1987).

stratum corneum, which is the outermost layer. Extensive research has revealed that the stratum corneum constitutes the principal barrier for transdermal diffusion (Scheuplein and Blank, 1971), and that the primary purpose of the lower layers of the epidermis is to build and maintain the stratum corneum (Elias, 1989).

1.2.1 Stratum Corneum Structure

The stratum corneum is a composite structure, with keratinocytes embedded in a lipid matrix, as shown in Figure 1.3. The keratinocytes, also known as corneocytes, are the metabolically inactive *cells* of the stratum corneum (El-Shimi and Goddard, 1975). They are typically broad, 30-40 μm in diameter, and thin, 0.5-1 μm thick (Mershon, 1975; Wildnauer et al., 1975). Keratinocytes account for 80-95% of the stratum corneum by weight (Anderson et al., 1988; Bissett, 1987; Miller, 1991), and for approximately 99-99.9% of its surface area (Mershon, 1975). They are filled with keratin fibers and surrounded by a highly impermeable membrane of cross-linked proteins (Rice and Green, 1978). This protein membrane, known as the corneocyte-envelope, is formed in the lower epidermal cells as proteins replace the phospholipid cell membranes (Elias, 1988).

The stratum corneum is a relatively thin tissue, typically 10-15 μm thick (Mershon, 1975). It is often described in the literature in terms of the *brick and mortar* analogy (Elias, 1983). In this analogy, the keratinocytes (which are colored white in the electron micrograph shown in Figure 1.3) are the bricks, and the lipids (which are colored black in Figure 1.3) are the mortar. This analogy accurately reflects the high degree of organization within the stratum corneum (Elias, 1983). Keratinocytes are typically stacked in well ordered columns, 10-20 layers thick, as shown in Figure 1.3 (Marks, 1988; Mershon, 1975). This analogy

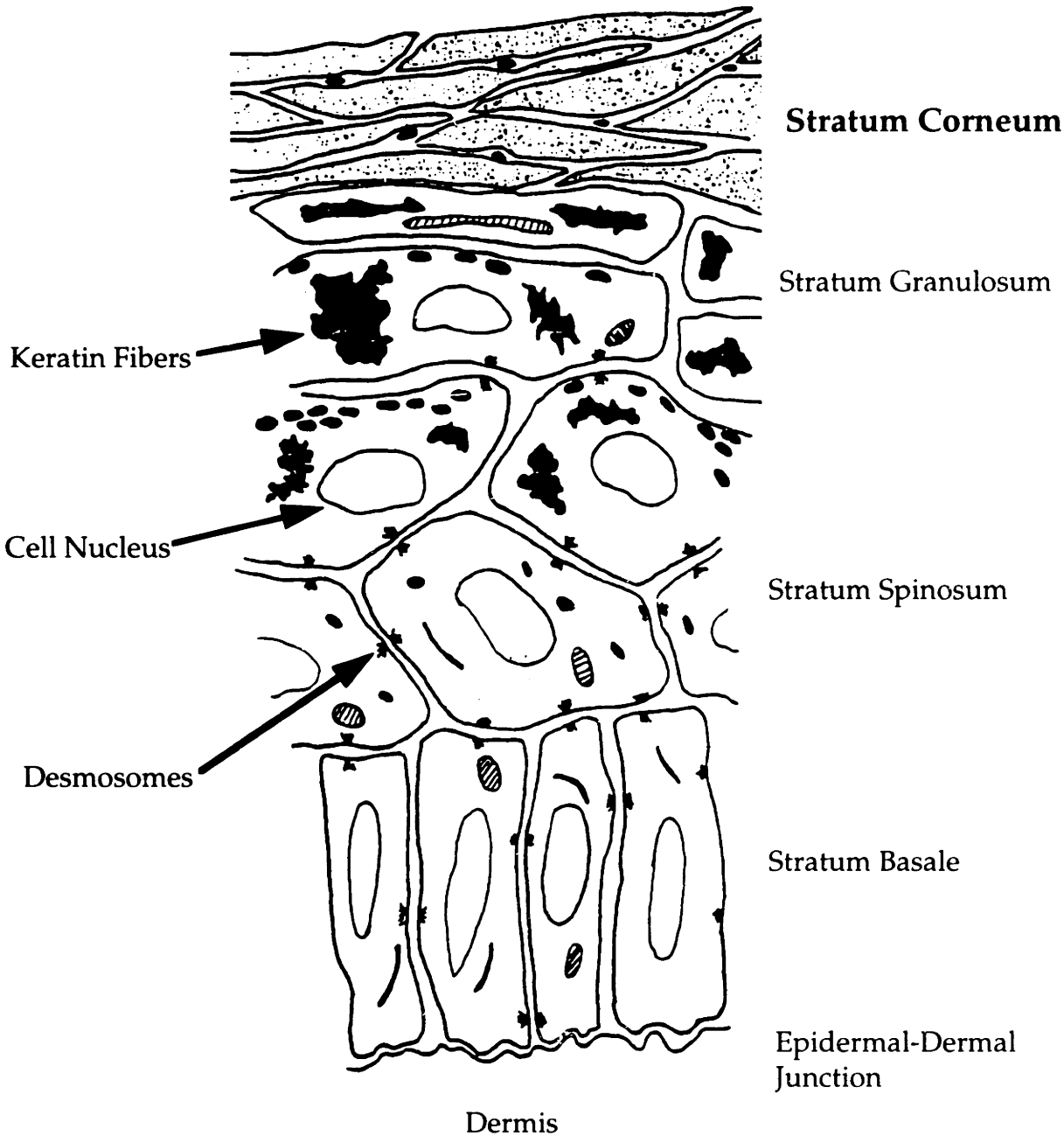

Figure 1.2 Schematic diagram of the epidermis. Epidermal cells migrate upwards in time. The outermost layer of the epidermis, the stratum corneum, is metabolically inactive and provides the principal barrier to drug transport into the body (Friberg, personal communication).

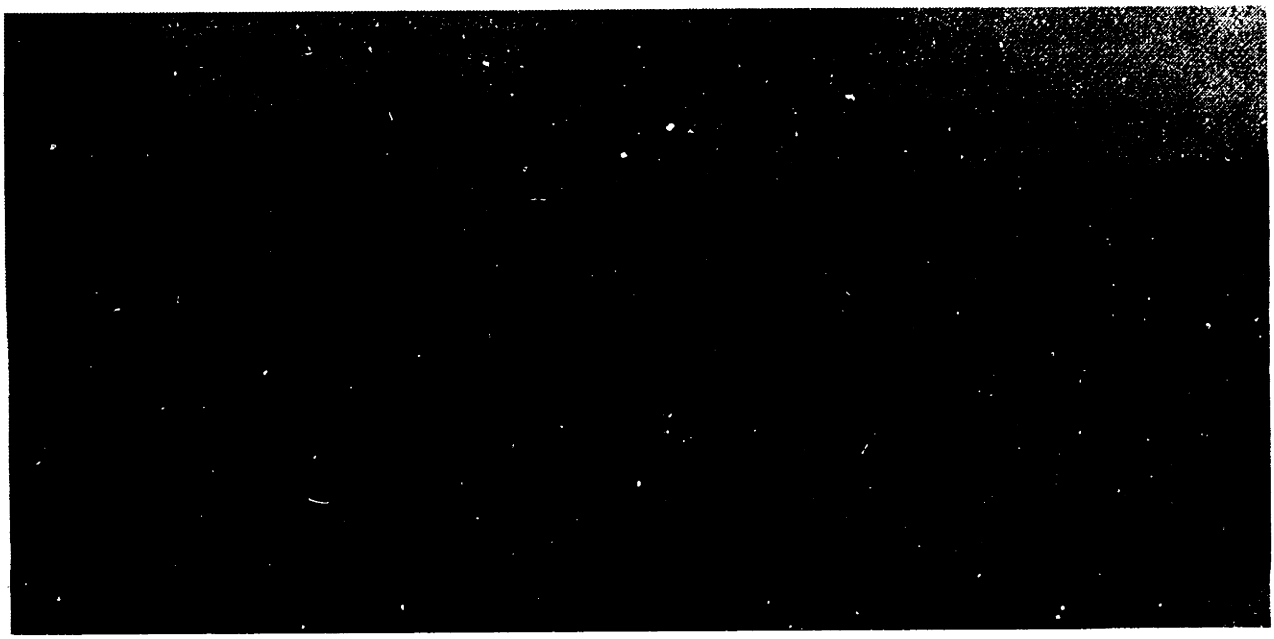

Figure 1.3 Electron micrograph of the stratum corneum. In this cross-section, keratinocytes are shown as the broad, thin white regions, while the black region illustrates the lipid bilayers domain. The keratinocytes are stacked in columns (see arrows) which overlap slightly with adjacent keratinocyte columns. Reproduced from (Menton, 1976).

also correctly reflects the fact that the lipids are the only continuous phase throughout the stratum corneum.

1.2.2 Stratum Corneum Lipid Composition

The extracellular stratum corneum lipids play an essential role in drug diffusion through the skin. The extracellular lipid domain constitutes the only continuous pathway through the skin, and furthermore, has been shown to be the primary route through which drugs permeate the stratum corneum (Johnson et al., in press; Knutson, 1987; Potts and Francoeur, 1990; Raykar, 1988; Wertz and Downing, 1989). The most basic characterization of the stratum corneum lipids is a compositional analysis of the various components. Such analyses have typically identified at least four major lipid classes: (1) ceramides, (2) neutral lipids, including sterols and fatty acids, (3) cholesterol sulfate, and (4) phospholipids. The chemical structures of several of the important components of these classes, including ceramide, palmitic acid, cholesterol, and cholesterol sulfate, are shown in Figure 1.4. These classes are then subdivided into different subclasses, depending upon the researcher. In the most comprehensive and detailed analysis of stratum corneum lipids to date, more than 70 different lipid species were detected and quantified (Lampe et al., 1983). This analysis was performed on stratum corneum samples obtained from four different regions of the body, abdomen, leg, face, and sole of the foot. A summary of the results of Lampe et al., as well as of those from other studies, are shown in Table 1.2.

Interestingly, the results obtained by the various researchers (Lampe et al., 1983; Miller, 1991; Yardley and Summerly, 1981) vary, often quite considerably, with each other. Table 1.3 summarizes these variations by showing the ranges of values obtained for the different lipid classes. The highest value in each range is

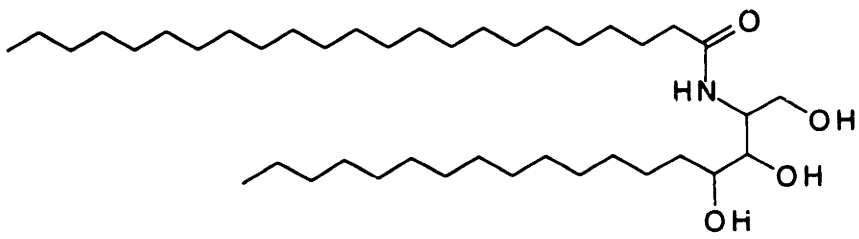

Ceramide

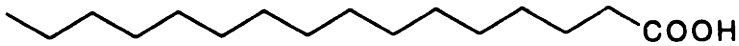

Palmitic Acid

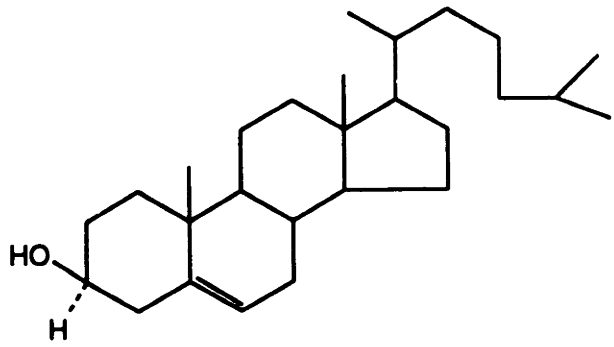

Cholesterol

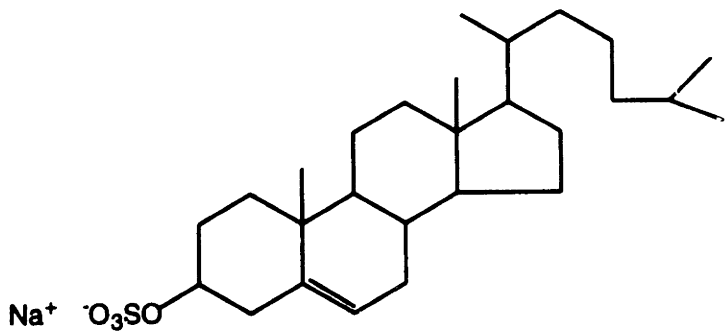

Cholesterol Sulfate

Figure 1.4 The chemical structures of several of the important components of the stratum corneum lipids, including ceramide, palmitic acid, cholesterol, and cholesterol sulfate.

Table 1.2 Detailed compositional analyses of stratum corneum lipids.

Lipid Component	Lipid Composition (wt%) A	B	C	D	E	F	G	H
1. Ceramides	18.2	25.9	26.5	34.8	26.6	22.4	23.4	52
2. Neutral Lipids	77.7	65.7	66.4	60.4	68.4	60.5	56.4	48
2a. Sterols	14	20.1	17.3	32.8	18.8	17.3	14.1	20
2b. Fatty Acids	19.3	13.9	19.7	9	15.6	28.4	28.4	22
2c. Other	44.4	31.7	29.4	18.6	34	14.8	13.9	6
3. Cholesterol-Sulfate	1.5	6	2.7	3.4	3.4	3	3	0
4. Phospholipids	4.9	5.2	3.3	3.2	2.3	15.1	13.4	0
Total	102.3	102.8	98.9	101.8	100.7	101	96.2	100

A Abdomen SC. Organic liquid extraction (Lampe et al., 1983).
B Leg SC. Organic liquid extraction (Lampe et al., 1983).
C Face SC. Organic liquid extraction (Lampe et al., 1983).
D Plantar SC. Organic liquid extraction (Lampe et al., 1983).
E Outer SC. Organic liquid extraction (Lampe et al., 1983).
F Whole SC. Supercritical fluid extraction(Miller, 1991).
G Whole SC. Organic liquid extraction (Miller, 1991).
H: Whole pig SC. Organic liquid extraction (Yardley and Summerly, 1981).

Table 1.3 Summary of stratum corneum lipid analyses.

Lipid Component	Range of Values* (wt%)	Mean Value* (wt%)	Median Value* (wt%)
Ceramides	18-52	28.7	26.2
Cholesterol	14-33	19.3	18
Fatty Acids	9-28	19.5	19.5
Phospholipids	0-15	5.9	3
Cholesterol Sulfate	0-6	2.9	3.3
Others	--	23.6	30

* Based upon the eight analyses presented in Table 1.2.

at least a factor of two larger than the smallest value. While the observed variations are nct entirely unexpected in this complex human tissue, they do create an apparent ambiguity regarding the relative composition of the stratum corneum lipids. This ambiguity has generally been avoided by other researchers by focusing on one particular set of results.

Nevertheless, by combining the results of Lampe et al., Miller et al., and Yardley et al., a characteristic composition emerges, as shown in Table 1.3. The mean and median values of the eight analyses are very consistent, suggesting a characteristic composition. Ceramides are the predominant lipid class, while sterols (represented by cholesterol) and fatty acids are present in significant, and approximately equal, quantities. Phospholipids and cholesterol sulfate, on the other hand, are only minor components.

In addition to representing the largest single lipid class, ceramides are also believed to be the most important ones. Specifically, ceramides have been shown to help form and stabilize the lipid bilayer structures (Elias and Menon, 1991; Grubauer et al., 1989). Cholesterol, the principal component of the sterols, has also been shown to have a significant impact on the properties and behavior of lipid structures of all types. Sterol and wax esters, squalene and n-alkanes, however, are present in relatively small quantities and are not believed to have a significant impact on the properties of lipid structures (Lampe et al., 1983; Lampe et al., 1983; Wertz et al., 1986). Free fatty acids, which comprise approximately 20% of the stratum corneum lipids, have been further analyzed for chain length and degree of saturation (Lampe et al., 1983). More than 90% of the fatty acids are either 16 or 18 carbons long, having between zero and three double bonds. The single largest fatty acid fraction was found to be palmitic acid, a sixteen-carbon fatty acid with no double bonds. Palmitic acid alone comprises approximately one-third of the fatty acids by weight.

1.2.3 Lipid Bilayer Structure

The organization of the stratum corneum lipids has been well characterized through the use of small angle x-ray scattering (SAXS) (Bouwstra et al., 1991; Friberg and Osborne, 1985), and electron microscopy (EM) (Madison et al., 1987; Swartzendruber et al., 1989). These studies have shown that stratum corneum lipids form multibilayers. The SAXS studies have also revealed that the bilayers have a characteristic thickness of 65 Å, which is in agreement with the expected bilayer thickness given the lipid composition of the SC (Bouwstra et al., 1991; Friberg and Osborne, 1985). Electron microscopy performed on ruthenium-tetroxide stained SC have produced clear images of the bilayer structures, as shown in Figure 1.5 (Elias, 1991). The lipid bilayers in Figure 1.5 are the parallel regions of thin white and black bands, wherein the white bands are the electron lucent lipophilic lipid tail-group regions and the black bands are the electron dense hydrophilic lipid head-group regions. Six sets of bilayers can be seen between the keratinocytes in this figure, which is within the range of 2-20 bilayers previously reported (Elias and Friend, 1975; Madison et al., 1987; Swartzendruber et al., 1989). These electron microscopy studies have shown that the lipid multibilayers, or *lamellae*, exist at all levels of the stratum corneum and are fairly continuous. Interestingly, lipid bilayers are often continuous at keratinocyte junctions. Figure 1.6 shows three lamellar regimes coming together at a junction, and reveals that there is at least one bilayer which connects each regime with the other in a continuous manner (Hou et al., 1991). Similar findings have also been reported by others (Hou et al., 1991; Swartzendruber et al., 1989). The implication of the lamellae remaining continuous at junctions is that solutes can diffuse towards the epidermis in a direction which is perpendicular to the

Figure 1.5 Electron micrograph showing the lamellar structure of the stratum corneum lipids. The electron lucent regions are white, and indicate the location of the lipophilic lipid tail-group regions. The electron dense regions are black, and indicate the hydrophilic lipid head-group regions of the multibilayers as well as the keratinocytes surrounding the bilayers. Between two and twenty sets of bilayers typically separate keratinocytes, while six sets of bilayers are shown this figure. Reproduced from (Elias, 1991).

Figure 1.6 Electron micrograph of the stratum corneum lipid lamellae at a keratinocyte junction. Three separate lamellar regimes come together at this location. At least one bilayer continuously connects each of the lamellar regimes with one another. Reproduced from (Hou et al., 1991).

plane of the skin while remaining within a bilayer (that is, via lateral diffusion (see Chapter 6 for further discussion)).

The prevalence and continuity of lipid bilayers shown in Figure 1.6 are consistent with the results obtained by Downing et al. who found that a significant percentage of the ceramides, 10-20%, are covalently bound to the keratinocytes (Wertz et al., 1989). They proposed that these lipids serve as templates to orient the other lipids into bilayers. Downing et al. also found a particular ceramide having a tail twice as long as that of most others (Wertz and Downing, 1983), a length which is approximately equal in length to the thickness of two bilayers, and hypothesized that such lipids help stabilize the lamellae. These results provide a strong biochemical explanation for how and why stratum corneum lipids form extensive bilayers and, hence, support the findings from EM and SAXS.

1.3 Transport Pathways

There are three discernible pathways by which drugs may diffuse through the stratum corneum, as shown schematically in Figure 1.7. First, drugs can bypass the stratum corneum by diffusing through either the hair follicles or sweat ducts, referred to as *shunt* pathways. While shunt pathways may be important in electrically enhanced stratum corneum permeation (Cullander and Guy, 1992), they are generally considered to be unimportant for passive (that is, without the application of external energy, such as an electrical current or ultrasound) diffusion in healthy stratum corneum (Scheuplein and Bronaugh, 1983). Hair follicles and sweat ducts comprise such a small fraction of the skin's surface area, typically less than 0.1% (Mershon, 1975), that the shunt pathway would not be of importance even if its resistance was smaller than that of the other two routes. In

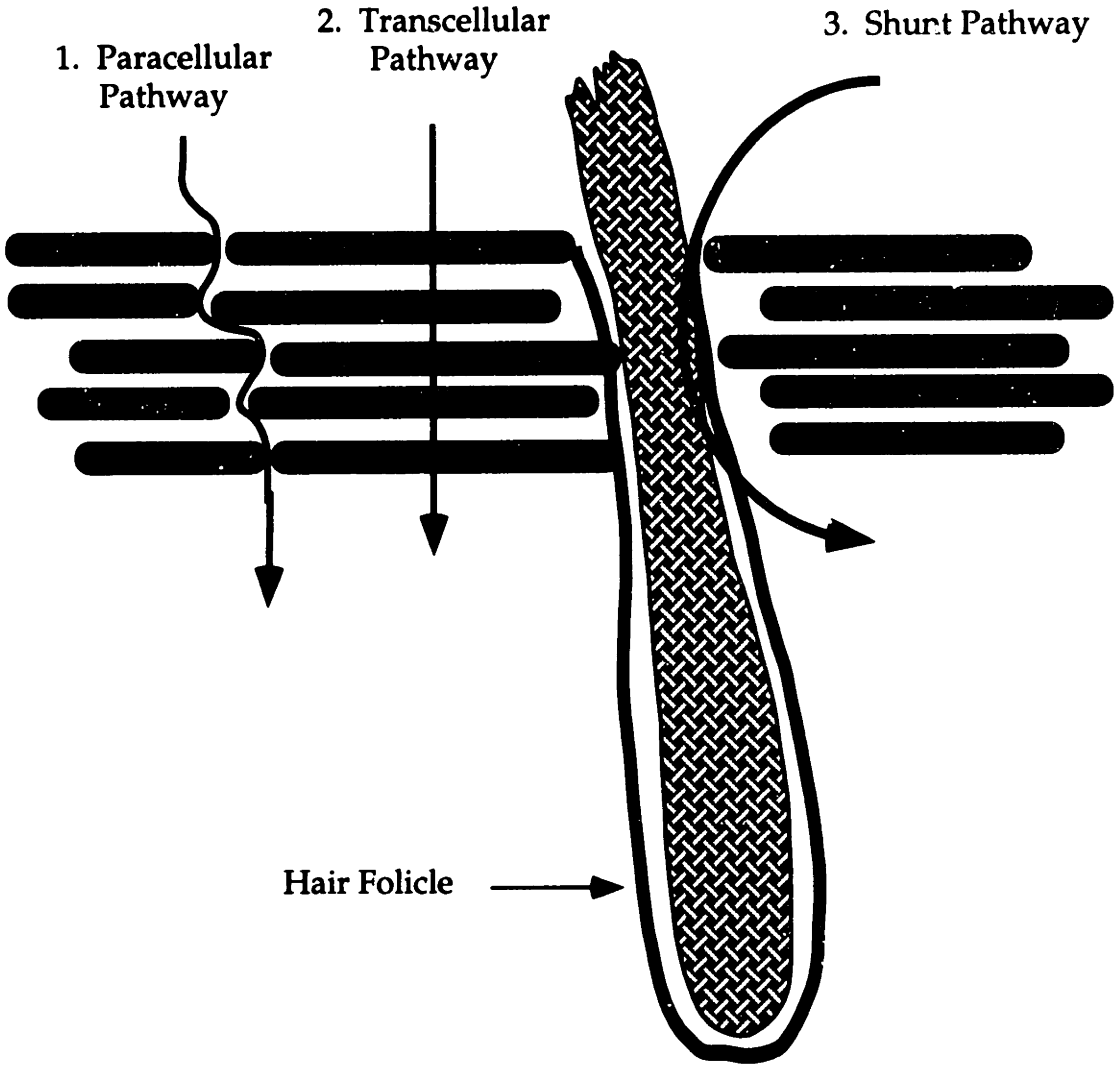

Figure 1.7 Schematic diagram of the possible pathways of drug diffusion through the stratum corneum. The paracellular route is through the tortuous lipid domain, and is the primary pathway for lipophilic compounds. The transcellular route is through the successive layers of lipids and keratinocytes, and may be important for electrically enhanced drug delivery (that is, iontophoresis and electroporation). The shunt route is through hair follicles and sweat ducts, but is not believed to be a significant pathway through the stratum corneum. Indirect evidence is accumulating implying the presence of an 'aqueous pore' pathway through the stratum corneum, although its precise physical nature has not yet been identified.

fact, there is little reason to believe that diffusion through the shunts is easier, since drugs still have to diffuse through the lipid bilayers lining these paths, and then pass through follicle membrane cells, as shown in Figure 1.7.

The second possible route of diffusion through the skin is transcellularly, that is, across successive layers of keratinocytes and the extracellular lipids. As with the shunt pathways, there is general agreement that there is not substantial solute diffusion across keratinocytes in the case of passive transport (Scheuplein and Bronaugh, 1983). However, recent work has suggested that keratinocytes may be the primary route of drug transport in the presence of electricity (that is, with iontophoresis or electroporation).

Drugs can permeate the skin via the paracellular route, that is, solely through the lipid domain, which constitutes the only continuous phase through the stratum corneum. This pathway has been shown to be the primary route of lipophilic drug diffusion through the skin (Elias et al., 1981; Grubauer et al., 1989). In the past fifteen years, the fundamental work on transdermal drug delivery has focused almost entirely on stratum corneum lipids and their properties. Likewise, stratum corneum permeabilities are related to the properties of the drugs and the stratum corneum lipids in Chapter 6. In this thesis, the keratinocytes will be considered as macroscopic obstacles around which the lipid pathway meanders.

Lastly, indirect evidence is accumulating that there is an 'aqueous pore' pathway through the stratum corneum. Specifically, hydrophilic solutes tend to exhibit permeabilities which are considerably larger than would be expected if the lipid domain was the primary route of transport. Moreover, a recent study (Yoneto et al., 1995) reveals that permeabilities of hydrophilic solutes across the 10-15μm thick stratum corneum are orders of magnitude greater than the permeabilities of the same solutes across a single lipid bilayer. This implies that

the lipid bilayer regime is circumvented by hydrophilic solutes. Although the idea of an 'aqueous pore' pathway was first proposed more than two decades ago (Scheuplein and Blank, 1971), the precise identity of this hypothetical pathway is still not known.

1.4 Methods of Transport Enhancement

The tremendous barrier properties of the skin successfully inhibit most drugs from diffusing through the skin at a rate sufficiently high to achieve the therapeutically effective dose of the drug using a reasonably sized patch (less than ~100 cm^2). In order to increase the number of drugs that can be used for transdermal drug delivery, several enhancement approaches have been, and continue to be explored. The most thoroughly studied method of enhancement has been to treat the skin with a chemical enhancer (see below) (Smith and Maibach, 1995). All seven of the drugs currently approved for transdermal delivery (see Table 1.1) are coupled with chemical enhancers. The use of electricity to provide an additional driving force for transport, referred to as iontophoresis (Guy, 1992), or to physically alter the lipid structure of the stratum corneum, referred to as electroporation (Prausnitz et al., 1993), has more recently become the subject of increased research efforts. The use of ultrasound to increase transdermal transport, referred to as sonophoresis (Kost et al., 1989), has recently been shown to be effective when applied at therapeutic frequencies (1-3 MHz) (Mitragotri et al., 1995), in combination with chemical enhancers (Johnson et al., in press), as well as at low frequencies (20 kHz) (Mitragotri et al., 1995). For example, low-frequency ultrasound is able to transdermally deliver proteins at therapeutically active levels (Mitragotri et al., 1995). Lastly, the use of drug derivatives, referred to as prodrugs (Sloan et al., 1984), which permeate the skin

faster than the original drug and can then be metabolized back to the therapeutically active agent, has also been studied.

1.5 Review on Chemical Enhancers

The use of chemical enhancers offers several advantages over other methods for increasing the rate of transdermal drug delivery. First, no external energy is required in the case of chemical enhancers. In contrast, iontophoresis, electroporation, and sonophoresis all require complex and expensive circuitry. The devices that may be used to generate iontophoresis, electroporation, and sonophoresis are not yet fully developed, but are envisioned to be comparable in weight and size to a large wrist watch. In contrast, transdermal drug delivery systems using chemical enhancers can be, and in fact are, as thin as a few hundred microns, and hence, are considerably less obtrusive.

Chemical enhancers are typically lipophilic or amphiphilic compounds which are applied to the skin surface together with the drug of interest. A recent review on chemical enhancers has compiled a list of nearly two hundred different compounds which have been studied for their ability to increase transdermal drug transport (Chattaraj and Walker, 1995). Table 1.4 shows the major classes of chemical enhancers, as grouped by the chemical structure of the enhancer, as well as several examples for each class. Table 1.4 also shows that a wide variety of compounds having different chemical properties have been examined. In Chapter 7, the effects of bilayer disrupting agents will be discussed. Note that *bilayer disrupting agents* is a classification based on the mode of action of the chemical enhancer, rather than on the chemical structure alone, and, hence, suggests that the direct comparisons of the effects of different compounds within this class are appropriate. Specifically, the effects of linoleic

Table 1.4 Chemical classes and examples of chemical enhancers.

Chemical Class	Examples
Alcohols	ethanol, butanol, hexanol, octanol, benzyl alcohol
Alkanones	n-heptane, n-octane, n-dodecane, n-hexadecane
Amides	urea, mehtyl pyrrolidone, cyclohexylpyrrolidone
Fatty Acids	heptanoic, linoleic, oleic, isostearic, neoheptanoic
Fatty Acid Esters	n-butyrate, isopropyl myristate, ethyl acetate
Organic Acids	citric acid, succinic acid,propyl glycol derivates
Polyols	propylene glycol, polyethylene glycol, glycerol
Sulfoxides	dimethylsulfoxide, decylmethylsulfoxide
Surfactants	sodium laurate, sodium cholate, lecithin
Terpenes	D-limonene, carvol, cyclohexene, anise, eucalyptus

Summary of enhancer list compiled by Chattaraj and Walker (1995).

acid, Azone, oleic acid, lauric acid, neodecanoic acid, and capric acid, will be considered.

Certain drug/enhancer combinations can increase transdermal drug fluxes by several orders of magnitude (Johnson et al., in press; Walters, 1989; Williams and Barry, 1991). One of the possible enhancement mechanisms that has received considerable attention is that some chemical enhancers can increase the *fluidity* of the stratum corneum bilayers (Allenby et al., 1969; Green et al., 1988; Johnson et al., in press; Williams and Barry, 1991). This is an intuitively appealing concept, yet is difficult to quantify experimentally. Despite many attempts, until very recently (Johnson et al., in press) neither a qualitative nor a quantitative correlation has been found between the nature of the drug, the type of chemical enhancer, and the observed enhancement.

The most fundamental investigations of the mechanisms of enhancement have attempted to correlate physical properties of the skin with the observed enhancement. Studies of this type have examined the results of differential scanning calorimetry (DSC) and Fourier transform infrared spectroscopy (FTIR) with limited success (Francoeur et al., 1990; Knutson, 1987; Oertel, 1977; Potts and Francoeur, 1990). Since the mechanisms of flux enhancement are not well understood, researchers have been limited to a trial-and-error approach for choosing effective drug/enhancer combinations.

1.6 Motivation

Transdermal drug delivery is a safe and effective means of systemically administering many different pharmacologically active substances (see section 1.1). The success of the nicotine patches (Nicoderm, Nicotrol, Habitrol, and Prostep), serves as an illustration of the tremendous benefits that transdermal

delivery systems can produce, both in terms of the savings in medical costs as well as by enhancing the quality of people's lives. That is, by doubling the success rate of smokers trying to quit, the nicotine patches are reducing the deleterious effects that smoking has on people's lives and health, and are also reducing the smoking related health care costs, estimated at $65 billion annually in the United States alone (Cleary, 1993).

Over the past fifteen years, there has been tremendous interest in delivering other drugs transdermally. The process of choosing a drug and the associated formulation, including the possible presence of chemical enhancers, is primarily conducted via the slow, and costly trial-and-error approach. This is due to the complex nature of transdermal solute transport and, even more so, of chemically enhanced solute transport (see Chapters 6 and 7). A byproduct of these investigations has been the generation and publication of a significant body of experiment data, much of which has not been closely examined. For example, over one hundred and fifty different measurements of transdermal solute permeabilities across human skin from aqueous solutions have been compiled from the literature (including measurements made by the author), and are presented and discussed in Chapters 3, 6, and 7. Hundreds of additional permeability measurements from aqueous solutions have similarly been measured across the skin of various animal models, including hairless rats, hairless mice, snakes, pigs, and many others.§ This large pool of data of aqueous skin permeabilities is particularly remarkable, since there is no serious interest in having an aqueous based transdermal delivery system (see chemical enhancers review in section 1.5). Moreover, there are hundreds of other permeability and

§ Extensive research has shown that transport measurements across animal skin models do not correlate well with those made across human skin, and hence, are not always comparable to the data obtained with human skin.

flux measurements across human and animal skin from non-aqueous formulations, that is, with the use of chemical enhancers.

The abundance of literature data is a tantalizing aspect of performing fundamental research on transdermal drug delivery and its enhancement using chemical enhancers. Indeed, the abundance of literature data provides researchers examining the more fundamental aspects of transdermal transport and chemical enhancement with a potentially rich source of independent measurements with which to examine hypotheses, compare original data, and draw conclusions.

However, it is difficult to compare transport measurements made with different non-aqueous systems at a level deeper than face value, even if the same drug has been examined. This is due, in part, to the multiple effects that enhancers can have on the drug and on the stratum corneum, the net product of which produces the observed drug flux. For example, ethanol is a simple chemical enhancer which can increase the solubility of many drugs, including many steroids, by several orders of magnitude (see Chapter 7), relative to their solubility in aqueous solution, due to the lesser degree of polarity of ethanol. Nevertheless, since drugs of this type 'like' ethanol better than the buffer, the extent of drug partitioning into the lipid bilayers of the stratum corneum tends to decrease, as revealed by the decrease in steroid permeabilities from ethanol solutions (see Chapter 7). In other words, the increase of steroid solubility in ethanol solutions is counteracted by the decrease of the steroid partition coefficient into the skin. Assuming that ethanol does not substantively affect the stratum corneum, which it appears to do at high concentrations, the degree of enhancement of a specific steroid by ethanol is purely a quantitative balance between these two effects.

Theories or correlations capable of effectively predicting solute solubilities in ethanol solutions, which is one of the simplest chemical enhancer systems utilized, without an extensive experimental characterization of the solutes are currently lacking. The prediction of partition coefficients from non-aqueous systems into the stratum corneum lipids is even more complex. The mere identification of the key effects that an enhancer exhibits at a qualitative level is often difficult. Ethanol differs in this respect, since the two primary effects it exhibits on transport, increasing the drug solubility and decreasing the drug partition coefficient, are intuitive and easily corroborated by experiments. Many other chemical enhancers affect drug solubilities and partitioning to lesser extents, but may also affect the bilayer structure as well as the keratinocytes. These effects can be difficult to isolate and quantify.

As a result of these complexities, it is useful to consider classes of enhancers, that is, groups of chemicals which have similar chemical structures (see section 1.5) or exhibit similar effects upon the skin and drug transport. One particular class of chemical enhancers, bilayer disrupting agents, is considered in Chapter 7, in which novel experiments, literature data, as well as transport mechanisms are discussed. In particular, a mechanism of transport enhancement is proposed, and supported by experimental data, which predicts that the extent of enhancement by bilayer disordering agents exhibits a size dependence, resulting in increasing enhancement with increasing size of the diffusing solute. This work illustrates the need for a more fundamental understanding of the transport and enhancement processes in order to draw broader connections between various drugs and chemical enhancers.

1.7 Objectives

The primary objective of this thesis is to develop a more fundamental understanding of the processes by which solutes permeate through the skin, and to use this understanding to facilitate the development of effective chemical enhancer/drug combinations. The following specific goals will be pursued: (i) The bilayer-scale transport properties, that is the lateral diffusion coefficient and partition coefficient of SCE lipids will be characterized experimentally. (ii) Macroscopic transdermal permeation will also be characterized experimentally, and then modeled theoretically in terms of the stratum corneum structure and the bilayer-scale properties. (iii) The effects of chemical enhancers, as well as of a combinations of therapeutic ultrasound and chemical enhancers, will be experimentally studied for several model drugs. (iv) Finally, the mechanisms responsible for the effects of these enhancers will be investigated.

1.8 Thesis Overview

This thesis is organized as follows. Chapter 2 provides background on transdermal drug delivery, including a discussion of the advantages of transdermal delivery systems, the structure of the skin and the stratum corneum, the possible pathways through the skin, and an overview on chemical enhancers and other enhancement methods. The experimental and analytical tools which were utilized in this thesis are described in Chapter 2. The experimental tools include human skin permeability measurements, FRAP experiments with stratum corneum lipids as well as with model lipid bilayer systems, partition coefficient measurements, and solubility measurements. In Chapter 3, the experimental results of human skin permeability measurements made for a

variety of steroids are presented and compared with values taken from the literature. A striking finding, discussed in Chapter 3, is that an important set of literature data (the 14 steroid permeability measurements of Scheuplein et al. (1969)) deviates from other values by an average of 16-fold, and hence, should be reconsidered.

Chapter 4 discusses the lateral diffusion measurements of a series of lipophilic probes having varying molecular weight (223-854 Da) in extracted stratum corneum lipids and in two model bilayer systems. The magnitude of the diffusion coefficients were greater for the cases of the two phospholipid model systems than for the case of the stratum corneum lipids. The data for all three lipid systems are also shown to exhibit a strong dependence on solute size. This strong size dependence is described well by a two-parameter empirical model, and is shown to extend to even smaller solutes (<223 Da) using literature data. Chapter 5 describes the measurements of stratum corneum lipid/water partition coefficients for a variety of drugs. Four additional experimental systems are examined, including octanol/water and three different liposome formulations, as possible experimental models of stratum corneum lipids. A series of extractions of radiolabeled, hydrophobic drugs using octanol and water are also described, as is the subsequent use of this data to characterize impurities in the radiolabeled drug samples.

In Chapter 6, the bilayer-scale solute transport properties are described and utilized in a model to predict the macroscopically measured stratum corneum permeabilities. Specifically, the diffusive resistance to lateral diffusion is shown to be sufficient to account for the permeabilities of 120 different lipophilic solutes across the skin. In contrast, transbilayer transport is shown to be inconsistent with the observed permeability values. Chapter 7 describes the application of the insights, gained in the studies described in the earlier chapters,

to the development of effective transdermal delivery systems and in understanding the mechanism of enhancement. Specifically, the combined application of ethanol and an unsaturated fatty acid, linoleic acid, are shown together to effectively increase transdermal drug transport. The application of therapeutic ultrasound (1 MHz, 1.4 W/cm^2) in conjunction with this enhancer combination further increases transport. Moreover, the observed enhancements exhibit a molecular weight dependence, with larger enhancements obtained for larger solutes. Finally, Chapter 8 presents the main conclusions of this thesis, and describes future promising research directions.

Chapter 2

Methods

2.1 Skin Preparation and Stratum Corneum Isolation

Human skin was obtained from the local hospitals (Beth Israel Hospital) and the National Disease Research Institute (NDRI, Philadelphia, PA). NDRI typically provided tissue from cadavers, breast reductions, or amputations that had been dermatomed to a thickness of several millimeters, and hence, was largely free of fat or excess tissue. Cadaver skin from local hospitals was typically harvested from the chest, abdominal, or back regions. Note that the SC lipid composition is fairly uniform for various body sites (Lampe et al., 1983). Preliminary cuts produced large tissue samples, which were subsequently scrapped to remove excess fat and divided into smaller pieces of 40-100 square inches. Samples were stored at -80°C for up to 6 months prior to use. Storage longer than 6 months tended to result in damaged skin, and hence, was avoided.

The epidermis was always separated from the lower skin layers, since the additional layers are not the rate limiting barrier to transport. This was accomplished by immersion of the full-thickness tissue in 60°C water for two minutes. The epidermis was then carefully peeled from the dermis. Heat-stripped skin was stored at 95% humidity and 5°C for up to one week prior to use. Longer periods of storage resulted in skin degradation, and hence, were not employed.

The SC was separated from the heat-stripped epidermis for select permeation experiments and for experiments which required extracted SC lipids

(see below). This was accomplished by soaking the epidermis in a 0.5% trypsin solution overnight at 5°C (Anderson et al., 1988), followed by extensive rinsing with Milli-Q water. Permeation experiments performed with the stratum corneum alone did not exhibit substantively different solute permeability values than did experiments which were performed with the whole epidermis. This was expected, given the consensus that the stratum corneum is the rate limiting skin structure, and confirmed that the epidermis was a suitable tissue for conducting permeation experiments.

2.2 Extraction of Stratum Corneum Lipids

Extraction of stratum corneum lipids was accomplished by first separating it from the epidermis, as described above. The SC was then cleaned with distilled water, rinsed in cold hexane to remove exogenous lipids, and lyophilized for 24 hours or more to remove all water. Dried SC was cut into pieces of approximately 10 mg, weighed, and placed in a 7 ml vial with a ground glass cap. 5 ml of chloroform:methanol (2:1 v/v) were added to the vial. After at least 24 hours, the delipidized SC (specifically, the remaining keratinocytes) was removed, lyophilized, and again weighed (Anderson et al., 1988). The amount of lipids in the vial was determined by taking the difference of the weights of the SC before and after delipidization. In control experiments, the weight of the vial was measured before and after the lipid extraction. The lipid weight was taken as the difference in these measurements. The lipid content determined by these two methods was generally in good agreement. Typical lipid contents of the SC were 5-20% on a weight basis, in good agreement with the literature (Lampe et al., 1983; Miller, 1991; Raykar, 1988). Extracted SC lipids were stored in chloroform:methanol (2:1 v/v) at -20°C until usage.

2.3 Transdermal Drug Permeation Measurements

2.3.1 Passive Permeation Measurements

The passive permeabilities (that is, permeabilities in the absence of ultrasound) of various solutes through human cadaver skin were typically measured using trace quantities of the corresponding radiolabeled drugs. These drugs were labeled with tritium (^3H) or carbon-14 (^{14}C). The radiolabeled drugs were rotary evaporated in order to remove the solvent in which they were shipped, as well as any tritium which might have reverse-exchanged onto them. The radiolabeled drugs were then redissolved in either phosphate buffered saline (PBS) or in an enhancer formulation, to a typical concentration of 1 μCi/ml, and added to the donor compartment of a diffusion cell.

Passive permeation experiments were performed using stirred side-by-side diffusion cells (#DC-100B, Crown Bioscientific; Sommerville, NJ), typically at room temperature. The donor and receiver volumes of these cells are both 3.3 ml. The available area for transport is about 0.64 cm^2. Select permeation experiments were performed at 37°C, which was maintained by using a water bath and a temperature controller. The receiver compartment for all experiments contained pH 7.4 phosphate buffered saline (PBS, phosphate concentration = 0.01 M, NaCl concentration = 0.137M) (Sigma Chemical Co., St. Louis, MO). Mild (~100-300 rpm) stirring rates provided adequate mixing for the solutes examined, since the boundary layer resistances are small due to the low skin permeabilities.

The concentrations of drug in the donor and the receiver compartments for the experiments with radiolabeled drugs were measured using a scintillation counter (model 2000 CA, Packard Instruments Co., Downers Grove, IL). A

minimum of three permeation experiments were performed for each enhancer/drug combination. The permeability values, P, were calculated under steady-state (SS) conditions from the relationship:

$$P = \left(\frac{dN_r}{dt}\right)_{ss}\left(\frac{1}{A(C_d - C_r)}\right) \tag{2.1}$$

where N_r is the cumulative amount of drug which has permeated into the receiver compartment at time, t, A is the surface area of the skin sample available for transport, C_d is the drug concentration in the donor compartment, and C_r is the drug concentration in the receiver compartment. The area of skin available for transport was 0.64 cm^2. Relatively large sample volumes of the receiver solution (0.5-3.3 ml) were taken in experiments involving compounds having low permeabilities, otherwise the sample volumes were 10-200 µl. For such compounds, the value of N_r, could not be approximated as the product of the sample concentration and the receptor volume (typically 3.3 ml) due to the fact that a significant fraction of the drug which had permeated the skin was removed during the sampling procedure. Consequently, N_r, was calculated using the relationship:

$$N_r(n) = C_r(n)V_r + \sum_{i=1}^{n-1} N_{s,i} \tag{2.2}$$

where $N_r(n)$ is the total amount of drug to have permeated the skin at the time that the n^{th} sample was taken, $C_r(n)$ is the drug concentration in the n^{th} sample, V_r is the receptor volume, and $N_{s,i}$ is the amount of drug in the i^{th} sample taken.

The results of a typical permeation experiment are shown in Figure 2.1, in which the cumulative drug transported, N_r, is plotted versus time for ^{14}C-(2-

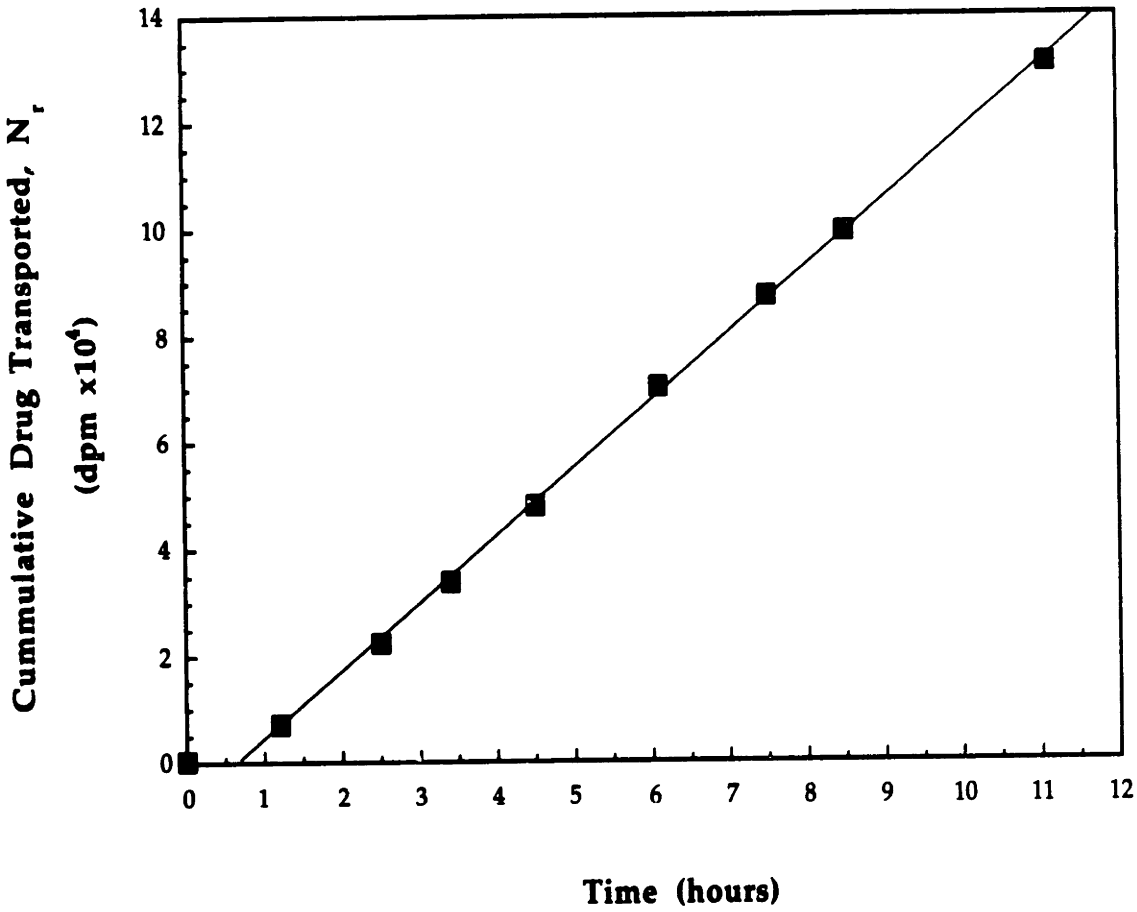

Figure 2.1 Permeation of ^{14}C-(2-napthol) across human skin from aqueous solutions at 25°C. After a lag-time of 45 minutes, the data exhibits a linear dependence upon time. The permeability is calculated from the slope of this profile. The line is drawn to guide the eye.

napthol). 100 μl samples were taken periodically from the receiver compartment of this experiment performed at 25°C. After a brief lag-time of approximately 45 minutes, the behavior shown in Figure 2.1 is linear in time (R^2=0.9995). The permeability of 2-napthol in this experiment, 4.3×10^{-2} cm/hr, was calculated using Eq. (2.1) and is in good agreement with the value reported in the literature, 2.8×10^{-2} cm/hr (Roberts et al., 1977). The observed inter-subject variability of the human skin permeability values observed with 2-napthol, as well as for the those measured with the other drugs examined, are consistent with the previously established 40% inter-subject variability of human skin permeabilities (Williams et al., 1992).

The experimentally observed lag-times for the permeation experiments varied with the compound examined. A long lag-time was observed for aldosterone, 21 hours on average, while the lag-times for many other compounds, including decanol, estradiol, hexanol, napthol, octanol, and progesterone, were under one hour.

2.3.2 Ultrasound-Mediated Permeation Measurements

The ultrasound-mediated permeabilities of various solutes through human cadaver skin were typically measured using trace quantities of the corresponding radiolabeled drugs, labeled with tritium (^{3}H) or carbon-14 (^{14}C), and prepared in a manner described above (section 2.3.1).

Ultrasound was applied under therapeutically approved conditions (1 MHz, 1.4 W/cm^2, continuous) for 24 hours using a sonicator (Sonopuls 463, Henley International, Sugar Land, TX). The ultrasound transducer was located approximately 3 cm from the surface of the skin. Permeation experiments were performed using customized side-by-side diffusion cells having an area of 3.1

cm^2 and a receiver compartment volume of 7.5 ml. These cells consisted of two flange glass cylinders (20 mm in diameter) with a ground glass joint (FDC 400, Crown Bioscientific; Sommerville, NJ) clamped together. The end of one cap was sealed with glass, while the other cap was sealed to the ultrasound transducer using epoxy. Samples were periodically taken from the receiver compartment over 24 hours. The concentrations of radiolabeled drug in these samples, as well as those in the donor compartment, were measured using a scintillation counter. Three or more permeation experiments were performed with ultrasound for each enhancer/drug combination examined. PBS was always used in the receiver compartment.

For most drugs, the measured sonophoretic permeabilities were constant once steady-state was achieved for most drugs.§ Accordingly, drug permeabilities in the presence of ultrasound, P_{us}, were calculated using the same relationship used in the passive case (Eq. (2.1)), $P_{us} = (dN_r/dt)/(AC_d)$.

2.4 Fluorescence Recovery After Photobleaching (FRAP)

Fluorescence recovery after photobleaching (FRAP) is a commonly used technique to measure diffusion coefficients in lipid bilayers. FRAP was first developed in the early 1980's, and has gained popularity as an analytical technique due in part to: i) the importance of lipid bilayer and cell membrane diffusion in a variety of fields, and ii) the reliability and reproducibility of these measurements.

The basic principle of FRAP is to irreversibly bleach the fluorescent bilayers in a certain bilayer region, and then to monitor the fluorescence recovery

§ A notable exception is corticosterone. The permeability of corticosterone continually increase when ultrasound was applied inconjunction with linoleic acid in ethanol/PBS (50:50 v/v) (see Chapter 7 for further discussion).

in that region as the non-bleached fluorophores diffuses back into the region. Most FRAP experiments are performed with fluorescently labeled integral proteins (that is, proteins which predominantly reside in the cell membrane or lipid bilayer), some of which are up to several-hundred thousand daltons in size, as well as fluorescently labeled lipid probes, which are typically 700-1000 Da in size. A key challenge of this thesis was to find fluorescent probes which are representative of the physical properties of potential transdermal drugs, specifically, probes which are small (<500 Da) and lipophilic. However, the fluorescent function groups which are often used to label proteins are nearly this large. Hence, the range of fluorescent compounds that could be examined in the FRAP studies was inherently limited.

The fluorescent probes are added to the bilayer in trace quantities (typically at concentrations of less than 0.1%), since higher probe concentrations can influence the bilayer structure and, hence, artificially alter the probe diffusion coefficient. Much of the previous FRAP work has been performed with cell membranes, which are typically fairly large (>10 μm), composed of phospholipids, cholesterol, and integral proteins, and comprised of a single bilayer. Extensive FRAP studies have also been performed with very large liposomes (>10 μm), which are often multilamellar in nature. A basic requirement of studies performed with these systems is that the structure is larger than the laser bleach spot. In general, this requirement is not a problem. The standard FRAP technique involves monitoring the fluorescence recovery at a single spatial location in the center of the bleached region over time using a photomultiplier. The plot of the normalized fluorescence intensity versus time is then fit to an approximate solution to the diffusion equation to obtain the diffusion coefficient, D, and the immobile fraction, ε (Yguerabide, 1982). The

equation most commonly used to calculate the diffusion coefficient with photomultiplier FRAP is (Yguerabide, 1982):

$$F(t) = \left\{ \frac{f(t) - \left[F(0)/F^o \right]}{1 - \left[F(0)/F^o \right]} \right\} [F(\infty) - F(0)] + F(0) \qquad (2.3)$$

where $F(t)$, $F(0)$, and $F(\infty)$ are the experimentally measured fluorescent intensities at the monitoring spot at time t, time zero, and infinite time, respectively, and F^0 is the pre-bleach fluorescence intensity. The function, $f(t)$, is given by:

$$f(t) = \sum_{n=0}^{\infty} \left[(-K)^n / n! \right] \left[1 + n(1 + 2t / \tau_D) \right]^{-1} \qquad (2.4)$$

where τ_D is given by $\tau_D = w^2/4D$, with w the half-width at the 1/e height of the laser beam at its point of focus. The parameter, K, is related to the fraction of probe that is bleached by the laser pulse, and is described by the expression:

$$\frac{F(0)}{F^0} = K^{-1}\left(1 - e^{-K}\right) \qquad (2.5)$$

As will be shown in section 2.4.3, the analysis utilized for the FRAP experiments conducted in this thesis is more powerful and, in some ways, also simpler.

Recently, FRAP is beginning to be used for characterizing transport in more diverse and complex systems. For example, the measurement of protein diffusion in aqueous gels (Berk et al., 1993; Johnson et al., 1995; Johnson et al., 1996), and of protein convection and diffusion in normal and noeplastic tissues have been reported (Chary and Jain, 1989). Likewise, diffusion in the complex lipid bilayers of human stratum corneum is examined in this thesis (see Chapter

4). These studies could not have effectively been performed with photomultiplier-FRAP, due to light scattering, inhomogeneities of the samples, and in some cases, convection. Instead, an image based FRAP system was utilized for these studies (see description in section 2.4.2) (Berk et al., 1993). Briefly, two dimensional images of the sample region are digitized over time and analyzed with a Fourier transform. The spatial resolution allows for rigorous analysis of transport in complex, inhomogeneous samples, such as the stratum corneum lipid bilayers.

2.4.1 Sample Preparations

Dimyristoylphosphatidylcholine (DMPC) was obtained from Avanti Polar Lipids (Alabaster, AL). Cholesterol was obtained from Sigma Chemical (St. Louis, MO) and stored at -20°C. DMPC was stored in chloroform and also at -20°C. All lipids were used without further purification.

DMPC and DMPC/cholesterol (40 mol%) multibilayers were prepared with the appropriate fluorescent probes by first combining the lipids and the probe in a chloroform solution. The lipid-to-probe ratio was at least 1000. The solvent was removed by rotary-evaporation at 40-45°C, followed by lyophilization, which produced a thin lipid film in the round-bottomed flask. Milli-Q water heated to 45°C (namely, above the phase transition temperature, T_m, of DMPC, 23.9°C (Mabrey and Sturtevant, 1976)) was added to the lipid film and vigorously mixed to produce the liposomes. The overall lipid concentration of the liposome solutions were about 10 mg/ml. The liposome solutions were annealed at 45°C under a nitrogen atmosphere for an hour. 10 µl of the solution, representing 100 µg of total lipids, were placed on a microscope slide cover, and dried for at least 4 hours at 45°C. The complete removal of the water was not

required, as was the case for removal of the solvent in the earlier steps, but was employed since dry lipid films formed in this manner tend to produce very large liposomes which are conducive to FRAP experiments. The lipid films were finally hydrated by placing the cover slips on a microscope slide with a 10 µl drop of phosphate buffered saline (PBS, pH 7.4, 10 mM phosphate, and 137 mM NaCl). The cover slip was sealed with silicone paste (Baxter SP, #S9003-1) to prevent water evaporation (Almeida et al., 1992). Sealed samples were annealed at 45°C overnight, and utilized within three days. Large multibilayer liposomes were selected by inspection using the FRAP video system, which is described below.

Several samples of DMPC/cholesterol liposomes were prepared in the same manner outlined above, but at an elevated temperature, as has been performed by others (Almeida et al., 1992). These liposomes were formed after preheating the lipids and Milli-Q water to 70°C. The microscope slide cover slip with the dried lipid film was preheated to 70°C for 10-30 minutes prior to the final hydration. Diffusion coefficients obtained with these samples were erroneously large. These results were likely due to thermal degradation of the probe or of the phospholipids, despite efforts to prevent exposure of the samples to oxygen for extended periods of time. Consequently, DMPC/cholesterol liposomes were prepared at lower temperatures, which proved to result in large liposomes which are conducive to the FRAP experiments.

Extracted SC lipid (SCE) solutions, obtained by the method outlined in section 2.2, were combined with the fluorescent probes in chloroform:methanol (2:1 v/v). The lipid-to-probe ratio was 1000. 50 µg of lipids in solution were placed on a microscope slide cover slip through successive application of a small amount of solution and drying. Typically 10-20 µl of solution were deposited per aliquot. Samples prepared in this manner tended to result in more homogenous

lipid films than samples in which all the lipids were deposited at once. After all the lipids were deposited, the cover slips were dried under low pressure to ensure removal of all the solvent. SC lipid films were hydrated by placing the cover slips on a microscope slide having a 10 µl drop of PBS on it, sealed with silicone paste to prevent water evaporation and annealed at 45°C overnight. Large lipid domains were selected by inspection using the FRAP video system.

2.4.2 Video-FRAP System and Lateral Diffusion Measurements

Diffusion coefficients were measured using an image-based fluorescence recovery after photobleaching (FRAP) technique. The reliability of this method has been previously established for the measurement of diffusion in gels and aqueous systems (Berk et al., 1993; Johnson et al., 1995). Utilization of the image-based FRAP technique offers several advantages over the conventional photomultiplier FRAP technique, as discussed in section 2.4, including a simplified solution to the 2-dimensional diffusion equation (see Eqs. (2.8)-(2.11) below). Detailed knowledge about the size, shape, and radial intensity distribution of the laser-beam radius are not needed. In photomultiplier-FRAP, the shape and Gaussian distribution of the laser beam must be carefully calibrated and constitute critical input parameters for calculating diffusion coefficients. Moreover, the image-based FRAP technique utilizes the fluorescence intensities measured at more than ten-thousand spatial locations at each time point to obtain the diffusion coefficient. This allows for the effective characterization of diffusion in heterogeneous media (Tsay and Jacobson, 1991).

The microscope slide was placed on the stage of an upright microscope (Universal; Zeiss, Thornwood, NY), and the sample was examined using epi-illumination, as shown in Figure 2.2. A beam splitter allowed the samples to be

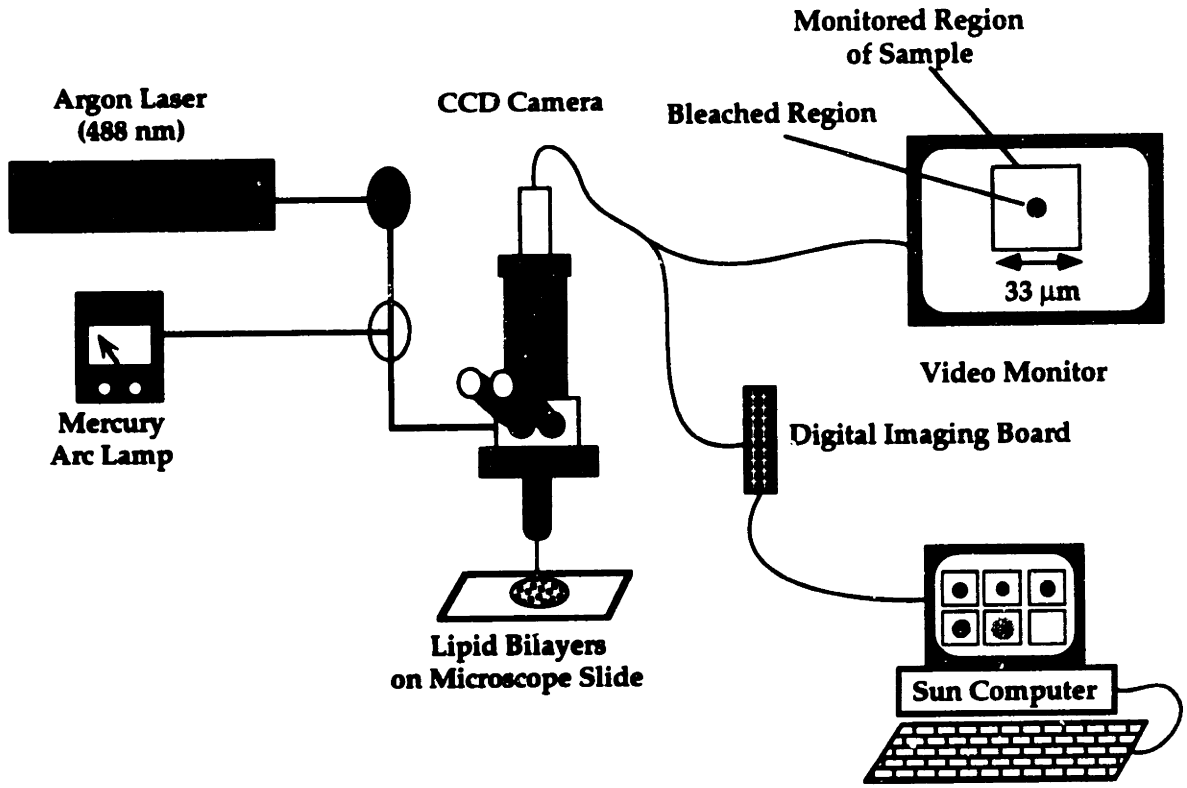

Figure 2.2 Schematic diagram of the image based fluorescence recovery after photobleaching (video-FRAP) apparatus. Samples are prepared on a microscope slide and examined on a video monitor while illuminated by a mercury arc lamp. At t=0, the sample is briefly exposed to the laser beam, resulting in the irreversible quenching of the fluophores in a small region. Two-dimensional images of the fluorescence distribution are captured over time, and analyzed to determine the diffusion coefficient.

either illuminated by a mercury arc lamp (100 W lamp (Osram, Munich) with stabilized power supply and convection-cooled housing (models 68806 and 60000, Oriel Corp., Stratford, CT)), or exposed to a laser pulse for fluorophore bleaching. An argon laser (model 2020 (Spectra Physics, Mountain View, CA)) operated in the TEM_{00} mode, such that the beam intensity was radially symmetric and obeyed a Gaussian profile, was used for the fluorophore bleaching. The beam passed through a focusing lens into the microscope epi-illumination port and was focused by the objective onto the sample. A 40X objective (N.A. 0.65) was used, which produced a laser spot radius (that is, the Gaussian radius of the attenuated beam projected onto a fluorescent sample) of 5 μm. Experiments were performed at 27±1°C. This warm temperature was obtained as a result of the heat produced by the arc lamp, computers, monitors, and other equipment in the small FRAP room. For those few cases when the temperature was below 26.0°C, an electric heat source placed near the microscope was used to elevate the temperature.

Under conventional epi-fluorescence illumination, the samples were examined and suitable lipid structures were chosen using an intensified CCD camera (model 2400 (Hamamatsu, Japan)) and video monitor. The fluorescence image of the 33 μm x 33 μm region of each sample was digitized using a monochrome video digitization board (model S1V (EDT, Beaverton, OR)). Only a portion (128 x 128 pixels) of the full (640 x 480 pixel) images were stored for analysis. The spatial sampling rates (that is, the vertical and horizontal distances between pixels) were determined using a stage micrometer (Edmund Scientific, Barington, NJ). FRAP experiments were performed by briefly exposing each sample to the laser, typically for 10-100 msec, in order to produce a bleached spot on the sample. A longer exposure time of 200 msec was used with the one particular probe, (dimethylaminocinnamylidene)malononitrile (DACM), since it

was found to be especially resistant to fluorescence quenching. Under conventional epi-illumination, fifty post-bleach images were obtained over the course of 20-120 seconds, depending upon the diffusion coefficient of the probe/lipid system. The first ten images were obtained at the maximum sampling rate of 30 images per second, while ten or more images were obtained at one-tenth of the maximum sampling rate, 3 images per second. The other 30 images were obtained at rates suitable to the time scale of the experiment.

2.4.3 Fourier Transform Analysis of FRAP Data

Two dimensional diffusion is described by Fick's second law:

$$\frac{\partial C(x,y,t)}{\partial t} = D\nabla^2 C(x,y,t) \tag{2.6}$$

where C is the concentration of the probe species, D is the diffusion coefficient, t is time, and x and y are the two-dimensional spatial coordinates. The Fourier-transform representation of this partial differential equation is a simpler ordinary differential equation, namely,

$$\frac{d\tilde{C}(u,v,t)}{dt} = -4\pi^2 D(u^2+v^2)\tilde{C}(u,v,t) \tag{2.7}$$

where $\tilde{C}(u,v,t)$ is the Fourier-transform of the concentration, and u and v are the spatial frequency components. The solution of Eq. (2.7) is a simple exponential equation. In contrast, the solution to Eq. (2.6) with the complex boundary conditions necessary to describe FRAP experiments (that is, that at time equals zero the initial fluorescence profile obeys a Gaussian distribution) is more

complex and cumbersome. Specifically, the solution of Eq. (2.7) in Fourier-space is the following simple exponential relationship:

$$\tilde{C}(u,v,t) = \tilde{C}(u,v,0)e^{(-4\pi^2 q^2 Dt)} \tag{2.8}$$

where q represents the spatial frequencies and is given by $q^2 = u^2 + v^2$. The fluorescence intensity in Fourier space, $\tilde{I}(u,v,t)$, is related to the fluorophore concentration, $\tilde{C}(u,v,t)$, such that:

$$\frac{\tilde{I}(u,v,t)}{\tilde{I}(u,v,0)} = \frac{\tilde{C}(u,v,t)}{\tilde{C}(u,v,0)} = e^{(-4\pi^2 q^2 Dt)} \tag{2.9}$$

Equation (2.9) describes a complete dissipation of the photobleached pattern. However, the fluorophore pattern in some FRAP experiments performed with lipid bilayer systems exhibits an incomplete or biphasic recovery. A modified form of Eq. (2.9), based on the assumption of an immobile or slow component, can be utilized to analyze the FRAP data and obtain the primary parameter of interest, D. Specifically,

$$\frac{\tilde{I}(u,v,t)}{\tilde{I}(u,v,0)} = \varepsilon + (1-\varepsilon)e^{(-4\pi^2 q^2 Dt)} \tag{2.10}$$

where ε denotes the immobile fraction.

Analyses of the representative FRAP recovery profiles for each probe in each lipid system were performed using a two diffusion coefficient model, namely:

$$\frac{\tilde{I}(u,v,t)}{\tilde{I}(u,v,0)} = f_1 e^{(-4\pi^2 q^2 D_1 t)} + (1 - f_1) e^{(-4\pi^2 q^2 D_2 t)} \qquad (2.11)$$

where D_1 and D_2 are the diffusion coefficients, and f_1 denotes the fraction of the probe diffusing in a regime characterized by D_1. Use of Eq. (2.11) proved statistically unnecessary for all but one of the probe/lipid systems, as will be discussed in Chapter 4. This was determined using the F statistic, namely:

$$F_n = \frac{(\chi^2_{n-1} - \chi^2_n)(N - 2n - 1)}{2\chi^2_n} \qquad (2.12)$$

where χ^2_n is the chi-squared goodness-of-fit statistic for n diffusing components, and N is the number of experimental data points (1000) (Wright et al., 1988). F_2 values of less than the critical value of 3.0 indicated that analyses utilizing Eq. (2.11) did not result in a statistically significant improvement over those utilizing Eq. (2.10). However, one probe, cholesteryl 4,4-difluoro-5,7-dimethyl-4-bora-3a,4a-diaza-s-indacene-3-dodecanoate (BOD-Chol), in SCE bilayers, consistently exhibited F_2 values greater than 3.0, and will be considered more thoroughly in the Chapter 4.

Values of $\tilde{I}(u,v,t)$ were obtained from the real values of the digitized images by first subtracting each post-bleach image from the pre-bleach image and then subjecting it to a discrete Fourier transform (Berk et al., 1993). Artifacts associated with the discrete transform were minimized by a digital windowing technique, as previously described (Johnson et al., 1994). Specifically, each differential image was padded at its edges (to a size of 256x256 pixels), then multiplied by a two-dimensional windowing function that smoothly attenuated the intensity to zero at the boundaries. A two dimensional fast Fourier transform (FFT) algorithm was then applied to produce an array of complex coefficients

corresponding to discrete spatial frequencies, $i\Delta u$ and $j\Delta v$ (where i and j range from -127 to 128). From each of the fifty post-bleach images, a total of twenty unique components were utilized for fitting to the decay equations (Eqs. (2.9)-(2.11)), as depicted in Figure 2.3. The components most useful for this purpose were the low spatial frequency components, although the lowest-frequency group was ignored since it does not decay. More frequencies were utilized in this work (20) than in earlier studies (8) due to the use of the faster video digitization board which can sample at a rate which is 6-fold faster than before. The faster sampling rate resulted in an increased signal-to-noise ratio of the higher frequencies, enabling more frequencies to be usable. The set of Fourier coefficients was then fit to the decay equation with one, two, or three parameters (Eqs. (2.9)-(2.11)) by a nonlinear least-squares algorithm, as described previously (Berk et al., 1993; Johnson et al., 1994).

2.5 Partition Coefficient Measurements

The extent to which a given solute is lipophilic (hydrophobic) or hydrophilic can be quantified by measuring the equilibrium distribution, that is, the partition coefficient, of the solute between two immiscable fluid phase, one that is organic and the other that is aqueous. Partition coefficients typically exhibit only a weak dependence upon solute concentration. Partition coefficients have been measured for tens of thousands of compounds using a variety of different organic phases, including olive oil, chloroform, and octanol, many of which have been compiled in one list (Hansch and Leo, 1979). Efforts to find a simple organic fluid which mimics the partitioning behavior of biological systems, such as phospholipid cell membranes, have shown that n-octanol to be the best (Leo et al., 1971). In fact, octanol/water partition coefficients, $K_{o/w}$, have been measured

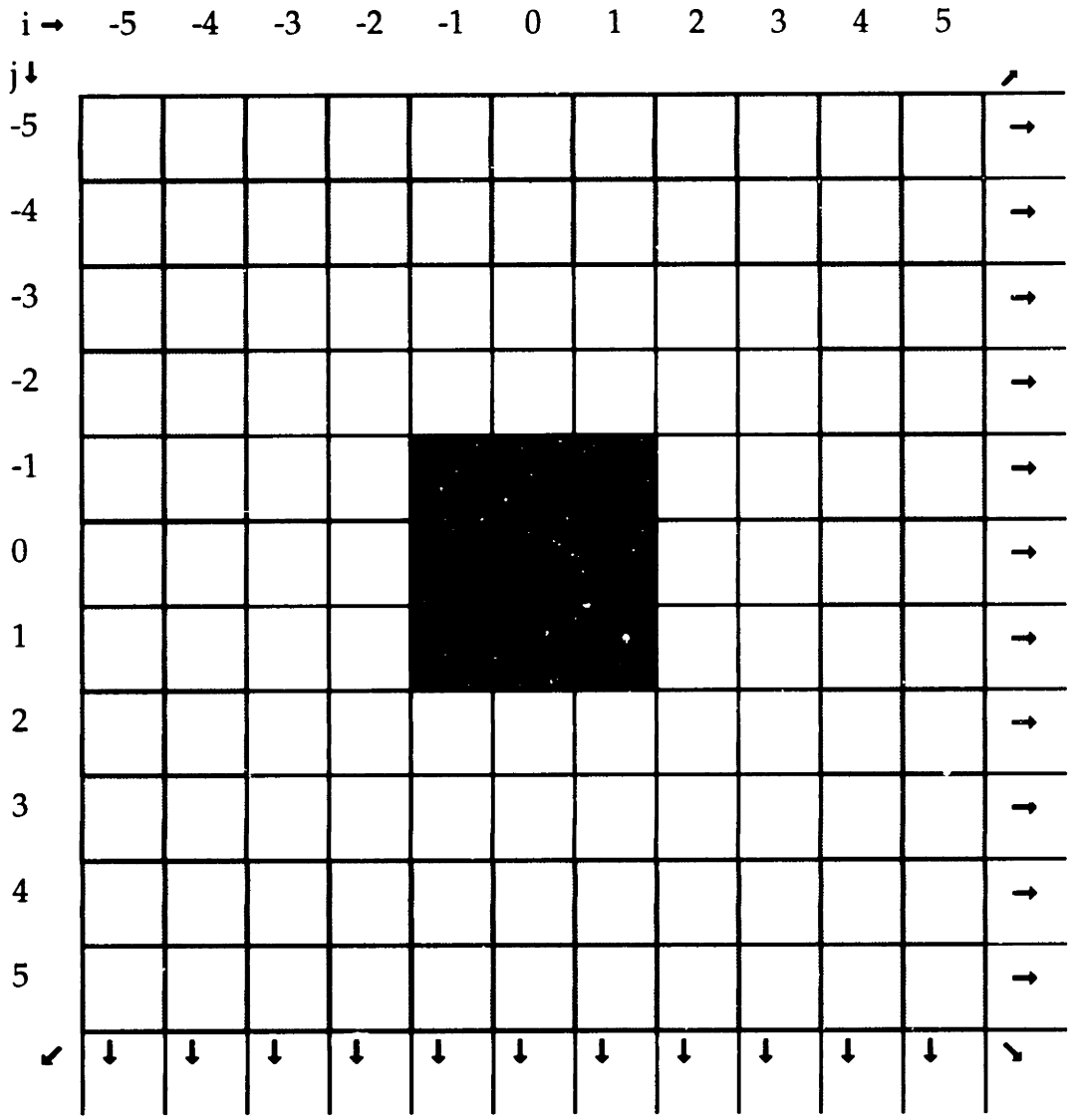

Figure 2.3 Selection of fast Fourier transform (FFT) components for use in the calculation of the pattern decay rate. The discrete components are grouped in 'levels' corresponding to the maximum index value (absolute values of i or j). The central component (black; i=j=0) does not decay. The next level of components (shaded dark gray; i or j = ±1) is affected by the windowing process, and is not used. The next two levels of components (white; i, j = ±2 and ±3) were utilized to determine the diffusion coefficient. Components with higher spatial frequencies (shaded light gray; |i or j| > 3) were not used due to their lower signal-to-noise ratio. Because the starting image intensity values are real-valued, the array is symmetrical, and half of the 40 acceptable components are redundant.

and reported for thousands of compounds (Hansch and Leo, 1979), including many drugs (see Tables 5. 1 and 5.2). $K_{o/w}$ values were also measured in this thesis for a variety of hydrophilic and lipophilic compounds. In addition, liposomes composed of dimyristoylphosphatidylcholine (DMPC) and DMPC/cholesterol (40 mol%) were used as a model system. Partition coefficients were made with these systems for a series of hydrophobic compounds, and compared with partition coefficients made with extracted stratum corneum lipids, K_{sce}.

2.5.1 Octanol/Water Partition Coefficients

Octanol/water partition coefficients were measured primarily using radiolabeled solutes, except the case of estradiol, which was measured with both radiolabeled and non-radiolabeled compound. Radiolabeled solutes were rotary-evaporated to remove any tritium which may have reverse-exchanged onto the solvent. The solute (radiolabeled or non-radiolabeled) was then redissolved in either octanol or water, and added to a separatory funnel. Appropriate volumes of octanol and pH 7.4 phosphate buffered saline (PBS) solution or distilled water were then added. The funnel was mixed by inversion 100 times, so as to facilitate solute equilibration between the two phases without promoting the formation of an emulsion, and allowed to settle for 24 hours or more at room temperature (Leo et al., 1971). Aliquots of octanol and the aqueous medium were then collected and centrifuged at 1000 rpm (212xg) for 10 minutes. Samples from each phase were taken and counted using a liquid scintillation counter or HPLC analysis. All measurements were made in triplicate. The value of apparent $K_{o/w}$ was taken to be the ratio of the volume-based concentration of each phase.

The $K_{o/w}$ measurements in the cases of hydrophilic solutes, such as sucrose, glucose, and oubain, were found to be independent of the aqueous and octanol volumes used, as expected. The $K_{o/w}$ values for some of the hydrophobic solutes, such the steroids, were obtained after repeated extractions were made. That is, radiolabeled-solute dissolved in large volumes (200-900 ml) of water were combined with approximately 5-15 ml of octanol, and mixed. Samples of each phase were centrifuged and analyzed to determine the apparent partition coefficient. The aqueous phase was removed and 900 ml more of water were added. This procedure was repeated until the apparent $K_{o/w}$ value was found to be constant for at least three consecutive extractions.

2.5.2 Liposome/Water Partition Coefficients

2.5.2.1 Liposome Formation

DMPC and DMPC/cholesterol (40 mol%) liposomes were prepared by placing a known amount of the lipids, dissolved in chloroform, in a round-bottom flask. The solvent was removed by rotary evaporation followed by lyophilization for at least one hour. A known amount of PBS pH 7.4, preheated to 40°C, was added to the flask, also preheated to 40°C. The final lipid concentration of these liposome systems was between 4 and 200 mg/ml, corresponding to an overall lipid content of 0.4-20% of the solution, by weight. The flask contents were annealed at 40°C for approximately 30 minutes, with periodic mixing to promote liposome formation.

Stratum Corneum model liposomes (SCM) were prepared by weighing out the individual lipid components in order to achieve a composition of 40% ceramides, 25% cholesterol, 25% palmitic acid, and 10% cholesterol sulfate, by

weight. The lipids fractions were dissolved in chloroform:methanol (2:1) and combined in a round bottom flask. The solvent was removed by rotary evaporation followed by lyophilization for at least 1 hour, resulting in the formation of a thin lipid film inside the flask. A known amount of Trizma pH 7.4 buffer, preheated to 80°C, was added to the flask, also preheated to 80°C. The final lipid concentration of the SCM systems was typically between 2 and 20 mg/ml. The flask contents were annealed at 80°C for approximately 30 minutes, with periodic mixing to promote liposome formation. The freeze-and-thaw technique (FAT) was used to facilitate lipid incorporation, since mixing alone was insufficient to incorporate all of the lipids into liposomes. That is, the lipid/buffer mixture was alternately frozen with liquid nitrogen (-196°C) and heated to 80°C in a water bath. Sonication was also used on occasion to facilitate liposome formation.

2.5.2.2 Partition Coefficient Measurements with DMPC and DMPC/Cholesterol liposomes

DMPC and DMPC/cholesterol liposome solutions were mixed with radiolabeled solutes to achieve a final overall solute concentration of approximately 0.5 μCi/ml and a total lipid concentration of approximately 4 mg/ml. The solutions were allowed to equilibrate for 24 hours or more in a water bath set at 25°C (±0.2°C). 5 ml of solution were centrifuged at 50,000 rpm (300,000xg; Beckman L-8 80-M Ultracentrifuge) and 25°C for approximately 2 hours. The supernatant was removed from tube, leaving a tightly packed 'pellet' of liposomes on the bottom. Care was taken to ensure that the pellet was not disturbed so that the supernatant remained free from liposomes. As a result of this precaution, a small volume of supernatant was left with the pellet phase. The presence of this extra

supernatant in the pellet phase simply increased the already substantial fraction of the water inherently present in the pellet, and was taken into account in the calculation of the partition coefficient. Three samples were taken from the supernatant phase and analyzed for ^{3}H or ^{14}C content utilizing a liquid scintillation counter, yielding the aqueous phase solute concentration, C_w.

The solute concentrations in the liposome lipid bilayers, C_b, were determined in a more indirect manner, since solute was present in the aqueous liposome core as well as in the water outside of the liposomes. Specifically, the solute concentration in the pellet, C_p, is related to the solute concentrations in the bilayer, C_b, and in the water, C_w, by their respective volume fractions in the pellet, namely,

$$C_p = \left(\frac{V_b}{V_b + V_w}\right) C_b + \left(\frac{V_w}{V_b + V_w}\right) C_w \tag{2.13}$$

where V_b and V_w are the total volumes of the lipid bilayers and the water in the pellet, respectively. Note that the water solute concentration in the pellet is identical as that in bulk supernatant, C_w, since the system is at equilibrium. The value of C_p can be determined experimentally, and V_b can be determined from the total amount of lipids in the sample and the bilayer density, which is assumed to be approximately unity. Therefore, only the volume of water in the pellet is left to be determined in order to be able to calculate C_b, using Eq. (2.13). The volume of water can be expressed in terms of the total pellet volume, V_p, namely,

$$V_w = V_p - V_b \tag{2.14}$$

The total pellet volume is then given by the ratio of the total solute content of the pellet, N_p, and the overall solute concentration in the pellet, namely,

$$V_p = {}^{N_p}\!/_{C_p} \tag{2.15}$$

where C_p can be determined by taking pellet samples of known volumes, and N_p can be determined by summing the amount of solute in the pellet samples taken with the amount of solute remaining in the pellet (note that liquid scintillation counting gives the amount of solute in the sample, such that no direct measurements of the volume of the unsampled pellet need to be made). By combining Eqs. (2.13), (2.14), and (2.15), the value of the solute concentration in the bilayer, C_b, can be expressed as follows:

$$C_b = \left(\frac{N_p}{V_b}\right) - \left(\frac{N_p}{V_b C_p} - 1\right) C_w \tag{2.16}$$

An additional step was needed in order to calculate the value of C_b, and hence, of the partition coefficient, since the ultracentrifugation of DMPC and DMPC/cholesterol liposomes produced heterogeneous pellets. These pellets, which were typically 40-100 mg in weight, were viscous and had an uneven distribution of water and lipid. Mixing the pellet proved ineffective, due to the viscosity of the pellet and the loss of pellet material on the stirring rod. Therefore, a known volume of water, V_a, (100 µl) was added to the pellet to reduce the viscosity of the pellet and allow for thorough mixing. Three 10 µl samples were then taken from the diluted pellet to determine the solute concentration, $C_{p,d}$. By noting that the total solute content is the same in both the

original and diluted pellet, the solute concentration in the original pellet can be written as follows:

$$V_p = {}^{N_p}\!/_{C_{p,d}} - V_a \tag{2.17}$$

where V_a is known (100 µl) and $C_{p,d}$ and N_p are determined by the method described above. Since the solute concentration in the original pellet is given by $C_p = N_p/V_b$, Eqs. (2.16) and (2.17) can be combined to express C_b in terms of known and experimentally measurable quantities. Specifically,

$$C_b = \left(\frac{N_p}{V_b}\right) - \left(\frac{N_p - V_a C_{p,d}}{V_b C_{p,d}} - 1\right) C_w \tag{2.18}$$

The bilayer/water partition coefficient was taken as the ratio of C_b, determined using Eq. (2.18), and the value of C_w. At least three separate experiments were performed for each drug/liposome combination.

2.5.2.3 Stratum Corneum Model Liposomes/Water Partition Coefficients

Solute partition coefficients for the SCM liposomes, K_{scm}, could not be measured using the ultracentrifugation technique at 25°C, described above (although measurements were made at 15°C with this technique), since these liposomes did not consistently pack into a pellet. That is, the supernatant contained liposomes for some samples, such that the true solute concentration could not be determined. For these samples, 6 hours of centrifugation did not completely remove the liposomes from the supernatant, while centrifugations at lower

temperatures (5-15°C) did. It is not clear why some samples would fully separate at 25°C while others would not.

Partition coefficients for the SCM liposomes at 25°C were measured using dialysis membranes to separate the liposomes from supernatant. One milliliter of SCM liposomes, with a known total-lipid content and containing approximately 0.5 μCi of solute, was added to 1 ml Spectro/Por® DispoDialyzer® tubes (Spectrum, Houston, TX) having a molecular weight cut-off (MWCO) of 10,000 Da. These tubes were sealed inside 13x110 mm glass test tubes filled with approximately 4 ml of buffer. The use of membranes having a low molecular weight cut-off ensured that the solutes, which were less than 500 Da in size, could readily pass through while the liposomes would be retained. The test-tubes/DispoDialyzer® systems were placed in a water bath maintained at 25°C (±0.2°C) and allowed to equilibrate for at least 24 hours. The liposome solution was removed, placed in a clean glass test-tube, and mixed prior to being sampled to determine the solute concentration, C_{lip}. Likewise, the external aqueous phase was well mixed prior to sampling. Three samples were taken from each phase and analyzed for solute content by liquid scintillation counting.

The partition coefficient was determined from the following relationship:

$$K_{sce} = \frac{\left(\frac{C_{lip}}{\phi_l} - \frac{C_w}{1-\phi_l} \right)}{C_w} \tag{2.19}$$

where ϕ_l is the volume fraction of lipids in the liposome phase. The value of ϕ_l was determined from the known lipid content by weight and assuming the density of the lipid and aqueous phases are 1 g/ml. At least three separate experiments were performed for each drug/liposome combination.

2.5.3 Stratum Corneum Lipid/Water Partition Coefficients

Lipids from human stratum corneum were extracted and placed in a 5 ml vial, as described in section 2.2. The solvent was removed by rotary evaporation and at least one hour of lyophilization, resulting in a dry lipid film on the inner surface of the lower portion of the vial. A buffer solution containing radiolabeled drug (~0.5 μCi/ml) was carefully added to the vial. 2.0 or 3.0 ml was typically sufficient to ensure that the entire lipid film was covered by solution. The system was allowed to equilibrate for 48 hours, with care being taken not to agitate the vials. Three samples were taken from the stock solute solution, as well as from the aqueous phase of the equilibrated vials, and the solute content determined by liquid scintillation counting. The partition coefficient of the solute between the extracted SC lipids and water were calculated with the following relationship:

$$K_{sce} = \frac{\left[\left(C_i - C_f\right)V_w / V_l\right]}{C_f} \tag{2.20}$$

where C_i is the initial aqueous solute concentration, C_f is the aqueous solute concentration after equilibration with the SC lipids, V_w is the volume of buffer added to the vial, and V_l is the volume of lipids, determined from the measured weight of the lipids and assuming a lipid density of 1 g/ml. Note that the amount of solute in the lipid phase was determined indirectly, by determining the difference in the aqueous solute concentration before and after equilibration. For select systems, the solute content of the lipids was also determined directly. That is, the entire aqueous phase was carefully pipetted away. Trace amounts of water remained, and were removed by gently tapping the vial on the bench top.

The remaining lipids were dissolved in liquid scintillation cocktail (Aquasol-2, New England Nuclear) and analyzed for solute content.

2.6 Solubility Measurements

The solubilities of non-radiolabeled solutes (corticosterone, dexamethasone, estradiol, lidocaine, and testosterone) were determined by placing excess amounts of each solute in several milliliters of buffer or an enhancer formulation. The system was thoroughly mixed and allowed to equilibrate for at least 24 hours. The solutions were then centrifuged at 1000 rpm (212xg) for 10 minutes and sampled. Samples were diluted to a concentration appropriate for high performance liquid chromatographic (HPLC) analysis utilizing the appropriate HPLC mobile phase.

Methanol and water (60:40 v/v) was the mobile phase used in the corticosterone and testosterone HPLC analyses, acetonitrile and water (35:65 v/v) was used in the dexamethasone HPLC analysis, and acetonitrile and water (60:40 v/v) was used in the estradiol analysis. The mobile phase used for the lidocaine HPLC analysis was acetonitrile and an aqueous phase (25:75 v/v), with the aqueous phase consisting of a mixture of water and acetic acid (93:5 v/v) whose pH was adjusted to 3.4 through the addition of NaOH. The mobile phases were filtered with 0.22 μm PTFE hydrophobic filters and degassed prior to use. A μ-Bondapak C18 (30 cm x 4 mm, i.d.) HPLC column was used. The sample volume was 40 μl and the mobile phase flow rate was 2.0 ml/min. An ultraviolet detector (Waters 490) was used at a wavelength of 240 nm for the corticosterone, dexamethasone, and testosterone analysis. Estradiol was detected at 220 nm, and lidocaine at 254 nm. Standards were prepared by diluting a stock solution of

each non-radiolabeled drug, prepared by weight, with the mobile phases. Measurements performed in triplicate had a standard deviation of less than 4%.

Chapter 3

Permeation of Steroids Through Human Skin

3.1 Introduction

Steroids are an important class of pharmacologically active drugs which have been found to be well suited for transdermal delivery. As a class, they tend to be hydrophobic, relatively small (for example, molecular weight<400 Da), and highly potent. Two different steroids, estradiol and testosterone, are currently delivered transdermally. Understanding why certain steroids have sufficient transdermal fluxes to be clinically effective, as well as how to increase the flux of other steroids, possibly utilizing chemical enhancers, in order that they may be delivered transdermally, is strongly dependent upon an accurate database of their properties. Foremost among these properties is the transdermal permeability, P, of the steroid.

The permeabilities of 14 steroids through human skin at 26°C were measured by Scheuplein et al. in 1969, and are listed in Table 3.1 (Scheuplein et al., 1969). This work constitutes the first, and the single most extensive study on the permeability of steroids through human skin to date. Table 3.1 shows that these steroids exhibit a wide range of characteristic properties, including permeabilities through human skin, which vary from as large as 3.6×10^{-3} cm/hr for estrone to as small as 3.0×10^{-6} cm/hr for aldosterone and hydrocortisone. The relative hydrophobicities of these steroids also vary considerably, as reflected in

Table 3.1 Steroid permeabilities through human skin.

Steroid	MW (Da)	$K_{o/w}$ [a]	P_s [b] (Scheuplein, 1969) (cm/hr)	P_o [c] (Other Groups) (cm/hr)	P_o/P_s	T (°C)	Ref.
Aldosterone	360.4	12	3.0×10^{-6}	5.0×10^{-5}	16.7	25	1
				5.8×10^{-5}	19.3	25	2
Hydrocortisone	362.5	34	3.0×10^{-6}	1.6×10^{-5}	5.3	37	3
				1.2×10^{-4}	40.0	30	4
				2.3×10^{-4}	76.7	37	2
Cortisone	360.5	26	1.0×10^{-5}				
Estriol	288.4	295	4.0×10^{-5}				
Corticosterone	346.5	87	6.0×10^{-5}	1.0×10^{-4}	1.7	25	5
				3.0×10^{-4}	5.0	25	6
				5.5×10^{-4}	9.2	27	7
Cortexolone	346.5	331	7.5×10^{-5}				
Estradiol	272.4	7200[d]	3.0×10^{-4}	3.0×10^{-3}	10.0	25	1
				3.2×10^{-3}	10.7	25	6
				3.4×10^{-3}	11.3	32	8
				3.5×10^{-3} [e]	11.7	32	9
				3.9×10^{-3}	13.0	30	10
				4.0×10^{-3} [f]	13.3	32	11
				4.1×10^{-3}	13.7	25	2
				4.2×10^{-3}	14.0	25	5
				5.2×10^{-3}	17.3	30	12
				5.4×10^{-3}	18.0	32	13
				6.1×10^{-3}	20.3	37	14
Hydroxyprogesterone	330.5	550	6.0×10^{-4}				
Testosterone	288.4	2042	4.0×10^{-4}	2.2×10^{-3}	5.5	25	6
				5.4×10^{-3}	13.5	25	5
Cortexone	330.5	759	4.5×10^{-4}				
Hydroxypregnenolone	330.5	1000	6.0×10^{-4}				
Pregnenolone	316.5	1349	1.5×10^{-3}				
Progesterone	314.5	5888	1.5×10^{-3}	1.3×10^{-2}	8.7	25	6
				3.0×10^{-2}	20.0	37	2
Estrone	270.4	575	3.6×10^{-3}				

[a] Data obtained from Hansch and Leo (Hansch and Leo, 1979) unless otherwise specified. [b] Permeability measurements made at 25°C. [c] Data obtained from the literature as referenced in column *Ref.* [d] Measurement made by Johnson et al. (see Chapter 5 and (Johnson et al., submitted, c)). [e] Calculated using the equation, $P = J_{ss} / \Delta c$, where values for the steady-state flux, J_{ss} (0.056 μg/cm^2-hr), and concentration gradient, Δc (16 μg/ml), were obtained from graphical representations of the experimental data (Goodman and Barry, 1988). [f] The arithmetic average of 211 different measurements after rejection of outliers (Williams et al., 1992). Outliers were generally attributed to the use of damaged skin, and resulted in erroneously large permeability values. [1] (Mitragotri et al., 1996). [2] (Johnson et al., 1995). [3] (Hou and Flynn, 1989). [4] (Hadgraft and Ridout, 1987). [5] (Johnson et al., submitted, a). [6] (Mitragotri et al., 1995). [7] (Peck et al., 1995). [8] (Goodman and Barry, 1988). [9] (Yum et al., 1994). [10] (Galey et al., 1976). [11] (Williams et al., 1992). [12] (Michaels et al., 1975). [13] (Perry, 1990). [14] (Knutson et al., 1993).

the values of the octanol/water partition coefficients, $K_{o/w}$, which are mostly taken from the literature (Hansch and Leo, 1979) and are also listed in Table 3.1. As can be seen, the $K_{o/w}$ values, taken primarily from the list compiled by Hansch and Leo (Hansch and Leo, 1979), vary from as low as 12 for aldosterone to as large as 7200 for estradiol (see section 2.4 for experimental details).

3.2 Materials and Methods

Permeability measurements were made with human cadaver skin obtained from the chest, abdomen, and back regions which was obtained from the National Disease Research Institute (Philadelphia, PA) and local hospitals, as fully described in section 2.3.1. The skin was stored at -80°C until use. The epidermis was obtained from the full-thickness tissue by immersion in 60°C water for two minutes. Heat-stripped skin was stored at 95% humidity and 5°C for up to one week prior to use. ^{3}H-aldosterone, ^{3}H-corticosterone, ^{3}H-estradiol, ^{3}H-hydrocortisone, ^{3}H-progesterone, and ^{3}H-testosterone were obtained from DuPont/NEN (Boston, MA) and American Radio Chemical (St. Louis, MO). The radiolabeled drugs were purchased in a solvent, typically ethanol, which was evaporated prior to use in order to remove any tritium which had reverse-exchanged onto the solvent. The drugs were redissolved in phosphate buffered saline (PBS, pH 7.4, 10 mM phosphate, and 137 mM NaCl) to a concentration of approximately 1 μCi/ml and added to the donor side of the permeation cell. PBS was utilized in the receptor compartment.

Permeation experiments were performed using stirred side-by-side diffusion cells (Crown Glass, #DC-100B). Typically, permeation experiments were performed at room temperature, although select experiments were also performed at a temperature of 37°C, which was maintained by using a water

bath and a temperature controller. Samples were taken periodically and counted using a Packard liquid scintillation counter (model 2000 CA, Packard Instruments Co., Downers Grove, IL). A minimum of three experiments were performed for each drug. The permeability values were determined under steady-state conditions using Eq. (2.1), $P = \left(\frac{dN_r}{dt}\right)_{ss}\left(\frac{1}{A(C_d - C_r)}\right)$, where N_r is the total amount of drug that permeated through the skin at time t, A is the available surface area of the skin, C_d is the drug concentration in the donor compartment, and C_r is the drug concentration in the receiver compartment. The experimental lag-times for these drugs were typically less than a few hours.

3.3 Discussion

The results of the permeability experiments with aldosterone, corticosterone, estradiol, progesterone, and testosterone are shown in Table 3.1, along with the data of Scheuplein et al. (1969) and that of various other groups taken from the literature.

An examination of Table 3.1 reveals that there are significant discrepancies between the steroid permeabilities reported by Scheuplein et al. and those measured by a number of other research groups. For example, I have also measured the permeability of estradiol through human skin and found it to be 4.1×10^{-3} cm/hr at 25°C (see Table 3.1) (Johnson et al., 1995). Several groups have reported human skin permeability measurements for estradiol (Galey et al., 1976; Goodman and Barry, 1988; Johnson et al., 1995; Johnson et al., in press; Knutson et al., 1993; Michaels et al., 1975; Mitragotri et al., 1996; Mitragotri et al., 1995; Perry, 1990; Williams et al., 1992; Yum et al., 1994) as shown in Table 3.1. These permeability values, ranging from 3.0×10^{-3} to 6.1×10^{-3} cm/hr, are between 10 and

20 times greater than the value of $3.0x10^{-4}$ cm/hr reported by Scheuplein et al. (1969). The estradiol permeability measurement reported by Williams et al., $4.0x10^{-3}$ cm/hr (see Table 3.1), is based upon an enormous data base of 211 individual permeability measurements (Williams et al., 1992). In addition, significant discrepancies exist between the data of Scheuplein et al. and that of others on the maximum estradiol flux through human skin from saturated aqueous solutions. Experimental values of 0.016 $\mu g/cm^2$-hr at 30°C (Michaels et al., 1975), 0.0314 $\mu g/cm^2$-hr at 32°C (Liu et al., 1991), and 0.056 $\mu g/cm^2$-hr at 32°C (Yum et al., 1994) are approximately two orders of magnitude larger than the value of 0.00036 $\mu g/cm^2$-hr at 26°C reported by Scheuplein et al. (1969) for the maximum estradiol flux through human skin.

As in the case of estradiol, values of the human skin permeability of hydrocortisone measured by other groups follow a similar trend in that they are considerably larger than those reported by Scheuplein et al. (1969). As shown in Table 3.1, values of $1.6x10^{-5}$ cm/hr (Hou and Flynn, 1989) and $1.2x10^{-4}$ cm/hr (Hadgraft and Ridout, 1987) have been reported. I have measured the permeability of hydrocortisone through human skin utilizing and found it to be $2.3x10^{-4}$ cm/hr at 37°C (Johnson et al., 1995). These permeability values are one to two orders of magnitude larger than the permeability value of $3.0x10^{-6}$ cm/hr reported by Scheuplein et al. (1969) at a temperature of 26°C.

The human skin permeabilities for several other steroids (Johnson et al., 1995; Johnson et al., in press) are reported in Table 3.1 and are in good agreement with those of others, sans Scheuplein et al. These include the measurement of aldosterone, $5.8x10^{-5}$ cm/hr at 25°C, of corticosterone, $4.1x10^{-3}$ cm/hr at 25°C, of testosterone, $5.4x10^{-3}$ cm/hr at 25°C, and of progesterone, $3.0x10^{-2}$ cm/hr at 25°C. Mitragotri et al. have also recently reported (Mitragotri et al., 1995) permeability measurements for several steroids through human skin, including

corticosterone, progesterone, and testosterone. These values, which were obtained at a temperature of 25°C, are also listed in Table 3.1. As shown in Table 3.1, the new permeability values measured for aldosterone, corticosterone, progesterone, and testosterone are between 1.7 and 19 times larger than those obtained by Scheuplein et al. (1969).

The reason behind the exceptionally low permeability values measured by Scheuplein et al. (1969) is not clear. A certain degree of variability is inherently associated with skin permeability measurements owing to differences in the physical properties of the skin samples. For example, the stratum corneum thickness, lipid content, and the keratinocyte dimensions, are all known to vary between individuals and between different locations on an individual. Yet, intersubject variability of human skin permeabilities has been reported to be approximately 40% (Williams et al., 1992). Consequently, random errors stemming from the variability of the skin properties cannot account for the magnitude of the discrepancies shown in Table 1, nor for the fact that the measurements of Scheuplein et al. (Scheuplein et al., 1969) tend to be consistently lower than those of made by others.

There are several other experimental factors which could result in systematically lower apparent skin permeabilities. The presence of air bubbles on the surface of the skin has been noted as a possible source of experimental error (Williams et al., 1992). Specifically, air-bubbles would result in lower apparent skin permeabilities by reducing the area available for drug transport (Williams et al., 1992). However, this source of error constitutes an unlikely explanation since 90% of the skin area would have to be covered by bubbles in order to achieve, for example, a 10-fold decrease in the apparent skin permeability. The effect of temperature on the permeability through human skin is also unable to explain the observed discrepancies reported in Table 3.1.

Specifically, assuming an activation energy of 10 kcal/mol (Scheuplein and Blank, 1971), the skin permeability would increase by less than a factor of two over the temperature range, 25-37°C, spanned by the measurements reported in Table 3.1. After correcting to a temperature of 32°C, utilizing an activation energy of 10 kcal/mol (Scheuplein and Blank, 1971), the estradiol permeabilities measured by other groups , listed in Table 3.1, average to 4.7×10^{-3} cm/hr with a 21% standard deviation, which is well within the intersubject variability of approximately 40% observed by Williams et al (Williams et al., 1992). Permeability measurements made prior to the establishment of steady-state could result in lower apparent skin permeabilities. Yet, Scheuplein et al. (1969) were careful to ensure that steady-state conditions had in fact been achieved prior to making their permeability measurements. This is illustrated in Figure 2 of (Scheuplein et al., 1969), which shows flux profiles from permeation experiments which lasted 100 hours and longer. The diffusional resistance of the dermis has been shown to contribute to and result in lower apparent skin permeabilities for certain compounds which have relatively large skin permeabilities (e.g., greater than approximately 1×10^{-2} cm/hr) (Flynn, 1990). However, heat-stripped epidermal membranes were used for the majority of the measurements listed in Table 3.1, including the measurements made by Scheuplein et al. (Scheuplein, 1967; Scheuplein et al., 1969), thus precluding the dermal resistance from explaining the observed discrepancies reported in Table 3.1. The use of radiolabeled drugs can also lead to possible errors in permeability measurements due to tritium exchange with the solvent and metabolism of the drug within the skin. However, the majority of the measurements reported in Table 3.1 were made with radiolabeled drugs, including those made by Scheuplein et al. (1969). In addition, the experimental transdermal flux of estradiol from saturated aqueous solutions measured by Liu et al., 0.0314

$\mu g/cm^2$-hr (Liu et al., 1991), using high-performance liquid chromatography as a detection method is in good agreement with the fluxes measured using radiolabeled estradiol by Michaels et al. (Michaels et al., 1975) and Yum et al. (Yum et al., 1994), 0.016 and 0.056 $\mu g/cm^2$-hr, respectively. Consequently, the use of radiolabeled drugs does not account for the discrepancies observed in Table 3.1. Other experimental factors, including the skin preparation technique, the skin storage conditions, and the buffer and salt content of the donor and receptor solutions can also possibly effect permeability measurements, but are not considered to be critical for nonelectrolytes (Bronaugh, 1989; Gummer, 1989; Harrison et al., 1984). However, these experimental factors are not able to explain deviations as large as those shown in Table 3.1, nor the fact that the measurements of Scheuplein et al. are consistently lower than those made by other groups. Therefore, there is no immediately obvious explanation as to why the steroid permeability values reported by Scheuplein et al. (1969) are much lower than those measured by other groups.

3.4 Conclusions

Numerous groups have examined the human skin permeabilities of six out of the fourteen steroids originally examined by Scheuplein et al. (1969), aldosterone, corticosterone, estradiol, hydrocortisone, progesterone, and testosterone, and found significant discrepancies. Table 3.1 shows that the permeabilities reported by Scheuplein et al. are consistently smaller than the twenty-three measurements made by other groups, by an average factor of 167, and by up to nearly two orders of magnitude. The properties of these six steroids, in terms of molecular weight, $K_{o/w}$, and permeability, span the range covered by the 14 steroids

examined by Scheuplein et al. (1969). This suggests that the permeability values for the other eight steroids should also be reexamined.

It is also worth noting that the 14 steroids examined by Scheuplein et al. comprise a substantial fraction of the compounds for which human skin permeabilities have been reported and compiled, such as those found in the Flynn list (Flynn, 1990). Moreover, the permeability values reported by Scheuplein et al. represent some of the lowest permeability values measured for hydrophobic non-electrolytes, and account for a significant fraction of the larger molecular-weight compounds found on the Flynn list (Flynn, 1990), which was published before most of the data in Table 3.1 had been reported. In other words, correlations to predict human skin permeabilities which have been based upon these data may in fact be skewed, particularly in the higher molecular-weight regime (Kasting et al., 1992; Kasting et al., 1987; Potts and Guy, 1992; Wilschut et al., 1995).

Chapter 4

Lateral Diffusion of Small Compounds in Human Stratum Corneum and Model Lipid Bilayer Systems

4.1 Introduction

Over the past two decades, lateral diffusion in phospholipid bilayer systems has been extensively studied using a variety of experimental and theoretical techniques. The majority of this work has been performed with the ultimate purpose of developing a better understanding of the fundamental and practical aspects of lateral diffusion in cell membranes. As such, these studies have focused on the diffusion of lipids and integral membrane proteins, and on the relationships between lateral diffusion rates and the probe's intrinsic properties, such as size and shape (Clegg and Vaz, 1985; Saffman and Delbrück, 1975). For example, integral protein diffusion has been found to exhibit a weak dependence on molecular size, and is effectively described using existing continuum theories (Clegg and Vaz, 1985; Saffman and Delbrück, 1975). The effects of temperature, cholesterol content, and lipid tail-length on the diffusion of lipid probes in model bilayer systems have also been effectively evaluated experimentally and theoretically (Almeida et al., 1992; Clegg and Vaz, 1985; Derzko and Jacobson, 1980; Rubenstein et al., 1979; Tocanne et al., 1989; Vaz et al., 1985).

In contrast, lateral diffusion in the lipid multibilayers of the stratum corneum (SC), the outermost layer of the skin which constitutes the primary

barrier to solute transport (Scheuplein and Blank, 1971), has been essentially unexplored despite the tremendous attention paid to SC transport (see Chapter 1). A better understanding of transdermal transport is desired in order to facilitate the development of, for example, therapeutically effective drug delivery systems. To this end, measurements have been made of the SC permeability of more than one hundred compounds, almost all of which are lipophilic and smaller than ~500 Da in molecular weight (Flynn, 1990; Johnson et al., 1995; Kasting et al., 1992) (see Tables 6.1 and 6.2). These compounds diffuse through the SC primarily via the inter-keratinocyte lipids, which include ceramides, fatty acids, and sterols but essentially no phospholipids (Lampe et al., 1983). Detailed studies using electron microscopy (Hou et al., 1991; Madison et al., 1987) and small-angle x-ray diffraction (Bouwstra et al., 1991; Fäberg and Osborne, 1985) have further revealed that the SC lipids are in the form of multibilayers (see Chapter 1).

Comparisons of the molecular weight dependence of SC permeabilities have been made with transbilayer permeability measurements of various phospholipid bilayer systems (Potts and Guy, 1992; Scheuplein and Blank, 1971). These studies have shown that the molecular weight dependence of SC permeation of small, lipophilic drugs is strong, and similar to that exhibited by small, mostly hydrophilic compounds diffusing across phospholipid bilayers. In contrast, little attention has been devoted to the potential importance of lateral diffusion in SC transport, even though lateral and transbilayer diffusion are different processes and occur at significantly different rates (Diamond and Katz, 1974; Lange-Lieckfeldt and Lee, 1992). This lack of attention is largely due to the unavailability of experimental data on the lateral diffusion coefficients of any size compounds (with the exception of molecular oxygen (Hatcher and Plachy, 1993))

in SCE bilayers and on the lateral diffusion coefficients of small probes (<500 Da) in other bilayer systems.

In this chapter, lateral diffusion in SCE lipid bilayers is explored by using the image-based fluorescence recovery after photobleaching (video-FRAP) technique to measure the diffusion coefficients of a series of nine fluorescent probes of varying molecular weight (223-854 Da) in lipids extracted from the SC (SCE lipids). Diffusion of these nine probes is also measured in two model lipid systems, dimyristoylphosphatidylcholine (DMPC) and DMPC/cholesterol (40 mol%; referred to as *DMPC/cholesterol*). The goals of this study were to: (i) characterize experimentally lateral diffusion in SCE bilayers, (ii) characterize experimentally lateral diffusion of small lipid and non-lipid probes in DMPC and DMPC/cholesterol model bilayer systems. (iii) determine the molecular weight dependence of lateral diffusion in DMPC and DMPC/cholesterol model bilayer systems, using the experimental results presented in this chapter, supplemented with available literature data to extend the size range to smaller probes, and (iv) determine the molecular weight dependence of lateral diffusion in SCE bilayers using the experimental results presented in this chapter, as well as the diffusion coefficient of a previously examined probe (Hatcher and Plachy, 1993).

4.2 Materials and Methods

4.2.1 Materials

The fluorescent probes examined in this study were obtained from Molecular Probes (Eugene, OR) and used without further purification. The structures of these probes - (a) 4-(dimethylaminocinnamylidene)malononitrile (DACM, 223 Da), (b) 4,4-difluoro-1,3,5,7,8-pentamethyl-4-bora-3a,4a-diaza-s-indacene (BOD,

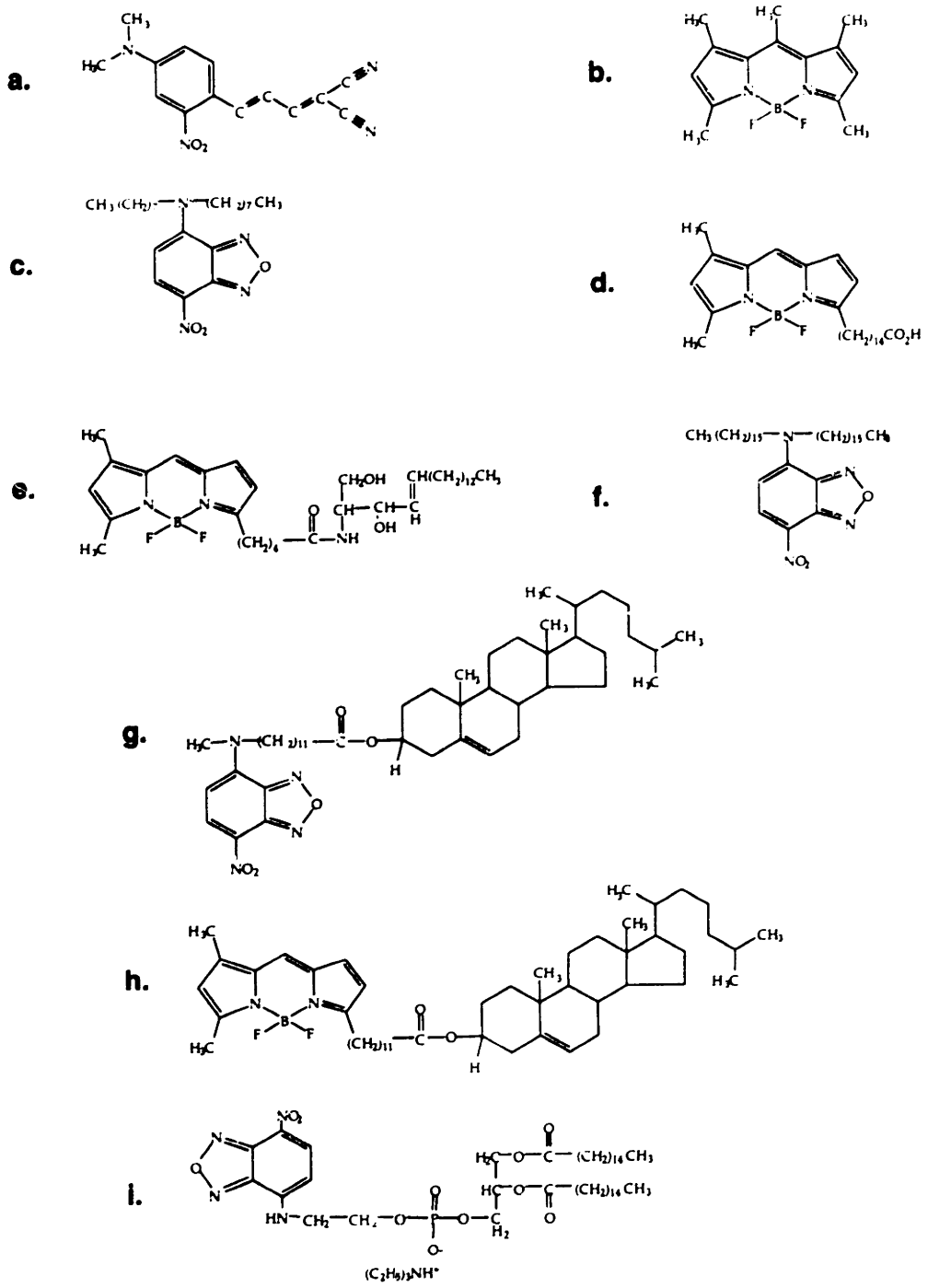

Figure 4.1 The chemical structures of the fluorescent probes utilized for the characterization of lateral diffusion in SCE lipids and DMPC and DMPC/cholesterol model bilayer systems: (a) DACM, (b) BOD, (c) NBD-dioct, (d) BOD-FA, (e) BOD-Cer, (f) NBD-dihexdec, (g) NBD-Chol, (h) BOD-Chol, and (i) NBD-PE.

262 Da), (c) 4-(N,N-dioctyl)amino-7-nitrobenz-2-oxa-1,3-diazole (NBD-dioct, 405 Da), (d) 4,4-difluoro-5,7-dimethyl-4-bora-3a,4a-diaza-s-indacene-3-hexadecanoic acid (BOD-FA, 474 Da), (e) N-(4,4-difluoro-5,7-dimethyl-4-bora-3a,4a-diaza-s-indacene-3-pentanoyl)sphingosine (BOD-Cer, 602 Da), (f) 4-(N,N-dihexadecyl)amino-7-nitrobenz-2-oxa-1,3-diazole (NBD-dihexdec, 629 Da), (g) cholesteryl 12-(N-methyl-N-(7-nitrobenz-2-oxa-1,3-diazol-4-yl)amino)dodecanoate (NBD-Chol, 761 Da), (h) cholesteryl 4,4-difluoro-5,7-dimethyl-4-bora-3a,4a-diaza-s-indacene-3-dodecanoate (BOD-Chol. 787 Da), and (i) N-(7-nitrobenz-2-oxa-1,3-diazol-4-yl)-1,2-dipalmitoyl-sn-glycero-3-phosphoethanolamine (NBD-PE, 854 Da) - are shown in Figure 4.1. The wavelengths of the peak absorption and emission of these probes are listed in Table 4.1.

DMPC was obtained from Avanti Polar Lipids (Alabaster, AL), and was stored in chloroform at -20°C. Cholesterol was obtained from Sigma Chemical (St. Louis, MO), and was also stored at -20°C. All lipids were used without further purification.

4.2.2 Sample Preparation

The methods utilized for the experiments described in this chapter are presented in detail in Chapter 2, and are summarized in the remainder of this section. Specifically, SC lipids were extracted from human cadaver skin. The skin was from the chest, back, and abdominal regions, and was obtained from local hospitals and the National Disease Research Institute (Philadelphia, PA). Note that the SC lipid composition is fairly uniform for various body sites (Lampe et al., 1983). The skin was stored at -80°C until usage. The epidermis was separated from the full-thickness tissue after immersion in 60°C water for 2

Table 4.1 Physical Properties of Fluorescent Probes

Probe Name	Molecular Weight (Da)	Absorption Peak (nm)	Emission Peak (nm)
DACM	223	482	577
BOD	262	491	505
NBD-dioct	404	486	543
BOD-FA	474	474	505
BOD-Cer	602	505	511
NBD-dihexdec	629	485	542
NBD-Chol	761	482	540
BOD-Chol	787	504	511
NBD-PE	854	460	534

Absorption and emission peak values from Molecular Probes (Eugene, OR).

minutes. The SC was then separated from the heat-stripped epidermis by soaking the epidermis in a 0.5% trypsin solution overnight at 5°C (Anderson et al., 1988). The SC was cleaned with distilled water, rinsed in cold hexane to remove exogenous lipids, and lyophilized for 24 hours or more to remove all water. Dried SC was cut into pieces of approximately 10 mg, weighed, and placed in a 7 ml vial with a ground glass cap. 5 ml of chloroform:methanol (2:1 v/v) were added to the vial. After at least 24 hours, the delipidized SC (specifically, the remaining keratinocytes) was removed, lyophilized, and again weighed (Anderson et al., 1988). The amount of lipids in the vial was determined by taking the difference between the weights of the SC before and after delipidization. Typical lipid contents of the SC were 10-20% on a weight basis. Extracted SC lipid solutions were stored at -20°C until usage.

DMPC and DMPC/cholesterol multibilayers were prepared with the appropriate probes by first combining the lipids and the probe in chloroform (see Chapter 2). The lipid-to-probe mole ratio was at least 1000. The solvent was removed by rotary-evaporation followed by lyophilization. Milli-Q water heated to 45°C was added to the lipid film and vigorously mixed to produce an overall lipid concentration of approximately 10 mg/ml. The resulting liposome solutions were annealed at 45°C under a nitrogen atmosphere for an hour. 10 µl of solution, representing 100 µg of total lipids, were placed on a microscope slide cover slip, and dried for at least 4 hours at 45°C. The lipid films were finally hydrated by placing the cover slips on a microscope slide with a 10 µl drop of phosphate buffered saline (PBS, pH 7.4, 10 mM phosphate, 137 mM NaCl). The cover slip was sealed with silicone paste (Baxter SP, #S9003-1) to prevent water evaporation (Almeida et al., 1992). Sealed samples were annealed at 45°C overnight, and utilized within three days. Large multibilayer liposomes were selected by inspection using the FRAP video system, which is described below.

Extracted SC lipid solutions were combined with the fluorescent probes in chloroform:methanol (2:1 v/v). The lipid-to-probe mole ratio was 1000. 50 μg of lipids in solution were placed on a microscope slide cover slip through successive application of a small amount of solution and drying. Once all the lipids were deposited, the cover slips were dried under low pressure to ensure removal of all the solvent. SC lipid films were hydrated by placing the cover slips on a microscope slide onto which a 10 μl drop of PBS had been placed, sealed with silicone paste (Baxter SP, #S9003-1) to prevent water evaporation and annealed at 45°C overnight. Large lipid domains were selected by inspection using the FRAP video system.

4.2.3 Diffusion Measurements

Diffusion coefficients were measured using an image-based fluorescence recovery after photobleaching (FRAP) technique (see Chapter 2). The reliability of this method has been previously established for the measurement of diffusion in gels and aqueous systems (Berk et al., 1993; Johnson et al., 1995). Utilization of the image-based FRAP technique offers several advantages over the conventional photomultiplier FRAP technique, including a simplified solution to the 2-dimensional diffusion equation (see Eqs. (4.1)-(4.4) below). Detailed knowledge about the size, shape, and radial intensity distribution of the laser-beam radius are not needed. Moreover, the image-based FRAP technique utilizes the fluorescence intensities measured at more than ten-thousand spatial locations at each time point to obtain the diffusion coefficient. This allows for the characterization of diffusion in heterogeneous media (Tsay and Jacobson, 1991).

The microscope slide was placed on the stage of an upright microscope (Universal; Zeiss, Thornwood, NY), and the sample was examined using epi-

illumination. A beam splitter allowed the samples to be either illuminated by a mercury arc lamp (100 W lamp (Osram, Munich) with stabilized power supply and convection-cooled housing (models 68806 and 60000, Oriel Corp., Stratford, CT)), or exposed to a laser pulse for fluorophore bleaching. An argon laser (model 2020 (Spectra Physics, Mountain View, CA)) operated in the TEM_{00} mode, such that the beam intensity was radially symmetric and obeyed a Gaussian profile, was used for the fluorophore bleaching. The beam passed through a focusing lens into the microscope epi-illumination port and was focused by the objective onto the sample. A 40X objective (N.A. 0.65) produced a laser spot radius (that is, the Gaussian radius of the attenuated beam projected onto a fluorescent sample) of 5 μm. Experiments were performed at 27±1.0°C. This warm temperature resulted from the heat produced by the arc lamp, computers, monitors, and other equipment in the small FRAP room. For those few cases when the temperature was below 26.5°C, an electric heat source placed near the microscope was used to elevate the temperature.

Samples were examined and suitable lipid structures were chosen using conventional epi-fluorescence illumination and an intensified CCD camera (model 2400 (Hamamatsu, Japan)) and video monitor. The fluorescence image of the 33 μm x 33 μm region of each sample was digitized using a monochrome video digitization board (model S1V (EDT, Beaverton, OR)). Only a portion (128 x 128 pixels) of the full (640 x 480 pixel) images were stored for analysis. The spatial sampling rates (that is, the vertical and horizontal distances between pixels) were determined using a stage micrometer (Edmund Scientific, Barington, NJ). FRAP experiments were performed by briefly exposing each sample to the laser, typically for 10-100 msec, in order to produce a bleached spot on the sample. A longer exposure time of 200 msec was used for the probe DACM, because this probe was found to be especially resistant to photobleaching. Under

conventional epi-illumination, fifty post-bleach images were obtained over the course of 20-120 seconds, depending upon the diffusion coefficient of the probe/lipid system. The first ten images were obtained at the maximum sampling rate of 30 images per second, and ten or more additional images were obtained at one-tenth of the maximum sampling rate, or 3 images per second. Thirty additional images were obtained at rates suitable to the time-scale of the experiment.

4.2.4 Analysis of FRAP Data

Two dimensional diffusion is described by Fick's second law:

$$\frac{\partial C(x,y,t)}{\partial t} = D\nabla^2 C(x,y,t) \tag{4.1}$$

where C is the concentration of the probe species, D is the lateral diffusion coefficient, t is time, and x and y are the two-dimensional spatial coordinates. The Fourier-transform representation of this partial differential equation is a simple ordinary differential equation, namely,

$$\frac{d\tilde{C}(u,v,t)}{dt} = -4\pi^2 D(u^2+v^2)\tilde{C}(u,v,t) \tag{4.2}$$

where $\tilde{C}(u,v,t)$ is the Fourier-transform of the concentration, and u and v are the spatial frequency components. The solution of Eq. (4.2) is a simple exponential equation, rather than the more complex and cumbersome solutions of Eq. (4.1). Specifically,

$$\tilde{C}(u,v,t) = \tilde{C}(u,v,0)e^{(-4\pi^2 q^2 Dt)} \tag{4.3}$$

where q represents the spatial frequencies and is given by $q^2=u^2+v^2$. The fluorescence intensity in Fourier space, $\tilde{I}(u,v,t)$, is related to the fluorophore concentration, $\tilde{C}(u,v,t)$, such that:

$$\frac{\tilde{I}(u,v,t)}{\tilde{I}(u,v,0)} = \frac{\tilde{C}(u,v,t)}{\tilde{C}(u,v,0)} = e^{(-4\pi^2 q^2 Dt)} \tag{4.4}$$

Equation (4.4) describes a complete dissipation of the photobleached pattern. However, the fluorophore pattern in some FRAP experiments performed using lipid bilayer systems exhibits an incomplete or biphasic recovery. A modified form of Eq. (4.4), based on the assumption of an immobile or slow component, was utilized to analyze the FRAP data and obtain the primary parameter of interest, D. Specifically,

$$\frac{\tilde{I}(u,v,t)}{\tilde{I}(u,v,0)} = \varepsilon + (1-\varepsilon)e^{(-4\pi^2 q^2 Dt)} \tag{4.5}$$

where ε represents the immobile fraction.

Analyses of representative FRAP recovery profiles for each probe in each lipid system were also performed using a two diffusion coefficient model, namely,

$$\frac{\tilde{I}(u,v,t)}{\tilde{I}(u,v,0)} = f_1 e^{(-4\pi^2 q^2 D_1 t)} + (1-f_1)e^{(-4\pi^2 q^2 D_2 t)} \tag{4.6}$$

where D_1 and D_2 are the diffusion coefficients, and f_1 represents the fraction of the probe diffusing in a regime characterized by D_1. Use of Eq. (4.6) proved statistically unnecessary for all but one of the probe/lipid systems. This was determined using the F statistic, namely:

$$F_n = \frac{(\chi^2_{n-1} - \chi^2_n)(N - 2n - 1)}{2\chi^2_n} \tag{4.7}$$

where χ^2_n is the chi-squared goodness-of-fit statistic for n diffusing components, and N is the number of experimental data points (1000) (Wright et al., 1988). F_2 values less than the critical value of 3.0 indicated that analyses using Eq. (4.6) did not result in a statistically significant improvement over those using Eq. (4.5). However, the diffusion of one probe, BOD-Chol in SCE bilayers, did consistently exhibit F_2 values greater than 3.0, and is considered more thoroughly in the Discussion.

Values of $\tilde{I}(u,v,t)$ were obtained from the real values of the digitized images by first subtracting each post-bleach image from the pre-bleach image and then subjecting it to a discrete Fourier transform (Berk et al., 1993). Artifacts associated with the discrete transform were minimized by a digital windowing technique, as previously described (Johnson et al., 1994). Specifically, each differential image was padded at its edges (to a size of 256x256 pixels), then multiplied by a two-dimensional windowing function that smoothly attenuated the intensity to zero at the boundaries. A two-dimensional fast Fourier transform (FFT) algorithm was then applied to produce an array of complex coefficients corresponding to discrete spatial frequencies, $i\Delta u$ and $j\Delta v$ (where i and j ranged from -127 to 128). From each of the fifty post-bleach images, a total of twenty unique components were utilized for fitting to the decay equations (Eq. (4.4)-

(4.6)). The components most useful for this purpose were the low spatial frequency components, although the lowest-frequency group was ignored since it does not decay. More frequencies were utilized in this work (20) than in earlier studies (8) due to the use of a video digitization board which could acquire images at a 6-fold faster rate. The faster sampling rate resulted in an increased signal-to-noise ratio of the higher frequencies, thus enabling more frequencies to be useful. The set of Fourier coefficients was then fit to the decay equation with one, two, or three parameters (Eqs. (4.4)-(4.6)) by using a nonlinear least-squares algorithm, as described previously (Berk et al., 1993; Johnson et al., 1994).

4.3 Results

4.3.1 Diffusion in DMPC and DMPC/Cholesterol Lipid Bilayers

Representative recovery plots of the recovery of the diffusion of BOD in DMPC, DMPC/cholesterol, and SCE lipid bilayers are shown in Figure 4.2, where the Fourier coefficients, $\tilde{I}/\tilde{I}_o$, corresponding to the twenty lowest spatial frequencies from each of the fifty post-bleach images are plotted against frequency-scaled time, $4\pi^2 q^2 t$. Since each component is scaled by its value in the first post-bleach image, dissipation of the photobleached pattern is represented by a decay from 1 to 0. The recovery of BOD in DMPC is faster than in DMPC/cholesterol and, hence, its diffusion coefficient, 1.27×10^{-7} cm^2/sec (R=0.998), is greater than that in DMPC/cholesterol, 2.57×10^{-8} cm^2/sec (R=0.989). Figure 4.2 also shows that the recovery profiles are all well represented by Eq. (4.5), from which the diffusion coefficient, D, and the immobile fraction, ε, were determined using a least-squares regression. The recovery profiles for the other eight probes in DMPC

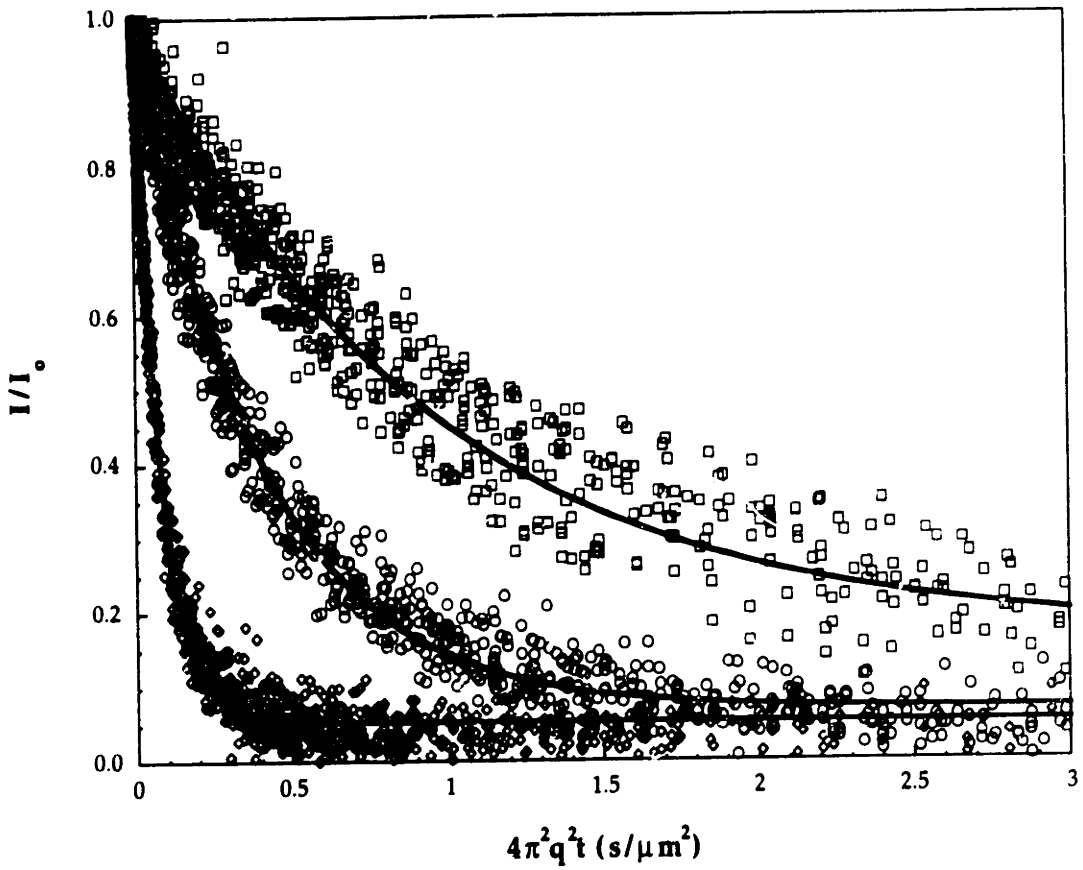

Figure 4.2 Recovery profiles of BOD in DMPC lipid bilayers (◇), DMPC/cholesterol lipid bilayers (○), and SCE lipid bilayers (□). The Fourier coefficients, $\tilde{I}_i/\tilde{I}_o$, corresponding to the twelve lowest spatial frequencies from each of the fifty post-bleach images are plotted against frequency-scaled time, $4\pi^2q^2t$. Since each component is scaled by its value in the first post-bleach image, dissipation of the photobleached pattern is represented by a decay from 1 to 0. The lines were obtained by performing a least-squares regression on the data using Eq. (4.5).

and DMPC/cholesterol lipid bilayers are qualitatively similar to those shown in Figure 4.2, and are also well described by Eq. (4.5).

Results of the analyses for the nine fluorescent probes examined in DMPC bilayers are summarized in Table 4.2. The diffusion coefficients in DMPC, measured at 27°C, range from as large as 16.2×10^{-8} cm^2/sec for DACM, the smallest probe, to 6.75×10^{-8} cm^2/sec for NBD-Chol. The diffusion coefficient for NBD-PE is 6.88×10^{-8} cm^2/sec. This value is in good agreement with previously reported values of the NBD-PE§ diffusion coefficient in DMPC lipid bilayers, which range from 4.3×10^{-8} cm^2/sec (Galla et al., 1979) to 8.2×10^{-8} cm^2/sec (Wu et al., 1977) (Table 4.3). The average immobile fractions of the probes in the DMPC bilayer experiments (Table 4.2) range from 2.6% to 4.6%, which is also in good agreement with the results of others (Balcom and Petersen, 1993). These favorable comparisons of the data presented in this chapter with those in the literature confirm that video-FRAP is an effective and accurate method for measuring lateral diffusion in lipid bilayer systems.

Results of analyses for the nine fluorescent probes in DMPC/cholesterol bilayers are also summarized in Table 4.2. Values of the diffusion coefficients in DMPC/cholesterol, obtained at 27°C, range from 5.60×10^{-8} cm^2/sec for DACM,

---

§ The length of the alkyl chains of the various NBD-PE probes used in previous studies were not all the same. The NBD-PE probe used in this and other studies (Balcom and Petersen, 1993; Paprica, 1994), NBD-dipalmitoylphosphatidylethanolamine, has an alkyl chain length of 16. NBD-dimyristoylphosphatidylethanolamine, with an alkyl chain length of 14, was also used (Vaz et al., 1985), while Almeida et al. (Almeida et al., 1992) used NBD-didecanoylphosphatidylethanolamine. At the time of the earlier studies (Chang et al., 1981; Derzko and Jacobson, 1980; Galla et al., 1979; Rubenstein et al., 1979; Wu et al., 1977), the NBD-PE probe which was commercially available (Avanti Polar Lipids, Alabaster, AL) had a slightly larger molecular weight of 880 Da. Since previous work has shown that differences in alkyl tail length of a series of NBD-PE probes does not substantially affect the diffusion coefficient in distearoylphosphatidylcholine lipid bilayers, due to the restrictions on the large head group in the more highly ordered head-group region (Vaz et al., 1985), the diffusion coefficients of these similar probes should be comparable.

Table 4.2 Diffusion coefficients and immobile fractions of low molecular weight probes in DMPC and DMPC/cholesterol 40 mol% bilayers.

Probe	DMPC			DMPC/Cholesterol 40 mol%		
	D (10^{-8} cm^2/sec)	ε (%)	*n*	*D* (10^{-8} cm^2/sec)	ε (%)	*n*
DACM	16.2 ± 2.0	4.6 ± 2.3	12	5.60 ± 1.5	16 ± 8.5	13
BOD	12.5 ± 1.3	2.6 ± 1.0	14	2.33 ± 0.20	6.5 ± 1.9	32
NBD-dioct	10.1 ± 1.2	4.8 ± 1.4	12	2.87 ± 0.38	5.2 ± 4.3	27
BOD-FA	7.89 ± 0.41	3.3 ± 1.0	20	1.92 ± 0.17	4.5 ± 1.9	36
BOD-Cer	7.52 ± 0.29	3.6 ± 0.4	16	1.88 ± 0.07	7.2 ± 2.8	24
NBD-dihexdec	7.80 ± 0.47	4.3 ± 1.2	16	1.65 ± 0.16	4.9 ± 1.9	26
NBD-Chol	6.75 ± 0.45	4.8 ± 1.7	11	1.32 ± 0.09	6.7 ± 1.5	14
BOD-Chol	7.24 ± 0.46	4.3 ± 0.6	12	1.69 ± 0.18	7.5 ± 3.2	27
NBD-PE	6.88 ± 0.59	4.1 ± 1.2	23	1.62 ± 0.16	6.5 ± 2.6	44

Values were measured at 27 °C, and are given as mean ± SD. *n* is the number of measurements.

Table 4.3 Summary of literature values of lipid and small probe lateral diffusion coefficients in DMPC lipid bilayers.

Probe	T (°C)	D † (10^{-8} cm^2/sec)	D_c § (10^{-8} cm^2/sec)	Ref.
NBD-PE	30	5.9	5.9	(Almeida et al., 1992)
Nifedipine analogue	47	130 ¶	710	(Alper and Stouch, 1995)
NBD-citronello	29	4.8	5.0	(Balcom and Petersen, 1993)
NBD-PE	29	5.0	5.2	(Balcom and Petersen, 1993)
NBD-solanesol	29	5.3	5.5	(Balcom and Petersen, 1993)
NBD-dolichol	29	4.6	4.8	(Balcom and Petersen, 1993)
Tetracene	29	11	11	(Balcom and Petersen, 1993)
Rubrene	29	5.8	6.0	(Balcom and Petersen, 1993)
Benzene	47	280 ¶	154	(Bassolino-Klimas et al., 1993)
NBD-PE	30	7.6	7.6	(Chang et al., 1981)
NBD-dodecanoic acid	24	7.2	11	(Derzko and Jacobson, 1980)
3,3'-dihexyloxacarbocyanine iodide	33	8.2	7.7	(Derzko and Jacobson, 1980)
3,3'-didodecanoylindocarbocyanine iodide	24	5.2	7.3	(Derzko and Jacobson, 1980)
3,3'-dioctadecyloxacarbocyanine iodide	24	6.7	7.7	(Derzko and Jacobson, 1980)
3,3'-dioctadecylindocarbocyanine iodide	24	8.4	9.8	(Derzko and Jacobson, 1980)
NBD-PE	24	6.3	7.7	(Derzko and Jacobson, 1980)
NBD-PE	30	4.3	4.3	(Kapitza et al., 1984)
NBD-Macrocyclic Polyamide Dimer	36	7.5	5.9	(Paprica, 1994)
NBD-Macrocyclic Polyamide Trimer	36	7.4	5.8	(Paprica, 1994)
NBD-PE	36	8.0	6.3	(Paprica, 1994)
NBD-Macrocyclic Polyamide Quatramer	36	6.3	5.0	(Paprica, 1994)
NBD-Macrocyclic Polyamide Pentamer	36	6.6	5.2	(Paprica, 1994)
NBD-Macrocyclic Polyamide Hexamer	36	4.2	3.3	(Paprica, 1994)
3,3'-dioctadecyloxacarbocyanine iodide	29	6.9	7.4	(Peters and Cherry, 1982)
NBD-PE	26	4.8	5.7	(Rubenstein et al., 1979)

Oxygen	40	2700 ¥	1800	(Subczynski et al., 1991)
1-methylpyrene	30	55 £	55	(Van den Zegel et al., 1984)
NBD-PE	30	5.3	5.3	(Vaz et al., 1985)
3,3'-dioctadecyloxacarbocyanine iodide	30	5.5	5.5	(Wu et al., 1977)
NBD-PE	30	8.2	8.2	(Wu et al., 1977)

† Diffusion coefficients were measured using FRAP unless otherwise noted.

§ Diffusion coefficient corrected to 30°C using either the activation energy reported in the same reference in which the diffusion coefficient measurement was reported, or the typical value of 7.4 kcal/ mole (Almeida et al., 1992; Chang et al., 1981; Peters and Cherry, 1982; Van den Zegel et al., 1984).

£ Measured using the fluorescence decay technique.

¶ Average values of the calculated diffusion coefficients in a DMPC bilayer determined from a molecular dynamic simulation (MDS).

¥ Calculated from measurements of the bilayer permeability, P, using $D = P\delta/K$, where δ is the bilayer thickness, and K is the bilayer/water partition coefficient, estimated from its octanol/water partition coefficient, $K_{o/w}$ (3.68, (Hansch and Leo, 1979)), by $K = K_{o/w}^{0.87}$. This value constitutes an upper estimate of the diffusion coefficient due to the resistance associated with crossing the bilayer head-group region (Diamond and Katz, 1974).

the smallest probe, to 1.32×10^{-8} cm^2/sec for NBD-Chol. The value for the diffusion coefficient of NBD-PE in DMPC/cholesterol lipid bilayers obtained using the video-FRAP technique, 1.62×10^{-8} cm^2/sec, is also in good agreement with previously reported measurements of NBD-PE in DMPC bilayers with 40-50 mol% cholesterol: 1.1×10^{-8} cm^2/sec at 30°C (Chang et al., 1981), 1.3×10^{-8} cm^2/sec at 26°C (Rubenstein et al., 1979), 2×10^{-8} cm^2/sec at 30°C (Wu et al., 1977), and 2.7×10^{-8} cm^2/sec at 30°C (Almeida et al., 1992). Combined with the results obtained for NBD-PE diffusion in DMPC, these results confirm the ability of the video-FRAP technique to measure diffusion coefficients spanning a wide range of values. The immobile fractions of the probes in DMPC/cholesterol are 5-7% (±3%), except for DACM, which has an immobile fraction of 16% (±9%) due to the higher noise levels obtained with this probe. Table 4.2 also shows that the diffusion coefficient values in DMPC are all greater than those in DMPC/cholesterol. This finding is in agreement with the general findings of many others that the isothermal addition of cholesterol to fluid phase phospholipid bilayers (that is, at $T > T_m$, where T_m=23.9°C for DMPC (Mabrey and Sturtevant, 1976)) produces a more ordered bilayer structure in which the diffusion coefficients are reduced. The diffusion coefficient of each probe in DMPC is consistently greater than that in DMPC/cholesterol, by an average factor of 4.3 (standard deviation of 18%).

4.3.2 Diffusion in SCE Lipid Bilayers

The recovery profile of BOD in SCE lipid bilayers is qualitatively similar to those for BOD diffusion in DMPC and DMPC/cholesterol bilayers (Figure 4.2) except that it exhibits a significantly longer characteristic recovery time, which corresponds to a smaller value of the diffusion coefficient, 1.28×10^{-8} cm^2/sec

(R=0.980). Figure 4.2 also shows that there was incomplete recovery of BOD diffusion in SCE, with an immobile fraction of 21%. Importantly, this figure also shows that the recovery was fairly uniform, confirming that the fluorescence recovery process was governed by diffusion of a single population. The recovery profiles for DACM, NBD-dioct, NBD-dihexdec, and NBD-Chol were also uniform and well described by Eq. (4.5). The diffusion coefficients and immobile fractions of these five probes in SCE bilayers are shown in Table 4.4. The diffusion coefficients of DACM, BOD, NBD-dioct, NBD-dihexdec, and NBD-Chol in SCE lipids range from as great as 2.34×10^{-8} cm^2/sec for the smallest probe, DACM, to 3.06×10^{-9} cm^2/sec for NBD-dihexdec. The immobile fractions of these probes vary from 17% to 32%. Similar immobile fractions (17-60%) have also been observed in other complex lipid systems, including multi-component bilayers (Vaz et al., 1989; Vaz et al., 1990), biological membranes characterized by slow diffusion ($D \leq 10^{-9}$ cm^2/sec) (Cherry, 1979), and gel-phase phospholipid bilayers (Balcom and Petersen, 1993).

Recovery curves of BOD diffusion in SCE bilayers were analyzed using the two diffusion coefficient model, Eq. (4.6), since the F statistic, Eq. (4.7), revealed that Eq. (4.6) provided a statistically significant improvement in accuracy over Eq. (4.5). These results suggested that the majority of BOD-Chol, 78±5%, diffused at a rate of 1.25×10^{-9} cm^2/sec, while the remainder of the probe, 22%, exhibited a diffusion coefficient that was more than an order of magnitude greater, 1.59×10^{-8} cm^2/sec. The recovery profiles for BOD-FA, BOD-Cer, and NBD-PE in SCE bilayers did not exhibit exponential decays, in contrast to the results for BOD (Figure 4.2) and the other probes examined, and are considered further in section 4.4.2.

Table 4.4 Diffusion coefficients and immobile fractions of low molecular weight probes in SCE bilayers

Probe	D (10^{-8} cm^2/sec)	ε (%)	n
DACM	2.34 ± 0.41	17 ± 3.6	16
BOD	1.22 ± 0.17	27 ± 10	20
NBD-dioct	0.712 ± 0.20	19 ± 8.0	22
BOD-FA	*	*	27
BOD-Cer	*	*	29
NBD-dihexdec	0.306 ± 0.181	32 ± 20	12
NBD-Chol	0.385 ± 0.19	22 ± 12	16
BOD-Chol	0.125 ± 0.07 §	22 ± 4.8 §	22
NBD-PE	*	*	24

Values were measured at 27°C, and are given as mean ± SD. n is the number of measurements. * The fluorescence intensity recovery curves in Fourier space did not exhibit an exponential decay. § Analyzed with Eq. (4.6). The two calculated diffusion coefficients were 0.125(±0.07)x10^{-8} cm^2/sec and 1.59(±0.57)x10^{-8} cm^2/sec, and the distribution coefficient was f_1=78% (±5%). That is, 78% of the probe appeared to diffuse at the slower rate, and 22% at the faster rate.

4.4 Discussion

4.4.1 Molecular Weight Dependence of Lateral Diffusion in DMPC Lipid Bilayers

The measured diffusion coefficients of the nine probes in DMPC bilayers are shown in Figure 4.3a plotted against the probe molecular weight. These data exhibit a molecular weight dependence, with the smaller probes tending to diffuse faster than the larger probes. The diffusion coefficient of the fastest probe, DACM, is 2.4-fold greater than that of the slowest probe, NBD-Chol. With respect to diffusion in DMPC bilayers, this change is dramatic. To illustrate the significance of this finding, consider the Saffman-Delbrück equation (Saffman and Delbrück, 1975), which effectively describes the diffusion of integral proteins in fluid phase lipid bilayers, namely,

$$D = \left(\frac{k_b T}{4\pi\eta_o h}\right)\left[\ln\left(\frac{\eta_o h}{\eta r_c}\right) - \gamma_e\right] \tag{4.8}$$

where k_b is Boltzmann's constant, T is temperature (303 K), η_o is the effective viscosity of the bilayer, η is the viscosity of the surrounding aqueous medium, h is the 'height' of the protein, which is assumed to span the bilayer, and is equivalent to the bilayer thickness (55 Å), and γ_e is Euler's constant (0.5772). Using a value of 0.75 P for η_o (Vaz et al., 1984), 0.01 P for η (Bird et al., 1960), and assuming a specific gravity of 0.9,§ the Saffman-Delbrück equation predicts that

§ For the purposes of this study, the molecular weights of the probes are related to their molecular volumes through, $M=vN_a g$ where M is the molecular weight, v is the molecular volume, N_a is Avogadro's number, and g is the specific gravity. The specific gravity of the probes is taken to be a typical value for organic molecules, 0.9 (Weast, 1975).

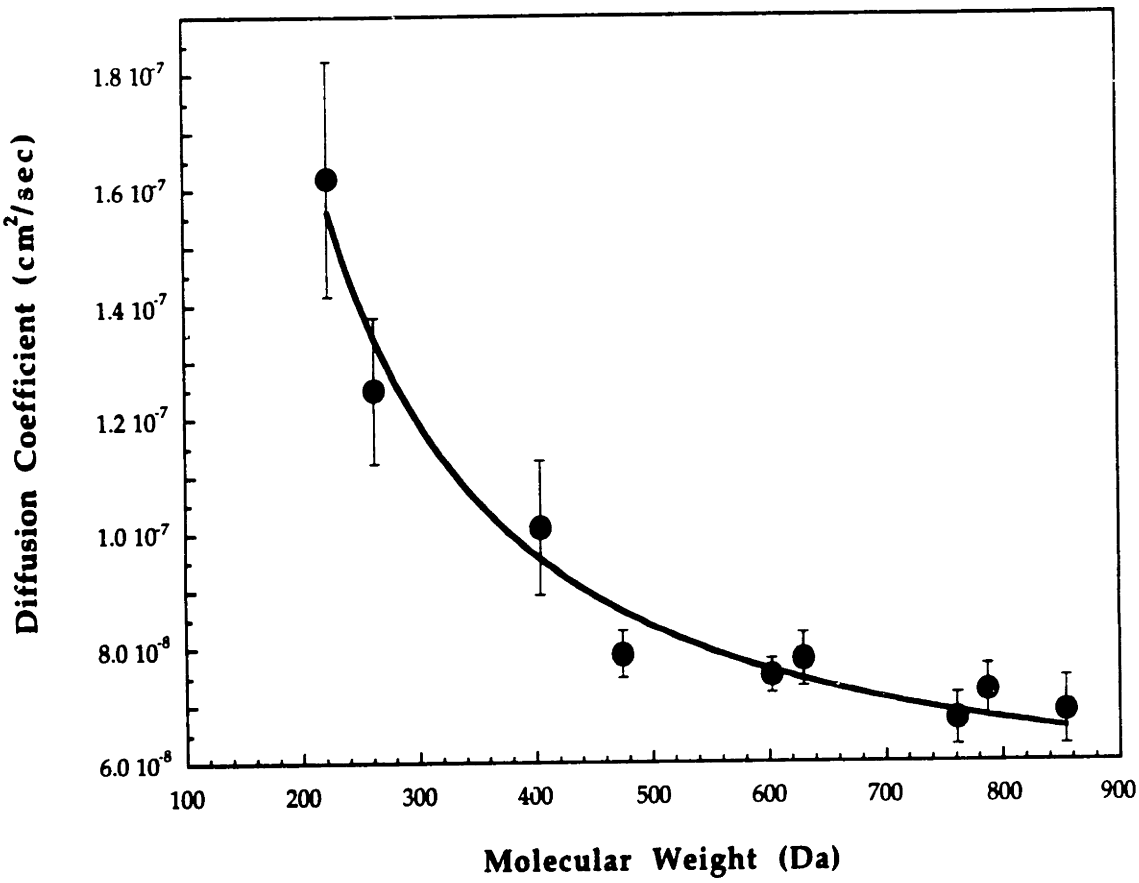

Figure 4.3a Diffusion coefficients of the fluorescent probes in DMPC, as measured by the video FRAP technique at 27°C, versus the probe molecular weight. These data exhibit a distinct molecular weight dependence with the diffusion coefficients decreasing with increasing probe size. The line represents the semi-empirical model (Eq. (4.9)), which combines the strong size dependence of free-volume theory in the lower molecular weight regime with the weak size dependence of continuum theories in the larger molecular weight regime. The error bars represent standard deviations of the measurements.

a 470,000 Da probe, a molecular weight nearly three-orders of magnitude greater than those of the probes examined in this study, would have a diffusion coefficient that is only 2.4-fold less than that of NBD-Chol. Equation (4.8) illustrates that the diffusion coefficients of larger probes in DMPC bilayers exhibit a very weak dependence on probe size. In contrast, the diffusion coefficients of smaller compounds in DMPC bilayers increase dramatically with decreasing probe molecular weight (Figure 4.3a, and discussion below).

Figure 4.3a shows several cases in which a larger probe has an apparent greater diffusion coefficient than a smaller probe, including the pair NBD-dihexdec and BOD-Cer, as well as the pair BOD-Chol and NBD-Chol. However, these differences are not statistically significant at the 95% confidence level using the two-tailed Student's t-test Table 4.2 and Figure 4.3a also show that the standard deviation of the DACM diffusion coefficient is unusually large (13%). This is due, in part, to the photostability of DACM, which makes it more resistant to bleaching than the other probes and, hence, results in weaker bleach spots and noisier recovery profiles.

Also shown in Figure 4.3a is the dependence of the diffusion coefficient on molecular weight, obtained by performing a least-squares regression on the DMPC data using the equation:

$$D = aM^{-b} + \left(\frac{k_b T}{4\pi\eta_o h}\right)\left[\ln\left(\frac{\eta_o h}{\eta r_c}\right) - \gamma_e\right] \qquad (4.9)$$

where M is the probe molecular weight and a and b are empirically determined parameters, and where M and the probe radius. The probe radius, r_c, in the second term of Eq. (4.9) and M are related by $r_c = \left[M/(\pi h N_a \rho)\right]^{1/2}$, where ρ is the solute density. The remaining parameters in Eq. (4.9) were described above.

Equation (4.9) combines a term exhibiting a strong molecular weight dependence, aM^{-b}, with a term exhibiting a weak size dependence as given by the Saffman-Delbrück relationship (Eq. (4.8)). The first term, aM^{-b}, which has been effectively used to describe the diffusion of small solutes in various biological tissues, including human stratum corneum permeabilities (Anderson and Raykar, 1989), red blood cells (Lieb and Stein, 1986), and stroma (Cooper and Kasting, 1987), is included to capture the dramatic increase in diffusion coefficients as the probe molecular weight decreases below ~400 Da, while the second term is included to account for the weaker molecular weight dependence which appears to begin at ~500 Da. These terms are effectively used in an additive manner since, in the low molecular weight regime, the contribution of the first term is much greater than that of the second, while in the high molecular weight regime the contribution of the first term becomes insignificant and the second term dominates. The values obtained for the empirical parameters, a and b, are 1.45×10^{-4} cm^2/sec and 1.32, respectively. Equation (4.9) describes well the molecular weight dependence of the diffusion coefficient in DMPC bilayers, as shown in Figure 4.3a.

4.4.2 Molecular Weight Dependence of Lateral Diffusion in DMPC/Cholesterol Lipid Bilayers

Figure 4.3b shows a plot of the diffusion coefficients of the nine fluorescent probes in DMPC/cholesterol bilayers versus the probe molecular weight. Similar to the results obtained in DMPC bilayers (Figure 4.3a), the diffusion coefficients initially decrease rapidly with increasing probe molecular weight, while the values for probes larger than ~500 Da decrease at a more moderate rate. The fastest probe in this system, DACM, diffuses 4.2-fold faster than the

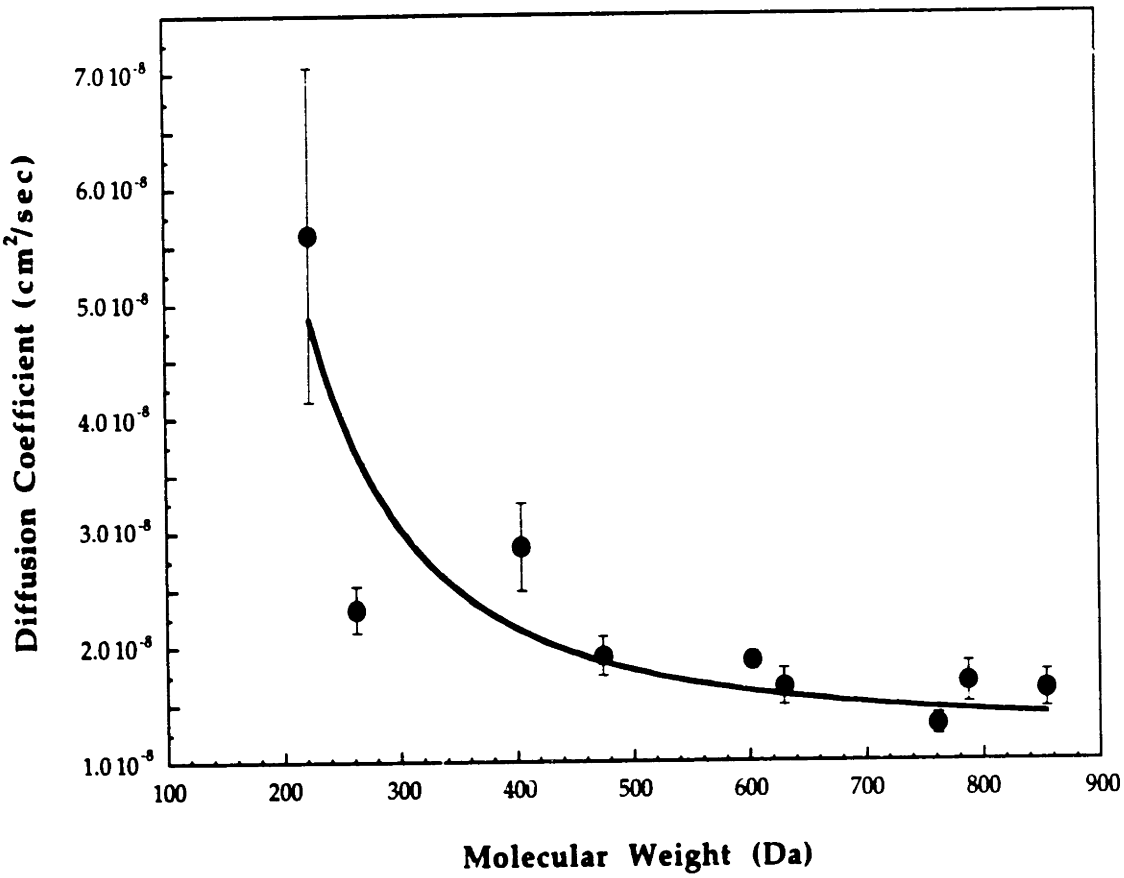

Figure 4.3b Diffusion coefficients of the fluorescent probes in DMPC/cholesterol, as measured by the video FRAP technique at 27°C, versus the probe molecular weight. These data exhibit a distinct molecular weight dependence with the diffusion coefficients decreasing with increasing probe size. The line represents the semi-empirical model (Eq. (4.9)), which combines the strong size dependence of free-volume theory in the lower molecular weight regime with the weak size dependence of continuum theories in the larger molecular weight regime. The error bars represent standard deviations of the measurements.

slowest probe, NBD-Chol. This increase suggests that the molecular weight dependence of diffusion in DMPC/cholesterol is greater than that in DMPC, for which a 2.4-fold increase is found. For SCE lipids this dependence is even greater, as discussed in the following section. The error of the DACM diffusion coefficient (26% standard deviation) is larger than that of the other probes due, in part, to the higher noise level resulting from the photostability of the probe, as discussed above.

The diffusion coefficient of BOD in DMPC/cholesterol, 2.33×10^{-8} cm^2/sec, lies below the expected trend (Figure 4.3b). This value is less than that of the larger probe, NBD-dioct, and is nearly as low as those of the larger probes examined (500-900 Da). This behavior is in contrast to the results shown in Figure 4.3a, in which the diffusion coefficient of BOD in DMPC bilayers follows the trend quite well, and is significantly greater than those of NBD-dioct and the larger probes. The reason for the observed discrepancy is not clear. One possible explanation is that the localization of BOD within the bilayer is different than that of the other probes. In fact, small solutes are not evenly distributed across lipid bilayers, but exhibit characteristic concentration profiles which depend upon the chemical-physical properties of the solute (Bassolino-Klimas et al., 1993; Gawrisch and Janz, 1991; Marqusee and Dill, 1986; Martel et al., 1993; White et al., 1981). The diffusion coefficient of a given solute has been shown to vary with its location in the bilayer. Specifically, greater diffusion coefficients have been observed at the terminal ends of the alkyl chains than at the head-group region (Alper and Stouch, 1995; Bassolino-Klimas et al., 1993; Dix et al., 1978; Marrink and Berendsen, 1994). However, this explanation does not account for the observed behavior since a given probe (namely, BOD) is likely to have similar bilayer distribution profiles in both DMPC and DMPC/cholesterol systems. A second possible explanation is that cholesterol causes BOD to segregate laterally.

For example, the addition of cholesterol to DMPC bilayers causes certain proteins to segregate and exhibit reduced rotational diffusion (Cherry et al., 1980; Nigg and Cherry, 1979). However, it is not clear why BOD would segregate in a similar manner to these membrane proteins while the other probes did not, the likelihood of this occurring given the low concentrations of the probes in the bilayers (0.1 mol%), or the reason why this would slow down the lateral diffusion of this small probe. A third possible explanation is that the diffusion coefficient scales more precisely with molecular area or molecular volume than with molecular weight. However, since the sizes of the probes do not change from one lipid system to the other, this explanation does not account for the qualitative variations in the profiles observed in DMPC (Figure 4.3a) and DMPC/cholesterol (Figure 4.3b). Such variations suggest the need for more sophisticated models to describe small solute diffusion in lipid bilayer systems.

Figure 4.3b also shows the results of a least-squares regression of Eq. (4.9) applied to the DMPC/cholesterol diffusion data. 3.9 P was used as the bilayer viscosity, η_o, rather than the value of 0.75 P which describes DMPC bilayers, in order to account for the lower values of the diffusion coefficients. This viscosity was determined such that the ratio of the diffusion coefficients (calculated using Eq. (4.8)) of the largest probe, NBD-PE, in DMPC and DMPC/cholesterol was the same as the experimentally measured ratio of 4.3. The values of the empirical parameters, a and b, are 2.32×10^{-2} cm^2/sec and 2.48. Figure 4.3b shows that Eq. (4.9) describes well the molecular weight dependence of the diffusion coefficient in DMPC/cholesterol bilayers.

4.4.3 Molecular Weight Dependence of Lateral Diffusion in SCE Lipid Bilayers

The diffusion coefficients of DACM, BOD, NBD-dioct, NBD-dihexdec, and NBD-Chol in SCE lipid bilayers are plotted in Figure 4.3c versus the probe molecular weight. As observed in DMPC and DMPC/cholesterol bilayers, the diffusion coefficients in SCE bilayers decrease with increasing probe molecular weight. The values shown in Figure 4.3c however, are considerably lower than those for diffusion in DMPC and DMPC/cholesterol, by average ratios of 15 (±7) and 3.4 (±1.4), respectively. The ratio of the largest diffusion coefficient in SCE bilayers (that of DACM) to the smallest (that of NBD-dihexdec) is 7.6, which is considerably greater than the corresponding ratios in DMPC (2.4) and DMPC/cholesterol (4.4). Although this ratio constitutes only a rough indication of the molecular weight dependencies of diffusion in these three lipid systems, it does show that those lipid systems characterized by lower diffusion coefficients exhibit greater molecular weight dependencies. The reason for this may be that the diffusion coefficients of the smallest compounds (such as the molecular gas, O_2) are less sensitive to the effective viscosity of the system than are those of the larger compounds, and hence, the diffusion coefficient in more 'viscous' systems (SCE>DMPC/cholesterol>DMPC) increases to a greater extent with decreasing solute molecular weight. This conjecture is supported by literature data for a variety of systems, as discussed below.

The molecular weight dependence given by Eq. (4.9) nicely describes the SCE bilayer experimental data (Figure 4.3c). The value for the effective bilayer viscosity, η_o, used in this equation is 21.3 P. This viscosity was determined such that the ratio of the diffusion coefficients (calculated using Eq. (4.8)) of the two largest probes in SCE (NBD-dihexdec and NBD-Chol) with their diffusion

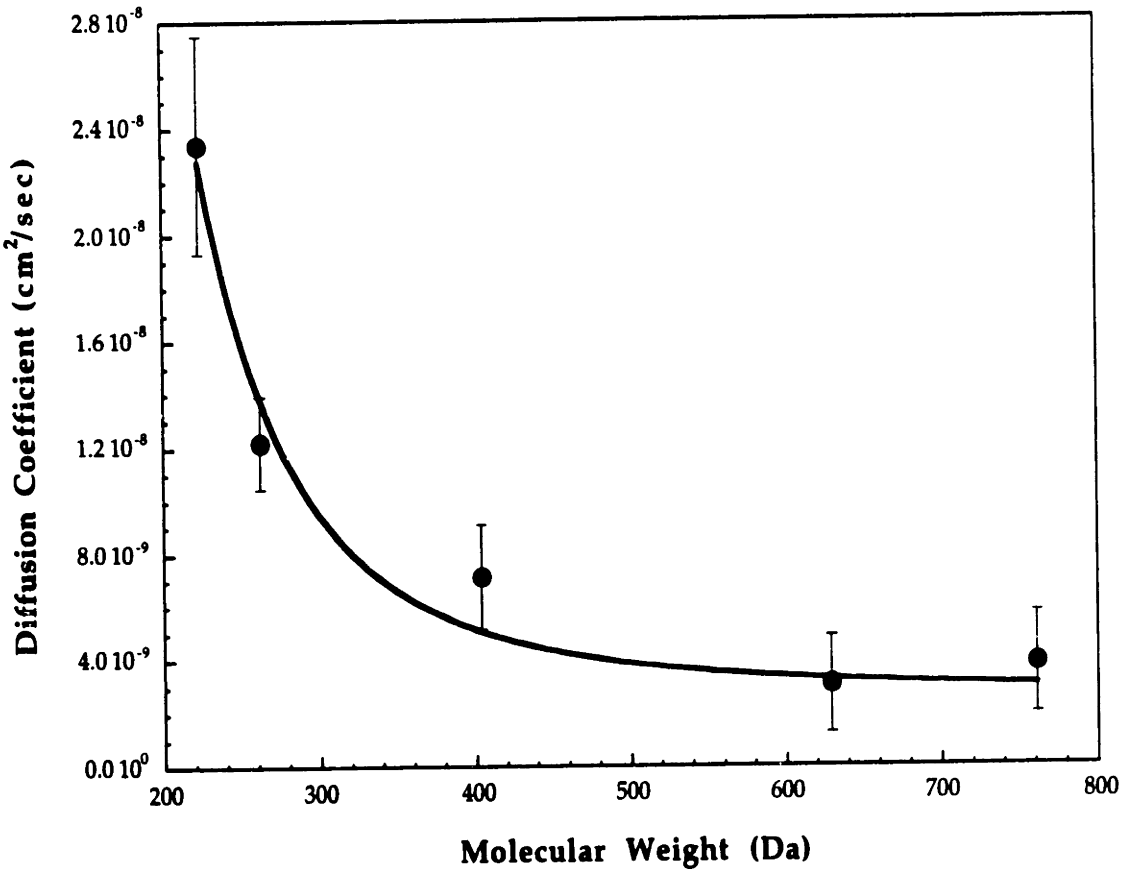

Figure 4.3c Diffusion coefficients of the fluorescent probes in SCE, as measured by the video FRAP technique at 27°C, versus the probe molecular weight. These data exhibit a distinct molecular weight dependence with the diffusion coefficients decreasing with increasing probe size. The line represents the semi-empirical model (Eq. (4.9)), which combines the strong size dependence of free-volume theory in the lower molecular weight regime with the weak size dependence of continuum theories in the larger molecular weight regime. The error bars represent standard deviations of the measurements.

coefficients in DMPC was the same as the experimentally measured ratio of 24. For reference, note that the viscosity of glycerol is 11 P at 20°C (Bird et al., 1960). Caution should be exercised in interpreting these bilayer viscosities and in making comparisons with the viscosities of bulk fluids, such as glycerol. While the diffusion of large probes in lipid bilayers can be modeled in terms of a viscosity, this property has yet to be linked with the chemical structure of the lipids, and hence, represents an effective property of the bilayer (see Clegg and Vaz, (Clegg and Vaz, 1985) for a thorough critique of bilayer hydrodynamic theories). Free-area/free-volume theories can also effectively describe diffusion of lipid probes in bilayers under a variety of conditions (Almeida et al., 1992). The values of the empirical parameters, a and b, for the SCE diffusion data obtained using Eq. (4.9), are 13 cm^2/sec and 3.75, respectively. The value of, b, the exponent of Eq. (4.9), 3.75 (±0.83) is in agreement with the exponent previously obtained in describing SC permeabilities, 4.6 (Anderson and Raykar, 1989).

The predominant diffusion coefficient describing BOD-Chol diffusion in SCE bilayers, 1.25×10^{-9} cm^2/sec, corresponds to 78% of the diffusing species, as determined using the two-diffusion coefficient model (Eq. (4.6)). As BOD-Chol has a molecular weight of 787 Da, this value is consistent with the molecular weight dependence shown in Figure 4.3c. Interestingly, the diffusion coefficient of the smaller population, 1.59×10^{-8} cm^2/sec, is essentially the same as that of BOD-Chol in DMPC/cholesterol, 1.69×10^{-8} cm^2/sec. Various physical explanations have been proposed to rationalize the results of polymodal models in other complex bilayer systems, including (i) 'fast' probe diffusion along structural defects or partially disordered bands in single-component, gel phase DMPC bilayers (Derzko and Jacobson, 1980; Schneider et al., 1983), (ii) kinetic binding of proteins coupled with lateral diffusion (Huang et al., 1994), and (iii)

probe distribution between the inner and outer leaflets of erythrocyte membranes (Schroeder et al., 1991). However, these explanations are not applicable to diffusion in SCE lipids since: (i) the DMPC gel-phase represents a special case in that it is a highly ordered, single-component system, the transport characteristics of which are not observed even in two-component lipid systems, (Almeida et al., 1992; Almeida et al., 1992), let alone in SCE lipids, (ii) there is no physical basis for assuming that there is kinetic binding in the present work, as there is in previous studies with proteins (Huang et al., 1994), and (iii) there is no evidence that SCE bilayer leaflets exhibit the anisotropy observed in erythrocytes. Therefore, it is not clear whether the results for BOD-Chol in SCE, which suggest bimodal diffusion, are correctly capturing probe diffusion in two distinct domains of SCE lipids, or whether the results could be induced by some other mechanism.

Experiments on BOD-FA and BOD-Cer diffusion in SCE lipids did not exhibit the discernible exponential decays observed with the other probes and lipid systems, such as those shown in Figure 4.2, although qualitative observations of the bleach spots revealed that there was fluorescence recovery on a time-scale similar to those of the other probes in SCE lipids (~20-30 seconds). This apparent failure of the data to collapse into a discernible pattern when plotted against the frequency-scaled time indicates that phenomenon other than simple, homogeneous diffusion are affecting the recovery process. In contrast, qualitative observations of the NBD-PE bleach spot in SCE lipids revealed that there was very little fluorescence recovery even after more than 10 minutes. Similarly, the fluorescence decay plots of the NBD-PE experimental results showed that the noise of the data in the NBD-PE decay profiles was greater than any recovery that took place. One possible explanation for these results is that there are disclinations or domain boundaries within SCE lipid bilayers, and that

a given probe has to cross such boundaries in order to access more distant parts of the lipid structure. These crossings may involve transbilayer diffusion, also referred to as flip-flop for phospholipid molecules. Large, long-tailed lipids exhibit great difficulty in crossing bilayers (Homan and Pownall, 1988; Lipka et al., 1991), and hence, their recovery in these experiments could be significantly hindered by such boundary crossings. This conjecture could explain the results obtained for BOD-FA, BOD-Cer, and NBD-PE in SCE lipids. An analogous finding was made by Kitson et al., who examined palmitic acid in human stratum corneum using deuterium nuclear magnetic resonance, and concluded that the diffusion of palmitic acid effectively does not occur (Kitson et al., 1994). In contrast, small, lipophilic compounds have been shown to diffuse readily across lipid bilayers (Lieb and Stein, 1969), suggesting that boundary crossings in SCE lipids would not play a significant role in the diffusive recoveries of such probes as DACM, BOD, NBD-dioct, and NBD-dihexdec. Cholesterol is also able to diffuse across bilayers much better than phospholipid molecules (Bittman, 1993), suggesting that NBD-Chol and BOD-Chol are similarly unhindered by any potential domain boundaries in SCE lipids. Hence, the experimental observations on the nine probes in SCE lipids are at least in qualitative agreement with this mechanism, although additional studies are needed to fully elucidate these issues.

The transport of molecular oxygen in human stratum corneum and model SC lipids has been examined using electron paramagnetic resonance (EPR) spectroscopy (Hatcher and Plachy, 1993). The effective diffusion coefficient in the SC, 3×10^{-7} cm^2/sec, was not corrected for SC tortuosity. Hence, the diffusion coefficient measured in the model SC lipids, 2×10^{-6} cm^2/sec, represents a better estimation of the true oxygen diffusion coefficient. This relatively large diffusion

coefficient illustrates the significant molecular weight dependence of diffusion in the very low molecular weight regime (<200 Da).

4.5 Comparison of the Lateral Diffusion Coefficient-Molecular Weight Dependence of Small Probes in SCE and Model Lipid Bilayer Systems

The probes examined in this study exhibit increasing lateral diffusion coefficients with decreasing probe molecular weight, down to 223 Da (DACM) (Figure 4.3). The extent to which this trend continues for even smaller probes cannot be discerned from these data, nor is it likely to be determined using the FRAP technique due to the lack of smaller (<223 Da), lipophilic, fluorescent probes which can absorb and emit light at appropriate wavelengths. Fortunately, lateral diffusion coefficients for several small molecules have been determined using other techniques. A summary of literature values of various lipid and non-lipid probes in DMPC fluid bilayers ($T>T_m$) are shown in Table 4.3. Table 4.3 also shows the lateral diffusion coefficients corrected to 30°C using the activation energies reported in the same reference in which the diffusion coefficients are reported, or using the typical value of 7.4 kcal/mole. 7.4 kcal/mole is the average of the activation energies of diffusion of 1-methylpyrene (7.0 kcal/mol, (Van den Zegel et al., 1984)), NBD-PE (8.1 kcal/mol, (Almeida et al., 1992); 6.9 kcal/mol, (Chang et al., 1981)), and 3,3'-dioctadecyloxacarbocyanine iodide (7.6 kcal/mol, (Derzko and Jacobson, 1980)). Table 4.3 illustrates the sparsity of lateral diffusion measurements of small probes in DMPC, and the lipid nature of the majority of these probes. Nevertheless, DMPC is one of the most studied lipid bilayer systems and, hence, these data provide one of the clearest portraits of small probe lateral diffusion (Table 4.3).

Lateral diffusion coefficients, including data presented in this chapter (Table 4.2; corrected to 30°C using an activation energy of 7.4 kcal/mol) and taken from the literature (Table 4.3), are shown in Figure 4.4 as a function of probe molecular weight. The top line represents the results of a least-squares regression using Eq. (4.9) to all the DMPC data reported in Tables 4.2 and 4.3, and describes the data well. Also shown in this figure are the results presented in the chapter for probe diffusion in DMPC/cholesterol (Table 4.2) and SCE (Table 4.4) lipid bilayer systems, as well as literature values for diffusion in DMPC/cholesterol 40-50 mol% (NBD-PE values are listed in the Results section; the diffusion coefficient for molecular oxygen was determined in the same manner as that for molecular oxygen in DMPC bilayers (see Table 4.3)) and in SCE (molecular oxygen, discussed above). The middle and bottom lines in Figure 4.4 represent the regressions using Eq. (4.9) of the total data sets for the DMPC/cholesterol and SCE lipid systems, respectively, and describe these data reasonably well.

The lateral diffusion coefficients for probes smaller than ~200 Da increase by orders of magnitude in DMPC, DMPC/cholesterol and SCE bilayer systems (Figure 4.4) (note that the value for molecular oxygen in DMPC, 1.8×10^{-5} cm^2/sec, is off the scale). This suggests that the 2.4-fold to 7-fold increases observed for DACM (223 Da) over larger probes in DMPC, DMPC/cholesterol, and SCE (Figure 4.3) represent the beginnings of the low molecular weight regime which is characterized by this strong molecular weight dependence. Diffusion experiments performed in other single component phospholipid bilayer systems support the findings in Figure 4.4 that small probes (molecular weights of less than ~200 Da) diffuse very rapidly relative to larger probes. Dix and Diamond (Dix et al., 1978) examined diffusion of four small probes in dipalmitoyl-lecithin (DPL) bilayers using ESR spectroscopy at 50°C: di-t-butyl

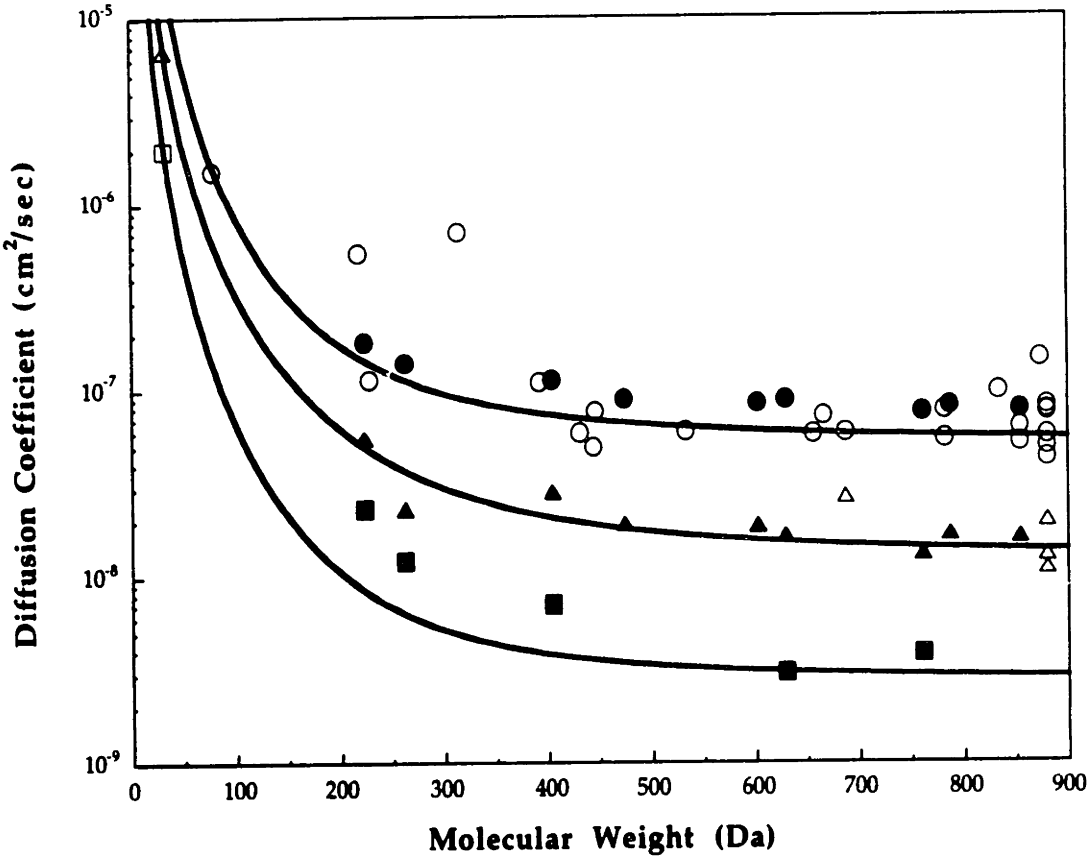

Figure 4.4 Comparisons of the dependencies of lateral diffusion coefficients on molecular weight in DMPC fluid phase bilayers (●, ○), DMPC/cholesterol (40-50 mol% cholesterol) bilayers (▲, △) and SCE bilayers (■, □). The filled symbols represent measurements presented in this paper, and the open symbols represent literature data (see Table 4.3 for details on the DMPC literature data, and the text for details on the DMPC/cholesterol and SCE literature data). All DMPC data points were corrected to 30°C (see Table 4.3 for details) The lines are the results of least-squares regressions of the semi-empirical model (Eq. (4.9)) to the combined data sets for these lipid systems, using T=30°C and η_0=0.75, 3.9, and 21.3 P for the effective viscosities of DMPC, DMPC/cholesterol, and SCE bilayers, respectively.

nitroxide (144 Da), 2,2,6,6-tetramethylpiperidine-1-oxyl (TEMPO, 156 Da), carbonyl-TEMPO (170 Da), and benzoyloxy-TEMPO (276 Da). Their reported diffusion coefficients, 1.0×10^{-6}, 0.9×10^{-6}, 0.7×10^{-6}, and 0.6×10^{-6} cm^2/sec, respectively, agree very well with the trend shown in Figure 4.4 for DMPC bilayers. Likewise, the diffusion coefficient of pyrene (202 Da) measured in dipalmitoylphosphatidylcholine (DPPC) bilayers by the fluorescence decay technique, 1.2×10^{-6} cm^2/sec at 50°C, is also in good agreement with the trend of DMPC in Figure 4.4 (Daems et al., 1985).

While the molecular weight dependencies for DMPC, DMPC/cholesterol, and SCE lipid bilayer systems appear to be analogous (Figure 4.4), it is still not clear what simple model bilayer system, if any, constitutes a reasonable model of SCE bilayers. The results in Figures 4.3 and 4.4 suggest that DMPC is not a quantitatively accurate model of SCE bilayers, as their diffusion coefficients differ by an average of 15-fold. Diffusion coefficients in DMPC/cholesterol and SCE bilayers also differ, but only by an average factor of three. Several other findings suggest that this difference may not be terribly significant, and that DMPC/cholesterol bilayers may be a reasonable model of SCE bilayers. First, a comparison of SCE diffusion data with that of gel-phase ($T<T_m$) DMPC bilayers, which is another potential model of the SCE system, suggests dramatic differences. For example, the average NBD-PE diffusion coefficient in gel-phase DMPC bilayers ($17.5 \leq T \leq 20.5$°C) is 1.6×10^{-10} cm^2/sec (Balcom and Petersen, 1993; Chang et al., 1981; Fahey and Webb, 1978; Rubenstein et al., 1979; Smith and McConnell, 1978; Wu et al., 1977), which is one hundred-fold lower than that in DMPC/cholesterol bilayers (Table 4.2), corresponding to a 30-fold difference with diffusion in SCE bilayers. Two recent studies of the structural aspects of SCE bilayers have also noted striking similarities between SCE lipids and phospholipid/cholesterol bilayers (Kitson et al., 1994; Ongpipattanakul et al.,

1994), again suggesting that SCE bilayers may be reasonably modeled by DMPC/cholesterol bilayers.

Additional evidence supporting the similarity of SCE and DMPC/cholesterol model bilayers is presented in Chapter 5. Specifically, the experimentally measured partition coefficients for a series of lipophilic drugs, between SCE lipids and water and between DMPC/cholesterol liposomes and water, are shown to correlate well (Figure 5.6). The value of the exponent in a power-law equation relating the partition coefficients in these two systems, β=0.97 ±0.01, was obtained by performing a least-squares regression on the partitioning data. This value of β, 0.97, is nearly unity, and illustrates the quantitative similarity of the partition coefficients made with these two systems.

4.6 Conclusions

The importance of lateral diffusion to the macroscopic stratum corneum permeability has yet to be elucidated, due in large part to the absence of a clear understanding of the nature of small solute diffusion in lipid bilayers. The results and analysis presented in this chapter, which establish the magnitude of diffusion in SCE lipids as well as the qualitative molecular weight dependence of lateral diffusion, are an important step in this direction. Chapter 6 utilizes these data to evaluate the contribution of lateral diffusion to transdermal transport, at both qualitative and quantitative levels.

Chapter 5

Partition Coefficient Measurements and Modeling

5.1 Introduction

The extent to which a given solute is lipophilic (hydrophobic) or hydrophilic can be quantified by measuring the equilibrium distribution, that is, the partition coefficient, of the solute between two immiscible fluid phases, one which is organic and the other which is aqueous. Partition coefficients have been measured for tens of thousands of compounds using a variety of different organic phases, including olive oil, chloroform, and octanol, many of which have been compiled in one list (Hansch and Leo, 1979). Efforts to find a simple organic fluid which mimics the partitioning behavior of biological systems, such as phospholipid cell membranes, have shown n-octanol to be the best (Leo et al., 1971). In fact, octanol/water partition coefficients, $K_{o/w}$, have been measured and reported for thousands of compounds (Hansch and Leo, 1979), including many drugs (see Tables 6. 1 and 6.2).

The partitioning of solutes into the lipids of the stratum corneum is an important aspect of transdermal transport. Stratum corneum lipid/water partition coefficients vary by orders of magnitude, depending upon the physicochemical properties of the solute. Yet, direct measurements of stratum corneum extracted lipid/water partition coefficients, K_{sce}, are experimentally cumbersome and financially expensive, due to the large quantities of skin needed

to extract sufficient quantities of lipids for such measurements. In this chapter, several different experimental model systems, including octanol/water, stratum corneum model (SCM) liposomes, dimyristoylphosphatidylcholine (DMPC) liposomes, and DMPC/cholesterol liposomes, were examined as possible models of the stratum corneum lipids and the associated partition coefficients, K_{sce}. These four systems all provided reasonable correlations with the K_{sce} data.

5.2 Materials and Methods

^{3}H-aldosterone, ^{3}H-corticosterone, ^{3}H-estradiol, ^{14}C-glucose, ^{3}H-hydrocortisone, ^{14}C-lidocaine, ^{14}C-napthol, ^{3}H-oubain, ^{3}H-progesterone, ^{14}C-sucrose, and ^{3}H-testosterone were obtained from DuPont/NEN (Boston, MA) and American Radio Chemical (St. Louis, MO). The radiolabeled drugs were purchased in a solvent, typically ethanol, which was evaporated prior to use in order to remove any tritium which had reverse-exchanged onto the solvent. Non-radiolabeled estradiol (>99.5%) was obtained from Sigma Chemical Co. (St. Louis, MO), and n-octanol (99.5%) was obtained from Mallinckrodt (Phillipsburgh, NJ). Dimyristoylphosphatidylcholine (DMPC) was obtained from Avanti Polar Lipids (Alabaster, AL). DMPC was stored in chloroform at -20°C. Cholesterol was obtained from Sigma Chemical (St. Louis, MO) and stored at -20°C. All lipids were used without further purification. Stratum corneum extracted lipids were obtained from human stratum corneum, as described in section 2.2.

5.2.1 Partition Coefficient Measurements and Extractions Performed with Octanol and Water

Octanol/water partition coefficients were measured primarily using radiolabeled solutes, except for the case of estradiol, which was measured using both the radiolabeled and the non-radiolabeled forms of the drug. Radiolabeled solutes were rotary-evaporated to remove any tritium which may have reverse-exchanged onto the solvent. The solute (radiolabeled or non-radiolabeled) was then dissolved in either octanol or water, and added to a separatory funnel. Appropriate volumes of octanol and pH 7.4 phosphate buffered saline (PBS) solution or distilled water were then added. The funnel was mixed by inversion 100 times, so as to facilitate solute equilibration between the two phases without promoting the formation of an emulsion, and allowed to settle for 24 hours or more at room temperature (Leo et al., 1971). Aliquots of octanol and the aqueous medium were then collected and centrifuged at 1000 rpm (212xg) for 10 minutes. Samples from each phase were taken and counted using a liquid scintillation counter or high-performance liquid chromatography (HPLC) analysis (see Chapter 2 for details on the HPLC analysis). All measurements were made in triplicate. The apparent octanol/water partition coefficient value, $K^a_{o/w}$, was taken to be the ratio of the volume-based concentration of each phase. The relationship between $K^a_{o/w}$ and the actual octanol/water partition coefficient, $K_{o/w}$, for the various compounds is discussed further below and in section 6.3.

The $K_{o/w}$ measurements in the case of hydrophilic solutes, such as sucrose, glucose, and oubain, were found to be independent of the aqueous and octanol volumes used, as expected, based on general thermodynamic considerations (see results in section 5.3.6). The $K_{o/w}$ values of some of the hydrophobic solutes examined, such as various steroids, were obtained from the analysis of the $K^a_{o/w}$

data which were obtained by repeated extractions of each solute using octanol and water. Specifically, radiolabeled-solute dissolved in large volumes (60-900 ml) of water were combined with much smaller volumes of octanol (5-20 ml), and then mixed. Samples of each phase were centrifuged and analyzed to determine the corresponding apparent partition coefficient, $K^a_{o/w}$. The aqueous phase was discarded, and fresh buffer or water was then added. This procedure was repeated between 6 and 13 times for each solute.

5.2.2 Interpretation of the Octanol/Water Extraction Data

Radiolabeled drug preparations often contain impurities, some of which are also radiolabeled (see section 5.3.1 for further discussion). The presence of these impurities was found to be qualitatively consistent with the extractions performed using octanol and water. Moreover, a technique was also developed, and described below, which allows for the characterization of the impurity, as well as for the determination of the actual octanol/water partition coefficient of the drugs based upon the results of the extraction experiments.

In the analysis that follows, each drug is assumed to contain only one impurity which is radiolabeled. The results of the analysis indicated that this was a reasonable assumption for all the drugs examined, except hydrocortisone, which appeared to contain both a hydrophilic and a hydrophobic impurity. The basic idea behind the analysis is that the value of $K^a_{o/w}$ can be predicted from knowledge of several experimental parameters, including the volumes of octanol, V_o, and water, V_w, the value of the actual octanol/water partition coefficient of a given drug, $K^d_{o/w}$, as well as that of the impurity, $K^i_{o/w}$, and the mole fraction of the radiolabeled impurity, ε. A spreadsheet was developed, utilizing the equations below, which calculates the value of $K^a_{o/w}$ from the values of the

octanol and aqueous volumes utilized in the extraction, and the initial guesses of the values of $K^d_{o/w}$, $K^i_{o/w}$, and ε.

The relationships in the spreadsheet represented the basic relationships between the various system and drug parameters. For example, the amount of total amounts of impurity, N^i, and drug, N^d, present in a given experimental system can be expressed in terms of the total amount of radiolabeled compounds present in the system, N_t and ε by: $N^i = \varepsilon N_t$ and $N^d = (1-\varepsilon)N_t$. The amount of impurity in the octanol and aqueous phases, N^i_o and N^i_w, respectively, can be written in terms of a material balance on the impurity present in the system, that is, $N^i = N^i_o + N^i_w$, as well as in terms of the definition of the partition coefficient, namely,

$$K^i_{o/w} = \frac{C^i_o}{C^i_w} = \frac{N^i_o / V_o}{N^i_w / V_w} \tag{5.1}$$

Equation (5.1) can be rewritten to express N^i_o and N^i_w in terms of the measurable experimental quantities and parameters to be optimized, using the above mentioned relationships. Specifically,

$$N^i_o = \frac{\varepsilon N_t V_o}{V_o - \left(V_w / K^i_{o/w} \right)} \tag{5.2}$$

and

$$N^i_w = \frac{\varepsilon N_t}{K^i_{o/w}\left(V_o / V_w \right) - 1} \tag{5.3}$$

Similar expressions describe the amounts of drug in the octanol and aqueous phases, N_o^d and N_w^d, respectively, in terms of N_t, V_o, V_w, ε, and $K_{o/w}^d$, that is,

$$N_o^d = \frac{(1-\varepsilon)N_t V_o}{V_o - \left(V_w / K_{o/w}^d\right)} \tag{5.4}$$

and

$$N_w^d = \frac{(1-\varepsilon)N_t}{K_{o/w}^d\left(V_o / V_w\right) - 1} \tag{5.5}$$

Given Eqs. (5.2)-(5.5), the value of $K_{o/w}^a$ is easily calculated from the following expression:

$$K_{o/w}^a = \frac{\left(N_o^d + N_o^i\right)/V_o}{\left(N_w^d + N_w^i\right)/V_w} \tag{5.6}$$

The values of $K_{o/w}^a$ were initially calculated using Eq. (5.6) for each of the extractions performed with a given drug using guessed values of $K_{o/w}^d$, $K_{o/w}^i$, and ε. The actual values of $K_{o/w}^d$, $K_{o/w}^i$, and ε were then determined by minimizing the sum of the squares of the differences between the values of $K_{o/w}^a$ calculated using Eq. (5.6), and the experimentally measured $K_{o/w}^a$ values. The minimization was performed by the *Solver* feature on a Microsoft Excel spreadsheet.

5.2.3 Stratum Corneum Lipid/Water Partition Coefficient Measurements

Lipids from human stratum corneum were extracted and placed in a 5 ml vial (see section 2.2 for details). The solvent was removed by rotary evaporation at 40-45°C, and at least one hour of lyophilization, resulting in a dry lipid film on the inner surface of the lower portion of the vial. Typically, 1-3 milligrams of lipids were utilized per experiment. A buffer solution containing radiolabeled drug (~0.5 μCi/ml) was carefully added to the vial. 2.0 or 3.0 ml was typically sufficient to ensure that the entire lipid film was covered by solution. The system was allowed to equilibrate for 48 hours, with care being taken not to agitate the vials. Three samples were taken from the stock solute solution, as well as from the aqueous phase of the equilibrated vials, and the solute content was then determined by liquid scintillation counting. The partition coefficient of the solute between the extracted SC lipids and water was calculated using the following relationship:

$$K_{sce} = \frac{(C_i - C_f)V_w}{C_f V_l} \qquad (5.7)$$

where C_i is the initial aqueous solute concentration, C_f is the aqueous solute concentration after equilibration with the SC lipids, V_w is the volume of buffer added to the vial, and V_l is the volume of lipids, determined from the measured weight of the lipids and assuming a lipid density of 1 g/ml. Note that the amount of solute in the lipid phase was determined indirectly, by determining the difference in the aqueous solute concentration before and after equilibration. For several experiments, the solute content of the lipids was also determined

directly. Specifically, the entire aqueous phase was carefully pipetted away. Trace amounts of water remained, and were removed by gently tapping the vial on the bench top. The remaining lipids were dissolved in liquid scintillation cocktail (Aquasol-2, New England Nuclear) and analyzed for solute content. Partition coefficients calculated in this direct manner agreed with those calculated using the difference method, described above, to within the typical experimental error of about 35%.

5.2.4 Liposome/Water Partition Coefficient Measurements

5.2.4.1 Liposome Formation

DMPC and DMPC/cholesterol (40 mol%) liposomes were prepared by placing a known amount of the lipids, dissolved in chloroform, in a round-bottomed flask. The solvent was removed by rotary evaporation followed by lyophilization for at least one hour. A known amount of PBS pH 7.4, preheated to 40°C, was added to the flask, also preheated to 40°C. The final lipid concentration of these liposome systems was typically between 4 and 10 mg/ml, corresponding to an overall lipid content of typically 0.4-1% of the solution, by weight. The flask contents were annealed at 40°C for approximately 30 minutes, with periodic mixing to promote liposome formation.

Stratum Corneum model liposomes (SCM) were prepared by weighing out the individual lipid components in order to achieve a composition of 40% ceramides, 25% cholesterol, 25% palmitic acid, and 10% cholesterol sulfate, by weight, which is characteristic of the stratum corneum (see section 1.2.2). The lipid fractions were dissolved in chloroform:methanol (2:1 v/v) and combined in a round-bottomed flask. The solvent was removed by rotary evaporation

followed by lyophilization for at least 1 hour, resulting in the formation of a thin lipid film inside the flask. A known amount of Trizma pH 7.4 buffer, preheated to 80°C, was added to the flask, also preheated to 80°C. The final lipid concentration of the SCM systems was typically between 2 and 20 mg/ml. The flask contents were annealed at 80°C for approximately 30 minutes, with periodic mixing to promote liposome formation. The freeze-and-thaw technique was used to facilitate lipid incorporation, since mixing alone was insufficient to incorporate all the lipids into liposomes. Specifically, the lipid/buffer mixture was alternately frozen with liquid nitrogen (-196°C), and then rapidly heated to 80°C in a water bath. Sonication was also used on occasion to facilitate liposome formation.

5.2.4.2 Partition Coefficient Measurements with DMPC, DMPC/Cholesterol, and Stratum Corneum Model Liposomes

DMPC, DMPC/cholesterol, and SCM liposome solutions were mixed with radiolabeled solutes to achieve a final overall solute concentration of approximately 0.5 μCi/ml and a total lipid concentration of approximately 4-6 mg/ml. The DMPC and DMPC/cholesterol solutions were allowed to equilibrate for 24 hours or more in a water bath set at 25°C (±0.2°C). 4 ml of solution were centrifuged at 50,000 rpm (300,000xg; Beckman L-8 80-M Ultracentrifuge) and 25°C for approximately 2 hours. The supernatant was removed from the tube, leaving a tightly packed 'pellet' of liposomes on the bottom. Care was taken to ensure that the pellet was not disturbed so that the supernatant remained free from liposomes. As a result of this precaution, a small volume of supernatant was left with the pellet phase. The presence of this extra

supernatant in the pellet phase simply increased the already substantial fraction of water inherently present in the pellet, and was taken into account in the calculation of the partition coefficient. Three samples were taken from the supernatant phase and analyzed for ^{3}H or ^{14}C content utilizing a liquid scintillation counter, yielding the aqueous phase solute concentration, C_w.

SCM liposome partition coefficient experiments were performed in a manner similar to the DMPC and DMPC/cholesterol liposomes partition coefficient experiments, described above. The only difference was that the SCM experiments were performed at a lower temperature of 15°C (±0.2°C). This was due to the fact that SCM liposomes did not consistently pack into a uniform, tightly packed pellet when ultracentrifuged at 25°C. In other words, the supernatant in some of the SCM experiments contained liposomes, such that the true solute concentration in the aqueous phase, C_w, could not be measured. For these samples, six hours of ultracentrifugation at 25°C did not produce a tight pellet with a liposome-free supernatant. The source of the observed intersample differences, with respect to the ability of the liposomes to be packed into a pellet, is not clear. However, ultracentrifugation at 15°C consistently produced good liposome pellets and a clear supernatant, and was therefore established as the experimental condition for the SCM partition coefficient experiments.

The solute concentration in the liposome lipid bilayers, C_b, was determined in a more indirect manner since the pellet contains solute in the water, which is present both in the liposome core as well as outside of the liposomes. Specifically, the solute concentration in the pellet, C_p, is related to the solute concentrations in the bilayer, C_b, and in the water, C_w, by their respective volume fractions in the pellet, namely,

$$C_p = \left(\frac{V_b}{V_b + V_w}\right) C_b + \left(\frac{V_w}{V_b + V_w}\right) C_w \tag{5.8}$$

where V_b and V_w are the total volumes of the lipid bilayers and the water in the pellet, respectively. Note that the water solute concentration in the pellet is identical to that in the bulk supernatant, C_w, since the system is at thermodynamic equilibrium. The value of C_p can be determined experimentally, and V_b can be determined from the total amount of lipids in the sample and the bilayer density, which is assumed to be approximately unity. Therefore, only the volume of water in the pellet is left to be determined in order to be able to calculate C_b, using Eq. (5.8). The volume of water can be expressed in terms of the total pellet volume, V_p, namely,

$$V_w = V_p - V_b \tag{5.9}$$

The total pellet volume is then given by the ratio of the total solute content of the pellet, N_p, and the overall solute concentration in the pellet, namely,

$$V_p = {}^{N_p}\!/_{C_p} \tag{5.10}$$

where C_p is determined by taking pellet samples of known volumes, and N_p is determined by summing the amounts of solute in the pellet samples taken, with the amount of solute remaining in the pellet (note that liquid scintillation counting gives the amount of solute in the sample, such that no direct measurement of the volume of the unsampled pellet needs to be made). By combining Eqs. (5.8), (5.9), and (5.10), the value of the solute concentration in the bilayer, C_b, can be expressed as follows:

$$C_b = \left(\frac{N_p}{V_b}\right) - \left(\frac{N_p}{V_b C_p} - 1\right) C_w \qquad (5.11)$$

An additional step was needed in order to calculate the value of C_b, and hence, of the partition coefficient, since the ultracentrifugation of DMPC and DMPC/cholesterol liposomes produced heterogeneous pellets. These pellets, which were typically 40-100 mg in weight, were viscous and had an uneven distribution of water and lipid. Mixing the pellet proved ineffective, due to the viscosity of the pellet and the loss of pellet material on the stirring rod. Therefore, a known volume of water, V_a, (100 µl) was added to the pellet to reduce the viscosity of the pellet and allow for thorough mixing. Three 10 µl samples were then taken from the diluted pellet to determine the solute concentration, $C_{p,d}$. By noting that the total solute content is the same in both the original and diluted pellets, the solute concentration in the original pellet can be written as follows:

$$V_p = {}^{N_p}\!/_{C_{p,d}} - V_a \qquad (5.12)$$

where V_a is known (100 µl) and $C_{p,d}$ and N_p are determined by the method described above. Since the solute concentration in the original pellet is given by $C_p = N_p/V_b$, Eqs. (5.11) and (5.12) can be combined to express C_b in terms of known and experimentally measurable quantities. Specifically,

$$C_b = \left(\frac{N_p}{V_b}\right) - \left(\frac{N_p - V_a C_{p,d}}{V_b C_{p,d}} - 1\right) C_w \qquad (5.13)$$

The bilayer/water partition coefficient was taken as the ratio of C_b, determined using Eq. (5.13), and the value of C_w. At least three separate experiments were performed for each drug/liposome combination.

5.2.5 Correction for the Presence of an Impurity in Lipid/Water Partition Coefficient Measurements

The presence of low levels of radiolabeled impurities can affect, sometimes substantially, the apparent octanol/water partition coefficients of lipophilic compounds. These impurities can also affect the various lipid/water partition coefficients, including those made with SCE lipids and SCM, DMPC, and DMPC/cholesterol liposomes (K_{sce}, K_{scm}, K_{dmpc}, and K_{chol}, respectively). However, the impact that these impurities have on the apparent partition coefficients can be calculated given the characterization of the impurities, which was accomplished in the octanol/water extraction experiments, the results of which are shown in Table 5.1. The ability to correct for the presence of impurities is important since the physical parameters of the various lipid/water partition coefficient measurements are not conducive to repeated extractions. Specifically, the sampling procedure consumes a large fraction of the lipid material (up to 100% for the SCM, DMPC, and DMPC/cholesterol experiments), and only moderate amounts of the drug remains in the lipid phase, due to the very small volumes of lipids utilized (~2-20 µl per experiment, which is about 1000-fold less than the volumes of octanol used).

The true partition coefficient of a drug in a particular lipid system (K^d, which represents either K_{sce}, K_{scm}, K_{dmpc}, or K_{chol}) can be expressed as a function of the experimental parameters (the volume of the lipid phase, V_l, and the volume of the aqueous phase, V_w), the characteristics of the impurity (the

lipid/water partition coefficient of the impurity, K^i, and the mole fraction of impurity, ε), and the experimentally measured apparent partition coefficient, K^a. Specifically,

$$K^d = \frac{K^a\left(V_l K^i + V_w\right) + \left(\frac{\varepsilon}{1-\varepsilon}\right)\left[V_w\left(K^a - K^i\right)\right]}{\left(V_l K^i + V_w\right) + \left(\frac{\varepsilon}{1-\varepsilon}\right)\left[V_o\left(K^i - K^a\right)\right]} \tag{5.14}$$

Equation (5.14) was obtained by combining the equations which define the basic system parameters, namely,

$$N_t = N^d + N^i \tag{5.15}$$

$$K^a = \left(\frac{C_l^a}{C_w^a}\right) = \frac{C_l^d + C_l^i}{C_w^d + C_w^i} \tag{5.16}$$

and

$$C_l^d = C_w^d K^d \tag{5.17}$$

where C denotes concentration, N is the amount of radiolabeled material (in μCi), t denotes total, a denotes apparent (that is, experimentally measured), l denotes lipid, w denotes water, d denotes drug, and i denotes impurity.

The values of K^i for the drugs in the various lipid systems were calculated from their octanol/water partition coefficients, shown in Table 5.1, using a power law relationship. Specifically,

$$K^i = \left(K_{o/w}^i\right)^{\beta} \tag{5.18}$$

where β was determined empirically. Specifically, an estimate of β was first made for each of the lipid systems (SCE, SCM, DMPC, and DMPC/cholesterol), allowing the estimation of the impurity lipid/water partition coefficient, K^i, using Eq. (5.18). Given the estimates of K^i for each of the drugs, the corrected lipid/water partition coefficients for the drugs were then calculated using Eq. (5.14). A least squares regression of the corrected drug partition coefficients was performed with their corresponding octanol/water partition coefficients, using Eq. (5.18), which yielded a revised value of β. In general, the corrections for the contaminants were small, and only two iterations on β were required to obtain a self-consistent value. The values of β determined by, and utilized in, this analysis are 0.76, 0.70, 0.92, and 0.72, for SCE, SCM, DMPC, and DMPC/cholesterol lipid systems, respectively. These values of β, which are less than unity, indicated that the drugs partition into the lipid systems to a lesser degree than they do into octanol. This is not surprising since the hydrophobic bilayer interior is considerable more ordered than the bulk fluid phase of octanol, and hence, is less able to accommodate exogenous species.

5.3 Results and Discussion

5.3.1 Octanol/Water Partition Coefficient Measurements and Impurity Corrections

The partition coefficient is an intensive thermodynamic property of a given system. The partition coefficient of a given solute depends upon the physicochemical properties of the solute, the experimental temperature, and the characteristics of the two immiscible phases, but should not depend on macroscopic system parameters, such as the volumes of the two coexisting

phases. However, results of preliminary octanol/water partition coefficient measurements performed with several radiolabeled, lipophilic compounds exhibited a dependence on the volumes of the octanol and water phases that were used. One possible mechanism which might account for these observations is that the radiolabeled solute, which is present in trace quantities, adsorbs onto the surfaces of test-tubes, pipette tips, separatory funnels, and other equipment with which it came in contact. To test this hypothesis, radiolabeled drug solutions were placed in contact with various pieces of glass and plastic laboratory equipment. After several hours, the solution was removed and the pieces of equipment were subsequently washed many times with water, ethanol, and acetone in order to remove any drug which had been adsorbed. These washings were then analyzed by liquid scintillation counting. The washings contained essentially no radiolabeled drug, suggesting that adsorption was not a major factor.

A second possible explanation for the dependence of $K^a_{o/w}$ on the macroscopic system parameters is that trace amounts of radiolabeled impurities may be affecting the partition coefficient measurements. To the author's best knowledge, the impact of impurities on partition coefficient measurements made with radiolabeled probes has not been addressed in the literature. However, the idea is appealing for several reasons. The manufacturers' specifications for the commercially obtained radiolabeled drugs (DuPont/NEN, and American Radiolabeled Chemicals, Co.) typically cite purities of 97-99%, indicating that 1-3% of the radiolabel probes are on compounds other than those which are desired. These other radiolabeled-compounds are referred to as *impurities* in this chapter. Moreover, many radiolabeled drugs are relatively unstable, and degrade over time due to chemical decomposition as well as atomic decay of the radiolabel probe itself (that is, tritium or carbon-14 atoms). This degradation can

further increase the impurity concentration in the sample. Since an impurity will generally have different physicochemical properties from those of the drug, the partition coefficient of the impurity will be different than that of the drug. Therefore, impurities will necessarily alter partition coefficient measurements made using radiolabeled drugs, with the extent of their effect left to be determined.

Figures 5.1 and 5.2 show the results of a series of extractions performed with ^{3}H-aldosterone and ^{3}H-estradiol, respectively, where the value of $K^a_{o/w}$ after each successive extraction is plotted against the ratio of the total volume of water used in the series of extractions, V_w, to the actual volume of octanol used in a given extraction, V_o. Although the value of $K^a_{o/w}$ is not unique for a given value of V_w/V_o, it is nevertheless useful for illustrative purposes. That is, V_w/V_o provides a semi-quantitative indication of the extent of extraction for a particular system, with large values of V_w/V_o indicating that large aqueous or small octanol volumes were used, that many extractions were performed, or that some combination of these was employed. Figure 5.1 shows that $K^a_{o/w}$ is essentially constant for the first four extractions performed. The fifth and sixth extractions were performed with large volumes of water (~900 ml), and produced $K^a_{o/w}$ values that were much larger. This profile suggests the presence of an impurity which is more hydrophobic than aldosterone. This impurity did not substantially affect the value of $K^a_{o/w}$ until substantial extractions were performed. In essence, the octanol/water extractions were purifying the impurity in the octanol phase. In contrast, Figure 5.2 shows that substantial extractions were required with the sample of estradiol to remove the contaminant to such a degree that $K^a_{o/w}$ became equal to the actual value for estradiol. This profile is consistent with an impurity that is lipophilic, but to a lesser degree than estradiol. Figures 5.1 and 5.2 also show the comparison of the

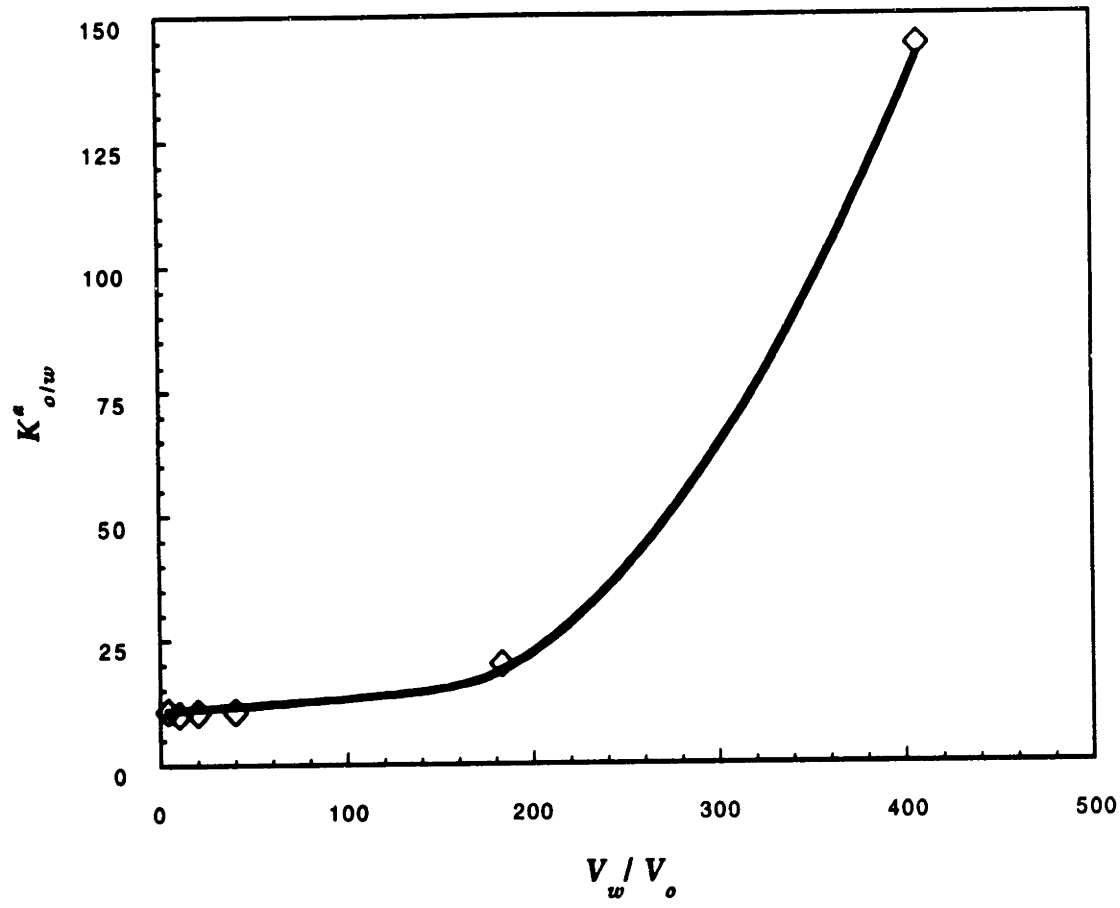

Figure 5.1 Extraction of ^{3}H-aldosterone using octanol and water. The $K^a_{o/w}$ values are plotted versus the ratio of the cumulative total volume of water used in the extractions, V_w, to the actual volume of octanol in a given extraction, V_o. The volume of octanol decreased slightly with each successive extraction, due to sampling and dissolution in the discarded aqueous phase. The line represents the results of a three-parameter least squares minimization which determines the $K_{o/w}$ values of aldosterone (11) and of the impurity (30,000), as well as the mole-fraction of the impurity in the sample (ε=1.3%) utilizing Eq. (5.6). The model appears to capture the partition coefficient of aldosterone, observed at low values of V_w/V_o, when the low-level contaminant is insignificant, as well as at high values of V_w/V_o, when the aldosterone has been largely extracted and the impurity remains.

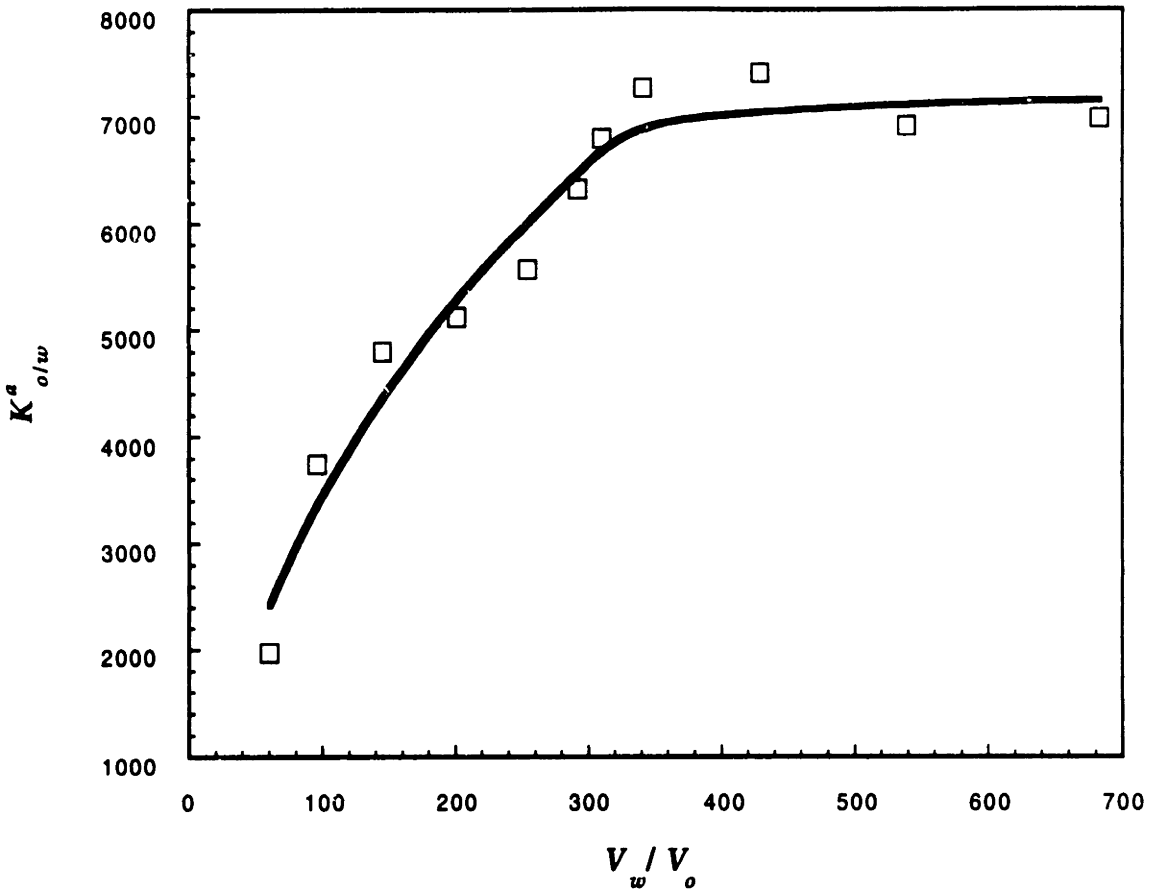

Figure 5.2 Extraction of ^{3}H-estradiol using octanol and water. The $K^a_{o/w}$ values are plotted versus the ratio of the cumulative total volume of water used in the extractions, V_w, to the actual volume of octanol in a given extraction, V_o. The volume of octanol decreased slightly with each successive extraction, due to sampling and dissolution in the discarded aqueous phase. The line represents the results of a three-parameter least squares minimization which determines the $K_{o/w}$ values of estradiol (7195) and the impurity (82), as well as the mole fraction of the impurity in the sample (ε=3.3%) using Eq. (5.6). The plateau of the $K^a_{o/w}$ for large V_w/V_o values indicates the removal of the impurity and the actual $K_{o/w}$ value of estradiol. The impurity is present at levels (3.3%) consistent with the specifications of the manufacturer (DuPont/NEN). Large volumes of water were used in the extractions (~900 ml), which tended to deplete the octanol volume, and required occasional replenishing of it.

experimentally measured (open symbols) and calculated values (lines), using Eq. (5.6), of $K^a_{o/w}$ for the cases of ^{3}H-aldosterone and ^{3}H-estradiol. In both figures, the profiles calculated using Eq. (5.6) agree well with the experimental measurements. Similar profiles were observed with the other lipophilic drugs examined.

The results of the analysis on the octanol/water extraction experiments for several lipophilic drugs are shown in Table 5.1. Between 6 and 13 extractions were performed for each drug. Also shown in Table 5.1 are the values of $K^i_{o/w}$ and ε for each drug. The mole fractions of impurity, ε, are all relatively low, averaging 2.6%. These low values are physically reasonable and consistent with the manufacturers' specifications. The values of $K^i_{o/w}$ are all reasonable. In the cases of aldosterone, corticosterone, and hydrocortisone, the least squares minimization calculated what should be considered as limiting values of $K^i_{o/w}$. That is, this analysis clearly indicates that the values of $K^i_{o/w}$ for aldosterone and hydrocortisone are much larger than those of the actual drugs (that is, $K^i_{o/w}>>33$), while their exact values can not be precisely

determined due to the limited number of extractions performed. Likewise, the value of $K^i_{o/w}$ for corticosterone is much less than that of the drug (that is, $K^i_{o/w}<<81$), while its precise value is also not clear. Interestingly, the corrections made to the experimentally measured partition coefficients using corticosterone and hydrocortisone with the other lipid systems (see Tables 5.2, 5.3 5.4, 5.5) based upon this contaminant analysis are not strongly influenced by the exact values of $K^i_{o/w}$, while the correction for aldosterone is (see section 5.3.2 for further discussion).

Also shown in Table 5.1 are literature values for the octanol/water partition coefficient measurements for these drugs compiled by Hansch and Leo (1979). Most values are in good agreement with the literature data. Estradiol is

Table 5.1 $K_{o/w}$ **measurements and impurity characterization.**

Drug	$K_{o/w}$ [a] (literature)	$K_{o/w}$	n	Impurity	
				$K_{o/w}$	ε
Aldosterone	35	11	6	30000	1.3%
Corticosterone	87	81	8	0	1.7%
Estradiol	495	7200	11	62	3.3%
Hydrocortisone [c]	34	33	13	10^5	0.6%
				1.0	6.4%
Lidocaine (pH 7.4)	44 [b]	207	10	6.9	6.1%
Napthol	692	896	6	n.d.	n.d.
Progesterone	5890	5480	10	80	2.5%
Testosterone	2040	1830	8	9.4	1.5%

n is the number of extractions utilized to calculate the $K_{o/w}$ values for the drugs and the impurities, as well as the mole fractions of impurity, ε. No impurity was detected (n.d.) by the extractions of ^{14}C-napthol. [a] Obtained from Hansch and Leo (1977), unless otherwise noted. [b] Strichartz et al., 1990. [c] Extractions with ^{3}H-hydrocortisone showed the presence of both a hydrophilic impurity ($K_{o/w}$=1.0, ε=6.4%) and a hydrophobic impurity ($K_{o/w}$~10^5, ε=0.6%). The calculated octanol/water partition coefficients of aldosterone and hydrocortisone were very large (3×10^4 and 10^5, respectively), and are likely over estimates of the actual values.

the primary exception to this, with the value determined from the extraction profile shown in Figure 5.2, 7195, being more than ten-fold greater than the literature value, 495. However, the additional experiments performed with unlabeled estradiol using HPLC analysis resulted in an octanol/water partition coefficient value of 7400, in good agreement with the results shown in Figure 5.2. As the citation from Hansch and Leo for the 495 value does not describe the experimental details, it is not possible to determine why this value is different.

5.3.2 Stratum Corneum Extracted Lipid/Water Partition Coefficients and Impurity Corrections

The results of partition coefficient experiments performed with extracted stratum corneum lipids (SCE) are shown in Table 5.2 (K_{sce}(uncorrected)). These values range from 19 (aldosterone) to 1020 (progesterone), with standard deviations of approximately 30-40%. Also listed in Table 5.2 are the corrected values of K_{sce}, obtained through the use of Eq. (5.14). The significance of this correction is most clearly seen by the ratio of the corrected to uncorrected partition coefficient values, f. Specifically, values of f are mostly between 1.00 (that is, no substantial correction was produced by the use of Eq. (5.14)) and 1.05 (that is, a 5% correction). Given that the error associated with these measurements is 30-40%, these corrections of 5% or less are insignificant.

The reason why some of the impurities exhibited significant effects in the case of the octanol/water partition coefficient measurements but do not in this case (with the exception of aldosterone, discussed below) relates to the total amount of drug that partitions into the octanol or lipid phase. For example, the vast majority of estradiol (in terms of μCi) lies in the octanol phase of the octanol/water experiments under the conditions described above, leaving very

Table 5.2 Partition coefficient measurements of various drugs between extracted stratum corneum lipids and water (K_{sce}).

Drug	K_{sce} (uncorrected)	n	S.D.	K_{sce} (corrected)	f
Aldosterone	19	6	33%	8	0.43
Corticosterone	32	7	26%	33	1.02
Estradiol	172	8	38%	177	1.03
Hydrocortisone	—	—	—	—	—
Lidocaine (pH 7.4)	23	2	38%	24	1.05
Napthol	954	3	11%	954	1.00
Progesterone	1020	3	48%	1060	1.05
Testosterone	80	6	38%	81	1.02

K_{sce} (uncorrected) values represent the average of n measurements. S.D. is the standard deviation. Values of K_{sce} (corrected) were calculated using the characteristics of the impurities, shown in Table 5.1. K_{sce} values for the impurities were calculated from: $K^i_{sce} = \left(K^i_{o/w}\right)^{0.76}$. f is the ratio of K_{sce} (corrected) to K_{sce} (uncorrected).

little estradiol (in terms of μCi) in the aqueous phase. As such, the relatively small quantities (3.3%) of the less hydrophobic impurity ($K_{o/w}$=82) raise the total concentration of radiolabeled compounds in the *aqueous phase* sufficiently to have an impact. In contrast, the volumes of the organic phase were 1000-fold smaller in the lipid experiments as compared to those used in the octanol experiments. As a result, the amount of estradiol present in the aqueous phase was large relative to the amount of impurity in the aqueous phase, resulting in the small correction shown in Table 5.2.

Use of Eq. (5.14) for aldosterone adjusts its SCE/water partition coefficient by more than two-fold. Although this correction is of the same order as the standard deviations, it is substantially greater than those for the other drugs. The corrections of the aldosterone partition coefficients in the other lipid systems (see Tables 5.3, 5.4, and 5.5) are similarly large. This is due to: (i) the large partition coefficient determined for the impurity (30,000), and (ii) the small experimental lipid/water partition coefficient value (19). The large impurity partition coefficient suggests that nearly all of the impurity is present in the lipid phase. Even though the contaminant mole fraction is small (1.3%), the contaminant still accounts for a large fraction of the total radiolabeled compound in the lipid system, resulting in a significant correction. However, the exact $K_{o/w}$ value of the impurity in this case should be viewed with caution, since the values of $K^a_{o/w}$ of aldosterone, shown in Figure 5.1, go only as high as 150. Clearly, more extractions would be needed to clarify the exact value of the partition coefficient of the impurity. In fact, since very few compounds have partition coefficient values as high as 30,000 (see Tables 5.1 and 5.2), it seems likely that this is an overestimation, and hence, that the corrections are excessively large. Therefore, the corrections for the aldosterone lipid/water partition coefficient experiments

should be viewed with caution, yet also serve as the exception which illustrates the soundness of the other corrections.

Partition coefficients for a given set of solutes measured with two different experimental systems, each containing an organic fluid and water, are typically related through a power-law relationship given by:

$$K = K_{o/w}^{\beta} \tag{5.19}$$

where K represents the partition coefficient with one experimental system, $K_{o/w}$ represents the partition coefficient in the often utilized octanol/water system, and β is an empirical parameter (Leo et al., 1971). Figure 5.3 shows the values of the corrected SCE lipid/water partition coefficients plotted against $K_{o/w}$. Also shown in this figure are the data for a series of hydrocortisone esters reported by Anderson et al. (1988). These data obey the expected power-law relationship of Eq. (5.19) with the value of β (0.76) determined by a least-squares regression. The 0.76 value compares favorably with previously reported values of 0.71 (Potts and Guy, 1992), 0.74 (Bunge and Creek, 1995), 0.75 (Morimoto et al., 1992), and 0.86 (Anderson and Raykar, 1989). The previous β values were deduced from regressions on sets of permeability, P, data using equations which express P as a functional of the physical properties of the solutes, including their $K_{o/w}$ values and molecular weights, MW. For example, Potts and Guy (Potts and Guy, 1992) fit the permeabilities compiled by Flynn (Flynn, 1990) to the equation:

$$\log(P) = \beta \log(K_{o/w}) - \gamma(MW) + \delta \tag{5.17}$$

where MW is the solute molecular weight, and γ and δ are correlative parameters.

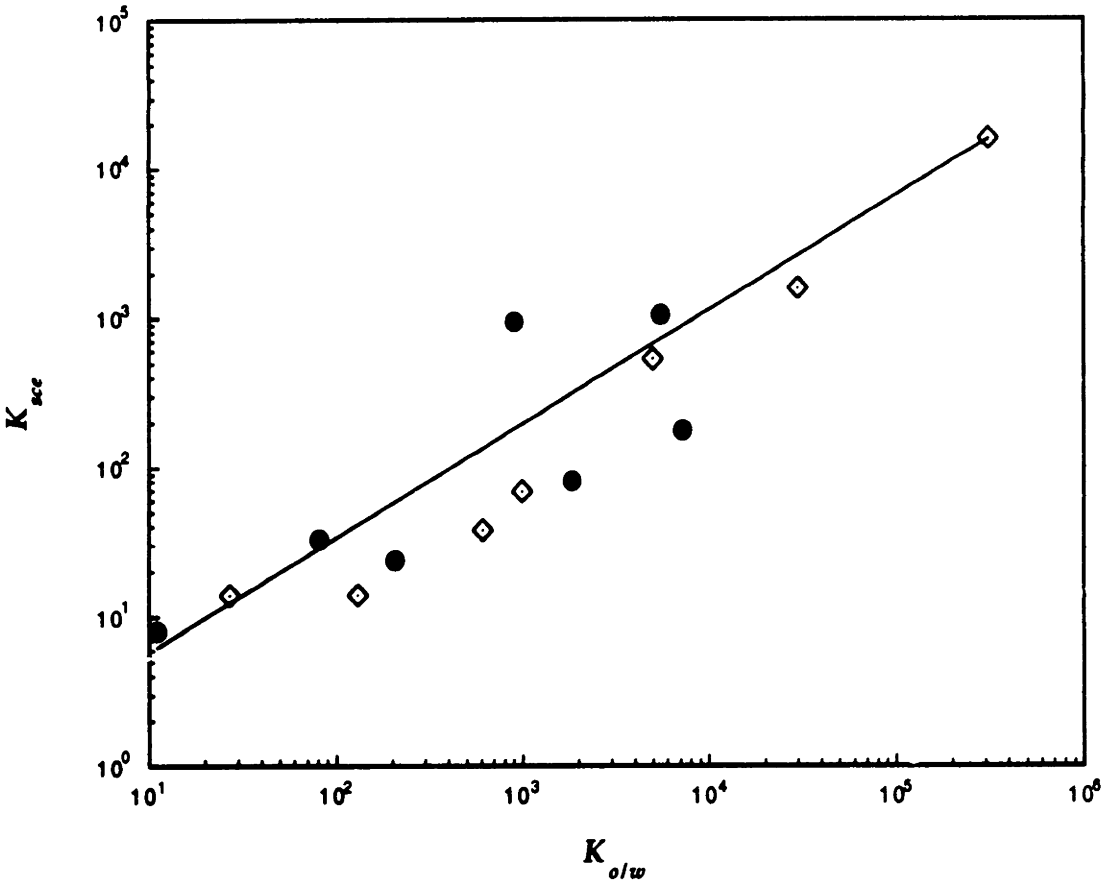

Figure 5.3 Values of the corrected stratum corneum lipid/water partition coefficient, K_{sce}, plotted versus the octanol/water partition coefficient values, $K_{o/w}$, for various solutes, reported in this chapter (●) as well as by Anderson et al. (1988) (◇). The best-fit line shows that the data obey a power-law relationship, $K_{sce} = K_{o/w}^{\beta}$, with β=0.76.

5.3.3 Stratum Corneum Model Liposome/Water Partition Coefficients and Impurity Correction

The experimental measurements of the partition coefficients obtained using stratum corneum model liposomes (SCM) are shown in Table 5.3. The values of K_{scm}(uncorrected) vary from 13 (aldosterone) to 728 (progesterone). As with the SCE measurements, the standard deviations are nearly 30% on average. The corrections for the impurity are relatively small, similar to the SCE results. The largest correction is only 17% (progesterone), which is within the error of the measurements. Even the correction for aldosterone is small (12%). This is due to the smaller value of β (0.70) used for estimating the SCM/water partition coefficient using Eq. (5.14) as compared to the value used in the SCE calculations above (0.76). The K_{scm}(corrected) correlation with $K_{o/w}$ is not as good as that of K_{sce}(corrected) as indicated the their regression coefficients, R, 0.65 and 0.99, respectively.

The use of stratum corneum model liposomes represents an attempt to create a system whose properties are an accurate reflection of the SC lipids. As such, the partition coefficients of these two systems would be expected to correlate. This is the case, as shown in Figure 5.4. Note that the value of β obtained from these data, 1.04 ± 0.05, is indistinguishable from unity, indicating that these model liposomes represent the partitioning behavior of SCE lipids. Unfortunately, experimental difficulties with this system (see section 5.2.4.2) make it difficult to work with, thus limiting its usefulness in experimental studies.

Table 5.3 Partition coefficient measurements of various drugs between stratum corneum model liposomes and water (K_{scm}).

Drug	K_{scm} (uncorrected)	n	S.D.	K_{scm} (corrected)	f
Aldosterone	13	4	66%	12	0.88
Corticosterone	24	2	36%	24	1.02
Estradiol	165	3	3%	176	1.06
Hydrocortisone	—	—	—	—	—
Lidocaine (pH 7.4)	49	2	10%	53	1.08
Napthol	74	4	47%	74	1.00
Progesterone	728	5	10%	849	1.17
Testosterone	102	2	5%	104	1.03

K_{scm} (uncorrected) values represent the average of n measurements. S.D. is the standard deviation. Values of K_{scm} (corrected) were calculated using the characteristics of the impurities, shown in Table 5.1. K_{scm} values for the impurities were calculated from: $K^i_{scm} = \left(K^i_{o/w}\right)^{0.70}$. f is the ratio of K_{scm} (corrected) to K_{scm} (uncorrected).

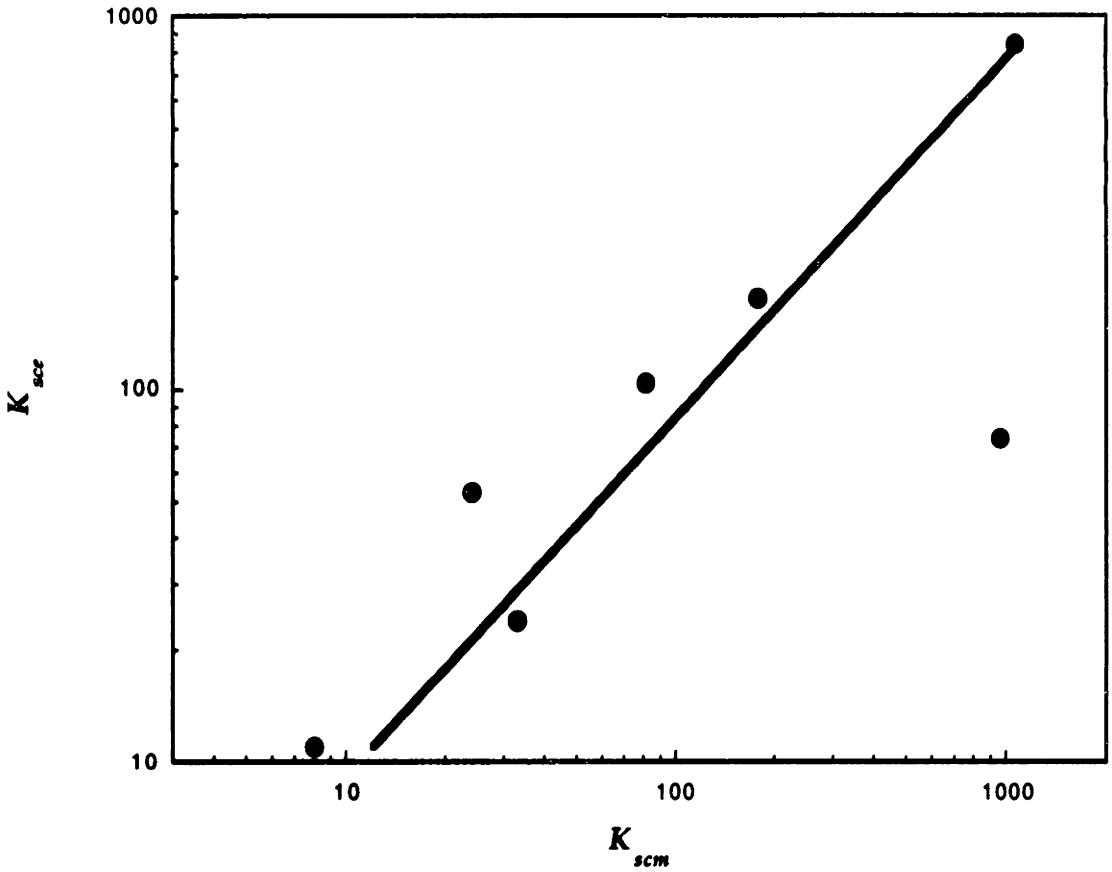

Figure 5.4 Values of the stratum corneum lipid/water partition coefficient, K_{sce}, plotted versus the stratum corneum model liposome/water partition coefficient, K_{scm}, for various solutes. The data obey a power-law relationship, $K_{sce} = K_{scm}^{\beta}$, with the value of β being essentially unity (1.04 ±0.05). This indicates that the SCM liposomes are a good quantitative model of the partitioning behavior of actual stratum corneum lipids.

5.3.4 DMPC Model Liposome/Water Partition Coefficients and Impurity Corrections

The results of the partitioning experiments performed with DMPC liposomes are shown in Table 5.4. The values of K_{dmpc}(uncorrected) vary from 18 (lidocaine) to 3870 (napthol). While only three experiments were performed per drug, the standard deviations of the measurements were all less than 4%. This enhanced reproducibility is a result of several factors including: (i) the synthetic nature of these liposomes, versus the varied lipid composition of SCE lipids; and (ii) a tighter liposome pellet was formed with DMPC liposomes as compared to that with SCM liposomes, resulting in a smaller correction for the water content of the pellet, which was the likely source of error in the SCM measurements. Table 5.4 also shows that the corrections for the impurities are still relatively small (0-41%), particularly given the fact that the partition coefficients in this table vary by 200-fold.

DMPC/water partition coefficients tend to correlate well with values of $K_{o/w}$. While the data in Table 5.4 correlate with $K_{o/w}$ (β=0.92), they do so to a more limited degree than the SCE and SCM systems, as indicated by the lower regression coefficient of R=0.57. However, the values of K_{sce} correlate well with these values of K_{dmpc}, as shown in Figure 5.5. The value of β determined from this plot is 0.82, indicating that the partition coefficients associated with DMPC liposomes are greater than those associated with SCE lipids. This is a result of DMPC liposomes being in a less ordered, more fluid-like phase than SCE lipids, which are more highly ordered and hence, are less able to accommodate solutes in their interior.

Table 5.4 Partition coefficient measurements of various drugs between DMPC model liposomes and water (K_{dmpc}).

Drug	K_{dmpc} (uncorrected)	n	S.D.	K_{dmpc} (corrected)	f
Aldosterone	38	3	3%	35	0.92
Corticosterone	364	3	1%	382	1.05
Estradiol	1830	3	3%	2500	1.37
Hydrocortisone	135	3	0%	142	1.05
Lidocaine (pH 7.4)	18	3	2%	19	1.05
Napthol	3870	3	2%	3870	1.00
Progesterone	2850	3	4%	4030	1.41
Testosterone	686	3	1%	733	1.07

K_{dmpc} (uncorrected) values represent the average of n measurements. S.D. is the standard deviation. Values of K_{dmpc} (corrected) were calculated using the characteristics of the impurities, shown in Table 5.1. K_{dmpc} values for the impurities were calculated from: $K^i_{dmpc} = \left(K^i_{o/w}\right)^{0.92}$. f is the ratio of K_{dmpc} (corrected) to K_{dmpc} (uncorrected).

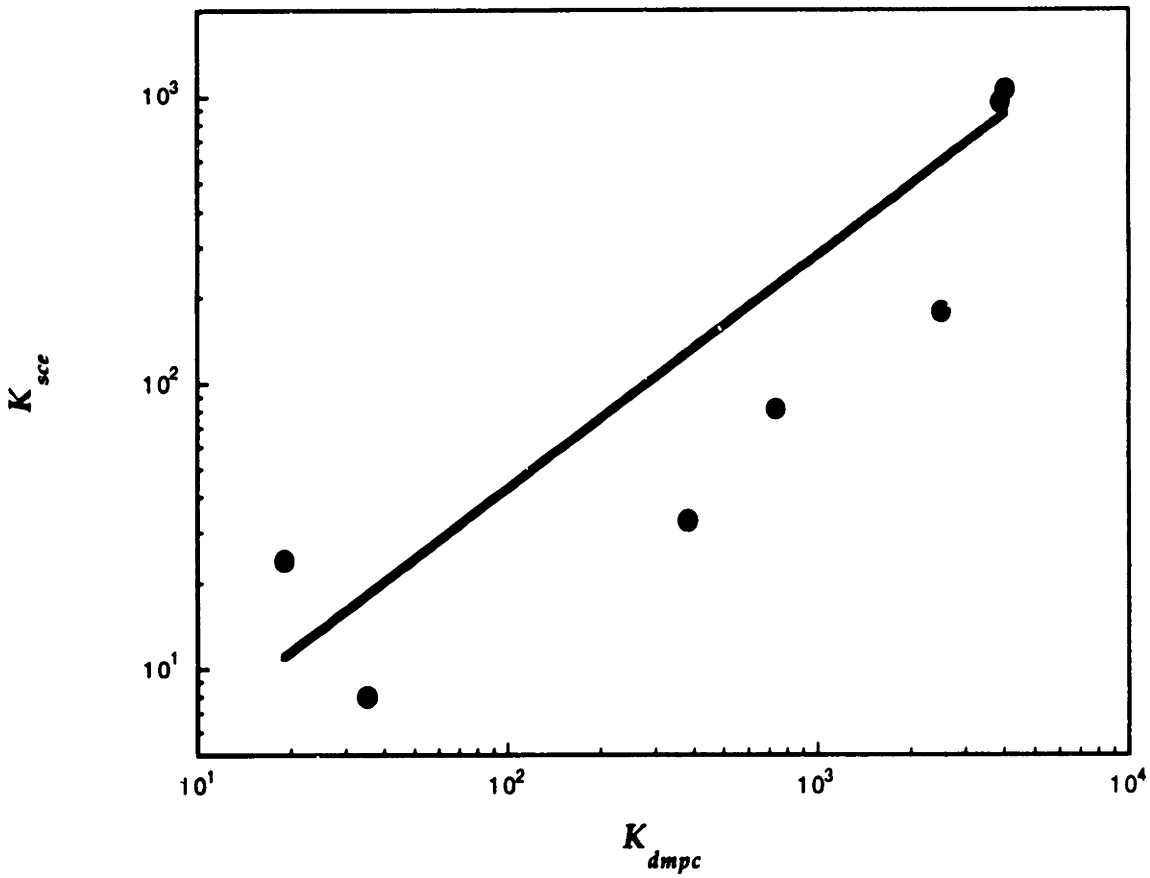

Figure 5.5 Values of the stratum corneum lipid/water partition coefficient, K_{sce}, plotted versus the DMPC liposome/water partition coefficient, K_{dmpc}, for various solutes. The data obey a power-law relationship, $K_{sce} = K_{dmpc}^{\beta}$, with the value of β less than unity (0.82 ± 0.02).

5.3.5 DMPC/Cholesterol Model Liposome/Water Partition Coefficients and Impurity Correction

The results of the partition coefficient experiments performed using DMPC/cholesterol liposomes are shown in Table 5.5. The values of K_{chol}(uncorrected) vary from 2.5 (aldosterone) to 793 (napthol). Similar to the results obtained with DMPC liposomes, the errors associated with these measurements are relatively small, as indicated by the standard deviations of 2-11% (see discussion above). The corrections for the impurity are also fairly small, 0-11%, for all the drugs examined except aldosterone. The 93% reduction in the value of K_{chol} due to the impurity is likely the result of an overestimate of the impact of the impurity resulting from an overestimation of its octanol/water partition coefficient.

Figure 5.6 shows the values of K_{sce} plotted as a function of K_{chol}. The results of this comparison bare a striking similarity with the comparison of K_{sce} with K_{dmpc} shown in Figure 5.5. The primary difference between these figures is that the magnitude of the partition coefficients are consistently larger with DMPC liposomes than with DMPC/cholesterol liposomes. Figure 5.6 shows that the DMPC/cholesterol (40 mol%) liposome partition coefficients correlate well with those measured with SCE lipids. Furthermore, the value of β (0.97 ± 0.01) is essentially unity, indicating that this is also a good quantitative model. This is an intriguing finding given the similiarity of the lateral diffusion coefficient values measured in SCE lipids and DMPC/cholesterol liposomes (see Chapter 5 and (Johnson et al., submitted[a])). Additionally, two recent studies of the structural aspects of SCE bilayers have also noted striking similarities between SCE lipids and phospholipid/cholesterol bilayers (Kitson et al., 1994; Ongpipattanakul et

Table 5.5 Partition coefficient measurements of various drugs between DMPC/cholesterol (40 mol%) model liposomes and water (K_{chol}).

Drug	K_{chol} (uncorrected)	n	S.D.	K_{chol} (corrected)	f
Aldosterone	2.5	3	6%	0.2 [a]	0.07 [a]
Corticosterone	15	3	5%	15	1.02
Estradiol	271	3	4%	290	1.07
Hydrocortisone	6.5	3	1%	142	1.05
Lidocaine (pH 7.4)	23	3	11%	25	1.06
Napthol	793	3	6%	793	1.00
Progesterone	736	3	2%	819	1.11
Testosterone	126	3	2%	129	1.02

K_{chol} (uncorrected) values represent the average of n measurements. S.D. is the standard deviation. Values of K_{chol} (corrected) were calculated using the characteristics of the impurities, shown in Table 5.1. K_{chol} values for the impurities were calculated from: $K^i_{chol} = \left(K^i_{o/w}\right)^{0.72}$. f is the ratio of K_{chol} (corrected) to K_{chol} (uncorrected). [a] The correction for aldosterone appears to be too large, and the resulting K_{chol} considerably lower than would seem reasonable. This is possibly the result of multiple impurities being present at low levels which are not adequately captured in terms of a one-component impurity model.

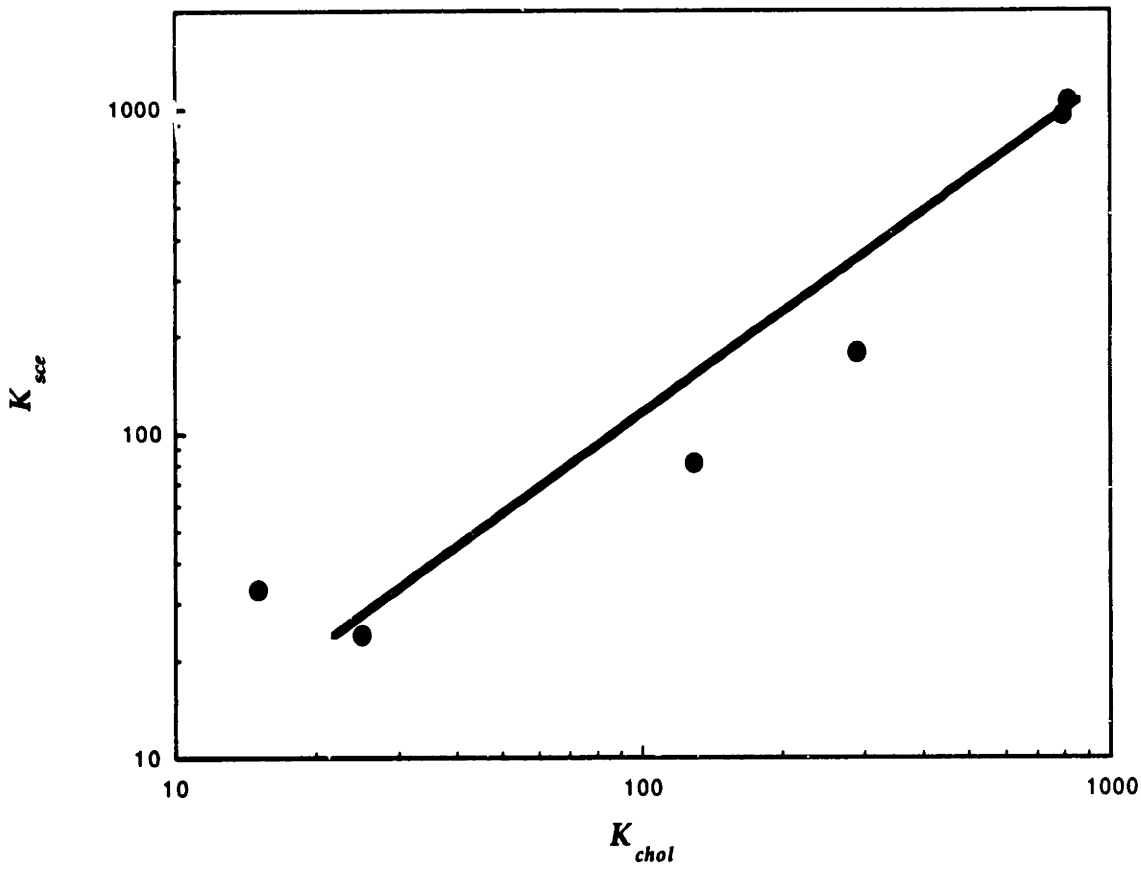

Figure 5.6 Values of the stratum corneum lipid/water partition coefficient, K_{sce}, plotted versus the DMPC/cholesterol (40 mol%) liposome/water partition coefficient, K_{chol}, for various solutes. The data obey a power-law relationship, $K_{sce} = K_{chol}^{\beta}$, with the value of β being essentially unity (0.97 ± 0.01). This indicates that the DMPC/cholesterol (40 mol%) liposomes are a good quantitative model of the partitioning behavior of actual stratum corneum lipids.

al., 1994), again suggesting that SCE bilayers may be modeled reasonably well by DMPC/cholesterol bilayers.

5.3.6 Octanol/Water Partition Coefficients of Hydrophilic Compounds

Octanol/water partition experiments performed with hydrophilic compounds, namely, ^{14}C-glucose, ^{3}H-oubain, and ^{14}C-sucrose, did not exhibit a dependence on the volumes of octanol and water utilized. Several factors may explain the lack of apparent impurities in these samples. First, these hydrophilic compounds are structurally simpler, such that their synthesis and subsequent purification may be more efficient than those for the complex steroids, hence, resulting in the generation of fewer impurities and the efficient removal of those that are produced. Second, these hydrophilic compounds are fairly stable, whereas steroids are known to decay at measurable rates. Hence, the experimentally measured $K_{o/w}$ value of glucose, oubain, and sucrose are 2.82×10^{-3} (±27%), 1.30×10^{-2} (±0.8%), and 3.93×10^{-4} (±44%), respectively.

5.4 Conclusions

In this chapter, $K_{o/w}$ values were measured for a variety of hydrophobic and hydrophilic compounds. Partition coefficients were also measured for a series of hydrophobic compounds with SCE lipids, as well as with three liposome model systems: SCM, DMPC, and DMPC/cholesterol. The partition coefficients for all four model systems correlated reasonably well with those of the SCE lipids. It is somewhat surprising that the three liposome systems did not exhibit a substantially better correlation than that exhibited by octanol/water, since

octanol/water lacks the lipid bilayer structure that is critical to the transport properties of the stratum corneum. Both SCM and DMPC/cholesterol liposomes where also found to be good quantitative models of the partition coefficients measured with SCE lipids, as indicated by their β values, 1.04 and 0.97, respectively, where β is the value of the exponent in the power-law relationship.

In this chapter, extraction experiments performed with octanol and water were also described. These experiments, and their subsequent analysis, produced the values of $K_{o/w}$ for the drugs as well as the characterization of the major radiolabeled impurity present in each drug. Specifically, the $K_{o/w}$ values and the mole fractions of the impurities were determined. The results of this analysis are generally consistent with the manufacturers' specifications for the purity of the drugs. This knowledge of the characteristics of the impurities allowed for the lipid/water partition coefficient measurements to be corrected for the presence of these impurities. Fortunately, these corrections were small and largely negligible, except in the case of aldosterone, for which the $K_{o/w}$ value of the impurity was only estimated approximately. This impurity analysis suggests that analytical methods which are more compound specific than the liquid scintillation counting of radiolabeled probes, such as HPLC, should be used in future partitioning experiments when possible. However, this study also shows that low level impurities can be corrected for, and will generally exhibit negligible effects on lipid/water partition coefficient measurements.

Chapter 6

Evaluation of Solute Permeation Through the Stratum Corneum: Lateral Bilayer Diffusion as the Primary Transport Mechanism

6.1 Introduction

Permeability and flux measurements are the primary experimental methods used to characterize transdermal solute transport. These macroscopic measurements are particularly useful for evaluating the potential efficacy of a specific transdermal drug delivery system, but by themselves do not provide much insight into the mechanisms of transport. Macroscopic transport measurements do not reveal, for example, the path by which a solute diffuses across the stratum corneum (SC), the outermost layer of the skin, whether it is through the lipid bilayer regime, the keratinized cells (keratinocytes), regions of disordered lipids (Johnson et al., in press; Mitragotri et al., 1995), or 'aqueous pores '(Peck et al., 1994; Yoneto et al., 1995). Many transport issues have been clarified, in part, by establishing the key structural aspects of the SC. For example, the SC has been shown to be a composite of ordered stacks of keratinocytes embedded in a lipid matrix. Electron microscopy (EM) (Elias and Menon, 1991; Madison et al., 1987; Odland and Holbrook, 1981; Swartzendruber et al., 1989) and small-angle x-ray scattering (SAXS) (Bouwstra et al., 1991; Friberg and Osborne, 1985; Garson et al., 1991) studies have further shown that the SC lipids reside in the form of lipid multibilayers in the interkeratinocyte regions of all parts of the SC.

Establishing the routes and mechanisms of transport through the SC is challenging due, in part, to our limited ability to 'see' the molecules and the pathways through which they are moving. Such determinations must be based upon indirect evidence. In fact, there is a substantial amount of such evidence which indicates that the interkeratinocyte lipids are the primary route of diffusion of lipophilic compounds through the SC. These findings include increased permeabilities upon removal or alteration of the SC lipids (Mitragotri et al., 1996; Wertz and Downing, 1989), high lipid/water partition coefficients and low keratinocyte/water partition coefficients (Raykar, 1988), and correlations between the transport enhancement of lipophilic compounds by chemicals and ultrasound and their site of action (that is, the lipid bilayers) (see Chapter 7 and (Johnson et al., in press; Knutson, 1987; Mitragotri et al., 1995; Potts and Francoeur, 1990)). Similarly, evidence is accumulating that very hydrophilic compounds are not limited to transport solely through the SC lipid bilayers, but may diffuse via an 'aqueous pore' pathway (Peck et al., 1994; Peck et al., 1995).

Studies on the nature of solute transport through the stratum corneum have generally focused on defining the domain through which solutes permeate through the skin, and not on the molecular-scale nature of the diffusion in the lipid bilayer medium. In contrast, extensive studies have been performed with phospholipids to characterize the partitioning of solutes between the bilayer and the surrounding aqueous medium (Arrowsmith et al., 1983; DeYoung and Dill, 1990; Knepp and Guy, 1989), the lateral transport along the plane of the bilayer (lateral diffusion) (Almeida et al., 1992; Tocanne et al., 1989; Vaz et al., 1984), and the transport across a phospholipid bilayer (transbilayer transport) (Cohen and Bangham, 1972; Lieb and Stein, 1986). From these studies, it is clear that the rate of lateral diffusion is considerably different from, and much faster than, that of

transbilayer transport, by up to a nine-orders of magnitude. Despite these differences, only one mode of bilayer transport, transbilayer transport, has been compared with transport through the skin. Several studies have noted that the size dependence of transbilayer transport measurements, typically made with phospholipid bilayers using hydrophilic compounds, is strong and comparable to that of SC permeabilities for lipophilic compounds (Cooper and Kasting, 1987; Potts and Guy, 1992). Little consideration has been given to the possible influence of solute lateral diffusion on SC permeabilities. This lack of attention is probably due to the previous absence of diffusion coefficient measurements in SC lipids, as well as the sparsity of lateral diffusion coefficient data of small probes (<600 Da) in other lipid systems.

In this chapter, transport at the lipid bilayer scale is examined by relating the micro-scale transport parameters to macroscopic SC permeability measurements. First, the bilayer-scale transport properties are introduced and described (section 6.2.1). Then, a mathematical expression is developed which describes the SC permeability, P, in terms of (i) bilayer-scale transport parameters, and (ii) characteristic dimensions of the SC and its microstructure (section 6.2.2). Experimental measurements of the bilayer-scale transport properties and of SC permeabilities, which are reported in section 6.3, and obtained from the literature, are then utilized to qualitatively and quantitatively evaluate the importance of the bilayer-scale transport parameters (section 6.4).

6.2 Model of Stratum Corneum Solute Permeation

To understand the macroscopic transport of solutes across the stratum corneum, it is first necessary to examine the microscopic transport properties of the SC lipid bilayers. By focusing on the lipid bilayer properties, hydrophilic solutes are

implicitly neglected, since very hydrophilic solutes (that is, solutes characterized by $\log(K_{o/w})$ values of less than -1.5) appear to permeate the skin through non-lipoidal pathways (referred to as 'aqueous pores') (Peck et al., 1994; Yoneto et al., 1995).

6.2.1 Microscale Description of Bilayer Transport

There are four intrinsic properties of the SC multibilayers which describe solute transport: (i) the lipid bilayer/water partition coefficient , K_m, (ii) diffusion along the plane of the bilayer, whether through the tail-group region, through the head-group region, or through both regions (lateral diffusion, characterized by a lateral diffusion coefficient, D_{lat}), (iii) transport from an external aqueous medium across the head-group region and into the lipid bilayer (interfacial transbilayer transport, characterized by a mass transfer coefficient, k_1), and (iv) transport from one bilayer in a multibilayer assembly, across two head-group regions, and into an adjacent bilayer (intramembrane transbilayer transport, characterized by a mass transfer coefficient, k').

The lipid bilayer/water partition coefficient, K_m, relates the equilibrium drug concentration in the aqueous medium surrounding the skin, C_w, to that in the SC bilayers, C_m , and is given by $K_m = C_m/C_w$. Partition coefficients have been measured for a variety of bilayer systems (see Chapter 5 and (Arrowsmith et al., 1983; DeYoung and Dill, 1990; Knepp and Guy, 1989; Vaara et al., 1990)), including lipids extracted from human stratum corneum (see Chapter 5 and (Anderson et al., 1988)). Knowing the value of K_m for a given drug allows the actual solute concentration in the stratum corneum lipid bilayers in a permeation experiment to be determined from the drug concentration in the surrounding medium, a value which is readily measurable.

Lateral diffusion in lipid bilayers, which has also been studied in various lipid bilayer systems (see (Johnson et al., submitted[a]; Vaz et al., 1984; Zhang et al., 1993) and Chapter 4), is analogous to diffusion in bulk solutions in several ways. Lateral diffusion does not involve diffusing between different phases, as is the case for transbilayer transport (see below), and can be effectively described by Fick's second law, $\partial C_m / \partial t = D_{lat} \nabla^2 C_m$. Measurements of lateral diffusion coefficients are typically made using the fluorescence recovery after photobleaching (FRAP) technique, and then fitting the data to the appropriate solution of Fick's second law to obtain the diffusion coefficient (Axelrod et al., 1976; Berk et al., 1993). The FRAP technique involves irreversibly bleaching fluorescent probe molecules dispersed in a small, typically circular, region of an extended lipid bilayer using a strong laser pulse, and subsequently monitoring the diffusive recovery of the non-bleached fluorescent probe molecules into this region over time. Measurements are typically made in phospholipid bilayer systems, and for fluorescently labeled lipids (>600 Da) and proteins as large as ~10^5 Da (Tocanne et al., 1989; Vaz et al., 1984). Due to the lack of experimental data on lateral diffusion in SC lipids and for low molecular weight solutes, the lateral diffusion coefficients of a series of small (223-787 Da), lipophilic, fluorescent probes in SC lipids, as well as in two model phospholipid bilayer systems, were recently measured (Chapter 5 and (Johnson et al., submitted[a])). Since lateral diffusion obeys the diffusion equation, that is, Fick's second law (Saffman and Delbrück, 1975; Yguerabide, 1982) the steady-state diffusive transport along a given bilayer is described by Fick's first law. Specifically,

$$J_l = \frac{D_{lat} \Delta C_m}{l} \tag{6.1}$$

where J_l is the lateral diffusive flux, ΔC_m is the solute concentration gradient along a bilayer, and l is the path length.

In contrast to lateral bilayer diffusion, interfacial transbilayer transport involves the discontinuous process associated with a solute molecule moving from an aqueous solution into the hydrophobic bilayer interior, or back out. The net interfacial transbilayer flux of a solute across the head-group region of a bilayer in contact with an aqueous medium, J_{if}, can be written as follows (Diamond and Katz, 1974):

$$J_{if} = k_1 C_w - k_{-1} C_m \tag{6.2}$$

where k_1 is the mass transfer coefficient for entering the bilayer from the surrounding aqueous solution, and k_{-1} is the mass transfer coefficient for exiting the bilayer into the surrounding aqueous solution. The processes of entering and exiting a bilayer from aqueous solution are not the same, both physically and quantitatively (Miller, 1991) . In particular, for solutes which form hydrogen bonds with water molecules, there is an energy penalty associated with the breaking of these bonds (desolvation) (Miller, 1991) and, hence, there is a corresponding transport resistance for entering the bilayer. Similarly, there is an entropy penalty for entering the aqueous medium associated with the reordering of the water molecules to accommodate the solute, and, hence, there is a corresponding transport resistance for exiting the bilayer. By considering diffusion into and out of a single bilayer under equilibrium conditions (that is, with no net flux across the interface, $J_{if}=0$), Eq. (6.2) can be used to relate k_{-1} to k_1 as follows:

$$k_{-1} = k_1\left(\frac{C_w}{C_m}\right) = \frac{k_1}{K_m} \tag{6.3}$$

Using Eq. (6.3), Eq. (6.2) can be rewritten in terms of a single mass transfer coefficient, k_1, that is,

$$J_{if} = k_1\left(C_w - \frac{C_m}{K_m}\right) \tag{6.4}$$

Measurements of k_1 have typically been made using biological and model phospholipid bilayer systems for relatively small compounds (typically <200 Da), which also tend to be hydrophilic (Cohen and Bangham, 1972; Lieb and Stein, 1986). Large, hydrophilic compounds have not been widely examined since they exhibit very low bilayer permeabilities (Brunner et al., 1980). Measurements of k_1 have not generally been made for lipophilic compounds since their transport is fast, and hence, is difficult to measure. For example, the characteristic time for the transport of several steroids (estrone, estradiol, progesterone, and testosterone) across human red blood cell ghosts has been determined to be less than 0.75 milliseconds, and, hence was too rapid to measure even with a highly specialized stop-flow technique (Koefoed and Brahm, 1994).

Intramembrane transbilayer transport involves the discontinuous process associated with solute diffusion from the tail-group region of a bilayer, across two ordered head-group regions of an adjacent lipid bilayer, and into the tail-group region of the adjacent bilayer. SC lipid bilayers are closely packed, with a 6.5 nm repeating unit and only a small amount of bound water in the head-group region (Bouwstra et al., 1991). As such, it is likely that solutes traverse the two head-group regions without the formation of extensive hydrogen bonds or the

subsequent desolvation, a key difference with the interfacial transbilayer transport process described earlier. The intramembrane transbilayer flux, J_{im}, can be written as follows:

$$J_{im} = k'\left(C_{m,r} - C_{m,r+1}\right) \tag{6.5}$$

where $C_{m,r}$ and $C_{m,r+1}$ are the solute concentrations in the adjacent bilayers, r and $r+1$. It is not clear how to reliably measure values of k'. Experiments involving multilamellar liposomes may seem like a logical way to proceed. However, several difficulties arise, including the fast time-scale associated with the transport of lipophilic solutes (see above), the dominant contribution of interfacial transbilayer transport in the case of hydrophilic solutes, and the creation and characterization of the multilamellar liposomes. Specifically, multilamellar liposomes tend to be polydisperse with respect to their overall size and their bilayer configurations, with large aqueous regions often present between adjacent bilayers (Cullis et al., 1987; Cussler et al., 1988). As such, it would be unlikely that the multibilayers present in a multilamellar liposome would be uniformly packed as closely, and contain as little water in the head-group region, as compared to those in the SC.

6.2.2 Description of Macroscopic Stratum Corneum Transport

Relating the bilayer-scale transport properties, K_m, D_{lat}, k_1, *and* k', described above, to the macroscopic SC permeability requires knowledge of the SC structure, the various dimensions of the keratinocytes, and several simplifying assumptions. Specifically, SC transport is assumed to occur solely through the interkeratinocyte lipid region (see section 6.1 and Chapter 1). Transport through

appendages, such as hair-follicles and sweat ducts, keratinocytes, and 'aqueous pore' pathways is neglected. The lipid bilayers are further assumed to be homogeneously dispersed (that is, the lipid composition is assumed to be the same in all parts of the SC lipid bilayers, such that the bilayer-scale transport properties are independent of position in the SC) (Lampe et al., 1983; Madison et al., 1987), continuous, and defect free.

A solute molecule traversing the SC under these conditions must first enter the top-most bilayer from the aqueous solution, a process which is described by Eq. (6.4) under steady-state conditions. Similarly, the solute molecule must exit the bottom-most bilayer on the epidermis side into another aqueous solution. Since there is no bulk water phase within the SC, interfacial transport occurs only at these two surfaces. Once in the lipid bilayers, diffusion through the SC is comprised of a series of segments of lateral diffusion and intramembrane transbilayer transport (see section 6.4.1 for additional discussion). In total, the solute crosses n bilayers internally and diffuses laterally over a total distance, l. The diffusive resistances of these three transport components (see Eqs. (6.1), (6.4), and (6.5)) can be combined to yield a mathematical description of the steady-state SC permeability, P, in resistance form for an average solute particle. Specifically,

$$\frac{1}{P} = \frac{h\tau^*}{K_m D_{lat}} + \frac{2}{k_1} + \frac{n}{K_m k'} \tag{6.6}$$

where h is the SC thickness and τ^* is the effective tortuosity (see Eq. (6.7) and Appendix 6A).

6.2.3 Calculation of the Stratum Corneum Tortuosity

Although solute diffusion occurs primarily in the SC lipids, the keratinocytes also play an important role in SC transport by acting as physical impediments and, hence, by reducing the overall solute transport. The spatial regularity of the keratinocytes, which are stacked in ordered columns (Menton, 1976; Mershon, 1975; Wildnauer et al., 1975), makes their presence amenable to analysis. Specifically, the extent to which the keratinocytes, which are taken to be impermeable in this analysis, reduce solute transport can be quantified using the established keratinocyte dimensions (see Figure 6.1) and the following relationship (see Appendix 6A):

$$\tau^* = 1 + \frac{2g}{h}\ln\left(\frac{d}{2s}\right) + \frac{Ndt}{sh} + \left(\frac{d}{1+\omega}\right)^2\left(\frac{\omega}{hg}\right)(N-1) \qquad (6.7)$$

where τ^* is the effective tortuosity and is defined as the ratio of the diffusive flux through a membrane without impediments to that through a membrane having impediments, d is the keratinocyte diameter, t is the keratinocyte thickness, N is the number of keratinocyte layers, h is the SC thickness, g is the vertical gap width between keratinocytes, s is the lateral space between keratinocytes, and ω is the offset ratio, described below (see Figure 6.1). The first three terms in Eq. (6.7) have been established previously (Cussler et al., 1988) and represent: i) the transport through a membrane with no impediments, ii) the resistance associated with necking down into the narrow lipid slits which laterally separate keratinocytes on the top layer, and out of the corresponding lipid slits of the bottom layer, and iii) the resistance of transport through the narrow lipid slits themselves. Using typical values for these parameters, which are shown in

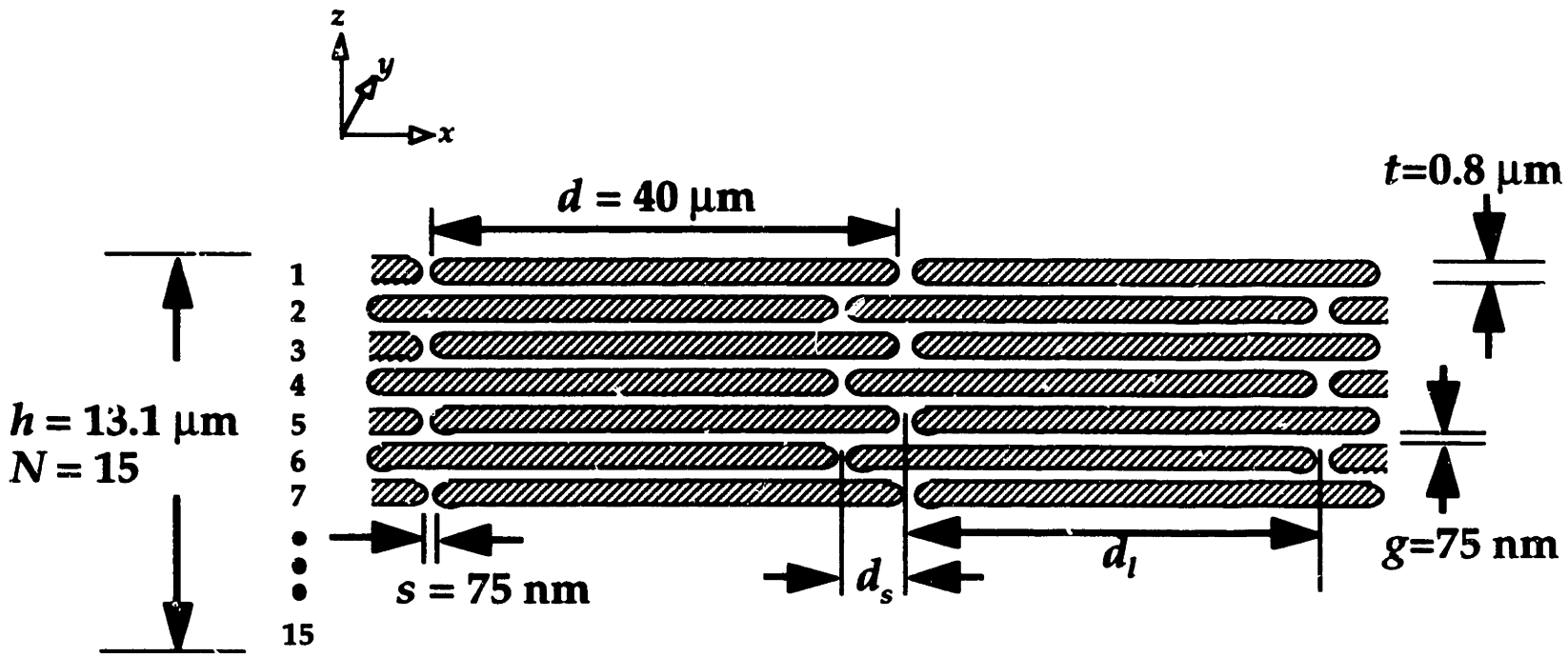

Figure 6.1 Schematic diagram of the cross-section of human stratum corneum. Keratinocytes are arranged in ordered, overlapping columns, and surrounded by lipid multibilayers. Representative values of the various dimensions are shown. Typical dimensions are shown for the keratinocyte diameter (d=40 μm, (Mershon, 1975; Wildnauer et al., 1975)), keratinocyte thickness (t=0.8 μm, (Mershon, 1975; Wildnauer et al., 1975)), number of keratinocyte layers (N=15,(Mershon, 1975; Wildnauer et al., 1975)), stratum corneum thickness (h=13.1 μm, calculated from $h=N(t+g)$), the vertical gap between keratinocytes (g=75 nm, (Elias and Friend, 1975)), the lateral spacing between keratinocytes (s=75 nm, (Elias and Friend, 1975)), and the offset ratio (ω=8, (Menton, 1976; Wildnauer et al., 1975)). The offset ratio, ω, is related to the path lengths from the interkeratinocyte lipid slit in one layer to the two closest slits in the next lower layer, d_s and d_l, by $\omega = d_l/d_s$.

Figure 6.1 (d=40 μm (Mershon, 1975; Wildnauer et al., 1975), t=0.8 μm (Mershon, 1975; Wildnauer et al., 1975), N=15 (Mershon, 1975; Wildnauer et al., 1975), h=13.1 μm[¶], g=75 nm (Elias and Friend, 1975), s=75 nm (Elias and Friend, 1975), and ω=8 (Menton, 1976; Wildnauer et al., 1975)),[¥] these first three terms can be shown to contribute less than 18% to the overall effective tortuosity. The contribution of the fourth term (see Appendix 6A), which accounts for the resistance of the parallel but unequal path lengths from a slit in one layer to the closest two slits in the next lower layer (Figure 6.1), dominates the value of the effective tortuosity. These parallel paths are unequal due to the partial overlap of the keratinocyte columns. The extent of this overlap is quantified by the offset ratio, ω, which is defined as the ratio of the non-equal path lengths from the slit in one layer to the two closest slits in the lower layer (Figure 6.1). Using the values shown in Figure 6.1 and listed above, the effective tortuosity of the SC, τ^*, is calculated to be 2740, and the product $h\tau^*$ is equal to 3.6 cm. These values are consistent with previous studies which estimated the effective tortuosity to be approximately 10^3 (Michaels et al., 1975; Potts and Francoeur, 1991).

The effectively tortuosity, τ^*, can also be expressed as the product, $\tau^*=\alpha\tau$, where α is the reduction in available area for the lipid path between keratinocytes, and τ is the tortuosity and describes the increased mean path length relative to the material thickness for the mean solute transport. Reported values of α, 250-1000 (Mershon, 1975) (that is, 0.1-0.25% of the surface area is comprised of lipid slits), are consistent with the value of 700 indicated by the SC

[¶] The SC thickness, h, was calculated from $h=N(t+g)$, in order to maintain self-consistency.

[¥] Taken as a whole, these values imply an overall lipid content of approximately 10%, which is consistent with experimental values (4.3-16% by weight) (Lampe et al., 1983; Miller, 1991; Raykar, 1988), and demonstrates the self-consistency of these values.

dimensions shown in Figure 6.1. The value of τ is, therefore, 3.9, consistent with the value of $\sqrt{7}$ (that is, ~2.6) estimated by Hatcher and Plachy (Hatcher and Plachy, 1993).

It seems unlikely that each term in Eq. (6.6) is of equal importance for every solute type. However, the relative contributions of the three terms in Eq. (6.6), corresponding to the three bilayer kinetic properties, to the overall permeability are currently not known, and will be considered in this chapter. First, however, the experimental measurements of the skin permeabilities for several solutes are described and reported.

6.3 Experimental Methods and Results

6.3.1 Passive Permeability Measurements

Human skin permeability measurements are described in detail in Chapter 2, and are briefly summarized in this section. Human cadaver skin from the chest, back, and abdominal regions was obtained from a local hospital (Brigham and Women's Hospital, Boston, MA) and the National Disease Research Institute (Philadelphia, PA). The skin was stored at -80°C until usage. The epidermis was separated from the full-thickness tissue after immersion in 60°C water for 2 minutes. Heat-stripped skin was stored at 5°C and 95% relative humidity for up to 1 week prior to usage. ^{14}C-n-decanol, ^{14}C-n-hexanol, ^{14}C-2-napthol, and ^{14}C-n-octanol were obtained from DuPont, New England Nuclear (Boston, MA) and American Radiolabeled Chemicals, Inc. (St. Louis, MO).

The permeabilities of n-decanol, n-hexanol, 2-napthol, and n-octanol through human cadaver skin were measured using trace quantities of the corresponding radiolabeled compounds. The radiolabeled compounds were

rotary evaporated in order to remove the solvent in which they were shipped, as well as any tritium which had reverse-exchanged onto them. The radiolabeled compounds were redissolved in pH 7.4 phosphate buffered saline (PBS, phosphate concentration = 0.01 M, NaCl concentration = 0.137M; Sigma Chemical Co., St. Louis, MO) to a typical concentration of 1 μCi/ml, and added to the donor compartment of a diffusion cell. Permeabilities were measured using stirred side-by-side diffusion cells (#DC-100B, Crown Bioscientific; Sommerville, NJ) at room temperature. The receiver compartment always contained PBS. The concentrations of radiolabeled drug in the donor and the receiver compartments were measured using a scintillation counter (model 2000 CA, Packard Instruments Co., Downers Grove, IL). A minimum of three permeation experiments were performed for each solute. The permeability values, P, were calculated under steady-state conditions from the relationship, $P = (dN_r/dt)/(A(C_d - C_r))$, where A is the surface area of the skin sample, C_d is the solute concentration in the donor compartment, C_r is the solute concentration in the receiver compartment, and N_r is the cumulative amount of drug which nas permeated into the receiver compartment at time, t. The experimentally observed lag-times for the permeation experiments were all less than one hour on average. The observed variability of the individual permeability values is consistent with the previously established 40% inter-subject variability of human skin permeabilities (Williams et al., 1992).

6.3.2 Experimental Results

The results of the permeability measurements performed with n-decanol, n-hexanol, 2-napthol, and n-octanol, 1.8×10^{-1}, 2.0×10^{-2}, 4.1×10^{-2}, and 1.1×10^{-1} cm/hr, respectively, are shown in Table 6.1, along with measurements obtained from the

Table 6.1 Human skin permeabilities, P, $K_{o/w}$ values, and lateral diffusion coefficients, D_{lat}, of various compounds.

Compound	MW (Da)	log($K_{o/w}$)	P (cm/hr)	Reference	D_{lat} (cm^2/sec)
aldosterone	360.4	1.08	5.00×10^{-5}	(Mitragotri et al., 1996)	7.55×10^{-9}
aldosterone	360.4	1.08	5.80×10^{-5}	(Johnson et al., 1995)	8.78×10^{-9}
anisole	108.1	2.11 Ω	7.37×10^{-2}	(Barry et al., 1985)	1.84×10^{-6}
benzaldehyde	106.1	1.45	6.08×10^{-2}	(Barry et al., 1985)	4.81×10^{-6}
benzene	78.0	2.1	1.11×10^{-1}	(Blank and McAuliffe, 1985)	2.81×10^{-6}
benzene	78.0	2.1	1.60×10^{-1}	(Mitragotri et al., 1995)	4.06×10^{-6}
benzyl alcohol	108.1	1.10	1.69×10^{-2}	(Barry et al., 1985)	2.47×10^{-6}
4-bromophenol	173.0	2.59	3.61×10^{-2}	(Roberts et al., 1977)	3.88×10^{-7}
2,3-butanediol	90.1	-0.92	5.00×10^{-5}	(Scheuplein, 1967)	2.50×10^{-7}
n-butanol	74.1	0.88	2.20×10^{-3}	(Mitragotri et al., 1995)	4.72×10^{-7}
n-butanol	74.1	0.88	2.50×10^{-3}	(Scheuplein and Blank, 1973)	5.36×10^{-7}
n-butanol	74.1	0.88	3.00×10^{-3}	(Scheuplein, 1967)	6.43×10^{-7}
2-butanone	72.1	0.28	4.50×10^{-3}	(Scheuplein, 1967)	2.76×10^{-6}
caffeine	194.0	-0.02	1.00×10^{-4}	(Mitragotri et al., 1995)	1.03×10^{-7}
4-chlorocresol	142.6	3.10	5.90×10^{-2}	(Roberts et al., 1977)	2.60×10^{-7}
2-chlorophenol	128.6	2.15	3.31×10^{-2}	(Roberts et al., 1977)	7.68×10^{-7}
4-chlorophenol	128.6	2.39	3.63×10^{-2}	(Roberts et al., 1977)	5.54×10^{-7}
chloroxylenol	156.6	3.39	5.28×10^{-2}	(Roberts et al., 1977)	1.40×10^{-7}
corticosterone	346.5	1.94	1.00×10^{-4}	(Johnson et al., sub.)	3.35×10^{-9}
corticosterone	346.5	1.94	3.00×10^{-4}	(Mitragotri et al., 1995)	1.01×10^{-8}
corticosterone	346.5	1.94	5.54×10^{-4}	(Peck et al., 1995)	1.86×10^{-8}
m-cresol	108.1	1.96	1.52×10^{-2}	(Roberts et al., 1977)	4.94×10^{-7}
o-cresol	108.1	1.95	1.57×10^{-2}	(Roberts et al., 1977)	5.18×10^{-7}
p-cresol	108.1	1.95	1.75×10^{-2}	(Roberts et al., 1977)	5.77×10^{-7}
n-decanol	158.3	4.24 §	8.00×10^{-2}	(Scheuplein and Blank, 1973)	4.79×10^{-8}
n-decanol	158.3	4.24 §	1.80×10^{-1} ¶		1.08×10^{-7}
dexamethasone	392.5	1.99	6.40×10^{-5}	(Johnson et al., sub.)	1.97×10^{-9}
2,4-dichlorophenol	127.6	3.08	6.01×10^{-2}	(Roberts et al., 1977)	2.74×10^{-7}
estradiol	272.4	3.86 £	3.00×10^{-3}	(Mitragotri et al., 1996)	3.51×10^{-9}
estradiol	272.4	3.86 £	3.20×10^{-3}	(Mitragotri et al., 1995)	3.75×10^{-9}
estradiol	272.4	3.86 £	3.40×10^{-3}	(Goodman and Barry, 1988)	3.98×10^{-9}
estradiol	272.4	3.86 £	3.50×10^{-3}	(Yum et al., 1994)	4.10×10^{-9}
estradiol	272.4	3.86 £	3.89×10^{-3}	(Galey et al., 1976)	4.55×10^{-9}
estradiol	272.4	3.86 £	4.00×10^{-3}	(Williams et al., 1992)	4.68×10^{-9}
estradiol	272.4	3.86 £	4.10×10^{-3}	(Johnson et al., 1995)	4.80×10^{-9}
estradiol	272.4	3.86 £	4.16×10^{-3}	(Johnson et al., sub.)	4.87×10^{-9}
estradiol	272.4	3.86 £	5.20×10^{-3}	(Michaels et al., 1975)	6.09×10^{-9}
estradiol	272.4	3.86 £	5.40×10^{-3}	(Perry, 1990)	6.32×10^{-9}
estradiol	272.4	3.86 £	6.10×10^{-3}	(Knutson et al., 1993)	7.14×10^{-9}
ethanol	46.1	-0.31	8.00×10^{-4}	(Scheuplein and Blank, 1973)	1.38×10^{-6}
2-ethoxy ethanol	90.1	-0.54	2.50×10^{-4}	(Scheuplein, 1967)	6.43×10^{-7}

ethyl benzene	106.2	3.15	1.22×10^{0}	(Dutkiewicz and Tyras, 1967)	4.91×10^{-6}
ethyl ether	74.1	0.80 ∞	1.60×10^{-2}	(Scheuplein, 1967)	3.95×10^{-6}
4-ethylphenol	122.2	2.40	3.49×10^{-2}	(Roberts et al., 1977)	5.23×10^{-7}
fluocinonide	494.6	3.19	1.70×10^{-3}	(Anderson et al., 1988)	6.40×10^{-9}
n-heptanol	116.2	2.72 §	3.20×10^{-2}	(Scheuplein and Blank, 1973)	2.74×10^{-7}
n-heptanol	116.2	2.72 §	3.76×10^{-2}	(Scheuplein, 1967)	3.22×10^{-7}
n-hexanol	102.2	2.03	1.30×10^{-2}	(Scheuplein and Blank, 1973)	3.73×10^{-7}
n-hexanol	102.2	2.03	2.00×10^{-2} ¶		5.73×10^{-7}
n-hexanol	102.2	2.03	2.77×10^{-2}	(Bond and Barry, 1988)	7.94×10^{-7}
hydrocortisone	362.5	1.53	1.60×10^{-5}	(Hou and Flynn, 1989)	1.10×10^{-9}
hydrocortisone	362.5	1.53	1.19×10^{-4}	(Hadgraft and Ridout, 1987)	8.19×10^{-9}
hydrocortisone	362.5	1.53	2.30×10^{-4}	(Johnson et al., 1995)	1.58×10^{-8}
hydrocortisone hydroxyhexanoate	476.6	2.79 †	9.10×10^{-4}	(Anderson et al., 1988)	6.95×10^{-9}
hydrocortisone hemipimelate	504.6	3.26 †	1.80×10^{-3}	(Anderson et al., 1988)	6.04×10^{-9}
hydrocortisone hemisuccinate	462.5	2.11 †	6.30×10^{-4}	(Anderson et al., 1988)	1.56×10^{-8}
hydrocortisone hexanoate	460.6	3.48 †	1.80×10^{-2}	(Anderson et al., 1988)	4.10×10^{-8}
hydrocortisone N,N dimethylsuccinamate	489.6	2.03 †	6.70×10^{-5}	(Anderson et al., 1988)	1.91×10^{-9}
hydrocortisone octanoate	488.7	5.49 †	6.20×10^{-2}	(Anderson et al., 1988)	4.16×10^{-9}
hydrocortisone pimelamate	503.6	2.30 †	8.90×10^{-4}	(Anderson et al., 1988)	1.59×10^{-8}
hydrocortisone proprinate	418.5	3.00 †	3.40×10^{-3}	(Anderson et al., 1988)	1.80×10^{-8}
hydrocortisone succinamate	461.6	1.43 †	2.60×10^{-5}	(Anderson et al., 1988)	2.12×10^{-9}
isoquinoline	129.2	2.08	1.68×10^{-2}	(Hadgraft and Ridout, 1987)	4.42×10^{-7}
methanol	32.0	-0.71	5.00×10^{-4}	(Scheuplein and Blank, 1973)	1.74×10^{-6}
methyl-4-hydroxy-benzoate	152.1	1.96	9.12×10^{-3}	(Roberts et al., 1977)	2.95×10^{-7}
hydrocortisone methylpimelate	518.6	3.30 †	5.40×10^{-3}	(Anderson et al., 1988)	1.67×10^{-8}
hydrocortisone methylsuccinate	476.6	2.58 †	2.10×10^{-4}	(Anderson et al., 1988)	2.30×10^{-9}
2-naphthol	144.2	2.84	2.56×10^{-2} ¶		1.78×10^{-7}
2-naphthol	144.2	2.84	2.79×10^{-2}	(Roberts et al., 1977)	1.94×10^{-7}
3-nitrophenol	139.1	2.00	5.58×10^{-3}	(Roberts et al., 1977)	1.69×10^{-7}
4-nitrophenol	139.1	1.96	5.64×10^{-3}	(Roberts et al., 1977)	1.83×10^{-7}
n-nonanol	144.3	3.68 §	6.00×10^{-2}	(Scheuplein and Blank, 1973)	9.58×10^{-8}
n-octanol	130.2	3.15	1.10×10^{-1} ¶		2.10×10^{-7}
n-octanol	130.2	3.15	5.20×10^{-2}	(Scheuplein and Blank, 1973)	4.44×10^{-7}
n-pentanol	88.2	1.56	6.00×10^{-3}	(Scheuplein and Blank, 1973)	3.91×10^{-7}
phenol	94.1	1.46	8.22×10^{-3}	(Roberts et al., 1977)	6.39×10^{-7}
phenol	94.1	1.46	1.30×10^{-2}	(Singh and Roberts, 1994)	1.20×10^{-6}
2-phenylethanol	122.2	1.36	1.30×10^{-2}	(Barry et al., 1985)	1.20×10^{-6}
progesterone	314.5	3.77	1.30×10^{-2}	(Mitragotri et al., 1995)	1.77×10^{-8}
progesterone	314.5	3.77	3.00×10^{-2}	(Johnson et al., 1995)	4.09×10^{-8}

n-propanol	60.1	0.25	1.20×10^{-3}	(Scheuplein and Blank, 1973)	7.75×10^{-7}
n-propanol	60.1	0.25	1.70×10^{-3}	(Scheuplein, 1967)	1.10×10^{-6}
resorcinol	110.1	0.80	2.40×10^{-4}	(Roberts et al., 1977)	5.92×10^{-8}
styrene	104.1	2.95	6.35×10^{-1}	(Dutkiewicz and Tyras, 1969)	3.64×10^{-6}
testosterone	288.4	3.31	2.20×10^{-3}	(Mitragotri et al., 1995)	6.71×10^{-9}
testosterone	288.4	3.31	5.36×10^{-3}	(Johnson et al., sub.)	1.64×10^{-8}
thymol	150.2	3.34	5.50×10^{-2}	(Roberts et al., 1977)	1.59×10^{-7}
toluene	92.1	2.70	1.00×10^{0}	(Dutkiewicz and Tyras, 1969)	8.87×10^{-6}
2,4,6-trichlorophenol	162.0	3.69	5.94×10^{-2}	(Roberts et al., 1977)	9.32×10^{-8}
water	18.0	-1.38	3.00×10^{-4}	(Mitragotri et al., 1996)	3.36×10^{-6}
water	18.0	-1.38	5.00×10^{-4}	(Scheuplein and Blank, 1973)	5.59×10^{-6}
water	18.0	-1.38	1.31×10^{-3}	(Astley and Levine, 1976)	1.47×10^{-5}
water	18.0	-1.38	1.40×10^{-3}	(Bond and Barry, 1988)	1.57×10^{-5}
water	18.0	-1.38	1.54×10^{-3}	(Bronaugh et al., 1986)	1.72×10^{-5}
water	18.0	-1.38	1.56×10^{-3}	(Barber et al., 1992)	1.75×10^{-5}
water	18.0	-1.38	1.58×10^{-3}	(Galey et al., 1976)	1.77×10^{-5}
water	18.0	-1.38	1.71×10^{-3}	(Harrison et al., 1984)	1.91×10^{-5}
3,4-xylenol	122.2	2.35	3.60×10^{-2}	(Roberts et al., 1977)	5.89×10^{-7}

References are for the permeability measurements. $K_{o/w}$ values are taken from Hansch and Leo (Hansch and Leo, 1979) unless otherwise noted. § Extrapolated from n-alcohol measurements. ¶ Reported in this chapter and in (Johnson, et al., submitted, c). £ Reported in Chapter 5. † Permeability and partition coefficient measurements were made at pH 4.0. ¥ (Peck et al., 1994) Ω (Barry et al., 1985) ∞ (Wilschut et al., 1995)

literature. These values are in good agreement with the previously published permeability values of n-hexanol (1.3×10^{-2} cm/hr) (Scheuplein and Blank, 1971), 2-napthol (2.8×10^{-2} cm/hr) (Roberts et al., 1977), and n-octanol (5.2×10^{-2} cm/hr) (Scheuplein and Blank, 1971).

6.4 Analysis

The human skin permeabilities of a variety of compounds having different sizes and hydrophobicities, along with their $K_{o/w}$ values, have been compiled from the literature in Table 6.1. This table lists permeabilities for which reported $K_{o/w}$ values are available, including measurements described in Chapter 5, and which are not adjusted for pH (see Table 6.2). One data set, that of steroid permeabilities by Scheuplein et al. (Scheuplein et al., 1969), is omitted from this table due to significant discrepancies (that is, between 5 and 77-fold differences) of their 14 measurements with those made by a variety of other groups (see (Johnson et al., 1995) and Chapter 3). A number of permeability measurements have been made with compounds which were partially ionized at the pH of the experiment. Table 6.2 lists these compounds along with their reported (uncorrected) permeabilities, the pH of the experiments, the pK's of the solutes, and the permeabilities of the non-ionized fraction of the compounds (corrected for pH using the Henderson-Hasselbalch equation§). Measurements made with highly ionized (>90%) or very hydrophilic compounds ($\log(K_{o/w}) < -1.5$) were not included due to the possible transport of charged species through non-lipoidal, 'aqueous pores' (Peck et al., 1994; Yoneto et al., 1995). The 120 permeability values listed in Tables 6.1 and 6.2 represent compounds which range in size from

---

§ $pH = pK + \log(f)$, where f is the ratio of non-protonated to protonated drug at the experimental pH.

Table 6.2 Human skin permeabilities, P, $K_{o/w}$ values, and lateral diffusion coefficients, D_{lat}, of various partially Ionized compounds.

Compound	MW (Da)	log($K_{o/w}$)	P (cm/hr)	pH	pK	P_c (cm/hr)	D_{lat} (cm^2/hr)
amylobarbital	226.3	1.96 [a]	2.27x10^{-3} [f]	5.0	7.8 [j]	2.28x10^{-3}	7.37x10^{-8}
barbital	184.2	0.65 [a]	1.11x10^{-4} [f]	5.0	7.4 [j]	1.12x10^{-4}	3.58x10^{-8}
butabarbital	212.2	1.65 [a]	1.93x10^{-4} [f]	5.0	8.0 [j]	1.94x10^{-4}	1.08x10^{-8}
4-chloro-m-phenylenediamine	142.6	0.85 [b]	2.10x10^{-3} [b]	9.7	4.1 [b]	2.10x10^{-3}	4.79x10^{-7}
codeine	299.3	1.25 [c]	4.90x10^{-5} [c]	7.4	8.1 [c]	2.94x10^{-4}	3.32x10^{-8}
diclofenac	318.0	4.31 [d]	1.82x10^{-2} [d]	§	4 [j]	1.82x10^{-2}	9.65x10^{-9}
ephedrine	165.2	1.03 [a]	6.00x10^{-3} [g]	10.8	9.6 [k]	6.38x10^{-3}	1.05x10^{-6}
fentanyl	336.5	4.37 [c]	5.60x10^{-3} [h]	§	9.0 [c]	5.60x10^{-3}	2.68x10^{-9}
hydromorphone	285.3	0.89 [c]	1.40x10^{-5} [c]	7.4	8.1 [c]	8.42x10^{-5}	1.78x10^{-8}
indomethacin	357.8	4.42 [d]	1.48x10^{-2} [d]	§	4.5 [j]	1.48x10^{-2}	6.47x10^{-9}
lidocaine	234.3	2.48 [e]	3.97x10^{-3} [i]	7.4	7.9 [k]	1.65x10^{-2}	2.14x10^{-7}
morphine	285.3	0.62 [c]	9.30x10^{-6} [c]	7.4	8.1 [c]	5.59x10^{-5}	1.88x10^{-8}
naproxen	230.3	3.18 [d]	3.82x10^{-2} [d]	§	4.15 [j]	3.82x10^{-2}	1.46x10^{-7}
nicotine	162.2	1.17 [a]	1.93x10^{-2} [f]	9.2	7.9 [k]	2.03x10^{-2}	2.62x10^{-6}
2-nitro-p-phenylenediamine	153.1	0.53 [b]	5.00x10^{-4} [b]	9.7	3.9 [b]	5.00x10^{-4}	1.97x10^{-7}
phenobarbital	232.2	1.47 [a]	4.53x10^{-4} [f]	5.0	7.4 [k]	4.55x10^{-4}	3.47x10^{-8}
o-phenylenediamine	108.1	0.15 [b]	4.50x10^{-4} [b]	9.7	4.8 [b]	4.50x10^{-4}	3.48x10^{-7}
p-phenylenediamine	108.1	-0.30 [b]	2.40x10^{-4} [b]	9.7	6.3 [b]	2.40x10^{-4}	4.07x10^{-7}
salicylic acid	138.1	2.24 [a]	3.04x10^{-2} [d]	§	3.0 [k]	3.04x10^{-2}	6.03x10^{-7}
salicylic acid	138.1	2.24 [a]	6.26x10^{-3} [f]	3.0	3.0 [k]	1.25x10^{-2}	2.48x10^{-7}
scopolamine	303.4	1.24 [a]	5.00x10^{-5} [g]	9.6	8.1 [k]	5.16x10^{-5}	5.89x10^{-9}
sufentanyl	386.6	4.59 [a]	1.20x10^{-2} [h]	§	8.5 [c]	1.20x10^{-2}	3.93x10^{-9}

$K_{o/w}$ values represent the equilbrium distribution of the non-ionized form of the drugs. Underlined pK values represent acids, while all others are bases. Permeabilities were corrected to represent the permeability of the non-ionized form of the compound, P_c, using the equation $P_c = P/(1-f)$, where f is the fraction of total compound in the solution that is ionized, and is calculated from the Henderson-Hasselbalch equation (see footnote in the text). Only permeabilities measured under conditions where at least 10% of the total compound was not ionized are listed. § Permeability value corrected for ionization by the original authors. Diffusion coefficients were calculated from the corrected skin permeability values using Eq. (6.9).

[a] (Hansch and Leo, 1979) [b] (Bronaugh and Congdon, 1984) [c] (Roy and Flynn, 1989) [d] (Singh and Roberts, 1994) [e] (Strichartz et al., 1990) [f] (Hadgraft and Ridout, 1987) [g] (Michaels et al., 1975) [h] (Roy and Flynn, 1990) [i] (Johnson et al., sub.) [j] (McEvoy, 1995) [k] (Katzung, 1995)

18 Da (water) to 518.6 Da (hydrocortisone methylpimelate), and in their $\log(K_{o/w})$ values from -1.38 (water) to 5.49 (hydrocortisone octanoate).

Values of the SC lipid/water partition coefficients, K_m, for the compounds listed in Tables 6.1 and 6.2 can be estimated from the octanol/water partition coefficients, $K_{o/w}$, listed in these tables using the relationship:

$$K_m = K_{o/w}^{\beta} \tag{6.8}$$

where β is an empirically determined parameter. The $K_{o/w}$ values in Table 6.2 are corrected for pH and represent partitioning of the non-ionized forms of the compounds. The value of β (0.76) was determined by performing a least-squares regression on K_m and $K_{o/w}$ data that are presented in Chapter 5 as well as by Anderson et al. (Anderson et al., 1988), using Eq. (6.8) (see Chapter 5 for further discussion of partition coefficients). The 0.76 value compares favorably with previously reported values of 0.71 (Potts and Guy, 1992), 0.74 (Bunge and Creek, 1995), 0.75 (Morimoto et al., 1992), and 0.86 (Anderson and Raykar, 1989). The previous values of β were deduced from regressions on sets of permeability data using equations which express P as a functional of the physical properties of the solutes, including their $K_{o/w}$ values and molecular weights. For example, Potts and Guy (Potts and Guy, 1992) fit the permeabilities compiled by Flynn (Flynn, 1990) to the equation:

$$\log(P) = \beta \log(K_{o/w}) - \gamma(MW) + \delta \tag{6.9}$$

where MW is the solute molecular weight, and β, γ, and δ are correlation parameters.

6.4.1 Comparison of Calculated and Experimental Lateral Diffusion Coefficients

The relative importance of lateral diffusion to the overall SC permeability can be examined by assuming that the resistance to transport resulting from lateral diffusion is greater than those from interfacial and intramembrane transbilayer transport. Hence, by neglecting the second and third terms in Eq. (6.6), an expression relating the lateral diffusion coefficient, D_{lat}, to the macroscopic SC permeability, P, is obtained, namely,

$$D_{lat} = \frac{Ph\tau^*}{K_m} \tag{6.10}$$

By substituting $h\tau^*$=3.6 cm and $K_m = K_{o/w}^{0.76}$ into Eq. (6.10), a relationship is obtained, which can be utilized to calculate the solute lateral diffusion coefficients in SC lipid bilayers from measured macroscopic skin permeabilities. Specifically,

$$D_{lat} = \frac{P}{K_{o/w}^{0.76}}\left(3.6\ cm\right) \tag{6.11}$$

Tables 6.1 and 6.2 list the diffusion coefficients that were calculated in this manner using Eq. (6.11), with the corresponding values of P and $K_{o/w}$ also listed in these tables. These calculated values of lateral diffusion coefficients span four orders of magnitude, ranging from 1.9×10^{-5} cm^2/sec for water to 1.1×10^{-9} cm^2/sec for hydrocortisone.

Figure 6.2 shows the calculated diffusion coefficients versus solute molecular weight. As can be seen, these diffusion coefficients exhibit a size

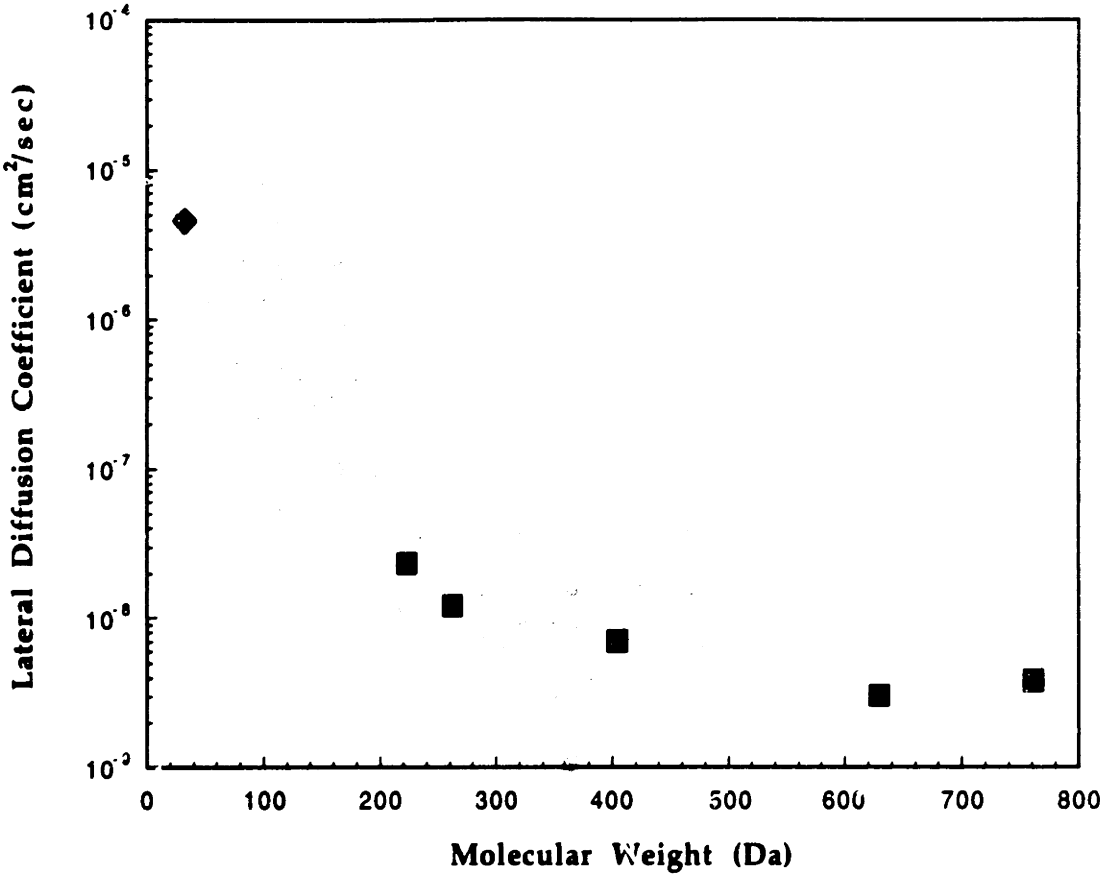

Figure 6.2 Comparison of experimentally measured lateral diffusion coefficients using video-FRAP (Johnson et al., submitted) (■) and EPR spectroscopy (molecular oxygen; diffusion coefficient corrected for the tortuosity of the SC, τ=3.9) (Hatcher and Plachy, 1993) (◆) with those calculated from human skin permeabilities using Eq. (6.10) (●). Both experimental and calculated values exhibit strong size dependencies in the low molecular weight regime, with a more gradual dependence for larger solutes. There is good qualitative and quantitative agreement between the experimental diffusion coefficients and those calculated by assuming that lateral diffusion is the rate limiting mechanism associated with SC permeation.

dependence, with values decreasing with increasing solute size. This dependence is particularly strong for the smallest compounds (<300 Da). The diffusion coefficients of the larger solutes (~350-500 Da) appear not to decrease at the same dramatic rate, but instead remain relatively constant at values of ~10^{-8}-10^{-9} cm^2/sec. The consistency of this trend is reasonable given the sources of potential error, including variability of the permeability measurements, and deviations from the partition coefficient correlation (Eq. (6.8)).

Also shown in Figure 6.2 are experimental values of lateral diffusion coefficients in SC lipids for lipophilic, fluorescent probes (223-787 Da) measured using video-FRAP (Johnson et al., submitted[a]). The diffusion coefficient for molecular oxygen in SC lipids, 4.6×10^{-6} cm^2/sec, is also shown in Figure 6.2. This value was calculated from the data of Hatcher and Plachy (Hatcher and Plachy, 1993), which was measured using electron paramagnetic resonance (EPR) spectroscopy, after correcting for the tortuosity of the SC using τ=3.9, as calculated above. Figure 6.2 shows that the direct experimental measurements of lateral diffusion in SC lipids agree well with the calculated values. The experimental data exhibits a strong size dependence in the low molecular weight regime (<300 Da), similar to that exhibited by the calculated values in Tables 6.1 and 6.2 (see Figure 6.2). The FRAP measurements also exhibit a much weaker size dependence for the larger probes (>350 Da), which is also consistent with the calculated trend for the solutes examined. Figure 6.2 shows good qualitative and quantitative agreement between the experimental lateral diffusion coefficient measurements and those calculated from skin permeability measurements using Eq. (6.11) without any fitted parameters.

This agreement indicates that the diffusive resistance of lateral diffusion in SC lipid bilayers is sufficient to account for the observed macroscopic permeabilities of the solutes listed in Tables 6.1 and 6.2. If transbilayer transport

provided the primary resistance for SC permeation, then the experimental lateral diffusion measurements could be larger than the values calculated using Eq. (6.11). Figure 6.2 shows that this is not the case. Similarly, if the experimental lateral diffusion coefficients were lower than those calculated using Eq. (6.11), or if the qualitative size dependence was different, the validity of the analysis would be in question. Figure 6.2 also shows that this is not so.

The above analysis indicates that there is a bimodal size dependence of transport within the SC, with a weaker size dependence for larger, lipophilic probes (≥350 Da) than for smaller probes. This is a novel finding, given that previous models and correlations of skin permeabilities have invariably assumed a unimodal size dependence (Anderson and Raykar, 1989; Bunge and Creek, 1995; Kasting et al., 1992; Kasting et al., 1987; Potts and Guy, 1992; Wilschut et al., 1995). In fact, there has not been a clear precedent for a bimodal size dependence of a given transport parameter in a given system until recently, when lateral diffusion in lipid bilayers was shown to be strong for small solutes (<300 Da) and weak for larger solutes (>350 Da) (Johnson et al., submitted[a]). Moreover, this bimodal distribution is consistent with the current understanding of small solute transport in complex media. First, the diffusion of solutes which are smaller than the solvent through which they diffuse, such as oxygen diffusing in lipid bilayers, is known to exhibit an exponential size dependence. Theories which describe such processes, that is, free-volume theories (Cohen and Bangham, 1972; Cohen and Turnbull, 1959; Lieb and Stein, 1969), uniformly assume that the solute is *smaller* than the solvent. Since the molecular weights of lipid molecules in biomembranes are typically 600-900 Da, this condition is clearly met for the majority of the compounds listed in Tables 6.1 and 6.2 as well as in Figure 6.2. However, the effective size of the lipid tail-groups, through which lipophilic solutes tend to diffuse, might be smaller than that of the entire lipid molecule.

For example, dexamethasone (392 Da) is smaller than a typical lipid molecule, taken as a whole, yet is large in comparison with the narrow, straight chain hydrocarbons which dominate the bilayer core through which dexamethasone diffuses. Dexamethasone is, in fact, larger than cholesterol (387 Da), a key component of SC lipid bilayers, illustrating the current ambiguity of effective tail-group size. Hence, the transition from a strong to a moderate size dependence at ~300-400 Da, shown in Figure 6.2, exhibited by both the experimentally measured and the calculated lateral diffusion coefficients, indicates that the effective 'size' of the lipid tails in the bilayer interior is about 300-400 Da. Second, lateral diffusion in phospholipid bilayer systems is known to exhibit a weak size dependence for solutes ranging in size from ~1000 Da up to 100,000 Da (Vaz et al., 1984). The lipid bilayer acts as a continuum for these solutes which are larger than the lipid molecules themselves. Hence, continuum theories, which have a weak size dependence, are able to effectively describe the diffusion of large solutes (≥1000 Da) (Saffman and Delbrück, 1975; Vaz et al., 1984), as well as that of solutes which are more moderate in size (~400-1000 Da), although to a lesser extent (Johnson et al., submitted[a]).

6.4.2 Transbilayer Transport

6.4.2.1 Interfacial Transbilayer Transport

Similarly, the relative importance of transbilayer transport to the macroscopic skin permeability can be examined. By assuming that the interfacial transbilayer transport resistance is the largest in Eq. (6.6), the following relationship between the skin permeability, P, and k_1 is obtained:

$$k_1 = 2P \tag{6.12}$$

Evaluation of skin permeabilities using Eq. (6.12) is more ambiguous, however, since almost all available interfacial transbilayer measurements have been made using lipid systems and solutes which are not representative of the human skin lipids or of the solutes listed in Tables 6.1 and 6.2. Phospholipid bilayer systems are typically used to examine small solutes having $K_{o/w}$ values of less than unity. In contrast, the data in Tables 6.1 and 6.2, using Eq. (6.12), are predominantly for very lipophilic compounds. Nevertheless, examination of transbilayer data is still valuable. Figure 6.3 shows a comparison of the values of k_1 calculated from the skin permeability measurements in Tables 6.1 and 6.2 with those measured in two phospholipid-based model bilayers systems, lecithin/cholesterol (50:50) liposomes (Cohen and Bangham, 1972) and human red blood cell ghosts (Lieb and Stein, 1986). The solutes used in these studies were mostly smaller than 100 Da, and hydrophilic, with a median $K_{o/w}$ value of 0.058. Both the measured and calculated values of k_1 are divided by $K_{o/w}^{0.76}$, an approximation of the bilayer/water partition coefficient, in order to illustrate their respective size-dependencies in Figure 6.3. Figure 6.3 shows that the experimental and calculated values of k_1 do not agree, with the values for the smallest solutes differing by 3-4 orders of magnitude. The experimental interfacial transbilayer measurements also exhibit a size-dependence, which appears to be considerably stronger than that exhibited by the skin. The fact that the experimental values of k_1 are larger than those calculated from skin permeabilities further indicates that the experimental resistance of interfacial transbilayer transport is less than that for the overall skin permeability. Hence, these data suggest that interfacial transbilayer transport does not constitute the primary resistance in skin

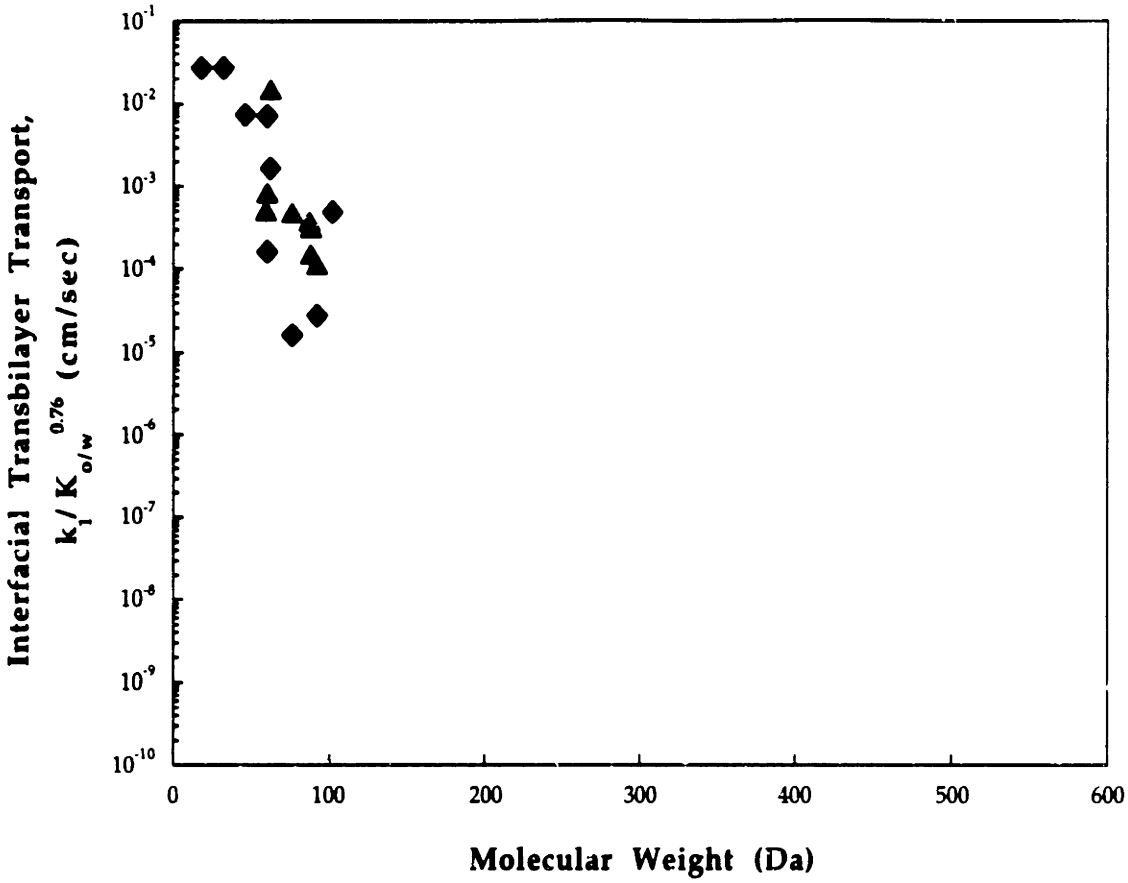

Figure 6.3 Comparison of experimentally measured interfacial transbilayer transport coefficients, $k_1/K_{o/w}^{0.76}$, for a series of small, mostly hydrophilic, solutes across lecithin/cholesterol (50:50) liposomes (▲) and human red blood cell ghosts (◆), with those calculated from human skin permeabilities using Eq. (6.11) (●). The experimental values are up to three orders of magnitude greater than the calculated values, indicating that the interfacial transbilayer resistance is insufficient to explain the measured SC permeabilities. The size dependence of the experimental data is also greater than that exhibited by the calculated values.

permeation, which is consistent with the findings in Figure 6.2, which show that lateral diffusion is likely to provide the primary resistance.

Additional evidence suggesting that interfacial transbilayer transport is not the rate limiting resistance to skin permeation is provided by a recent studies of liposomes composed of lipids which are representative of the SC (Johnson et al., 1993; Yoneto et al., 1995). For example, Yoneto et al. measured the permeability of hydrophilic solutes (glucose, mannitol, methylglucose, raffinose, and sucrose) across unilamellar liposomes. The results of these experiments are shown in Table 6.3, along with the molecular weights and $K_{o/w}$ values of the solutes examined. These data are in general agreement with bilayer permeability measurements of lecithin liposomes using similar compounds (Brunner et al., 1980), also shown in Table 6.3, but are three-orders of magnitude *lower* than the corresponding human skin permeabilities (Table 6.3) (Peck et al., 1994). The data in Table 6.3 indicate that the resistance associated with crossing a single lipid bilayer in aqueous solution is greater than that associated with crossing the entire stratum corneum, a tissue which is more than one thousand fold thicker. This finding reveals two important points: (i) very hydrophilic compounds may permeate the skin through non-lipoidal, 'aqueous pore' pathways, as has been previously suggested (Peck et al., 1994), and (ii) solutes can enter the stratum corneum without necessarily having to cross the ordered head-group region of the top-most bilayer. This second point contradicts the assumption made in the model presented in section 6.2 that the lipid bilayers are continuous and defect free. Note that without having made this assumption, there would be no physical basis for having examined interfacial transport (Figure 6.3), the only transbilayer transport mechanism for which direct experimental measurements are available. It seems physically unlikely that the stratum corneum lipid bilayers are perfectly continuous and defect free such that the top-most bilayer of

Table 6.3 Permeabilities of polar nonelectrolytes through lipid bilayers and human skin.

Solute	MW (Da)	log($K_{o/w}$)	P_{scm} (cm/sec)	P_l (cm/sec)	P (cm/sec)
fructose	180.2	-3.2 †	—	4.0×10^{-10}	—
glucose	180.2	-3.3	2.49×10^{-11}	3.0×10^{-11}	—
mannitol	182.2	-3.1	5.80×10^{-12}	—	1.15×10^{-8}
methylglucose	194.2	-2.5	5.82×10^{-11}	—	
raffinose	504.4	-4.3	2.60×10^{-12}	—	4.27×10^{-9}
sucrose	342.3	-3.7 §	4.80×10^{-12}	8.0×10^{-14}	5.75×10^{-9}

Permeabilities across (i) liposomes composed of model-SC lipids, P_{scm} (Yoneto et al., 1995), (ii) liposomes composed of egg-lecithin, P_l, (Brunner et al., 1980), and (ii) human skin, P (Peck et al., 1994). $K_{o/w}$ values from Yoneto et al. (Yoneto et al., 1995), unless otherwise noted.

† Estimated as the average of glucose and mannitol. § Reported in Chapter 5.

the skin is like the surface of a liposome. Taken together, Figure 6.3 and Table 6.3 provide compelling evidence that the diffusive resistance of interfacial transbilayer transport does not represent a significant contribution to the overall skin resistance, if it contributes at all.

6.4.2.2 Intramembrane Transbilayer Transport

By assuming that the intramembrane transbilayer transport resistance is greater than that associated with lateral diffusion and interfacial transbilayer transport, Eq. (6.6) yields:

$$k' = \frac{Pn}{K_{o/w}^{0.76}} \tag{6.13}$$

Since there are currently no available measurements of k', Eq. (6.13) cannot be fully evaluated at this time. However, the above discussion on interfacial bilayer transport, which indicates that the lipid bilayers on the SC surfaces are not continuous and defect-free, also suggests that the bilayers within the SC are not completely defect free. In fact, an examination of the SC bilayers using electron microscopy (EM) has revealed that adjacent bilayers often merge together, such that solutes can diffuse from one bilayer to another without having to necessarily cross the head-group regions (Elias and Menon, 1991; Swartzendruber et al., 1989). The presence of lacunae (Elias and Menon, 1991; Swartzendruber et al., 1989) within the interkeratinocyte domain provides another possible pathway by which solutes can diffuse from one bilayer to another. These alternative pathways for diffusion between bilayers may be important if the resistance associated with intramembrane transbilayer transport itself were significant.

Interestingly, the movement of lipid molecules, such as phospholipid molecules, between the two leaflets of a bilayer (a process which is referred to as *flip-flop*) is known to be very slow (Homan and Pownall, 1988; Lipka et al., 1991). Results from the recent examination of diffusion in SC bilayers using video-FRAP also suggest that transbilayer transport, or flip-flop, may be an important contributor to the overall movement of solutes which are lipid-like, having a hydrophilic head-group and a lipophilic tail-group to anchor the molecule into the bilayer (Chapter 5 and (Johnson et al., submitted[a])). Experiments performed in SC lipids with four probes, including a fluorescently labeled phospholipid molecule, which were chosen specifically for their lipid-like nature, exhibited anomalous behavior which could not be explained in terms of lateral diffusion. This behavior is consistent with the fact that the slow flip-flop of the probes significantly impede their movement at disclinations or domain boundaries. More work is needed to fully evaluate the importance of intramembrane transbilayer transport and lipid flip-flop to the macroscopic human skin permeabilities, particularly for lipid-like molecules.

6.5 Conclusions

Human stratum corneum is a complex tissue, and diffusive transport through it is, similarly, a complex phenomenon. In this chapter, the permeation of solutes through the lipid multibilayer regime of the stratum corneum and its relationship to the intrinsic transport properties of lipid bilayers were examined, specifically: bilayer/water partitioning, lateral diffusion, interfacial transbilayer transport, and intramembrane transbilayer transport. A model was developed which mathematically expresses the macroscopic skin permeability in terms of these bilayer-scale properties and geometric characteristics of the SC. Analysis using

this model showed that the diffusive resistance associated with lateral diffusion in the SC bilayers is sufficient to account for one hundred and twenty measurements of human skin permeabilities. These lateral diffusion coefficients exhibited a strong size dependence in the low molecular weight regime (<300 Da) and a weak size dependence for larger solutes (>350 Da), and are qualitatively consistent with free-volume models as well as with lateral diffusion coefficients measured in SC lipids using FRAP, presented in Chapter 5. Interfacial transbilayer transport was shown to be unimportant, owing to the low resistances exhibited by model bilayer systems for small (<150 Da) solutes and the apparent bypassing of the interfacial transbilayer transport route for very hydrophilic solutes ($\log(K_{o/w})$<-1.5) permeating the skin. While no measurements exist for intramembrane transbilayer transport, EM analyses have shown the existence of several possible routes by which solutes can pass from one bilayer to another, suggesting that the resistance associated with intramembrane transbilayer transport is not likely to significantly impede solute permeation through the SC. Further studies are still needed to fully elucidate the mechanisms by which hydrophilic and lipid-like solutes permeate the skin.

Appendix 6A Derivation of Tortuosity Expression

The diffusive transport through a unit area of a homogeneous membrane, M_o, is given by the expression:

$$M_o = D\Delta C(dW)/h \qquad (6A1)$$

where D is the diffusion coefficient, ΔC is the concentration gradient across the membrane, h is the total membrane thickness, d is the characteristic length-scale

in the x-direction, and W is the unit width in the y-direction (see Figure 6.1). The diffusive transport through a unit area of a membrane containing N layers of regularly ordered impediments, M_N, (such as the SC structure, shown in Figure 6.1) will be less than that through the homogeneous membrane, M_0. The ratio, M_0/M_N, is referred to here as the *effective tortuosity*, τ^*, namely,

$$\tau^* = \frac{M_o}{M_n} \tag{6A2}$$

The factors which affect the value of τ^*, given a specific membrane, include: (i) necking down into the slit between impediments at the top-most layer, and out of the slits of the bottom-most layer, (ii) diffusion through the vertical slits separating adjacent impediments, and (iii) tortuous diffusion in the x,y-direction from the slits in one layer to the slits in the next lowest layer. The contributions of the first two factors have been considered elsewhere (Cussler et al., 1988), and correspond to the first three terms in Eq. (6.7). Cussler et al. (1988) also considered the third factor for one specific case in which the layers of impediments are completely offset from one another (ω=1).

This appendix details the development of the expression which quantifies the effect of tortuous diffusion in the x,y-direction between slits in adjacent layers, for the generalized case in which the impediments of adjacent layers are off-set by ω, where $\omega = d_l/d_s$ (see Figure 6.1). The path lengths to the two closest slits, d_s and d_l, are depicted in Figure 6.1, and represent *parallel* pathways by which a solute molecule may diffuse. For simplicity, only transport to the two closest slits (in the next lower layer) is considered. The effects of transport to the other slits (in a given layer) are negligible, due to the greater distance of separation. Hence, the effective length, d_e, associated with transport in the x,y-direction between layers of impediments is given by:

$$d_e = \frac{d_s d_l}{(d_s + d_l)} \tag{6A3}$$

Noting that $d = (d_s + d_l)$ and $d_l = \omega d_s$, Eq. (B3) can be rewritten as:

$$d_e = \frac{\omega d}{(1+\omega)^2} \tag{6A4}$$

Hence, the total effective path length of diffusion in the x,y-direction in a N-layered membrane is $(N-1)d_e$, and the flux in the x,y-direction along a path length, $(N-1)d_e$, is given by:

$$J_{gw} = \frac{(1+\omega)^2}{(N-1)\omega d} D\Delta C \tag{6A5}$$

Note that the flux described in Eq. (6A5) is per unit area of the vertical (z direction) plane across which transport in the x,y direction occurs (see Figure 6.1). The actual area of transport for diffusion along a path of length $(N-1)d_e$ in the x,y-direction is gW. Hence, by considering only diffusion in the x,y-direction, the flux through across an N-layered membrane, J_N, (that is, in the vertical or z-direction) is given by:

$$J_N = \frac{(1+\omega)^2}{(N-1)\omega d} D\Delta C\left(\frac{gW}{dW}\right) \tag{6A6}$$

where (gW/dW) is the ratio of the area available for diffusion in the x,y-direction to that available for diffusion in the z-direction. The transport through a unit area of membrane having N layers of impediments is, therefore, given by:

$$M_N = \frac{(1+\omega)^2}{(N-1)\omega^2} D\Delta C\left(\frac{gW}{dW}\right)(dW) \tag{6A7}$$

Hence, the contribution to the overall tortuosity of diffusion in the x,y-direction between the lateral slits of an N-layered membrane, τ^*_ω, is given by substituting Eqs. (6A1) and (6A7) in Eq. (6A2), that is,

$$\tau^*_\omega = \left(\frac{d}{1+\omega}\right)^2\left(\frac{\omega}{hg}\right)(N-1) \tag{6A8}$$

Equation (6A8) is the fourth term in Eq. (6.7).

Chapter 7

Synergistic Effects of Chemical Enhancers and Therapeutic Ultrasound

7.1 Introduction

The outermost layer of the skin, the stratum corneum (SC), is a remarkable transport barrier which effectively retards the diffusion of exogenous compounds into the body (see Chapter 1). In recent years, researchers have studied a variety of different methods for increasing the transport of drug molecules across the skin in order to develop effective transdermal delivery systems. These methods include the use of (i) chemical enhancers (Walters, 1989), (ii) therapeutic (Levy et al., 1989; Mitragotri et al., 1995) and low-frequency (Mitragotri et al., 1995) ultrasound (sonophoresis), and (iii) electrical current (iontophoresis (Burnette, 1989) and electroporation (Prausnitz et al., 1993)). Considerable attention has been devoted both to developing practical systems as well as to understanding the mechanisms by which these methods work. For example, electroporation is believed to work in part by creating transient pores in the lipid bilayers of the SC (Prausnitz et al., 1993), while iontophoresis provides an electrical driving force (Burnette, 1989). Ultrasound has been shown to induce cavitation within the SC, which disorders the lipid bilayers thus increasing drug transport (Mitragotri et al., 1995). Chemical enhancers have been found to increase transdermal drug transport via several different mechanisms, including increased solubility of the drug in the donor formulation, increased partitioning into the SC, fluidization of

the lipid bilayers, and disruption of the intracellular proteins (Aungst et al., 1990; Barry, 1987; Goates and Knutson, 1994).

Since different chemical enhancers have been found to increase transdermal drug transport via different mechanisms, it was hypothesized that the combination of two chemical enhancers which act in different manners might be most effective in increasing the overall drug transport (Johnson et al., in press). Specifically, ethanol has been found to increase the solubility of drugs up to 10,000-fold (Knutson et al., 1993) resulting in, for example, a 140-fold transdermal flux increase of estradiol (Liu et al., 1991), while unsaturated fatty acids in propylene glycol have been shown to increase the fluidity of SC lipid bilayers and increase the transdermal transport of certain drugs (Aungst et al., 1990; Barry, 1987; Cooper, 1984; Cooper et al., 1985; Walters, 1989). Unlike ethanol, propylene glycol is not a very effective permeation enhancer by itself (Barry, 1987). Accordingly, a mixture of ethanol and the unsaturated fatty acid linoleic acid were combined (referred to as LA/EtOH) and examined in order to simultaneously exploit the solubility enhancement ability of ethanol solutions and the bilayer fluidity enhancement ability of linoleic acid. Linoleic acid was chosen as the model bilayer fluidizing enhancer over, for example, the commonly studied fatty acid oleic acid since linoleic acid has two double bonds in the acyl chain, which may better fluidize the bilayers (Cooper, 1984), in contrast to oleic acid, which has only one. Single component enhancer formulations were also examined, including polyethylene glycol 200 dilaurate (PEG), isopropyl myristate (IM), glycerol trioleate (GT), ethanol/pH 7.4 phosphate buffered saline in a one-to-one ratio (referred to as 50 % EtOH), and PBS, as a control. Furthermore, since chemical enhancers and ultrasound can each individually increase transdermal drug transport, it was further hypothesized that the combination of chemical enhancers and therapeutic ultrasound (1 MHz, 1.4

W/cm^2) may result in a greater enhancement than that resulting from each enhancement method alone (Johnson et al., in press). The validity of these hypotheses are examined in this chapter.

After a brief description of the materials and methods in section 7.2, the remainder of this chapter is organized as follows. In section 7.3.1, the effects of the chemical enhancers alone on the transdermal transport properties of a single model drug, corticosterone, are examined. The permeabilities, solubilities, and saturated fluxes of corticosterone with the various chemical enhancers are evaluated. Section 7.3.2 examines the effects of therapeutic ultrasound combined with these chemical enhancers on the transdermal transport of the model drug, corticosterone. Section 7.3.3 probes the generality of the key enhancement findings beyond corticosterone. Specifically, LA/EtOH and ultrasound as well as LA/EtOH alone are examined for their abilities to increase the transdermal transport of four additional model drugs, dexamethasone, estradiol, lidocaine, and testosterone. In section 7.3.4, a mechanism of transdermal permeation enhancement of lipophilic solutes by bilayer disordering agents is proposed and shown to be consistent with experimental data presented in this chapter. The generality of this mechanism is further examined by reevaluating permeation data available in the literature. Finally, some concluding remarks are presented in section 7.4.

7.2 Materials and Methods

A detailed description of the general techniques utilized to measure the permeabilities of solutes across the skin were presented in Chapter 2. This section summarizes these methods and connects them with the specific experiments described in this chapter. Human cadaver skin from the chest,

back, and abdominal regions was obtained from a local hospital (Brigham and Women's Hospital, Boston, MA) and the National Disease Research Institute (Philadelphia, PA). The skin was stored at -80°C until usage. The epidermis was separated from the full-thickness tissue after immersion in 60°C water for 2 minutes. Heat-stripped skin was stored at 5°C and 95% relative humidity for up to 1 week prior to usage. ^{3}H-corticosterone, ^{3}H-dexamethasone, ^{3}H-estradiol, ^{14}C-lidocaine, ^{3}H-testosterone, and ^{14}C-linoleic acid were obtained from DuPont, New England Nuclear (Boston, MA). Non-radiolabelled corticosterone (95%), dexamethasone (>99%), estradiol (>99.5%), lidocaine (>99%), testosterone (>99%), and linoleic acid (99%) were obtained from Sigma Chemical Co. (St. Louis, MO). Glycerol trioleate (>99%) and polyethylene glycol 200 dilaurate (>99%) were obtained from Henkel (Cincinnati, OH). Isopropyl myristate (98%) was obtained from Aldrich Chemicals (Milwaukee, WI), and butanediol (98%) was obtained from ISP Technologies (Wayne, NJ). Ethanol was obtained from Pharmco Products (Brookfield, CT).

The passive permeabilities (that is, permeabilities in the absence of ultrasound) of corticosterone, dexamethasone, estradiol, lidocaine, and testosterone through human cadaver skin were measured using trace quantities of the corresponding radiolabelled drugs. The radiolabelled drugs were rotary evaporated in order to remove the ethanol in which they were shipped, as well as any tritium which had reverse-exchanged onto them. The radiolabelled drugs were then redissolved in an enhancer formulation to a typical concentration of 1 μCi/ml, and added to the donor compartment of a diffusion cell. Note that the LA/EtOH formulation consisted of an ethanol/buffer (1:1, v/v) solution saturated with linoleic acid. Passive permeation experiments were performed using stirred side-by-side diffusion cells (#DC-100B, Crown Bioscientific; Sommerville, NJ) at room temperature. The receiver compartment always

contained pH 7.4 phosphate buffered saline (PBS, phosphate concentration = 0.01 M, NaCl concentration = 0.137M) (Sigma Chemical Co., St. Louis, MO). The concentrations of radiolabelled drug in the donor and the receiver compartments were measured using a scintillation counter (model 2000 CA, Packard Instruments Co., Downers Grove, IL). A minimum of three permeation experiments were performed for each enhancer/drug combination. The permeability values, P, were calculated under steady-state conditions from the relationship, $P = (dN_r/dt)/(A(C_d - C_r))$, where A is the surface area of the skin sample, C_d is the drug concentration in the donor compartment, C_r is the drug concentration in the receiver compartment, and N_r is the cumulative amount of drug which has permeated into the receiver compartment at time, t. The experimentally observed lag-times for the permeation experiments were 1-6 hours for corticosterone, 2-8 hours for dexamethasone, less than 1 hour for estradiol and testosterone, and 9-15 hours for lidocaine. The observed variability of the individual permeability values is consistent with the previously established 40% inter-subject variability of human skin permeabilities (Williams et al., 1992).

The passive permeability enhancement, ε_p, was calculated relative to the passive permeability from PBS according to the following relationship:

$$\varepsilon_p \equiv \frac{P(enhancer)}{P(PBS)} \tag{7.1}$$

where *P(enhancer)* and *P(PBS)* are the drug permeabilities from a given enhancer and from PBS, respectively. The flux from a saturated solution, J^{sat}, was calculated from $J^{sat}=PC^{sat}$, where C^{sat} is the drug concentration in the formulation saturated with the drug, whose measurement is discussed below. The flux enhancement, ε_j, was calculated according to the following relationship:

$$\varepsilon_J \equiv \frac{J^{sat}(enhancer)}{J^{sat}(PBS)} \tag{7.2}$$

where $J^{sat}(enhancer)$ and $J^{sat}(PBS)$ are the drug fluxes from saturated solutions of a given enhancer and PBS, respectively,

Ultrasound was applied under therapeutically approved conditions (1 MHz, 1.4 W/cm^2, continuous) for 24 hours using a sonicator (Sonopuls 463, Henley International, Sugar Land, TX). Earlier studies also showed that ultrasound (2 W/cm^2) is unlikely to cause a local temperature increase within the skin due to the well stirred conditions of the diffusion cell compartments, but does produce an overall temperature increase of several degrees (Mitragotri et al., 1995). This temperature increase was determined to be unimportant given the variability of skin permeability measurements (Mitragotri et al., 1995). The ultrasound transducer was located approximately 3 cm from the surface of the skin. Permeation experiments were performed using customized side-by-side diffusion cells having an area of 3.1 cm^2 and a receiver compartment volume of 7.5 ml. These cells consisted of two flange glass cylinders (20 mm diameter) with a ground glass joint (FDC 400, Crown Bioscientific; Sommerville, NJ) clamped together. The end of one cap was sealed with glass, while the other cap was sealed to the ultrasound transducer using epoxy. Samples were periodically taken from the receiver compartment over 24 hours. The concentrations of radiolabelled drug in these samples, as well as those in the donor compartment, were measured using a scintillation counter. Three or more permeation experiments were performed with ultrasound for each enhancer/drug combination examined. PBS was always used in the receiver compartment. The measured sonophoretic permeabilities were constant once steady-state was achieved. Accordingly, drug permeabilities in the presence of ultrasound, P_{us},

were calculated using the same relationship used in the passive case, $P_{us} = (dN_r/dt)/(A(C_d - C_r))$. The exception to this observation is the combination of therapeutic ultrasound and LA/EtOH, with which the corticosterone permeability continually increased, as will be discussed in section 7.3.4.

The transmission efficiency of ultrasound through the various enhancer formulations was measured using a hydrophone (model PZT 54, Specialty Engineering Associates, Milpitas, CA) coupled to a hydrophone preamplifier (model A17DB, Specialty Engineering Associates, Milpitas, CA), and connected to an oscilloscope (model 7623 A, Hewlett Packard, Cupertino, CA). The hydrophone was calibrated by Sonic Technologies (Hatboro, PA). The ultrasound intensity was first measured with both the transducer and the hydrophone submerged in an enhancer formulation while in close proximity to each other. The ultrasound intensity was subsequently measured with the transducer submerged in the enhancer formulation in the donor compartment and the hydrophone submerged in the enhancer formulation in the receiver compartment, 5-6 cm away. No difference in the measured intensities was observed for any formulation, thus indicating that all the chemical enhancer formulations examined were uniformly efficient in transmitting ultrasound.

The uptake of ^{14}C-linoleic acid into human SC was measured with and without the application of therapeutic ultrasound (1.4 W/cm^2, 1 MHz, continuous). This set of experiments was performed in order to examine the mechanism of enhancement (see section 7.3.4). The SC was separated from the heat-stripped epidermis by soaking the epidermis in a 0.5% Trypsin solution overnight at 5°C. The SC was cleaned with water, rinsed in cold hexane to remove any exogenous lipids, and lyophilized for at least 24 hours to remove all the water. Dried pieces of SC were cut into pieces approximately 10 mg in weight and weighed. These SC pieces were placed in a glass chamber (Crown

Glass), mounted on an ultrasound probe containing 3 ml of a solution of ^{14}C-linoleic acid in LA/EtOH, and sealed. 25 µl samples were taken from the chamber periodically, and counted with the liquid scintillation counter. The outcome of this experiment is discussed in section 7.3.4.

The drug solubilities in the various formulations were measured, using techniques described in detail in Chapter 2. Specifically, excess non-radiolabelled corticosterone, dexamethasone, estradiol, lidocaine, and testosterone were each placed in several milliliters of an enhancer formulation and thoroughly mixed. After allowing for equilibration for a minimum of 24 hours, the solutions were removed, centrifuged at 1000 rpm (212xg) for 10 minutes, and sampled. Samples were diluted to a concentration appropriate for high performance liquid chromatographic (HPLC) analysis utilizing the appropriate HPLC mobile phase. Specifically, methanol and water (60:40 v/v) was the mobile phase used in the corticosterone and testosterone HPLC analyses, acetonitrile and water (35:65 v/v) was used in the dexamethasone HPLC analysis, and acetonitrile and water (60:40 v/v) was used in the estradiol analysis. The mobile phase used for the lidocaine HPLC analysis was acetonitrile and an aqueous phase (25:75 v/v), with the aqueous phase consisting of a mixture of water and acetic acid (93:5 v/v) whose pH was adjusted to 3.4 through the addition of NaOH. The mobile phases were filtered with 0.22 µm PTFE hydrophobic filters and degassed prior to use. A µ-Bondapak C18 (30 cm x 4 mm, i.d.) HPLC column was used. The sample volume was 40 µl and the mobile phase flow rate was 2.0 ml/min. An ultraviolet detector (Waters 490) was used at a wavelength of 240 nm for the corticosterone, dexamethasone, and testosterone analysis. Estradiol was detected at 220 nm, and lidocaine at 254 nm. Standards were prepared by diluting a stock solution of each non-radiolabelled drug, prepared by weight, with the mobile phases. Measurements performed in triplicate had a standard deviation of less than 4%.

7.3 Results and Discussion

7.3.1 Passive Transdermal Transport Enhancement of Corticosterone

Results of the passive corticosterone transdermal transport experiments, presented in Table 7.1, reveal that the enhancer formulations examined fall into two groups. The first group of chemical enhancers, PEG, IM, and GT, produced only modest effects upon the corticosterone solubilities, permeabilities, and saturated fluxes relative to those with PBS, while the second group, 50% EtOH and LA/EtOH, resulted in significant changes in these properties. In the first group, PEG and IM are good solubilizers of corticosterone, with measured solubilities of 0.94 and 0.77 mg/ml, respectively. The solubility of corticosterone in PBS is considerably lower, 0.12 mg/ml, but is similar to the solubility of corticosterone in GT, 0.14 mg/ml. These increases in solubility for PEG and IM, however, do not translate into significantly greater saturated fluxes when compared to that from PBS. This is due to the lower corticosterone skin permeabilities from PEG and IM as compared to that from PBS. Specifically, the measured corticosterone skin permeability from PBS is 10×10^{-5} cm/hr, while those from PEG and IM are only 2.4×10^{-5} and 7.0×10^{-5} cm/hr, respectively. The standard errors on these measurements are 11%, 17%, and 22%, respectively. As a result, the flux enhancements from PEG and IM are moderate, 1.9 and 4.5, respectively. GT, whose corticosterone solubility is similar to that of PBS, has a corticosterone permeability of 7.1×10^{-5} cm/hr (±17%), which is similar to that from PBS, 1.0×10^{-4} cm/hr. Therefore, the corticosterone flux from a saturated solution of GT, 1.0×10^{-5} mg/cm^2/hr, is similar to that from a saturated solution

Table 7.1 Corticosterone transdermal transport properties with chemical enhancers.

Enhancer	C^{sat} (mg/ml)	P (cm/hr x10^5 ±SEM)	ε_p	J^{sat} (mg/cm^2/hr x10^5)	ε_j
PBS	0.12	10 ±11%	1.0	1.2	1.0
PEG	0.94	2.4 ±17%	0.24	2.2	1.9
IM	0.77	7.0 ±22%	0.70	5.4	4.5
GT	0.14	7.1 ±17%	0.71	1.0	0.8
50% EtOH	9.2	5.2 ±12%	0.52	48	40
LA/EtOH	12.4	87 ±14%	8.7	1080	903

of PBS, $1.2x10^{-5}$ mg/cm^2/hr. In short, the differences in the solubilities, permeabilities, and fluxes of corticosterone from PBS, PEG, IM, and GT are all relatively moderate and not noteworthy.

In contrast, 50% EtOH and LA/EtOH are both able to significantly impact the transdermal transport of corticosterone. The permeability of corticosterone from 50% EtOH, $5.2x10^{-5}$ (±12%) cm/hr, is nearly two-fold lower than that from PBS, $10x10^{-5}$ (±11%) cm/hr, and in the same range as those from PEG, IM, and GT. This permeability decrease reflects a lesser degree of polarity of 50% EtOH compared to PBS, thus making 50% EtOH a more attractive environment for lipophilic compounds like corticosterone. Accordingly, the equilibrium drug distribution shifts away from the skin and towards the donor solution, resulting in lower partitioning into the skin and, hence, in a lower skin permeability. However, 50% EtOH is also a very effective solubilizer of corticosterone. Specifically, the solubility of corticosterone in 50% EtOH is 9.2 mg/ml, which is nearly 100-fold greater than that in PBS, 0.12 mg/ml, as shown in Table 7.1. This greater extent of solubilization results in a significantly greater flux of $48x10^{-5}$ mg/cm^2/hr, which is 40 fold greater than that from PBS.

Even more effective is LA/EtOH, which is 50% ethanol (v/v) saturated with linoleic acid. Table 7.1 shows that the corticosterone permeability from LA/EtOH is $87x10^{-5}$ (±14%) cm/hr. Note that all the other formulations have lower skin permeabilities than that from PBS, while the permeability from LA/EtOH is nine-fold greater. The permeability enhancement achieved through the mere addition of linoleic acid to 50% EtOH is 17-fold, clearly showing the effectiveness of the unsaturated fatty acid in increasing corticosterone transdermal transport. Addition of linoleic acid to 50% EtOH increases the corticosterone solubility to 12.4 mg/ml in LA/EtOH from 9.2 mg/ml in 50% EtOH alone, as shown in Table 7.1. This is not surprising, since addition of the

oily linoleic acid makes the solution slightly less polar, thus increasing the solubility of lipophilic drugs, such as corticosterone. Even though linoleic acid decreases the polarity of the formulation, and may also slightly decrease corticosterone partitioning into the SC lipids, the corticosterone permeability is larger from LA/EtOH than from 50% EtOH due to the ability of linoleic acid to interact, and fluidize, the stratum corneum lipid bilayers. Likewise, Aungst et al.[8] found that the addition of fatty acids, such as capric acid, lauric acid, and neodecanoic acid, to propylene glycol tended to increase the solubilities of the model drugs naloxone, testosterone, benzoic acid, indomethacin, fluorouracil, and methotrexate (Aungst et al., 1990). The combined effects of enhanced permeation and increased corticosterone solubility arising from the use of linoleic acid in 50% EtOH results in a saturated corticosterone flux of 1080×10^{-5} $mg/cm^2/hr$, which is 900-fold greater than that from PBS and more than 20-fold greater than that from 50% EtOH, that is, in the absence of linoleic acid.

In order to further examine the impact of linoleic acid alone on corticosterone transport, experiments were conducted where corticosterone permeabilities were measured from PBS saturated with linoleic acid. The resulting corticosterone permeability, $(11 \pm 3.4) \times 10^{-5}$ cm/hr, is essentially indistinguishable from that from PBS alone, $(10 \pm 3.2) \times 10^{-4}$ cm/hr, as reported in Table 7.1. Clearly, ethanol and linoleic acid are each ineffective in increasing the corticosterone permeability when utilized with PBS individually, but when ethanol and linoleic acid are utilized together, they yield a substantial degree of enhancement.

7.3.2 Ultrasound-Mediated Transdermal Transport Enhancement of Corticosterone

Previous studies using therapeutic ultrasound (1 MHz, continuous) at an intensity of 2.0 W/cm^2 found that the continuous application of ultrasound increases transdermal permeabilities, but only for a limited period of time (Mitragotri et al., 1995). Specifically, after 5-6 hours, the sonophoretic enhancement diminished and the observed permeabilities returned to their passive values. The sonophoretic enhancement, while it lasted, was caused by cavitation within the SC, that is, the growth and oscillation of air bubbles which disorder the SC lipid bilayers (Mitragotri et al., 1995). In the presented in this chapter, ultrasound was applied at a lower intensity of 1.4 W/cm^2. At this lower intensity, the sonophoretic permeability enhancements lasted for extended periods of time for corticosterone, dexamethasone, estradiol, lidocaine, and testosterone. Specifically, the elevated transdermal permeabilities resulting from the continuous application of ultrasound at 1.4 W/cm^2 were maintained for up to 48 hours, the longest sonophoretic experiment conducted. As a control, the permeability of corticosterone was measured with therapeutic ultrasound applied at 2.0 W/cm^2. The permeation enhancement lasted only for 5-6 hours, as was previously observed for the ultrasound-mediated permeation of estradiol (Mitragotri et al., 1995). This difference in the duration of the sonophoretic enhancements observed at 1.4 and 2.0 W/cm^2 probably reflects changes in the extent of the cavitation activity, which increases as the ultrasound intensity increases. Since the ultrasound-induced cavitation results in the degassing of the system (Mitragotri et al., 1995), 1.4 W/cm^2 ultrasound may result in a more attenuated degassing of the system relative to that at 2.0 W/cm^2, thus leading to the longer durations of the permeability enhancements in the present studies.

Therapeutic ultrasound (1 MHz, 1.4 W/cm^2) was found to be effective in increasing the permeability of corticosterone from all the enhancer formulations examined, as shown in Table 7.2. The sonophoretic permeability enhancements, $\varepsilon_{p,us}$, defined as:

$$\varepsilon_{p,us} = \frac{P_{us}}{P} \tag{7.3}$$

where P_{us} is the sonophoretic skin permeability in a given enhancer formulation, and P is the passive skin permeability from the same formulation, are all greater than unity. The sonophoretic enhancement from PBS, 5.0, is in good agreement with the previously reported value of 4.0 (Mitragotri et al., 1995). The sonophoretic permeability enhancements for the first group of enhancers, PBS, PEG, IM, and GT, are all moderate, ranging from 1.3 for GT to 5.0 for PBS, while the enhancement from 50% EtOH, 1.9, is also moderate. The most significant sonophoretic enhancement is obtained with LA/EtOH. Interestingly, the sonophoretic permeability from LA/EtOH increased over the 24 hour experiments, as will be discussed in section 7.3.4. The sonophoretic permeability from LA/EtOH, as determined at the 24 hour mark of the experiments (n=6), is 1260x10^{-5} cm/hr, which is 14-fold greater than the passive permeability from LA/EtOH. These results show that ultrasound is effective in increasing transdermal corticosterone permeation when utilized with both aqueous as well as non-aqueous formulations, including PEG, IM, GT, and ethanol solutions.

The values of the ultrasound-mediated corticosterone fluxes from the saturated enhancer formulations, J_{us}^{sat}, where $J_{us}^{sat} = P_{us}C^{sat}$, are listed in Table 7.2. The fluxes from PBS, PEG, IM, and GT are all fairly low, ranging from 1.3x10^{-5} mg/cm^2/hr for GT to 6.0x10^{-5} mg/cm^2/hr for PBS. The flux from PBS is greater than those from PEG and GT, due to the greater sonophoretic permeability enhancement for PBS, as shown in Table 7.2. The saturated flux

Table 7.2 Ultrasound-mediated transdermal transport enhancement of corticosterone.

Enhancer	P (cm/hr x10^5 ±SEM)	P_{us} (cm/hr x10^5 ±SEM)	$\varepsilon_{p,us}$	J_{us}^{sat} (mg/cm^2/hr x10^5)	$\varepsilon_{j,us}$
PBS	10 ±11%	50 ±23%	5.0	6.0	5.0
PEG	2.4 ±17%	4.5 ±14%	1.9	4.2	3.5
IM	7.0 ±22%	25 ±19%	3.6	20	16
GT	7.1 ±17%	9.3 ±21%	1.3	1.3	1.1
50% EtOH	5.2 ±12%	9.8 ±11%	1.9	90	75
LA/EtOH ¥	87 ±14%	≥1260 ±60%	≥14.4	≥15,600	≥13,000

¥ The sonophoretic permeability, P_{us}, measured with LA/EtOH was observed to increase over time. The reported value is the average permeability calculated at the 24 hour mark of the experiments, and represents a lower bound on the actual steady-state permeability.

from IM is greater than that from PBS due primarily to the six-fold greater solubility of corticosterone in IM. While the flux from 50% EtOH, 90×10^{-5} mg/cm^2/hr, is 15-fold greater than that from PBS, it is still a relatively low value. Table 7.2 shows that the use of LA/EtOH and therapeutic ultrasound yields a flux greater than or equal to $15{,}600 \times 10^{-5}$ mg/cm^2/hr, which is more than two orders of magnitude greater than that from 50% EtOH with ultrasound, 90×10^{-5} mg/cm^2/hr. Also listed in Table 7.2 are the sonophoretic saturated flux enhancements, $\varepsilon_{J,us}$, defined as:

$$\varepsilon_{J,us} \equiv \frac{P_{us}(enhancer)C^{sat}(enhancer)}{P(PBS)C^{sat}(PBS)} \tag{7.4}$$

Note that $\varepsilon_{J,us}$ represents the flux enhancement relative to the passive flux from PBS, the base case condition. The flux enhancements for PBS, PEG, IM, GT, and 50% EtOH, range from 1.1 for GT to 75 for 50% EtOH. In contrast, LA/EtOH provides a tremendous flux enhancement of approximately 13,000 relative to the passive flux from saturated PBS. This enormous enhancement is the result of the synergistic combination of ethanol, linoleic acid, and ultrasound. Ethanol and PBS (1:1, v/v) greatly increase the saturated concentration of corticosterone (see Table 7.1). Linoleic acid increases both the corticosterone solubility in 50% EtOH as well as the corticosterone permeability, while ultrasound further increases the corticosterone permeability when applied in conjunction with linoleic acid.

7.3.3 Transdermal Transport Enhancement of Dexamethasone, Estradiol, Lidocaine, and Testosterone by Linoleic Acid and Ultrasound

To examine the generality of the effectiveness of LA/EtOH by itself, as well as of the combination of ultrasound and LA/EtOH, in enhancing transdermal transport, measurements were made with four additional model drugs, dexamethasone, estradiol, lidocaine, and testosterone. Solubility and passive permeability measurements were made with PBS, 50% EtOH, and LA/EtOH, as described above. Ultrasound-mediated transport was also measured with LA/EtOH and ultrasound for all four drugs (Table 7.3), since this was the most effective enhancer combination observed in the corticosterone experiments (Table 7.2).

The solubility of dexamethasone in PBS is 0.10 mg/ml, which is similar to the solubility of corticosterone in PBS, 0.12 mg/ml. This is not surprising since both drugs possess a similar degree of hydrophobicity, as revealed by their similar octanol/water partition coefficients of 97 for dexamethasone and 87 for corticosterone (Hansch and Leo, 1979). Likewise, the solubilities of estradiol and testosterone in PBS are much lower, 0.003 (Knutson et al., 1993; Michaels et al., 1975; Williams and Barry, 1991) and 0.023 mg/ml, respectively, which is consistent with their having much larger octanol/water partition coefficients of 7200 (see Chapter 5) and 2100 (Hansch and Leo, 1979), respectively. Lidocaine exists in aqueous solution as both a free-base (non-charged) form and an acid (charged) form. Consequently, the lidocaine solubility in PBS reported in Table 7.3, 3.8 mg/ml, represents the total lidocaine solubility, which includes the acid form which is freely soluble in aqueous solution. Corticosterone, dexamethasone, estradiol, and testosterone are much more soluble in 50% EtOH

Table 7.3 Passive and ultrasound-mediated transport properties of dexamethasone, estradiol, lidocaine and testosterone.

Drug	Enhancer	C^{sat} (mg/ml)[£]	P (cm/hr x10^5 ±SEM)	J^{sat} (mg/cm2/hr x10^5)	P_{us} (cm/hr x10^5 ±SEM)	J_{us}^{sat} (mg/cm^2/hr x10^5)
Dexamethasone	PBS	0.10	6.4 ±23%	0.66	—	—
	50% EtOH	2.39	1.7 ±13%	4.0	—	—
	LA/EtOH	4.36	217 ±24%	945	600 ±4%	2610
Estradiol	PBS	0.003[†]	416 ±13%	1.25	—	—
	50% EtOH	0.74	23 ±22%	17.2	—	—
	LA/EtOH	1.24	429 ±33%	531	787 ±10%	974
Lidocaine[§]	PBS	3.8	397±9%	1520	—	—
	50% EtOH	830/21[¶]	67 ±15%	55600/1410[¶,¥]	—	—
	LA/EtOH	732/648[¶]	576 ±13%	422000/373000[¶,¥]	1170 ±30%	855000/757000[¥]
Testosterone	PBS	0.023	536 ±10%	12.3	—	—
	50% EtOH	6.37	5.5±5%	35.2	—	—
	LA/EtOH	8.2	64 ±11%	525	449 ±30%	3680

[†] Average of values reported in the literature (Knutson et al., 1993; Michaels et al., 1975; Williams et al., 1992).

[§] The reported lidocaine passive and sonophoretic permeabilities are the overall lidocaine permeabilities. Lidocaine solutions contain both the free-base (that is, non-charged) and the acid (charged) forms of lidocaine. As charged compounds have very low permeabilities, the diffusion of the free-base form across the skin dominates.

[¶] The addition of excess lidocaine to 50% EtOH and LA/EtOH solutions resulted in the formation of two liquid phases. For 50% EtOH, one phase was rich in lidocaine, 830 mg/ml, while the other had little lidocaine, 21 mg/ml. For LA/EtOH, one phase contained 732 mg/ml of lidocaine while the other contained 648 mg/ml. Two values of the saturated lidocaine fluxes for both the 50% EtOH and LA/EtOH, calculated with the expression $J^{sat} = Pc^{sat}$ using the lidocaine solubilities in the two phases, are therefore reported.

[¥] Large concentrations of lidocaine in the enhancer formulation may alter the solution properties by making the solution less polar. As such, the skin/solution partition coefficient would be lower for a concentrated lidocaine solution than for a very dilute lidocaine solution, such as those solutions containing only radiolabelled lidocaine utilized for the permeation experiments. The lidocaine permeability, in turn, would be lower from a solution saturated with lidocaine than from a dilute solution. Hence, the reported passive and sonophoretic saturated fluxes are likely to be upper estimates of the actual values.

[£] The standard deviations on the solubility measurements were less than 4%.

than in PBS by factors of 77, 24, 247, and 280, respectively, and even more soluble in LA/EtOH, by an average factor of 1.5, than in 50% EtOH, as shown in Figure 7.1.

The measured passive permeabilities from 50% EtOH for dexamethasone, estradiol, lidocaine, and testosterone are $1.7x10^{-5}$, $23x10^{-5}$, $67x10^{-5}$, and $5.5x10^{-5}$ cm/hr, respectively, which are lower than their respective permeabilities from PBS by one to two orders of magnitude. These results are consistent with the observations made of corticosterone, presented in Table 7.1, and with previous reports for estradiol (Liu et al., 1991). These permeability decreases are a result of the decreased partitioning of the drugs into the skin, as discussed above. The permeability of dexamethasone from LA/EtOH, $217x10^{-5}$ cm/hr, is significantly greater than that from PBS, $6.4x10^{-5}$ cm/hr, as was also observed with corticosterone. However, the permeabilities of estradiol and lidocaine from LA/EtOH, $429x10^{-5}$ and $576x10^{-5}$ cm/hr, respectively, are both approximately the same as the permeabilities from PBS, while the permeability of testosterone from LA/EtOH, $64x10^{-5}$ cm/hr, is still eight-fold lower than that from PBS, $536x10^{-5}$ cm/hr.

The sonophoretically-enhanced permeabilities of dexamethasone, estradiol, lidocaine, and testosterone increased over time in these experiments, similar to what was observed with corticosterone. However, unlike the corticosterone experiments, the observed permeabilities were steady after 10-15 hours, thus enabling true steady-state measurements to be made. Specifically, the sonophoretic permeabilities of dexamethasone, estradiol, lidocaine, and testosterone are $600x10^{-5}$ (±4%) cm/hr, $787x10^{-5}$ (±10%) cm/hr, $1170x10^{-5}$ (±30%) cm/hr, and $450x10^{-5}$ (±30%) cm/hr, respectively. Similar to corticosterone, large sonophoretic saturated fluxes of $2610x10^{-5}$, $974x10^{-5}$, and $3680x10^{-5}$ mg/cm^2/hr were obtained for dexamethasone, estradiol, and testosterone, respectively.

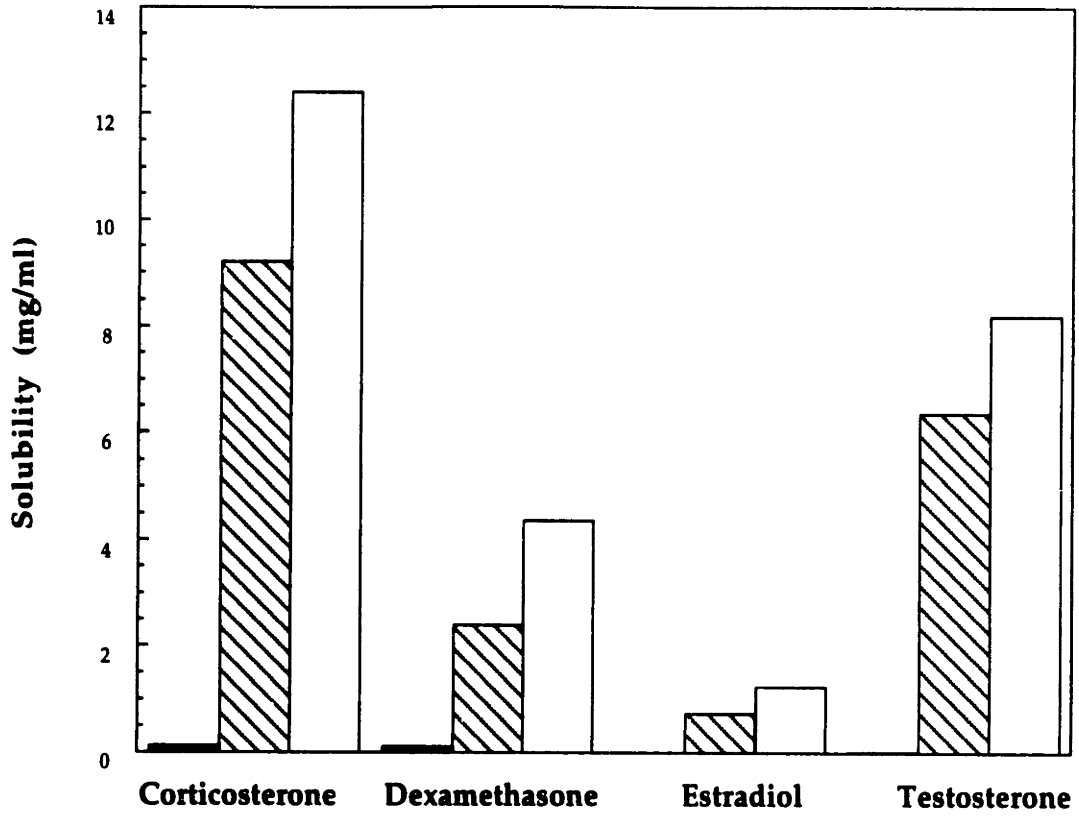

Figure 7.1 Solubilities of corticosterone, dexamethasone, estradiol, and testosterone in PBS (black bars; note that the bars representing the solubilities of estradiol and testosterone in PBS are too small to be discerned), 50% EtOH (cross-hatched bars), and LA/EtOH (white bars) measured using HPLC. The solubilities of these drugs in PBS, 0.12 mg/ml, 0.10 mg/ml, 0.003 mg/ml (Knutson et al., 1993; Michaels et al., 1975; Williams et al., 1992) and 0.023 mg/ml, respectively, are 77, 44, 246, and 360 fold lower than the solubilities in 50% EtOH. Corticosterone, dexamethasone, estradiol, and testosterone are even more soluble in 50% EtOH saturated with linoleic acid (LA/EtOH) by an average factor of 1.5. The standard deviation of each of these measurements is less than 4%.

Lastly, the saturated flux and sonophoretic saturated flux values for lidocaine from 50% EtOH and LA/EtOH, shown in Table 7.3, are large due to the exceptionally large lidocaine saturated concentrations in these formulations. However, the lidocaine permeabilities listed in Table 7.3, which were used as the basis for the flux calculations, were measured with radiolabelled lidocaine under dilute conditions. As large lidocaine concentrations would tend to decrease the polarity of the formulation, and hence decrease the drug permeability, the lidocaine flux values in Table 7.3 should be taken as upper estimates of the actual values.

7.3.4 Mechanisms of Enhancement and Synergistic Effects

7.3.4.1 Permeability Enhancement by Lipid Bilayer Disordering Enhancers

Unsaturated fatty acids, such as linoleic acid, are primarily thought to enhance skin permeabilities by disordering the SC intercellular lipid domain. Detailed studies of the SC with unsaturated fatty acids, for example, oleic acid, have been performed utilizing differential scanning calorimetry (Barry, 1987) and infrared spectroscopy (Mak et al., 1990; Ongpipattanakul et al., 1991). Oleic acid was found to disorder the highly ordered SC lipid bilayers, and to possibly form a separate, oil-like phase in the intercellular domain. SC lipid bilayers disordered by unsaturated fatty acids or other bilayer disrupters may be similar in nature to a lipid bilayer fluid phase. A separated oil phase, such as pools of linoleic acid within the SC, would likely have properties similar to a bulk oil phase. It was proposed that bilayer disordering agents, such as linoleic acid and ultrasound, transform SC lipids into a state analogous to fluid bilayers or a bulk oil phase,

and that the increased diffusion in these phases produces the observed permeability enhancements (Johnson et al., in press).

Diffusion in various lipid bilayer systems is characterized by a solute-size dependence (Clegg and Vaz, 1985; Cooper and Kasting, 1987; Johnson et al., submitted[a]; Kasting et al., 1992; Potts and Guy, 1992; Tocanne et al., 1989; Wilschut et al., 1995), with the rate of diffusion decreasing substantially with increasing size for solutes smaller than ~500 Da (Johnson et al., submitted[a]). The degree of this dependence is much greater for diffusion in the highly ordered SC lipids than for more fluid bilayers, such as dimyristoylphosphatidylcholine (DMPC), which in turn exhibits a stronger solute-size dependence than do bulk fluids, such as oils (Perry et al., 1984). This implies that the *difference* in diffusivity of a given solute in SC bilayers and in either DMPC bilayers or bulk oil is *larger for larger solutes.* Hence, the enhancement ability of a bilayer disordering compound which transforms the SC lipid bilayers into a fluid lipid bilayer phase or creates a separate bulk oil phase should be greater for larger compounds.

In fact, Figure 7.2 shows that the permeability enhancement resulting from the use of linoleic acid depends on the size of the drug. The permeability enhancements resulting from linoleic acid, that is, the ratio of the permeability from LA/EtOH and the permeability from 50% EtOH alone, are 8.6 for the smallest drug (lidocaine free-base, 234 Da), 18 for estradiol (272 Da), 12 for testosterone (288 Da), 17 for corticosterone (346 Da), and 130 for the largest drug (dexamethasone, 392 Da). The linoleic acid enhancement varies directly with the drug molecular weight, except in the case of estradiol, which exhibits a larger enhancement than the trend in Figure 7.2 predicts. These data are consistent with the proposed mechanism of enhancement.

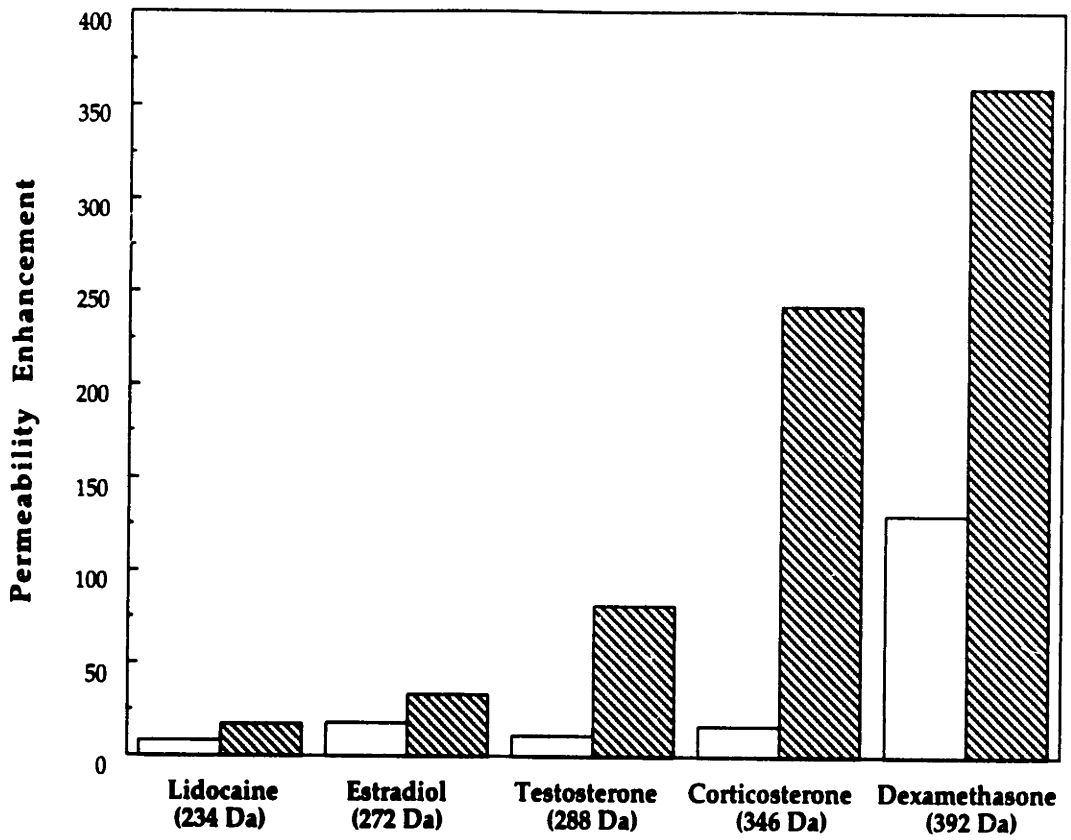

Figure 7.2 Permeability enhancements for lidocaine (free-base, 234 Da), estradiol (272 Da), testosterone (288 Da), corticosterone (346 Da), and dexamethasone (392 Da) through (1) the addition of linoleic acid to 50% EtOH (white bars), and (2) the addition of linoleic acid to 50% EtOH with the continuous application of therapeutic ultrasound (cross-hatched bars) relative to the permeabilities from 50% EtOH alone. The enhancements from linoleic acid exhibit a size dependence, with the larger compounds tending to have larger enhancements. Likewise, the enhancements with linoleic acid and therapeutic ultrasound exhibit a clear size dependence with greater enhancements observed for the larger compounds.

In order to assess the generality of the findings with linoleic acid, data associated with the permeation enhancement by other bilayer disordering agents were collected from the literature and analyzed. Specifically, Aungst et al. (Aungst et al., 1990) measured the permeabilities of six compounds with several different formulations across human skin, and concluded that there was no size dependence of the enhancement. Closer examination of their data, however, reveals that there is a size dependence of enhancement for the lipophilic compounds by the bilayer disrupting enhancers. Figure 7.3a shows the permeability enhancements for the four lipophilic compounds they examined, benzoic acid (122 Da), testosterone (288 Da), naloxone (328 Da), and indomethacin (359 Da), which were produced by the three bilayer disrupting compounds which they utilized, capric acid, lauric acid, and neodecanoic acid, all in propylene glycoi (Aungst et al., 1990). The data of Aungst et al. (Aungst et al., 1990) which are shown in Figure 7.3a support the conjecture that the permeability enhancements of lipophilic compounds by bilayer disrupting agents exhibit a size dependence. Note also that the permeability enhancements of the two hydrophilic compounds, fluorouracil and methotrexate, obtained with the bilayer disrupting enhancers do not support the idea of a molecular weight dependence. However, this is not surprising since hydrophilic compounds appear to permeate the skin through non-lipoidal pathways (Peck et al., 1995), and, hence, would not be expected to be affected by bilayer fluidizing enhancers via the same mechanism as that affecting lipophilic compounds which diffuse through the lipid bilayers.

Lambert et al. (1989) and Hirvonen et al. (Hirvonen et al., 1993; Hirvonen et al., 1991) examined the effects of a different, but commonly studied, bilayer disrupting compound, Azone, upon the permeability of a variety of lipophilic drugs. Lambert et al. measured the permeabilities of ethanol, butanol,

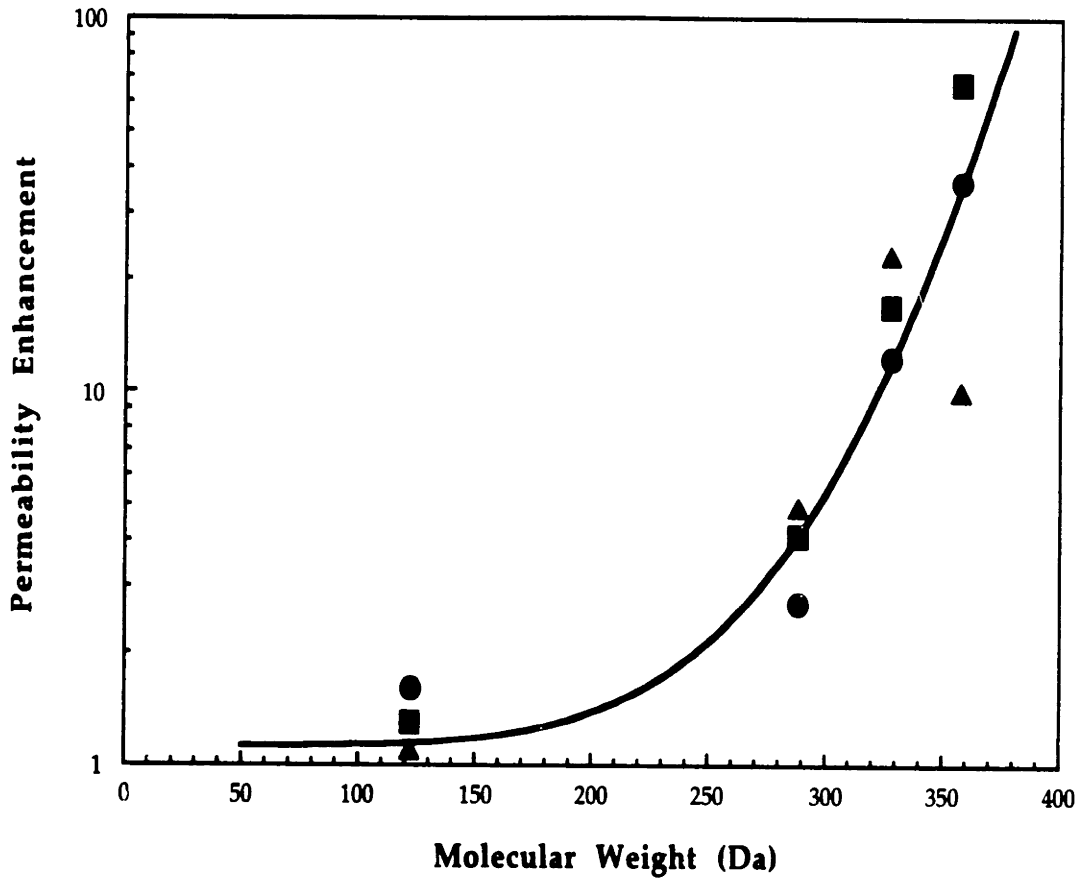

Figure 7.3a The enhancement effects of three different enhancers, capric acid (●), lauric acid (■), and neodecanoic acid (▲), on the human skin permeabilities of benzoic acid (122 Da), testosterone (288 Da), naloxone (328 Da), and indomethacin (359 Da), from propylene glycol. These enhancements exhibit a clear size dependence, with the larger compounds being enhanced to a greater extent than the smaller compounds. The permeability values were originally reported by Aungst et al. (1990). The line is drawn to guide the eye.

corticosterone, and hydrocortisone from aqueous solutions across hairless mouse skin which had been pretreated with Azone.§ Hirvonen et al. measured the permeabilities of propanolol, timolol, corticosterone, and indomethacin from aqueous solutions across human skin, rabbit skin, and snake skin, pretreated with Azone. Figure 7.3b shows that the permeability enhancements resulting from the use of Azone exhibit a size dependence, with the larger compounds exhibiting greater enhancements. These results, combined with those presented in Figures 7.2 and 7.3a, further support the proposed mechanism of permeability enhancement.

While the data discussed above are consistent with the proposed enhancement mechanism, other mechanisms could also contribute to the observed permeability enhancements. First, fluidization of the stratum corneum lipid bilayers can increase the solute partition coefficient between the bilayers and the donor medium in addition to increasing solute diffusion. However, partitioning is a function of the chemical nature of a solute (namely, of the hydrophobic/hydrophilic nature of a solute) and is not an independent function of molecular weight (Hansch and Leo, 1979). Therefore, the contributions of enhanced partitioning to the overall permeability would tend to obscure the size dependence of enhancement and cannot account for the results presented in Figures 7.2, 7.3a, and 7.3b. A second possible mechanism is that the bilayer disordering enhancers or ethanol may increase drug transport through alternate pathways, often referred to as aqueous pores (Peck et al., 1994). Consistent with

---

§ The permeabilities tended to increase with the amount of Azone used in the pretreatment up to 0.4 mg/cm^2 of Azone. Pretreatment with 0.4 mg/cm^2 or more of Azone produced the same, and the maximum, effects observed. The values of the permeabilities were obtained from graphical representations of the data in Ref. 25, and were utilized to calculate the enhancements according to $\varepsilon_A = P_{A/aq}/P_{aq}$, where $P_{A/aq}$ is the drug permeability with Azone pretreatment at 0.8 mg/cm^2, and P_{aq} is the permeability from aqueous solution alone.

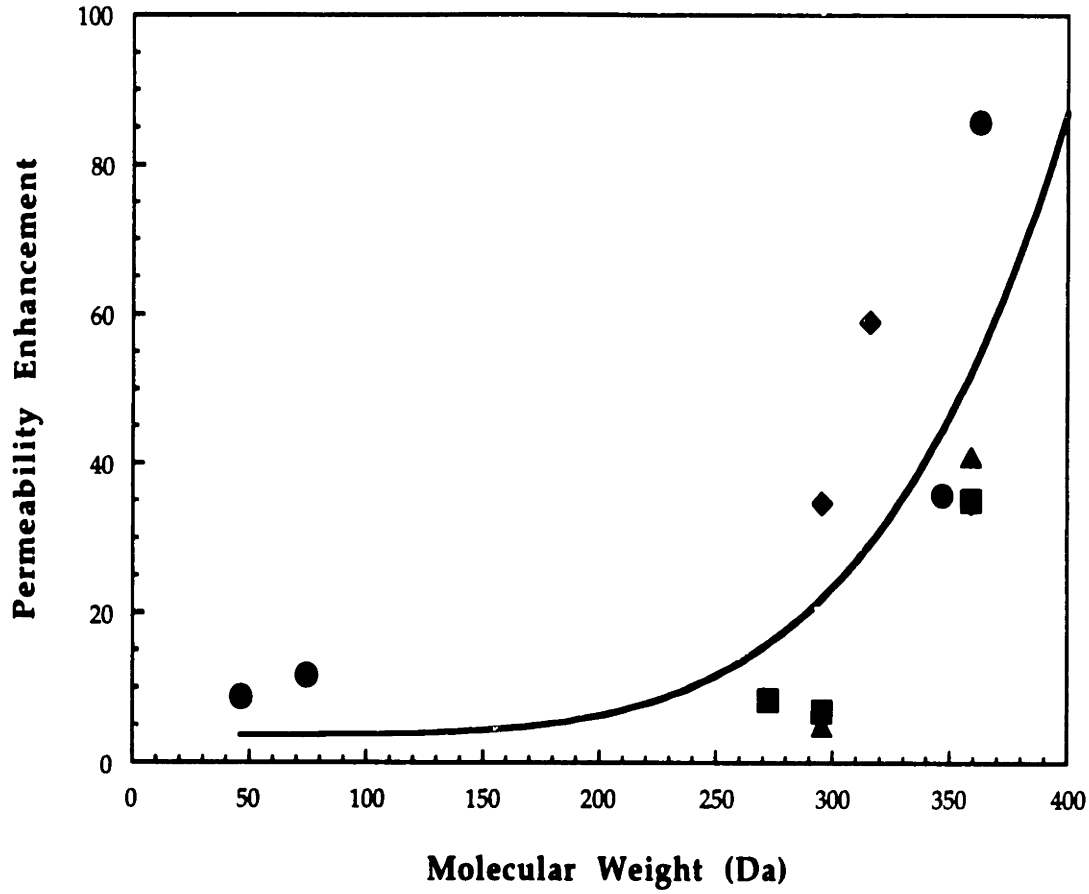

Figure 7.3b The enhancement of Azone on the permeabilities of a variety of compounds through hairless mouse skin (●) (Lambert et al., 1989), human skin (■) (Hirvonen et al., 1993; Hirvonen et al., 1991), snake skin (▲) (Hirvonen et al., 1991), and rabbit skin (◆) (Hirvonen et al., 1991). The degree of permeability enhancement correlates with the size of the solute. The line is drawn to guide the eye.

this mechanism, passive skin permeabilities of hydrophilic compounds, which are thought to diffuse through these aqueous pores, exhibit a weaker size dependence than that of hydrophobic compounds (Peck et al., 1994). However, since fatty acids interact predominantly with the intercellular lipids (Barry, 1987; Ongpipattanakul et al., 1991), this mechanism appears unlikely. High ethanol concentrations, about 75% (v/v) (Ghanem et al., 1992), can enhance the transport of both hydrophobic and hydrophilic compounds through these aqueous pore pathways. However, lipoidal compounds in solutions of 50% ethanol or less, as was used in the experiments described in this chapter, permeate the SC primarily through the lipoidal domain (Ghanem et al., 1992), suggesting that the results in Figure 7.2 do not stem from increased transport through an aqueous pore pathway (Ghanem et al., 1992). Furthermore, the results presented in Figures 7.3a and 7.3b were obtained from experiments performed with propylene glycol, and not ethanol. Nevertheless, these mechanisms, as well as others, are worthy of further investigation.

In summary, chemical enhancers can affect drug transport by (1) altering the donor solution properties, and (2) interacting with the SC. Results presented in this chapter, as well as those of others (Aungst et al., 1990; Lambert et al., 1989), suggest an explanation for some apparently disparate chemical enhancer data. Specifically, bilayer disrupting agents appear to increase the permeabilities of larger lipophilic compounds to a greater extent than those of smaller compounds. This is consistent with the proposed mechanism that bilayer disordering agents increase the fluidity of the intercellular lipid region, which in turn increases the solute diffusion coefficients and decreases the apparent size dependence.

7.3.4.2 Ultrasound as a Bilayer Disordering Agent

Figures 7.2, 7.3a, and 7.3b, show the effects of bilayer disordering agents which produce permeability enhancements which depend upon solute size. Therapeutic ultrasound has also been found to increase solute permeabilities by disordering the lipid bilayers. Mitragotri et al. (1995) have recently reported that the mechanism of sonophoretic enhancement is cavitation within the SC, a phenomenon that disorders the SC lipid bilayers. Since ultrasound by itself is a bilayer disordering agent, sonophoretic enhancement measured without chemical enhancers would also be expected to exhibit a size dependence. Mitragotri et al. have recently compiled the results of therapeutic sonophoretic enhancement experiments conducted over the last four decades for more than a dozen different drugs, ranging in size from 78 Da (benzene) up to 453 Da (fluocinolone acetonide) (submitted). These studies include both *in vitro* and *in vivo* experiments. While some studies quantified the degree of enhancement, others simply reported whether or not sonophoretic enhancement was observed. All of these data, except for that of hydrophilic drugs, are summarized in Figure 7.3c, where the molecular weights of the various drugs are shown. Hydrophilic drugs are not considered in this analysis since they may permeate the skin through aqueous pathways and, hence, would not be substantively affected by bilayer disordering. Drugs for which sonophoretic enhancements were observed are plotted as filled circles, while drugs for which no enhancements were observed are plotted as open circles. Figure 7.3c shows that there is a fairly sharp cut-off size of approximately 250 Da, above which ultrasound produces measurable enhancements and below which it does not. These therapeutic ultrasound enhancement data further support the chemical enhancer findings, discussed above, and the proposed enhancement mechanism.

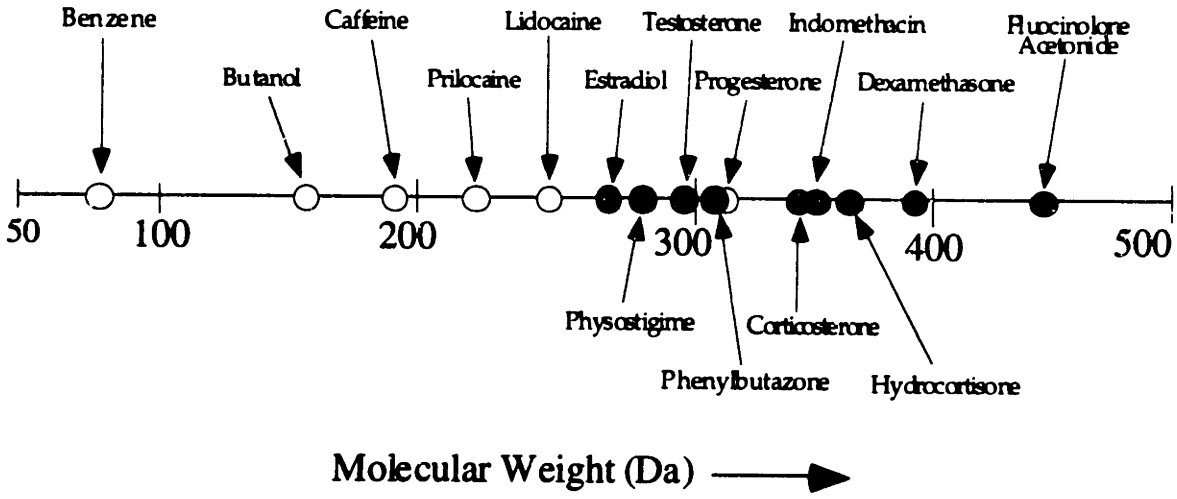

Figure 7.3c The figure shows molecular weights of various drugs that have been examined in the past with sonophoresis. Hydrophilic drugs, which may permeate the skin through aqueous pathways and, hence, would not be expected to be affected by bilayer disordering, are not included in this figure. Drugs indicated by empty circles (O) correspond to those for which no enhancement of transdermal delivery has been observed during sonophoresis. Drugs indicated by filled circles (●) correspond to those for which an experimentally observed enhancement has been reported. A molecular weight cut-off is observed at approximately 250 Da. No sonophoretic enhancement has been observed for drugs smaller than 250 Da, whereas sonophoretic enhancement has been observed for compounds larger than 250 Da, with the sole exception of progesterone. Data were originally compiled by Mitragotri et al. (Mitragotri et al., submitted), who report that sonophoretic enhancement correlates very well with the drug passive diffusion coefficient, which, in turn, is a strong function of molecular weight (see Chapter 4).

7.3.4.3 Synergistic Effects of Linoleic Acid and Therapeutic Ultrasound

As linoleic acid and ultrasound are both bilayer disordering agents, the enhancement arising from their combined use should also exhibit a size dependence. Figure 7.2 shows that the permeability enhancements resulting from the combined application of linoleic acid and ultrasound increase with the size of the drug. Lidocaine (free-base, 234 Da) exhibits a permeability enhancement of 17, estradiol (272 Da) of 34, testosterone (288 Da) of 81, corticosterone (346 Da) of 243, and dexamethasone (392 Da) of 360. As would be expected, the combination of linoleic acid and therapeutic ultrasound increases transdermal drug transport more than each agent by itself.

Lastly, an intriguing aspect of the synergistic effects of linoleic acid and therapeutic ultrasound was observed, and is shown in Figures 7.4a and 7.4b. These figures show the results of typical corticosterone transport experiments performed with LA/EtOH in the presence and absence of ultrasound, respectively. Corticosterone permeability from LA/EtOH achieved steady-state after several hours in the absence of ultrasound, but increased over the 24 hour experiment when ultrasound was applied. This synergistic relationship was further probed in a set of experiments with corticosterone in LA/EtOH in which ultrasound was applied for the first eight hours of the experiments, after which ultrasound was turned off. The results of one such experiment are shown in Figure 7.5. The corticosterone permeability continually increases for the first eight hours, during which ultrasound is applied. However, the slope of the curve is linear beginning at the eight hour mark ($R>0.999$) - at which time

ultrasound was turned off - and remains so for the remainder of the experiment, in contrast to the continual increase shown in Figure 7.4b.

Four possible mechanisms were considered to explain the experimental observations shown in Figures 7.4b and 7.5:

1. Ultrasound may be solely responsible for these behaviors by disordering the SC lipid bilayers through cavitation (Mitragotri et al., 1995). Cessation of ultrasound in corticosterone permeation experiments from PBS resulted in the recovery of the permeability back to passive levels after 1-2 hours. In contrast, Figure 7.5 shows that the corticosterone permeability from LA/EtOH does not decrease after ultrasound is removed. Instead, the corticosterone permeability is maintained at the same elevated values, 745×10^{-5} cm/hr - nearly an order of magnitude greater than the passive permeability - for more than 24 hours after ultrasound is removed. While cavitation induced bilayer disordering is likely to be occurring, additional mechanism(s) appear to be important and necessary to explain the results presented in Figures 7.4a, 7.4b, and 7.5.

2. Ultrasound might also be driving linoleic acid into the skin over time. This would increase the linoleic acid levels in the SC, which would likely result in increased bilayer fluidity relative to the passive case. To test this mechanism, the SC uptake of ^{14}C-linoleic acid from LA/EtOH was measured both with and without the application of therapeutic ultrasound (section 7.2). The rates of uptake were nearly identical over 24 hours, indicating that linoleic acid is not being driven into the skin at a significantly greater rate by ultrasound than as compared to the passive case.

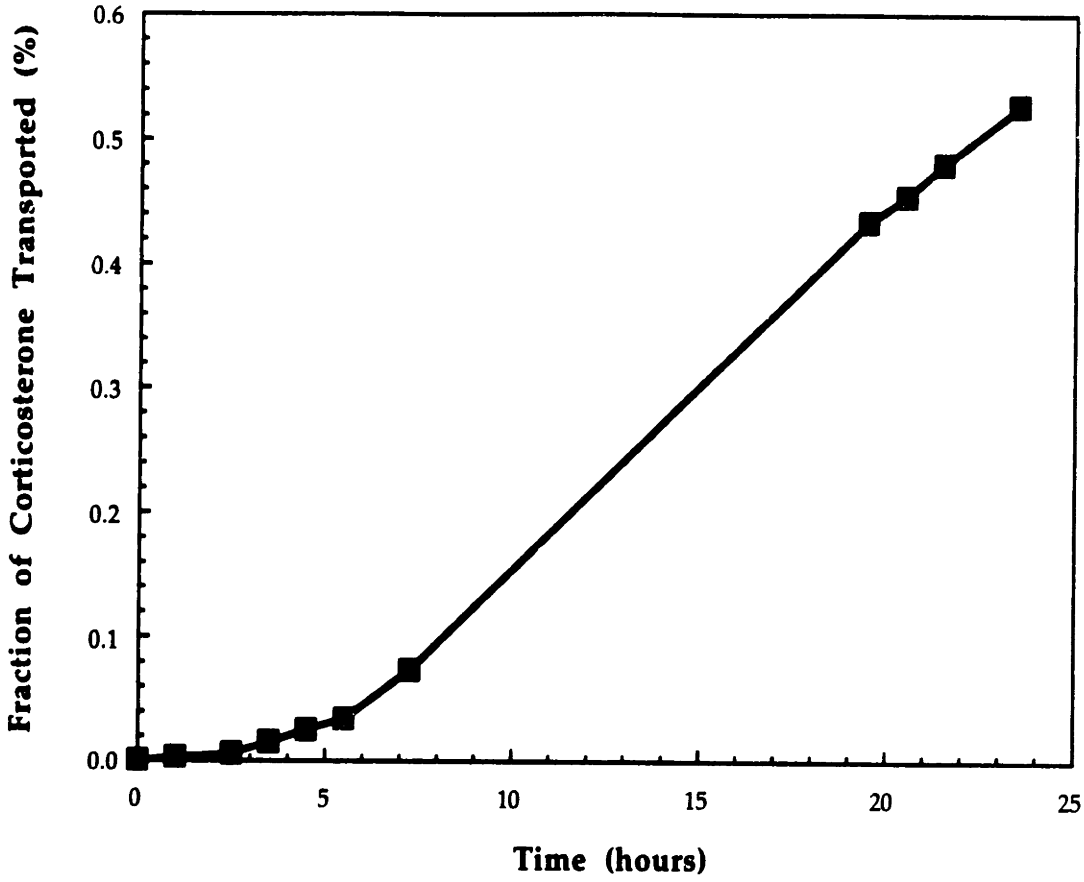

Figure 7.4a Time variation of corticosterone transport through human skin from PBS in the presence of therapeutic ultrasound (1 MHz, 1.4 W/cm^2, continuous). The corticosterone permeability (that is, the slope of the curve) is maintained at the steady-state value for the duration of the 24 hour experiment once the lag-time period of about 4 hours is surpassed. The typical error (SD) of the data points is 3%. The line is drawn to guide the eye.

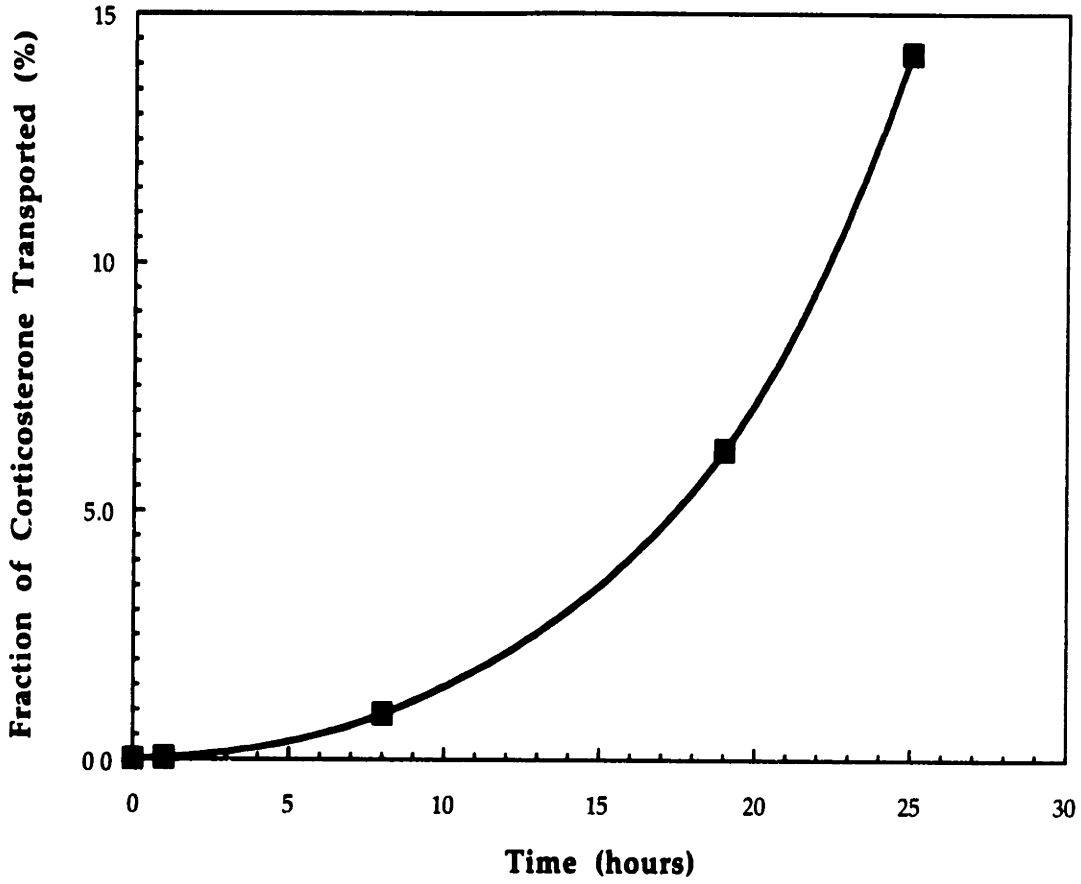

Figure 7.4b Time variation of corticosterone transport through human skin from LA/EtOH in the presence of therapeutic ultrasound (1 MHz, 1.4 W/cm^2, continuous). The corticosterone permeability (that is, the slope of the curve) continues to increase over time, in contrast to the transport experiments from PBS (Figure 7.4a), in which the permeability remained constant. The typical error (SD) of the data points is 3%. The line is drawn to guide the eye.

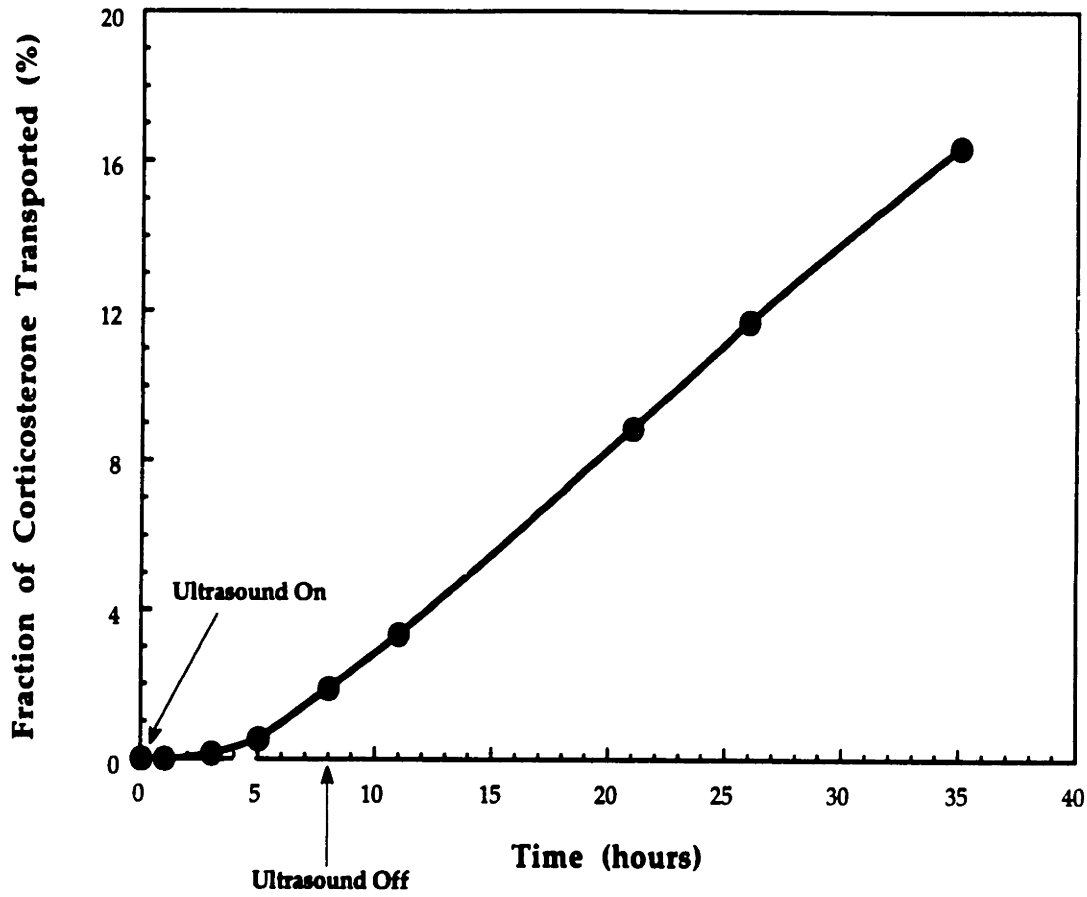

Figure 7.5 Time variation of corticosterone transport through human skin from LA/EtOH with the discontinuous application of therapeutic ultrasound (1 MHz, 1.4 W/cm^2). Ultrasound was applied for the first eight hours of the experiment, at which time it was turned off. In contrast with the results shown in Figure 7.4b, in which ultrasound was applied continuously and the permeability continued to rise for the entire 24 hour period, the corticosterone permeability increases up to the point at which the ultrasound is turned off, beyond which it remains constant for the remainder of the experiment. The typical error (SD) of the data points is 3%. The line is drawn to guide the eye.

3. LA/EtOH and ultrasound together might be inducing extraction of the SC lipids. The degree of lipid removal would be essentially constant for all five drugs, since the drugs were present in trace quantities and exert no influence on the extraction process. Since SC permeabilities are inversely proportional to the lipid content, the same degree of increase in the sonophoretic permeability over the passive values from LA/EtOH would be expected for all five of the drugs examined. However, the permeability enhancements from the application of ultrasound to LA/EtOH span an order of magnitude, from 1.8 for estradiol to 14 for corticosterone. This range is considerably greater than the characteristic error of permeability measurements. In addition, the 14-fold enhancement of corticosterone would imply that 13/14, or 93% of the stratum corneum lipids, would have been removed, which appears to be unlikely. Consequently, although lipid extraction may be occurring to a minor extent, it does not appear to be the primary mechanism behind the findings illustrated by Figures 7.4a, 7.4b, and 7.5.

4. Ultrasound may be aiding the dispersion of linoleic acid in the SC lipids. Previous studies have shown that fatty acids, such as oleic acid, form segregated phases within the SC (Ongpipattanakul et al., 1991; Walker and Hadgraft, 1991). Under passive conditions, linoleic acid may also tend to diffuse into the SC and collect in pools. The cavitation produced by ultrasound may induce mixing and facilitate the dispersion of linoleic acid and the SC lipids. The increased entropy of the resulting mixed system would make it a more favorable molecular arrangement which would remain stable even after ultrasound is turned off. The results presented in Figures 7.4a, 7.4b, and 7.5 are consistent with this last mechanism, but additional studies are needed to further elucidate the mechanisms.

7.4 Conclusions

Different enhancement agents, each of which are capable of increasing transdermal drug transport via a different mechanism, can be effectively combined, as shown in this chapter. Ethanol, which can effectively solubilize many lipophilic drugs, and linoleic acid, an unsaturated fatty acid which disorders bilayers, when combined (LA/EtOH), significantly increased the saturated fluxes of the model drugs corticosterone, dexamethasone, estradiol, lidocaine, and testosterone. Even greater enhancements were obtained by combining ultrasound with LA/EtOH. Ultrasound applied under the conditions described in this work (1 MHz, 1.4 W/cm^2) has been shown to be completely reversible for application times as long as 24 hours (Mitragotri et al., 1995), and is approved for therapeutic applications (Kost and Langer, 1993). Likewise, most of the enhancers examined in this work are generally considered to be safe by regulatory authorities.(1991) Nevertheless, *in vivo* toxicological studies will be required to fully assess the biocompatibility and reversibility of these enhancer/ultrasound combinations.

The magnitude of the permeability enhancements of the model drugs produced by LA/EtOH with and without ultrasound increased with increasing molecular weight. A mechanism of enhancement was proposed in this chapter to explain this size dependence. Specifically, it was proposed that bilayer disordering agents, including unsaturated fatty acids and therapeutic ultrasound, transforms the highly ordered SC lipid bilayers into a more fluid state, such as DMPC or a bulk oil phase. Diffusion in the highly ordered SC lipids exhibits a stronger size dependence than that in fluid phase lipid bilayers and bulk oil phases. Hence, the potential transdermal permeation enhancement

is greater for larger drugs. The data presented in this chapter, as well as a reevaluation of published data based on the use of several different bilayer disordering chemicals, supports the proposed mechanism. This size dependence of the permeability enhancement is applicable to a certain class of enhancers, bilayer disordering agents, and to lipophilic drugs. Further investigations may lead to analogous relationships for other classes of enhancers as well as for hydrophilic compounds.

Chapter 8

Concluding Remarks

8.1 Thesis Summary

Diffusive transport of solutes across the stratum corneum is an inherently complex phenomenon, due to the intricate structures which compose this tissue as well as the diverse physicochemical properties of the solutes considered. Connecting the macroscopic transport properties of interest, that is, the transdermal permeability and flux, to the underlying structure of the stratum corneum, including lipid bilayers and keratinocytes, continues to be a challenge to researchers. Furthermore, the process of choosing drug/chemical enhancer combinations is even more challenging due to the complex and multiple effects that chemical enhancers can introduce to the transport process, including increased drug solubility, decreased lipid bilayer/formulation partitioning, increased diffusion in lipid bilayers, as well as diffusion through other pathways. This thesis addressed these challenges, and in the process, has effectively coupled macroscopic transdermal transport with the lipid-bilayer scale transport properties, and showed that the permeability enhancement produced by bilayer disordering agents is generally predictable for lipophilic drugs.

Values of the fundamental bilayer transport properties (that is, partition coefficients, lateral diffusion coefficients, and transbilayer mass transfer coefficients) were directly measured in this thesis (Chapter 4 (lateral diffusion)

and Chapter 5 (partitioning)), and supplemented by data obtained from the literature for a variety of model systems.

The measurement of lateral diffusion coefficients for a series of lipophilic, fluorescent probes (223-854 Da), are described in Chapter 4. The diffusion experiments were performed using an image based fluorescence recovery after photobleaching (video-FRAP) technique, and represents the first time that this particular technique has been utilized to study diffusion in lipid bilayer systems. Measurements made with stratum corneum extracted lipids (SCE) exhibited a size dependence, with smaller probes diffusing at a faster rate than larger probes. These measurements represent the first, and most comprehensive, examination of lateral diffusion with stratum corneum lipids, a remarkable fact given the amount of attention paid to 'diffusion' in the stratum corneum, and were utilized in Chapter 6 to examine the importance of lateral diffusion to stratum corneum solute transport. Three out of the nine probes examined exhibited behaviors which indicate that their movement was not governed solely by diffusion, but that some other kinetic phenomenon was involved. Interestingly, these three probes had been chosen specifically for their lipid-like nature, and when viewed in terms of previous experiments which showed that lipid molecules cross bilayers much more slowly than non-lipoidal solutes, seems to suggest that the rate of 'flip-flop' of these probes may have played a role in the overall transport.

Lateral diffusion measurements made with liposomes composed of dimyristoylphosphatidylcholine (DMPC) and DMPC/cholesterol (40%) also exhibited size dependencies, with smaller probes diffusing at faster rates than larger probes (Chapter 4). These measurements represent the most comprehensive examination of small-molecule diffusion in DMPC and DMPC/cholesterol model lipid systems made to date. The molecular weight (size) dependence of the lateral diffusion coefficients for all three lipid systems in

the size regime examined (223-854 Da) is stronger than that predicted by continuum theory, but was well described by a two-parameter empirical expression. This expression combined a power-law molecular weight dependence with a dependence predicted by continuum theory (that is, the Saffman-Delbrück expression). The strong size dependence exhibited by my data was also found to extend to even smaller solutes (down to 32 Da, for molecular oxygen), through an examination of available literature data. Furthermore, this work constitutes the first systematic comparison of the magnitudes and size dependencies of lateral diffusion in different lipid systems. The size dependencies for SCE lipids, DMPC liposomes, and DMPC/cholesterol liposomes were shown to be analogous, but with the most fluid system (DMPC) characterized by greater diffusion coefficients than those for DMPC/cholesterol and SCE lipid bilayers, which were found to be approximately the same.

Partition coefficients were measured for a series of lipophilic solutes using a variety of model systems, including octanol/water and liposomes composed of stratum corneum model lipids (SCM), DMPC, and DMPC/cholesterol, and these were compared with partition coefficient values measured using SCE lipids (Chapter 5). The measurements made in all four of the model lipid systems were found to correlate reasonably well with the values obtained using SCE lipids, although the SCM and DMPC/cholesterol liposomes were the most quantitatively similar. While it is not surprising that the SCM liposomes are quantitatively similar to SCE lipids in their partitioning characteristics, the similarity of DMPC/cholesterol liposomes - combined with the similarity of the lateral diffusion measurements in this model lipid systems - suggests that the characteristics and behavior of DMPC/cholesterol liposomes provide a reasonable model system for SCE lipids. Further corroboration of this finding

was established through literature data, for which analogous similarities, obtained using FTIR and NMR techniques, were reported.

Octanol/water partition coefficient measurements made using radiolabeled compounds were found to be influenced by the presence of radiolabeled impurities present at trace levels (Chapter 5). These impurities were characterized, in terms of their octanol/water partition coefficients and their mole fraction of total radiation, through the analysis of successive octanol/water extraction experiments. The impurities were found to be present at levels of typically a few percent, consistent with the manufacturers' specifications, and to vary from hydrophilic to lipophilic, depending on the particular drug. Further analysis revealed that these contaminants exhibited negligible effects on the partition coefficient measurements made using the lipid systems, due in large part to the low lipid-to-water ratio utilized.

Macroscopic measurements of stratum corneum transport, specifically, of human skin permeabilities, were also made in this thesis (see Chapters 3, 6, and 7) for a variety of solutes. Chapter 3 examined the human skin permeabilities of one particular class of solutes, steroids. A surprising finding of Chapter 3 is that the often cited list of permeability measurements of 14 different steroids by Scheuplein et al. (1969) appears to be in error. That is, comparison of the Scheuplein et al. data, which is the single largest experimental examination of steroids to date, with more than twenty different measurements reported in this thesis and compiled from the literature, shows that those values are an average of 16-fold lower. For one steroid, estradiol, eleven different reported values of its permeability by various groups are in good agreement with each other, but are between 10-fold and 20-fold greater than that reported by Scheuplein et al. (1969). Although several possible reasons were considered (Chapter 3), the source of these discrepancies is still not clear. However, these data also

constitute a large fraction of the available permeability measurements made with large compounds, and their inclusion by other researchers in analyses of stratum corneum transport erroneously implies that the exponential size dependence of stratum corneum transport extends to larger compounds (greater than ~350 Da).

In Chapter 6, the values of 120 permeability measurements, which are reported in this thesis and compiled from the literature, were examined in terms of the bilayer-scale transport properties. Specifically, an expression was developed which expresses the macroscopic permeability in terms of the lipid/water partition coefficient, lateral diffusion coefficient, and transbilayer mass transfer coefficients. Evaluation of the contribution of lateral diffusion, through the use of this expression and the experimental data reported in Chapters 5 and 6, revealed that the diffusive resistance of lateral diffusion is sufficient to account for the experimental permeability values. The size dependence exhibited by stratum corneum transport also agrees with that of lateral diffusion, with a strong dependence for small solutes (<350 Da) and a moderate dependence for larger solutes. An analysis of transbilayer transport indicated that this process is not capable of accounting for the observed permeability values, although other factors may be important for the transport of hydrophilic and lipid-like solutes.

Lastly, Chapter 7 described the use of chemical enhancers and a combination of chemical enhancers and therapeutic ultrasound (1 MHz, 1.4 W/cm^2, continuous) to increase the transport of various drugs across human skin. Specifically, the unsaturated fatty acid, linoleic acid, saturated in ethanol/water (50:50, v/v) was found to be an effective formulation. The application of ultrasound further increased the extent of enhancement. Even more interesting, however, is the observation that the extent of enhancement of this formulation, either alone or in conjunction with ultrasound, exhibited a

dependence on the size of the solute, with larger enhancements observed for larger solutes. A reexamination of published permeation data obtained using other bilayer disordering chemical enhancers, including Azone, lauric acid, and capric acid, reveals similar size dependencies. These results are consistent with the mechanism, proposed in Chapter 7, that bilayer disordering agents fluidize the stratum corneum lipid bilayers. Disordered systems tend to be characterized by more moderate size dependencies than more ordered systems (Chapter 4), and hence, the difference in diffusion coefficients between two such systems (that is, the enhancement) should increase with increasing solute size.

8.2 Future Research Directions

Recently, low frequency ultrasound (20 kHz) has displayed a remarkable ability to deliver a wide variety of compounds, including large proteins like insulin, across the skin at therapeutically meaningful rates (see section 6.1). For small solutes (less than ~500 Da), however, passive transdermal patches will likely still be preferred, due to their significantly lower cost, smaller size, and general simplicity. As it seems unlikely that a universal chemical enhancer will be developed to enhance the transdermal transport of every possible compound, future formulations are likely to be composed of *multiple* chemical enhancers, each of which may act in a different manner. The number of experiments required to choose, for example, a three-component formulation for a given drug is prohibitively large, particularly given the broad, and growing, list of chemical enhancers to choose from (Chapter 1). While the ability to quantitatively predict the effects of a given chemical enhancer is still very limited, developing a semi-quantitative or qualitative understanding of the effects that a chemical enhancer will have on a given drug is essential.

In the past, researchers have generally focused on either a single chemical enhancer or on a chemical class of enhancers, or have attempted to find universal relationships between the nature of transdermal transport and chemical enhancement. The results presented in this thesis suggest that the best approach lies somewhere in between. Specifically, it has only recently become clear that hydrophilic solutes permeate the stratum corneum through non-lipoidal routes ('aqueous pore' pathways). The precise characterization of these routes, and the subsequent characterization of the associated transport process, constitutes an important next step in the field. Likewise, chemical enhancers are best considered by their *mechanism of action*, rather than simply by their chemical structure, although the two are, of course, related. In short, two of the key challenges and opportunities in the area of chemical enhancement of transdermal transport are: (i) the identification and possible optimization of the 'aqueous pore' pathways for hydrophilic, and possibly also for lipophilic, solutes, and (ii) the determination of the mechanisms of action of chemical enhancers, to allow more effective chemical enhancers combinations to be developed.

For example, further experimental characterization of the *direct* effects that specific chemicals have on the stratum corneum lipid bilayers needs to be carried out. In this thesis, the bilayer-scale transport properties were related to macroscopic permeability measurements, which were made in the absence of any chemical enhancers. Direct measurements of properties, such as partition coefficients and lateral diffusion coefficients, in the presence of chemical enhancers would undoubtedly help to clarify the roles of specific enhancers. The most readily measurable bilayer-scale property is lateral diffusion, using the video-FRAP technique. A comprehensive examination of lateral diffusion in the presence of chemical enhancers, such as linoleic acid and Azone, could be performed with the same nine fluorescent probes utilized in this thesis.

Caution should be exercised, however, since several of these probes are no longer commercially available (the samples purchased for this thesis were the last aliquots in stock (Molecular Probes, Eugene, OR, 1995), although sufficient quantities of those samples still remain for many additional experiments), and would likely be expensive to have synthesized. Additional fluorescent probes, having the necessary absorption and emission peak wavelengths, are also available but fairly large (greater than ~450-500 Da). An additional small probe, tetracene, was examined unsuccessfully in this thesis (228.3 Da; B240-3, Aldrich Chemicals, Milwaukee, WI), but successfully by Balcom et al. (1993) in DMPC fluid bilayers. Tetracene is very photolabile, and was excessively bleached by the mercury arc-lamp of the video-FRAP system, which continually illuminated the sample during the fluorescence recovery. However, by having the shutter on the arc-lamp closed during the bulk of the fluorescence recovery process in which images are not being taken, and having the computer software programmed to open the shutter when images are captured, this small probe may be useful. The DMPC/cholesterol (40 mol%) bilayer system should be seriously considered as a model with which to evaluate enhancers. It is an inexpensive and reliable system, which could nicely complement the more difficult experiments performed with SCE lipids.

Direct experimental measurements of solute partition coefficients between lipid bilayers and chemical enhancer formulations should also be calculated, but will require innovative experimental methods, due to the ability of many enhancer formulations to dissolve the lipids. For example, one method of determining lipid/enhancer partition coefficients for enhancers which dissolve lipids is to utilize a three-phase system. The partition coefficient of the drug would first be measured between the enhancer and an aqueous solution. In a subsequent experiment, the partition coefficient of the drug between the lipid

bilayer and the aqueous solution, saturated with the enhancer, would be measured. Since both measurements would be made at equilibrium, and since the aqueous phase would be common to both systems, the lipid/enhancer drug partition coefficient would be simply the ratio of the two measured partition coefficients. This technique would, of course, be limited to enhancers which are immiscible in water, but also illustrates the challenges in measuring the underlying transport properties with chemical enhancers. As mentioned in Chapter 5, caution should be taken in considering the use of radiolabeled solutes for such studies, due to the presence of impurities. HPLC analysis of non-radiolabeled solutes, while more cumbersome than analysis using radiolabeled solutes, could provide reliable data without the need to characterize and correct for the presence of contaminants.

An interesting set of experiments would involve measuring the key transport properties, that is, the lateral diffusion coefficient, SCE lipid/water partition coefficient, and stratum corneum permeability, for the same solute(s). That is, there are currently no compounds for which values of these three properties have been measured. The solutes most conducive to such experiments are the small, fluorescent probes utilized in the FRAP experiments (Chapter 4). A preliminary attempt to measure the stratum corneum permeability of BOD was unsuccessful (n=1), although the reason for this was not clear. A challenge in performing such experiments includes the low aqueous solubilities of the probes, owing to their lipophilic nature. Using low solute concentrations in the donor solution of a skin permeability experiment, detection of the concentration of solute appearing in the receiver compartment over time may be impossible, given the sensitivity of the current spectrofluorimeters. Photobleaching of the probes over time, due to any exposure to ambient light or to oxygen (oxygen tends to hasten the transition of a fluorophore from active to inactive) would be

potential sources of additional error. However, the custom labeling (with tritium) of such probes would allow the permeability and partition coefficient measurements to be readily measured using liquid scintillation counting, as described in this thesis (Chapters 2, 3, 5, and 7).

Molecular dynamics simulations (MDS) are an intriguing theoretical tool which has the potential to shed light on the more fundamental aspects of bilayer transport. To date, MDS 'experiments' have been carried out at relatively high temperatures (for example, 47°C), and in one-component lipid bilayers (DMPC). Since the primary limitation of this methodology is computational speed, the ever increasing speed of workstations suggests that MDS will become more powerful and effective in the near future. Use of MDS may help provide information on: (i) the distribution across, and orientation of drugs in, lipid bilayers, (ii) the rate of lateral diffusion of drugs in bilayers, and (iii) the effects of exogenous compounds (that is, chemical enhancers) on these properties. Owing to the complexity of stratum corneum lipids, the use of DMPC/cholesterol (40 mol%) as a model system for MDS again seems very attractive, due to the relative simplicity of this system.

In this thesis, experimental techniques, theoretical concepts, and literature data from a variety of different fields, were all brought together in a unique manner to probe the fundamental nature of transdermal solute transport and the enhancement (chemical and otherwise) of transdermal transport. The findings of this thesis have illustrated, at a more general level, that macroscopic skin transport properties can successfully be related to the properties of the underlying structural features of the skin. This thesis has also shown compelling parallels between the behavior of stratum corneum lipid bilayers and those of a simple model bilayer system (DMPC/cholesterol 40 mol%). Lastly, these

insights have led to the development of effective chemical enhancer formulations.

Chapter 9

References

Inert Ingredients Guide. Food and Drug Administration. 1991.

Ailenby, A. C., N. H. Creasey, J. A. G. Edginton, J. A. Fletcher, and C. Schock. 1969. Mechanism of action of accelerants on skin penetration. *Brit. J. Derm.* 81:47-55.

Almeida, P. F. F., W. L. C. Vaz, and T. E. Thompson. 1992. Lateral diffusion in the liquid phases of dimyristoylphosphatidylcholine/cholesterol lipid bilayers: A free-volume analysis. *Biochemistry.* 31:6739-47.

Alper, H. E., and T. R. Stouch. 1995. Orientation and diffusion of a drug analogue in biomembranes: Molecular dynamics simulations. *J. Phys. Chem.* 99:5724-5731.

Anderson, B. D., W. I. Higuchi, and P. V. Raykar. 1988. Heterogeneity effects on permeability-partition coefficient relationships in human stratum corneum. *Pharm. Res.* 5:566-573.

Anderson, B. D., and P. V. Raykar. 1989. Solute structure-permeability relationships in human stratum corneum. *J. Invest. Dermatol.* 93:280-86.

Arrowsmith, M., J. Hadgraft, and I. W. Kellaway. 1983. Thermodynamics of steroid partitioning in dimyristoylphsophatidylcholine liposomes. *Biochim. Biophys. Acta.* 750:149-56.

Astley, J. P., and M. Levine. 1976. Effect of dimethyl sulfoxide on permeability of human skin in vitro. *J. Pharm. Sci.* 65:210-215.

Aungst, B. J., J. A. Blake, and M. A. Hussain. 1990. Contributions of drug solubilization, partitioning, barrier disruption, and solvent permeation to

the enhancement of skin permeation of various compounds with fatty acids and amines. *Pharm. Res.* 7:712-718.

Axelrod, D., D. E. Koppel, J. Schlessinger, E. Elson, and W. W. Webb. 1976. Mobility measurment by analysis of fluorescence photobleaching recovery kinetics. *Biophys. J.* 16:1055-1069.

Balcom, B. J., and N. O. Petersen. 1993. Lateral diffusion in model membranes is independent of the size of the hydrophobic region of molecules. *Biophys. J.* 65:630-637.

Barber, E. D., N. M. Teetsel, K. F. Kolberg, and D. Guest. 1992. A comparative study of the rates of in vitro percutaneous absorption of eight chemicals using rat and human skin. *Fund. Appl. Tox.* 19:493-497.

Barry, B. 1987. Mode of action of penetration enhancers in human skin. *J. Control. Rel.* 6:85-97.

Barry, B. W., S. M. Harrison, and P. H. Dugard. 1985. Vapour and liquid diffusion of model penetrants through human skin; correlation with thermodynamic activity. *J. Pharm. Pharmacol.* 37:226-235.

Bassolino-Klimas, D., H. W. Alper, and T. R. Stouch. 1993. Solute diffusion in lipid bilayer membranes: an atomic level study by molecular dynamics simulations. *Biochemistry.* 32:12624-12637.

Berk, D. A., F. Yuan, M. Leunig, and R. K. Jain. 1993. Fluorescence photobleaching with spatial Fourier analysis: measurement of diffusion in light-scattering media. *Biophys. J.* 65:2428-2436.

Bird, R. B., W. E. Stewart, and E. N. Lightfoot. 1960. Transport Phenomena. John Wiley & Sons, New York.

Bissett, D. L. 1987. Anatomy and biochemistry of skin. *In* Transdermal Delivery of Drugs. A. F. Kydonieus, and B. Berner, ed. 29-42.

Bittman, R. 1993. A review of the kinetics of cholesterol movement between donor and acceptor bilayer membranes. *In* Cholesterol in Membrane Models. L. Finegold, ed. CRC Press. Boca Raton, FL. 45-65.

Blank, I. H., and D. J. McAuliffe. 1985. Penetration of benzene through human skin. *J. Invest. Dermatol.* 85:522-526.

Bond, J. R., and B. W. Barry. 1988. Limitations of hairless mouse skin as a model for in vitro permeation studies through human skin: hydration damage. *J. Invest. Dermatol.* 90:486-489.

Bouwstra, J. A., G. S. Gooris, J. A. v. d. Spek, and W. Bras. 1991. Structural investigations of human stratum corneum by small-angle X-ray scattering. *J. Invest. Dermatol.* 97:1005-1012.

Bronaugh, R. L. 1989. Determination of Percutaneous Absorption by In Vitro Techniques. *In* Percutaneous Absorption. R. L. Bronaugh and H. I. Maibach, ed. Marcel Dekker. New York. 239-258.

Bronaugh, R. L., and E. R. Congdon. 1984. Percutaneous absorption of hair dyes: correlation with partition coefficients. *J. Invest. Dermatol.* 83:124-127.

Bronaugh, R. L., R. F. Stewart, and M. Simon. 1986. Methods for in vitro percutaneous absorption studies VII: use of excised human skin. *J. Pharm. Sci.* 75:1094-1097.

Brunner, J., D. E. Graham, H. Hauser, and G. Semenza. 1980. Ion and sugar permeabilities of lecithin bilayers: Comparison of curved and planar bilayers. *J. Membrane Biol.* 57:133-141.

Bunge, A. L., and R. L. Creek. 1995. A new method for estimating dermal absorption from chemical exposure: 2. Effect of molecular weight and octanol-water partitioning. *Pharm. Res.* 12:88-95.

Burnette, R. R. 1989. Iontophoresis. *In* Transdermal Drug Delivery: Development Issues and Research Initiatives. J. Hadgraft, and R.H. Guy, ed. Marcel Dekker. New York. 247-291.

Chang, C.-H., H. Takeuchi, T. Ito, K. Machida, and S. Ohnishi. 1981. Lateral mobility of erythrocyte membrane proteins studied by the fluorescence photobleaching recovery technique. *Biochemistry.* 90:997-1004.

Chary, S. R., and R. K. Jain. 1989. Direct measurement of interstitial convection and diffusion of albumin in normal and neoplastic tissues by fluorescence photobleaching. *Proc. Natl. Acad. Sci. USA.* 86:5385-5389.

Chattaraj, S. C., and R. B. Walker. 1995. Penetration Enhancer Classificantion. *In* Percutaneous Penetration Enhancers. E. W. Smith and H. I. Maibach, ed. CRC Press. Boca Raton, FL. 5-20.

Cherry, R. J. 1979. Rotational and lateral diffusion of membrane proteins. *Biochim. Biophys. Acta.* 559:289-327.

Cherry, R. J., U. Muller, C. Holenstein, and M. P. Heyn. 1980. Lateral segregation of proteins induced by cholesterol in bacteriorhodopsin-phospholipid vesicles. *Biochim. Biophys. Acta.* 596:145-151.

Cleary, G. W. 1993. Transdermal Delivery Systems: A Medical Rationale. *In* Topical Drug Bioavailability, Bioequivalence, and Penetration. V. P. Shah and H. I. Maibach, ed. Plenum Press. New York. 452.

Clegg, R. M., and W. L. C. Vaz. 1985. Translational diffusion of proteins and lipids in artificial lipid bilayer membranes. A comparison of experiment with theory. *In* Progress in Protein-Lipid Interactions. A. Watts and J. J. H. H. M. DuPont, ed. Elsevier. Amsterdam. 173-229.

Cohen, B. E., and A. D. Bangham. 1972. Diffusion of small non-electrolytes across liposome membranes. *Nature.* 236:173-174.

Cohen, M. H., and D. Turnbull. 1959. Molecular transport in liquids and glasses. *J. Chem. Phys.* 31:1164-69.

Cooper, E. R. 1984. Increased skin permeability for lipophilic molecules. *J. Pharm. Sci.* 73:1153-1156.

Cooper, E. R., and G. Kasting. 1987. Transport across epithelial membranes. *J. Control. Rel.* 6:23-35.

Cooper, E. R., E. W. Merritt, and R. L. Smith. 1985. Effect of fatty acids and alcohols on the penetration of acyclovir across human skin in vitro. *J. Pharm. Sci.* 74:688-689.

Cullander, C., and R. Guy. 1992. Routes of delivery: Case studies. *Adv. Drug Deliv. Rev.* 8:291-329.

Cullis, P. R., M. J. Hope, M. B. Bally, R. D. Madden, L. D. Mayer, and A. S. Janoff. 1987. Liposomes as Pharmaceuticals. *In* Liposomes: From Biophysics to Therapeutics. M. J. Ostro, ed. Marcel Dekker. New York. 39-72.

Cussler, E. L., S. E. Hughes, W. J. Ward, and R. Aris. 1988. Barrier membranes. *J. Membrane Sci.* 38:161-174.

Daems, D., M. V. d. Zegel, N. Boens, and F. C. D. Schryver. 1985. Fluorescence decay of pyrene in small and large unilamellar L,a-dipalmitoylphosphatidylcholine vesicles above and below the phase transition temperature. *Eur. Biophys. J.* 12:97-105.

Derzko, Z., and K. Jacobson. 1980. Comparative lateral diffusion of fluorescent lipid analogues in phospholipid multibilayers. *Biochemistry.* 19:6050-6057.

DeYoung, L. R., and K. A. Dill. 1990. Partitioning of nonpolar solutes into bilayers and amorphous n-alkanes. *J. Phys. Chem.* 94:801-809.

Diamond, J. M., and Y. Katz. 1974. Interpretation of nonelectrolyte partition coefficients between dimyristoyl lecithin and water. *J. Membrane Biol.* 17:121-154.

Dix, J. A., D. Kivelson, and J. M. Diamond. 1978. Molecular motion of small nonelectrolyte molecules in lecithin bilayers. *J. Membrane Biol.* 40:315-342.

Dutkiewicz, T., and H. Tyras. 1967. A study of the skin absorption of ethylbenzene in man. *Brit. J. Ind. Med.* 24:330-3312.

Dutkiewicz, T., and H. Tyras. 1969. Skin absorption of toluene, styrenes, and xylenes by man. *Brit. J. Ind. Med.* 25:243.

El-Shimi, A., and E. D. Goddard. 1975. Wetting characteristics of keratin substrates. *In* Applied Chemistry at Protein Interfaces. R. F. Gould, ed. American Chemical Society. Washington, D.C. 141-154.

Elias, P. M. 1983. Epidermal lipids, barrier function, and desquamation. *Journal of Investigative Dermatology.* 80:44-49.

Elias, P. M. 1988. Structure and function of the stratum corneum permeability barrier. *Drug Devel. Res.* 19:97-105.

Elias, P. M. 1989. Microscopic Structure of the Epidermis. *In* Percutaneous Absorption: Mechanisms, Methodology, Drug Delivery. R. L. Bronaugh and H. I. Maibach, ed. Marcel Dekker. New York. 3-12.

Elias, P. M. 1991. Epidermal barrier function: intercellular lamellar lipid structures, origin, composition and metabolism. *J. Control. Rel.* 15:199-208.

Elias, P. M., E. R. Cooper, A. Korc, and B. E. Brown. 1981. Percutaneous transport in relation to stratum corneum structure and lipid composition. *J. Invest. Dermatol.* 76:297-301.

Elias, P. M., and D. S. Friend. 1975. The permeability barrier in mammalian epidermis. *J. Cell Biol.* 65:180-191.

Elias, P. M., and G. K. Menon. 1991. Structural and lipid biochemical correlates of the epidermal permeability barrier. *Adv. Lipid. Res.* 24:1-26.

Fahey, P. F., and W. W. Webb. 1978. Lateral diffusion in phospholipid bilayer membranes and multilamellar liquid crystals. *Biochemistry.* 17:3046-3053.

Flynn, G. L. 1990. Physiochemical determinants of skin absorption. *In* Principles of Route-to-Route Extrapolation for Risk Assessment. T. R. Gerrity and C. J. Henry, ed. Elsevier. New York. 93-127.

Francoeur, M. L., G. M. Golden, and R. O. Potts. 1990. Oleic Acid: Its effects on stratum corneum in relation to (trans)dermal drug delivery. *Pharm. Res.* 7:621-627.

Friberg, S. E., and D. W. Osborne. 1985. Small angle X-ray diffraction patterns of stratum corneum and a model structure for its lipids. *J. Disp. Sci. Tech.* 6:485-495.

Galey, W. R., H. K. Lonsdale, and S. Nacht. 1976. The in vitro permeability of skin and buccal mucosa to selected drugs and tritiated water. *J. Invest. Dermatol.* 67:713-717.

Galla, H. J., W. Hartmann, U. Theilen, and E. Sackman. 1979. On two-dimensional passive random walk in lipid bilayers and fluid pathways in biomembranes. *J. Membrane Biol.* 48:215-36.

Garson, J. C., J. Doucet, J. L. Leveque, and G. Tsoucaris. 1991. Oriented structure in human stratum corneum revealed by X-ray diffraction. *J. Invest. Dermat.* 96:43-49.

Gawrisch, K., and S. Janz. 1991. The uptake of pristane (2,6,10,14-tetramethylpentadecane) into phospholipid bilayers as assessed by NMR, DSC, and tritium labeling methods. *Biochim. Biophys. Acta.* 1070:409-418.

Ghanem, A., H. Mahmoud, W. I. Higuchi, P. Liu, and W. R. Good. 1992. The effect of ethanol on the transport of lipophilic and polar permeants across hairless mouse skin: methods/validation of a novel approach. *Int. J. Pharm.* 78:137-156.

Goates, C. Y., and K. Knutson. 1994. Enhanced permeation of polar compounds through human epidermis. I. Permeability and membrane structural changes in the presence of short chain alcohols. *Biochim. Biophys. Acta.* 1195:169-179.

Goodman, M., and B. W. Barry. 1988. Action of penetration enhancers on human skin as assessed by the permeation of model drugs 5-fluoracil and estradiol: I. Infinite dose technique. *J. Invest. Dermatol.* 91:323-27.

Green, P. G., R. H. Guy, and J. Hadgraft. 1988. In vitro and in vivo enhancement of skin permation with oleic and lauric acids. *Int. J. Pharm.* 48:103-111.

Grubauer, B., K. R. Feingold, R. M. Harris, and P. M. Elias. 1989. Lipid content and lipid type as determinants of the epidermal permeability barrier. *J. Lipid Res.* 30:89-96.

Gummer, C. L. 1989. The In Vitro Evaluation of Transdermal Delivery. *In* Trnasdermal Drug Delivery: Developmental Issues and Research Initiatives. J. Hadgraft and R. H. Guy, ed. Marcel Dekker. New York.

Guy, R. H. 1992. Iontophoresis. *Adv. Drug Deliv. Rev.* 9:

Hadgraft, J., and G. Ridout. 1987. Development of model membranes for percutaneous adsorption measurements: I. isopropy myristate. *Int. J. Pharm.* 39:149-156.

Hansch, C., and A. Leo. 1979. Substituent Constants for Correlation Analysis in Chemistry and Biology. Wiley, New York.

Harrison, S. M., B. W. Barry, and P. H. Dugard. 1984. Effects of freezing on human skin permeability. *J. Pharm. Sci.* 36:262-262.

Hatcher, M. E., and W. Z. Plachy. 1993. Dioxygen diffusion in the stratum corneum: an EPR spin label study. *Biochim. Biophys. Acta.* 1149:73-8.

Hirvonen, J., K. Kontturi, L. Murtomaki, P. Paronen, and A. Urtti. 1993. Transdermal iontophoresis of sotalol and salicylate; the effect of skin charge and penetration enhancers. *J. Control. Rel.* 26:109-117.

Hirvonen, J., J. H. Rytting, P. Paronen, and A. Urtti. 1991. Dodecyl N,N-Dimethylamino acetate and Azone enhance drug penetration across human, snake, and rabbit skin. *Pharm. Res.* 8:933-937.

Homan, R., and H. J. Pownall. 1988. Transbilayer diffusion of phospholipids: dependence on head group structure and acyl chain length. *Biochim. Biophys. Acta.* 938:155-166.

Hou, S. Y. E., and G. L. Flynn. 1989. Enhancement of hydrocortisone permeation of human and hairless mouse skin by 1-dodecylazacycloheptan-2-one. *J. Invest. Dermatol.* 93:774-779.

Hou, S. Y. E., A. K. Mitra, S. H. White, G. K. Menon, R. Ghadially, and P. M. Elias. 1991. Membrane structures in normal and essential fatty acid-deficient stratum corneum: Characterization by ruthenium tetroxide staining and X-ray diffraction. *J. Invest. Dermatol.* 96:215-223.

Huang, Z., K. H. Pearce, and N. L. Thompson. 1994. Translational diffusion of bovine prothrombin fragment 1 weakly bound to supported planar

membranes: Measurements by total internal reflection with fluorescence pattern photobleaching recovery. *Biophys. J.* 67:1754-1766.

Johnson, E. M., D. A. Berk, R. K. Jain, and W. M. Deen. 1995. Diffusion and partitioning of proteins in charged agarose gels. *Biophys. J.* 68:1561-1568.

Johnson, E. M., D. A. Berk, R. K. Jain, and W. M. Deen. 1996. Hindered diffusion in agarose gels: Test of effective medium model. *Biophys. J.* 70:1017-1026.

Johnson, M. E., D. Berk, D. Blankschtein, D. Golan, R. Jain, and R. Langer. Submitted[a]. Lateral diffusion of small compounds in stratum corneum and model lipid systems.

Johnson, M. E., D. Blankschtein, and R. Langer. 1995. Permeation of steroids through human skin. *J. Pharm. Sci.* 84:1144-1146.

Johnson, M. E., D. Blankschtein, and R. Langer. Submitted[b]. Evaluation of solute permeation through the stratum corneum: lateral bilayer diffusion as the primary transport mechanism.

Johnson, M. E., R. S. Langer, and D. Blankschtein. 1993. Fundamental studies of transbilayer diffusion and transport through the stratum corneum. *U.S.-Japan Symposium on Drug Delivery Systems*, Maui, HI.

Johnson, M. E., S. Mitragotri, A. Patel, D. Blankschtein, and R. Langer. In press. Synergistic effects of chemical enhancers and therapeutic ultrasound on transdermal drug delivery. *J. Pharm. Sci.*

Kapitza, H. G., D. A. Ruppel, H. J. Galla, and E. Sackmann. 1984. Lateral diffusion of lipids and glycophorin in solid phosphatidylcholine bilayers: The role of structural defects. *Biophys. J.* 45:577-587.

Kasting, G. B., R. L. Smith, and B. D. Anderson. 1992. Prodrugs for dermal delivery: solubility, molecular size, and functional group effects. *In* Prodrugs: Topical and Ocular Delivery. K. B. Sloan, ed. Marcel Dekker. New York. 117-61.

Kasting, G. B., R. L. Smith, and E. R. Cooper. 1987. Effect of lipid solubility and molecular size on percutaneous absorption. *In* Pharmacology and the Skin.

B. Shroot, H. Schaefer and Valbone, ed. Karger and Basel. Switzerland. 138-153.

Katzung, B. G. 1995. Basic and Clinical Pharmacology.

Kitson, N., J. Thewalt, M. Lafleu, and M. Bloom. 1994. A model membrane approach to the epidermal permeability barrier. *Biochemistry.* 33:6707-6715.

Knepp, V. M., and R. H. Guy. 1989. Transport of steroids at model biomembrane surfaces and across organic liquid-aqueous phase interfaces. *J. Phys. Chem.* 93:

Knutson, K., S.I. Krill, W.J. Lambert, and W.I. Higuchi. 1987. Probing the structure of the stratum corneum on the molecular level. *In* Controlled Release Technology: Pharmaceutical Applications. P. I. a. W. R. G. Lee, ed. American Chemical Society. Washington, DC. 241-66.

Knutson, K., D. J. Harrison, L. K. Pershing, and C. Y. Goates. 1993. Transdermal absorption of steroids. *J. Control. Rel.* 24:95-108.

Koefoed, P., and J. Brahm. 1994. The permeability of the human red cell membrane to steroid sex hormones. *Biochim. Biophys. Acta.* 1195:55-62.

Kost, J., and R. Langer. 1993. Ultrasound-Mediated Trnasdermal Drug Delivery. *In* Topical Drug Bioavaibility, Bioequivalency, and Penetration. V. Shah and H. I. Maibach, ed. Plennum. New York. 91-103.

Kost, J., D. Levy, and R. Langer. 1989. Ultrasound as a Transdermal Enhancer. *In* Percutaneous Absorption: Mechanisms-Methodology-Drug Delivery. R. L. Bronaugh and H. I. Maibach, ed. Marcel Dekker. New York. 595-602.

Lambert, W. J., W. I. Higuchi, K. Knutson, and S. L. Krill. 1989. Dose-dependent enhancement effects of Azone on skin permeability. *Pharm. Res.* 6:798-803.

Lampe, M. A., A. L. Burlingame, J. Whitney, M. L. Williamss, B. E. Brown, E. Roitman, and P. M. Elias. 1983. Human stratum corneum lipids: characterization and regional variations. *J. Lipid Res.* 24:120-130.

Lampe, M. A., M. L. Williams, and P. E. Elias. 1983. Human epidermal lipids: characterization and modulations during differentiation. *J. Lipid Res.* 24:131-140.

Lange-Lieckfeldt, R., and G. Lee. 1992. Use of a model lipid matrix to demonstrate the dependence of the stratum corneum's barrier properties on its internal geometry. *J. Control. Rel.* 20:183-194.

Leo, A., C. Hansch, and D. Elkins. 1971. Partition coefficients and their uses. *Chem. Rev.* 71:525-554.

Levy, D., J. Kost, Y. Meshulam, and R. Langer. 1989. *J. Clin. Invest.* 83:2074-2078.

Lieb, W. R., and W. D. Stein. 1969. Biological membranes behave as non-porous polymeric sheets with respect to the diffusion of non-electrolytes. *Nature.* 224:240-243.

Lieb, W. R., and W. D. Stein. 1986. Non-Stokesian nature of transverse diffusion within human red cell membranes. *J. Membrane Biol.* 92:111-119.

Lipka, G., J. A. F. O. d. Kamp, and H. Hauser. 1991. Lipid asymmetry in rabbit intestinal brush border membrane as probed by an intrinsic phospholipid exchange protein. *Biochemistry.* 30:11828-11836.

Liu, P., T. Kurihara-Bergstrom, and W. R. Good. 1991. Cotransport of estradiol and ethanol through human skin in vitro: Understanding the permeant/enhancer flux relationship. *Pharmaceutical Research.* 8:938-44.

Mabrey, S., and J. M. Sturtevant. 1976. Investigation of phase transitions of lipids and lipid mixtures by high sensitivity differential scanning calorimetry. *Proc. Natl. Acad. Sci. USA.* 73:3862-3866.

Madison, K. C., D. C. Swartzendruber, P. W. Wertz, and D. T. Downing. 1987. Presence of intact intercellular lipid lamellae in the upper layers of the stratum corneum. *J. Invest. Dermatol.* 88:714-718.

Mak, V. H. W., R. O. Potts, and R. H. Guy. 1990. Oleic acid concentration and effect in human stratum corneum: non-invasive determination by attenuated total reflectance infrared spectroscopy in vivo. *J. Control. Rel.* 12:67-75.

Marks, R. 1988. Skin under the microscope: The organization, kinetics and dimensions of skin. *In* The Physical Nature of the Skin. R. M. Marks, S. P. Barton and C. Edwards, ed. 3-12.

Marqusee, J. A., and K. A. Dill. 1986. Solute partitioning into chain molecule interphases: monolayers, bilayer membranes, and micelles. *J. Chem. Phys.* 85:434-444.

Marrink, S., and H. J. C. Berendsen. 1994. Simulation of water transport through a lipid membrane. *J. Phys. Chem.* 98:4155-68.

Martel, P., A. Makriyannis, T. Mavromoustakos, K. Kelly, and K. R. Jeffrey. 1993. Topography of tetrahydrocannabinol in model membranes using neutron diffraction. *Biophys. Biochem. Acta.* 1151:51-58.

McEvoy, G. K. 1995. AHFS Drug Information.

Menton, D. N. 1976. A minimum-surface mechanism to account for the organization of cells into columns in the mammalian epidermis. *Am. J. Anat.* 145:1-22.

Mershon, M. M. 1975. Barrier surfaces of skin. *In* Applied Chemistry at Protein Interfaces. R. F. Gould, ed. American Chemical Society. Washington D.C. 41-73.

Michaels, A. S., S. K. Chandraskeran, and J. E. Shaw. 1975. Drug permeation through human skin: theory and in vitro experimental measurement. *Amer. Inst. Chem. Eng.* 21:985-996.

Miller, B. A., R. Cambell, G. Bornett, and A. Weiss Jr. 1991. Supercritical fluid extraction of lipids from human skin. *International Symposium on Supercritical Fluid Chromatography and Extraction*, Park City, Utah.

Miller, D. M. 1991. Evidence that interfacial transport is rate-limiting during passive cell membrane permeation. *Biochim. Biophys. Acta.* 1065:75-81.

Mitragotri, S., D. Blankschtein, and R. Langer. 1995. Ultrasound-mediated transdermal protein delivery. *Science.* 269:850-853.

Mitragotri, S., D. Blankschtein, and R. Langer. 1996. Transdermal drug delivery using low-frequency sonophoresis. *Pharm. Res.* 13:411-420.

Mitragotri, S., D. Edwards, D. Blankschtein, and R. Langer. 1995. A mechanistic study of ultrasonically enhanced transdermal drug delivery. *J. Pharm. Sci.* 84:697-706.

Morimoto, Y., T. Hatanaka, K. Sugibayashi, and H. Omiya. 1992. Prediction of skin permeability of drugs: comparison of human and hairless rat skin. *J. Pharm. Pharmac.* 44:634-639.

Nigg, E. A., and R. J. Cherry. 1979. Influence of temperature and cholesterol on the rotational diffusion of band 3 in the human erythrocyte membrane. *Biochemistry*. 18:3457-3465.

Odland, G. F., and K. Holbrook. 1981. The lamellar granules of epidermis. *Curr. Prob. Derm.* 9:29-49.

Oertel, R. P. 1977. Protein conformational changes induced in human stratum corneum by organic sulfoxides: An infrared spectroscopic investigation. *Biopolymers*. 16:2329.

Ongpipattanakul, B., R. R. Burnette, R. O. Potts, and M. L. Francoeur. 1991. Evidence that oleic acid exists in a separate phase within stratum corneum lipids. *Pharm. Res.* 8:350-354.

Ongpipattanakul, B., M. L. Francoeur, and R. O. Potts. 1994. Polymorphism in stratum corneum lipids. *Biochim. Biophys. Acta.* 1190:115-122.

Paprica, P. 1994. Evidence for a continuum model of diffusion in lipid membranes. Ph.D., University of Western Ontario.

Peck, K. D., A. Ghanem, and W. I. Higuchi. 1994. Hindered diffusion of polar molecules through and effective pore radii estimates of intact and ethanol treated human epidermal membranes. *Pharm. Res.* 11:1306-1314.

Peck, K. D., A. H. Ghanem, and W. I. Higuchi. 1995. The effect of temperature upon the permeation of polar and ionic solutes throug h human epidermal membrane. *J. Pharm. Sci.* 84:975-982.

Perry, G. E. 1990. Percutaneous absorption of drugs across human skin. PhD, University of Utah.

Perry, R. H., D. W. Green, and e. J.O. Maloney. 1984. Perry's Chemical Engineering Handbook. McGraw-Hill, New York.

Peters, R., and R. J. Cherry. 1982. Lateral and rotational diffusion of bacteriorhodopsin in lipid bilayers: experimental test of the Saffman-Delbrück equations. *Proc. Natl. Acad. Sci. USA.* 79:4317-4321.

Potts, R. O., and M. L. Francoeur. 1990. Lipid biophysics of water loss through the skin. *Proc. Natl. Acad. Sci. USA.* 87:3871-3883.

Potts, R. O., and M. L. Francoeur. 1991. The influence of stratum corneum morphology on water permeability. *J. Invest. Dermatol.* 96:495-99.

Potts, R. O., and R. H. Guy. 1992. Predicting skin permeability. *Pharm. Res.* 9:663-669.

Prausnitz, M. R., V. G. Bose, R. Langer, and J. C. Weaver. 1993. Electroporation of mammalian skin: A mechanism to enhance transdermal drug delivery. *Proc. Nat. Acad. Sci.* 90:10504-10508.

Raykar, P. V., M.C. Fung, and B.D. Anderson. 1988. The role of protein and lipid domains in the uptake of solutes by human stratum corneum. *Pharm. Res.* 5:140-50.

Rice, R. J., and H. J. Green. 1978. Relationship of protein synthesis and transgulataminase activity to formation of the cross-linked envelope during terminal differentiation of the cultured epidermal keratinocyte. *J. Cell. Biol.* 76:705-711.

Roberts, M. S., R. A. Anderson, and J. Swarbrick. 1977. Permeability of human epidermis to phenolic compuonds. *J. Pharm. Pharmac.* 29:677-683.

Roy, S. D., and G. L. Flynn. 1989. Transdermal delivery of narcotic analgesics: comparative permeabilities of narcotic analgesics through human cadaver skin. *Pharm. Res.* 6:825-832.

Roy, S. D., and G. L. Flynn. 1990. Transdermal delivery of narcotic analgesics: pH, anatomical, and subject influences on cutaneous permeability of fentanyl and sufentanil. *Pharm. Res.* 7:842-847.

Rubenstein, J. L., B. A. Smith, and H. M. McConnell. 1979. Lateral diffusion in binary mixtures of cholesterol and phosphatidylcholines. *Proc. Natl. Acad. Sci. USA.* 76:15-18.

Saffman, P. G., and M. Delbrück. 1975. Brownian motion in biological membranes. *Proc. Natl. Acad. Sci. USA.* 72:3111-3113.

Scheuplein, R. J. 1967. Mechanism of percutaneous absorption: II. Transient diffusion and the relative importance of various routes of skin penetration. *J. Invest. Dermatol.* 48:79-88.

Scheuplein, R. J., and I. H. Blank. 1971. Permeability of the skin. *Physiol. Rev.* 51:702-47.

Scheuplein, R. J., and I. H. Blank. 1973. Mechanism of percutaneous absorption. IV.Penetration of nonelectrolytes (alcohols) from aqueous solutions and from pure liquids. *J. Invest. Dermatol.* 60:286-296.

Scheuplein, R. J., I. H. Blank, G. J. Brauner, and D. J. MacFarlane. 1969. Percutaneous absorption of steroids. *J. Invest. Dermatol.* 52:63-70.

Scheuplein, R. J., and R. L. Bronaugh. 1983. Percutaneous Absorption. *In* Biochemistry and Physiology of the Skin. Goldsmith, ed. 1255-1295.

Schroeder, F., G. Nemecz, W. G. Wood, C. Joiner, G. Morrot, M. Ayraut-Jarrier, and P. F. Devaux. 1991. Transmembrane distribution of sterol in the human erythrocyte. *Biochim. Biophys. Acta.* 1066:183-192.

Singh, P., and M. S. Roberts. 1994. Skin permeability and local tissue concentrations of nonsteroidal anti-inflammatory drugs after topical application. *J. Pharm. Expt. Ther.* 268:144-151.

Sloan, K. B., S. A. M. Koch, and K. G. Siver. 1984. Mannich base derivatives of theophylline and 5-fluorouracil: syntheses, properties, and topical delivery characteristics. *Int. J. Pharm.* 21:251-264.

Smith, B. A., and H. M. McConnell. 1978. Determination of molecular motion in membranes using periodic pattern photobleaching. *Proc. Natl. Acad. Sci. USA.* 75:2759-2763.

Smith, E. W., and H. I. Maibach. 1995. Percutaneous Penetration Enhancers. 500.

Strichartz, G. R., V. Sanchez, G. R. Arthur, R. Charetz, and D. Martin. 1990. Fundamental properties of local anesthetics. II. Measured octanol:buffer partition coefficients and pK_a values of clinically used drugs. *Anesth. Analg.* 71:158-170.

Subczynski, W., J. S. Hyde, and A. Kusumi. 1991. Effect of alkyl chain unsaturation and cholesterol intercalation on oxygen transport in membranes: A pulse ESR spin labeling study. *Biochemistry.* 30:8578-8590.

Swartzendruber, D. C., P. W. Wertz, D. J. Kitko, K. C. Madison, and D. T. Downing. 1989. Molecular models of the intercellular lipid lamellae in mammalian stratum corneum. *J. Invest. Dermatol.* 92:251-257.

Tocanne, J. F., L. Dupou-Cezanne, A. Lopez, and J. F. Tournier. 1989. Lipid lateral diffusion and membrane organization. *FEBS Lett.* 257:10-16.

Tsay, T. T., and K. A. Jacobson. 1991. Spatial Fourier analysis of video photobleaching measurements: Principles and optimization. *Biophys. J.* 60:360-368.

Vaara, M., W. Z. Plachy, and H. Nikaido. 1990. Partitioning hydrophobic probes into lipopolysaccharide bilayers. *Biochim. Biophys. Acta.* 1024:152-158.

Van den Zegel, M., N. Boens, and F. C. D. Schryver. 1984. Fluorescence decay of 1-methylpyrene in small unilamellar L-a-dimyristoylphosphatidylcholine vesicles. A temperature and concentration dependence study. *Biophys. Chem.* 20:333-345.

Vaz, W. L. C., R. M. Clegg, and D. Hallmann. 1985. Translational diffusion of lipids in liquid crystalline phase phosphatidylcholine multibilayers. A comparison of experiment with theory. *Biochemistry.* 24:781-86.

Vaz, W. L. C., F. Goodsaid-Salduondo, and K. Jacobson. 1984. Lateral diffusion of lipids and proteins in bilayer membranes. *FEBS Lett.* 174:199-207.

Vaz, W. L. C., E. C. C. Melo, and T. E. Thompson. 1989. Translational diffusion and fluid domain connectivity in a two-component, two-phase phospholipid system. *Biophys. J.* 56:869-876.

Vaz, W. L. C., E. C. C. Melo, and T. E. Thompson. 1990. Fluid phase connectivity in an isomorphous, two-component, two-phase phosphatidylcholine bilayer. *Biophys. J.* 58:273-275.

Walker, M., and J. Hadgraft. 1991. Oleic acid - a membrane 'fluidiser' or fluid within the membrane. *Int. J. Pharm.* 71:R1-R4.

Walters, K. A. 1989. Penetration Enhancers and Their Use in Transdermal Therapeutic Systems. *In* Transdermal Drug Delivery: Developmental Issues and Research Initiatives. J. Hadgraft and R. Guy, ed. Marcel Dekker. New York. 197-246.

Weast, R. C. 1975. Handbook of Chemistry and Physics. CRC Press, Cleveland, OH.

Wertz, P. W., W. A. Abraham, L. Landmann, and D. T. Downing. 1986. Preparation of liposomes from stratum corneum lipids. *J. Invest. Dermatol.* 87:582-584.

Wertz, P. W., and D. T. Downing. 1983. Ceramides of pig epidermis: structure determination. *J. Lipid Res.* 24:759-765.

Wertz, P. W., and D. T. Downing. 1989. Stratum corneum: Biological and biochemical considerations. *In* Transdermal Drug Delivery: Development Issues and Research Initiatives. J. Hadgraft and R. H. Guy, ed. Marcell Dekker. New York. 1-22.

Wertz, P. W., K. C. Madison, and D. T. Downing. 1989. Covalently bound lipids of human stratum corneum. *J. Invest. Dermatol.* 92:109-111.

White, S. H., G. I. King, and J. E. Cain. 1981. Location of hexane in lipid bilayers by neutron diffraction. *Nature.* 290:161-63.

Wildnauer, R. H., D. L. Miller, and W. T. Humphries. 1975. A physiochemical approach to the characterization of stratum corneum. *In* Applied Chemistry at Protein Interfaces. R. F. Gould, ed. American Chemical Society. Washington D.C. 74-124.

Williams, A. C., and B. W. Barry. 1991. The enhancement index concept to terpene penetration enhancers for human skin and model lipophilic (oestradiol) and hydrophilic (5-fluorouracil) drugs. *Int. J. Pharm.* 74:157-168.

Williams, A. C., and B. W. Barry. 1991. Terpenes and the lipid-protein partitioning theory of skin penetration enhancement. *Pharm. Res.* 8:17-24.

Williams, A. C., P. A. Cornwell, and B. W. Barry. 1992. On the non-Gaussian distribution of human skin permeabilities. *Int. J. Pharm.* 86:69-77.

Wilschut, A., W. F. T. Berge, P. J. Robinson, and T. E. McKone. 1995. Estimating skin permeation. The validation of five mathematical skin permeation models. *Chemosphere.* 30:1275-1296.

Wright, L. L., A. G. Palmer, and N. L. Thompson. 1988. Inhomogeneous translational diffusion of monoclonal antibodies on phospholipid Langmuir-Blodgett films. *Biophys. J.* 54:463-470.

Wu, E., K. Jacobson, and D. Papahadjcpoulos. 1977. Lateral diffusion in phospholipid multibilayers measured by fluorescence recovery after photobleaching. *Biochemistry.* 16:3936-41.

Yardley, H. J., and R. Summerly. 1981. Lipid composition and metabolism in normal and diseased epidermis. *Pharmac. Ther.* 13:357-383.

Yguerabide, J., J.A. Schmidt, and E.E. Yguerabide. 1982. Lateral mobility in membranes as detected by fluorescence recovery after photobleaching. *Biophys. J.* 39:69-75.

Yoneto, K., S. K. Li, A. H. Ghanem, D. J. Crommelin, and W. I. Higuchi. 1995. A mechanistic study of the effects of 1-alkyl-2-pyrrolidones on bilayer permeabilitiy of stratum corneum lipid liposomes: a comparison with hairless mouse skin studies. *J. Pharm. Sci.* 84:853-861.

Yum, S., E. Lee, L. Taskovich, and F. Theeuwes. 1994. Permeation Enhancement with Ethanol: Mechanism of Action Through Skin. *In* Drug Permeation Enhancement: Theory and Application. D. S. Hsieh, ed. Macel Dekker. New York. 143-170.

Zhang, F., G. M. Lee, and K. Jacobson. 1993. Protein lateral mobility as a reflection of membrane microstructure. *BioEssays*. 15:579-588.